

# ROBUST MULTI-MODE CONTROL OF HIGH PERFORMANCE AERO-ENGINES

Thesis submitted for the degree of  
Doctor of Philosophy  
at the University of Leicester

by

Raza Samar BSc Engg (Lahore), MS (Stanford)  
Department of Engineering  
University of Leicester

May 1995

*To my parents*

# Abstract

This thesis describes the application of  $H_\infty$  design techniques to the control of high performance aero-engines. The design study presented is practical and realistic, the work being motivated by problems that arise naturally in real engineering situations. The aero-engine is multivariable and highly nonlinear: the dynamics vary considerably with the thrust being produced, and with the altitude and forward speed of the aircraft. Moreover, there are operational constraints that must never be violated for reasons of safety: certain engine variables should always be limited to safe values. Furthermore, not all the engine parameters to be controlled are directly measurable; instead a number of related measurements are available. A methodology is presented to choose from the available measurements, those that are preferable for feedback control. Different techniques of model reduction using balanced realizations are considered. Two illustrative examples are presented, and the methods compared in detail. Explicit state-space formulae for an  $H_\infty$ -based two degrees-of-freedom robust controller are derived in discrete time. The controller provides robust stability with respect to coprime factor perturbations, and a degree of robust performance in the sense of making the closed-loop system match an ideal reference model. Special attention is paid to the structure of the controller. It is shown that the controller consists of a plant observer, the reference model, and a generalized state feedback law associated with the plant and model states. Multi-mode control logic is developed to ensure that safety limits are never violated. Actual engine test results are presented for sea-level static conditions. All the different modes of operation are tested. Full flight envelope evaluation of the controller is carried out using a nonlinear engine simulation. The robust performance of the controller is demonstrated and comparisons made with existing engine control systems.

# Acknowledgements

It is my pleasure to thank my supervisor, Professor Ian Postlethwaite, for his invaluable guidance, support and accessibility throughout the course of this work. I would also like to thank Dr. Da-Wei Gu for always being ready to help, and to provide constructive comments and suggestions. I thank my family, and in particular my parents, for their continual support and encouragement during my studies.

This work was carried out with financial support from the S&T scholarship scheme of the Government of Pakistan and the ORS awards scheme of the British Government. Support from both these funding bodies is gratefully acknowledged. I am also grateful to Professor Ian Postlethwaite for arranging additional funding when the scholarship finished, during which time much of this thesis was prepared.

The nonlinear thermodynamic model of the aero-engine used in the designs presented in this thesis was provided by Lucas Aerospace Limited, Birmingham. I would like to thank Mr. G.J. Dadd, Mr. M.J. Porter, Mr. A. Greig and Mr. J.W. Beard of the Defence Research Agency, Pyestock, and Mr. A.E. Sutton of Lucas Aerospace Limited, Birmingham, for organizing and arranging the engine tests, as well as for many helpful discussions and comments regarding the engine control problem.

Finally I would like to thank all my colleagues in the control systems research group for helping to create such a friendly and enjoyable work environment. In particular I would like to thank Abdul-Wahid, Byung-Wook, Chris, Ghassan, Song-Joo and Tim for being great company, and for their ever-readiness to discuss both work and non-work related matters.

Leicester  
May 1995

# Contents

<b>1</b>	<b>Introduction</b>	<b>1</b>
1.1	An overview . . . . .	1
1.2	Structure of thesis . . . . .	10
1.3	Notation . . . . .	15
1.3.1	Mathematical notation . . . . .	15
1.3.2	Abbreviations . . . . .	16
1.3.3	List of variable names . . . . .	17
<b>2</b>	<b>Background and preliminaries</b>	<b>19</b>
2.1	Introduction . . . . .	19
2.2	Motivation for robust multivariable control . . . . .	19
2.3	Singular values and the small gain theorem . . . . .	20
2.4	Normalized coprime factors and uncertain models . . . . .	23
2.5	The $H_\infty$ standard plant . . . . .	25
2.6	Summary . . . . .	27
<b>3</b>	<b>A multivariable multi-mode design problem</b>	<b>28</b>
3.1	Introduction to high performance aero-engines . . . . .	28
3.1.1	The compressor . . . . .	30

3.1.2	The combustor . . . . .	33
3.1.3	The turbine . . . . .	34
3.1.4	The nozzle . . . . .	35
3.2	Design specifications . . . . .	35
3.2.1	Steady-state accuracy . . . . .	35
3.2.2	Transient accuracy . . . . .	36
3.2.3	Disturbance rejection . . . . .	36
3.2.4	Stability . . . . .	36
3.2.5	Limiter loop exchange . . . . .	37
3.2.6	Robustness requirements . . . . .	37
3.3	The aero-engine control problem . . . . .	37
3.3.1	Parameters to be controlled/limited and available measurements . .	37
3.3.2	The control inputs . . . . .	39
3.3.3	The multi-mode (switching) strategy . . . . .	39
3.3.4	Engine non-linearities . . . . .	40
3.4	The aero-engine model . . . . .	42
3.4.1	Discretization: modelling of input delays . . . . .	42
3.4.2	Modelling of output delays . . . . .	48
3.5	Summary . . . . .	48
<b>4</b>	<b>Control structure design</b>	<b>49</b>
4.1	Introduction . . . . .	49
4.2	Input output scaling . . . . .	50
4.3	Practical considerations . . . . .	51
4.4	Right half-plane zeros . . . . .	51

4.5	The relative-gain array . . . . .	52
4.6	The condition number . . . . .	56
4.7	Hankel singular values . . . . .	59
4.8	Input output pairing . . . . .	62
4.9	Summary . . . . .	63
<b>5</b>	<b>Model reduction with balanced realizations</b>	<b>64</b>
5.1	Introduction . . . . .	64
5.2	Truncation and residualization . . . . .	66
5.3	Optimal approximations of stable transfer functions . . . . .	69
5.4	Error bound for balanced residualization . . . . .	71
5.5	Some multivariable examples . . . . .	72
5.5.1	Reduction of the aero-engine model . . . . .	72
5.5.2	Reduction of an aero-engine controller . . . . .	78
5.6	Conclusions . . . . .	90
5A	All-pass transfer functions . . . . .	92
5B	Error bound for balanced residualization . . . . .	92
5C	Manipulation of equations and some useful results . . . . .	97
5C.1	Expression (5B.8): (1,2)/(2,1) blocks . . . . .	97
5C.2	Expression (5B.10): (1,2)/(2,1) blocks . . . . .	98
5C.3	Proof of equation (5B.11) . . . . .	98
5C.4	Proof of equation (5B.12) . . . . .	99
5C.5	Proof of equation (5B.13) . . . . .	100
<b>6</b>	<b>Robust two degrees-of-freedom discrete time controller synthesis</b>	<b>101</b>
6.1	Introduction . . . . .	101

6.2	Robust stabilization in the normalized coprime factor framework . . . . .	102
6.3	$H_\infty$ loop-shaping . . . . .	104
6.4	Two degrees-of-freedom configuration . . . . .	108
6.5	$H_\infty$ two degrees-of-freedom controller synthesis . . . . .	111
6.6	$H_\infty$ full information control . . . . .	111
6.7	The disturbance feedforward problem . . . . .	115
6.8	Controller formulae and structure . . . . .	118
6.9	Design procedure . . . . .	123
6.10	Summary . . . . .	125
<b>7</b>	<b>Multi-mode controller design and implementation</b>	<b>126</b>
7.1	Introduction . . . . .	126
7.2	Design considerations for plants with more outputs than inputs . . . . .	127
7.3	Controller design . . . . .	130
7.3.1	PS6PS1 controller design . . . . .	131
7.3.2	NL limiter design . . . . .	135
7.3.3	TT15 limiter design . . . . .	136
7.4	Controller implementation . . . . .	138
7.5	Computational advantages gained by utilizing the controller structure . . . . .	142
7.6	The switched controller structure . . . . .	144
7.7	Anti-windup and bumpless transfer . . . . .	144
7.8	Summary . . . . .	149
<b>8</b>	<b>Engine test results</b>	<b>150</b>
8.1	Introduction . . . . .	150
8.2	Engine test results . . . . .	151

8.2.1	PS6PS1 (thrust) control mode . . . . .	151
8.2.2	NL limiting mode . . . . .	152
8.2.3	TT15 limiting mode . . . . .	158
8.3	Improving speed of response . . . . .	161
8.4	Full flight envelope evaluation . . . . .	162
8.5	Conclusions . . . . .	165
<b>9</b>	<b>Conclusions and suggestions for further research</b>	<b>169</b>
9.1	Conclusions . . . . .	169
9.2	Suggestions for future research . . . . .	172
	<b>References</b>	<b>176</b>

# Chapter 1

## Introduction

### 1.1 An overview

This thesis is about the application of linear robust control theory to high performance aero-engines. The need and importance of robustness in control system design though always appreciated, has been brought into the limelight during the last fifteen years. In classical single-input single-output control, robustness is achieved by ensuring good gain and phase margins. Designing for good stability margins also results in good, well-damped time responses, i.e., good performance [26]. When multivariable design techniques were first developed in the 1960s, the emphasis was laid on achieving good performance, and not on robustness. These multivariable techniques were based on linear quadratic performance indices and Gaussian disturbances, and proved to be successful in many aerospace applications. The main reason for this success was that accurate mathematical models of aerospace vehicles can be developed, and descriptions for external disturbances based on white noise are often appropriate in such applications. However, application of these methods, commonly referred to as the linear quadratic Gaussian (LQG) methods, to other industrial problems made apparent the poor robustness properties exhibited by LQG controllers. Doyle [15] and Doyle & Stein [18] later showed that LQG designs can exhibit arbitrarily poor stability margins. This led to a substantial research effort to develop a theory which could explicitly address the issue of robustness in feedback design. The pioneering work in the development of the forthcoming theory, now known as the  $H_\infty$  control theory, was performed in the early 80s by Zames [113] and Zames &

Francis [114]. In  $H_\infty$  design, the designer from the outset, specifies a model of system uncertainty (such as additive or input multiplicative) that is most suited to the problem at hand. A constrained optimization is then performed to maximize the robust stability of the closed-loop system to the type of uncertainty chosen, the constraint being that the feedback system be internally stable. Performance objectives can also be included in the optimization function. Design using the  $H_\infty$  approach has recently become very attractive with the efficient state-space solution of Doyle et al. [17]. This only requires the solution of two algebraic Riccati equations, and results in a controller of state dimension equal to that of the (weighted) plant. Earlier frequency domain methods (see for example, Francis [25]) resulted in controllers of a much higher order.

Alongside the theoretical developments in the field of  $H_\infty$  control, application studies also started appearing in the literature, see for example, Postlethwaite et al. [81, 83], Doyle et al. [14], and Safonov & Chiang [87]. Postlethwaite et al. [81, 83] considered a variety of industrial case studies: full authority flight control of a high performance helicopter, pitch axis control of an unstable aircraft, and control of a nuclear reactor and power plant. The performance and robustness objectives for the designs were taken to be the minimization of the weighted sensitivity function  $S$  and the weighted complementary sensitivity function  $T := I - S$ . Minimization of  $S$  gives good disturbance rejection properties at the plant output, while minimization of  $T$  gives robustness against output multiplicative uncertainty. The transfer function  $KS$  was also included in the cost to penalize the control energy,  $K$  being the  $H_\infty$  controller. The design procedure thus came to be known

as the  $S/T/KS$  procedure, the objective being to minimize  $\left\| \begin{array}{c} W_1 S \\ W_2 T \\ W_3 KS \end{array} \right\|_\infty$ , where  $W_i$  are

the weighting functions chosen by the designer. The weights were proposed to be chosen as simple first or second order filters:  $W_1$  chosen to be a low-pass filter, while  $W_2$  and  $W_3$  chosen as high-pass filters, to appropriately shape the different closed-loop transfer functions. Standard software for  $H_\infty$  design was not available then and a high level of software development was required to implement the designs; CAD packages such as *Stable-H* [82] were developed specially for this purpose. The choice of the weighting functions for the  $S/T/KS$  designs usually required numerous iterations and was cumbersome, hence the

$S/KS$  design formulation was adopted subsequently [83]. Note that the transfer function  $KS$  not only penalizes the control energy, but also provides robustness against additive plant perturbations.

Safonov & Chiang [87] advocated the use of the  $S/T$  design procedure. They studied an aircraft pitch axis control design example involving an unstable, non-minimum phase plant. The  $H_\infty$  design was compared to an earlier frequency-weighted LQG design, and it was concluded that the  $H_\infty$  theory easily produced a superior design, having both a higher bandwidth, and greater stability margins.

The software problems associated with  $H_\infty$  design were gradually overcome by the introduction of standard software packages such as MATLAB<sup>1</sup>, and specialized toolboxes, see for example [33, 10, 6]. This greatly facilitated design using the  $H_\infty$  approach. The  $S/KS$  and  $S/T$  techniques, commonly referred to as the *mixed sensitivity* techniques, were subsequently applied to various design problems. However, one major disadvantage of the mixed sensitivity approach became apparent: it results in pole-zero cancellations between the plant and the controller. All the stable poles of the open-loop plant are cancelled by the controller, and furthermore, the closed-loop poles include the mirror image positions (in the imaginary axis) of all the unstable poles of the plant [101, 62]. The consequences of this phenomenon are that the closed-loop properties of the system are directly determined by the properties of the open-loop plant, which may be undesirable in the following scenarios:

- (i) The cancellation of relatively slow or lightly damped resonant poles, means that the closed-loop system will exhibit undesirable properties. In particular, these modes will be uncontrollable from the controller input and unobservable from the controller output, leaving them as modes of the closed-loop system. These modes are not visible as long as we examine the transfer functions  $S$  or  $T$  or  $KS$ , but they become apparent once we consider how any disturbance at the plant input may propagate to the plant output. These modes will be excited in response to a disturbance which affects the control inputs, and the closed-loop system will exhibit undesirable behaviour.

---

<sup>1</sup>MATLAB is a registered trademark of The MathWorks, Inc.

- (ii) If the plant contains slow unstable poles compared to the rest of the system, some closed-loop transfer functions will contain slow stable poles, which again may result in undesirable behaviour.

Tsai et al. [101] gave some guidelines on how to choose the weighting functions to prevent undesirable pole-zero cancellations. They showed that with a particular construction of the weights, the designer can not only prevent undesirable pole-zero cancellations, but can also effect (partial) pole placement. This however, leads us to the other major drawback of the mixed sensitivity approach: the choice of the weighting functions is not straightforward, and it is often difficult to

- establish clear relationships between closed-loop design objectives and the choice of particular weighting functions,
- produce rules by which the weights are to be modified in the event of an unsuitable design.

A new approach to  $H_\infty$  design was developed by McFarlane & Glover [64, 63] in the late 1980s. This approach, referred to as the *loop-shaping design* approach, overcomes to a great extent, the main drawbacks of the mixed sensitivity approach. In particular, the problem of pole-zero cancellation is largely avoided, except for a certain special class of plants (i.e., those containing stable all-pass factors) [101]. As the name suggests, the loop-shaping approach is based on the multivariable generalization of classical loop-shaping ideas. The frequency response of the open-loop plant is shaped by augmenting it with appropriate weighting functions. The choice of the weights is, therefore, more intuitive and straightforward; the weights being selected for open-loop shaping and not for closed-loop shaping as in the mixed sensitivity approach. Moreover, the uncertainty in the plant is modelled in a fractional framework, which allows a much broader class of perturbations to be considered; this is discussed in detail in Chapter 2. Furthermore, the loop-shaping design approach has been shown (Chapter 6) to yield better robust performance properties than the mixed sensitivity approach, which places all the emphasis on the output of the plant, giving rise to possibly poor properties at the plant input. Also there is no need to iterate for the optimal solution, which in general, is a characteristic of all  $H_\infty$  designs.

These advantages led to the loop-shaping approach being applied successfully to various design problems, see for example [103, 48, 80].

It should be noted that all the design formulations considered so far rely on frequency shaping of various transfer functions, and time domain performance specifications cannot be incorporated directly into the design framework. In the loop-shaping approach, for example, the performance specifications are aimed for by appropriately shaping the open-loop plant. A more direct way of incorporating time domain specifications was proposed by Hoyle et al. [45] by extending the loop-shaping approach to a two degrees-of-freedom configuration. This allowed a model-matching problem to be included into the  $H_\infty$  cost function, and provided an explicit framework for robust performance design (in the model-matching sense). The two degrees-of-freedom design procedure has since been used successfully in various applications, examples are [104, 69]. It is emphasized however, that almost all these application studies have been based on computer simulations of the actual systems. Also the controller designs have mostly been performed in continuous time, and either used as such in the simulations, or discretized using certain  $s$ -plane to  $z$ -plane transformations. In this thesis, a discrete time design procedure based on the two degrees-of-freedom configuration is presented, and applied to the aero-engine control problem. The controller thus designed has been tested on an actual aero-engine, the Rolls Royce Spey Mk 202, and the test results discussed and compared with those obtained from existing engine control systems. The theory of discrete time  $H_\infty$ -optimization has been developed by Walker [107], and Iglesias & Glover [50].

The control of high performance aero-engines has been the subject of numerous papers over the last few years. All these papers can broadly be classified as belonging to one of two categories: (i) those in which the emphasis is on the controller design theory and the aero-engine control problem is presented as an illustrative (and in most cases trivial) example, and (ii) those in which the emphasis is on the aero-engine control problem, and simple classical controllers are designed and verified by simulation on the plant model. We shall now look at some of the work done in this field over the last ten years.

Kapasouris [52] presents controller designs for the GE-21 variable cycle turbofan jet engine using the LQR (linear quadratic regulator) and the LQG-LTR (linear quadratic Gaussian with loop transfer recovery) based methods of controller synthesis. The LTR

technique was introduced to improve the robustness of LQG controllers. It is well-known (see for example, [62]) that optimal state feedback (LQR controllers) and the Kalman filter, taken separately, have good robustness and performance properties. It might be expected therefore, that LQG compensators, which are constituted by combining the LQR state feedback with the Kalman state estimator, would also yield good robustness and performance. This, as indicated earlier, is generally not the case [15]. However, there is a way of designing the Kalman filter so that the full state feedback properties are ‘recovered’ at the input of the plant, this being referred to as the loop transfer recovery (LTR) procedure. What is needed is for some of the filter’s eigenvalues to be placed at the zeros of the plant, the remainder being allowed to become arbitrarily fast [18]. Since the procedure relies on cancellation of some of the plant dynamics (in particular the zeros) by the filter dynamics, it is guaranteed to work only with minimum phase plants. Kapasouris [52] selects nine operating points for linear designs. The linear compensators are scheduled using least-squares polynomial fitting methods to produce a ‘global’ nonlinear controller. The problem, however, is over-simplified, and the work is mainly of academic interest only. There have been some other studies on the application of the LQG-LTR technique to aero-engine control, see for example [76, 5, 65]. These again, are based on a simplified version of the problem, and serve mainly to illustrate the design technique.

Peczowski & Sain [73] have advocated the use of the ‘total synthesis’ approach for the design of multivariable controllers for gas turbine engines. They argue that in order to control the outputs of the plant independently with unique control inputs, the plant inverse must exist. Furthermore, for practical considerations, it should be well-conditioned. Given a plant  $G$  and a unity feedback error-actuated controller  $K$ , the transfer function from the reference input  $r$  to the plant output  $y$  is given by  $(I + GK)^{-1}GK$ . If the desired output response is given by  $y = Tr$ , where  $T$  is an ideal model, then equating the response of the feedback system to the ideal response gives the following expression for the controller:

$$K = G^{-1}T(I - T)^{-1}. \quad (1.1.1)$$

$K$  as given above is the ‘total synthesis’ controller. Peczowski & Sain [73] apply this scheme to a gas turbine engine model and design five linear controllers for different operating points. These controllers are then gain-scheduled to cover half of the thrust range

of the engine. In practice, the operating point of the aero-engine depends not only on thrust, but also on the operating altitude and forward speed. Hence a large number of such controllers would need to be designed to cover the full operating envelope of the engine. The design technique, however, has a number of obvious flaws: the requirement that the inverse of the plant must exist is not always a realistic one, and the controller given by (1.1.1) may not be realizable. Furthermore, the issue of robustness is not addressed; even the internal stability of the feedback system is not guaranteed.

Porter & Jones [78] have attempted to extend to multivariable plants, the classical proportional-integral-derivative (PID) based techniques of control system design. They assume the plant to be asymptotically stable, and propose a way to determine the proportional and integral gain matrices directly from step responses of the open-loop plant. These matrices are chosen so as to provide decoupling between the different controlled outputs. They propose the gains in each channel to be tuned on-line, and apply the technique to a linear engine model. The issue of robustness again, is not considered. PI controllers, nevertheless, have been successfully used in the aero-engine industry for a long time. However, with the future generation of engines being more complex and having a relatively large number of manipulated and controlled variables, there is a need to consider more sophisticated methods of control, and to analyse the benefits they may offer over the simpler PI schemes.

Eisa & Tyler [22] describe the development of a nonlinear multivariable controller for the F100 engine using the total synthesis theory of Peczkowski & Sain [73], as mentioned above. They use a fourth order nonlinear model of the engine, and linearize it at eight different points over the thrust range. Linear controllers are then designed at each of the chosen operating points using equation (1.1.1). These controllers are linked together using linear interpolation techniques to form a full range gain-scheduled nonlinear controller. The ideal response matrix  $T$  is chosen to be a diagonal matrix of first order lags. The controller is simulated on the nonlinear simulation, the responses are seen to be good for small steps, but with the full range reference step and a delay in fuel ignition, the controller performance is not good. This is not surprising as the issue of robustness is not addressed in the design procedure.

Polley et al. [77] describe the design of a full flight envelope nonlinear multivariable con-

troller for a single bypass variable-cycle jet engine. The nonlinear controller is obtained by scheduling linear compensator gains designed at selected operating points. Each individual linear controller is designed by parameter optimization techniques, using Edmund's algorithm [21] for optimizing the controller parameters. The algorithm aims at making the closed-loop transfer function approach a desired or 'target' transfer function as closely as possible over a specified frequency range. The design methodology is a frequency based one, and uses closed-loop Nyquist and Bode plots. The structure of the controller has to be specified by the designer, and the parameters of the controller are estimated by minimizing the square of the 2-norm of the error between the actual and target closed-loop transfer functions. This problem is shown to be reduced to a linear least-squares problem [21], to which a standard solution exists. Success of the algorithm depends on having a sufficiently good initial design and an appropriate choice of the controller structure. Polley et al. [77] choose a proportional plus integral (PI) based controller structure. After designing linear compensators at a number of operating points, the compensator gains are linked and scheduled using curve-fitting methods. The simulation results are seen to be good. Drawbacks of the design procedure are the lack of consideration to plant uncertainty and possibly undesirable pole-zero cancellations between the plant and the controller.

Leithead & O'Reilly [58] discuss multivariable control by the 'individual channel design' method. The multivariable problem is reduced to a set of single-loop design problems by taking into account the interaction between the different loops. The design technique is simple and manageable for 2-input 2-output systems, but for higher dimension systems, the procedure becomes complicated and cumbersome. Leithead & O'Reilly [58] apply the method to the design of a gas turbine control system. The example, however, is over-simplified and serves mainly to illustrate the main points of the proposed design procedure.

Recently there has been a study of the application of  $H_\infty$  mixed sensitivity control to gas turbine engines for helicopters [108]. This problem differs from the aero-engine control problem in several respects. Firstly, gas turbine engines for helicopters drive the rotor shaft, the rotational speed of the shaft being the most important output to be controlled. Aero-engines on the other hand, produce thrust by the expansion of hot compressed gases

in the nozzle. Secondly, for helicopter engines, the problem is basically that of regulation, the speed of the rotor shaft is required to be regulated to a desired value. There are some common attributes too, which both the aero-engine and the helicopter engine control problems share: the change in the dynamics of the engines with thrust and with the flight conditions is quite similar. A single-input single-output controller is designed in [108] for regulation of rotor shaft speed. Only one flight condition is considered.

Sutton [100] and Greig [37] have presented realistic case studies of the aero-engine control problem. They use simple PI controllers, which are gain-scheduled to produce a full range controller. It should be noted here that a very important issue in aero-engine control is the necessity of preventing violation of operational constraints. Since the principle of operation of a gas turbine engine is based on the compression, combustion and expansion of air, certain temperatures and rotational speeds in the engine can, under some conditions, rise to dangerously high levels. This can adversely affect engine life, and in some cases can cause catastrophic failure. Hence, critical engine variables are always required to be limited to specified safe values. In all the design studies considered so far, this important aspect of the engine control problem is completely neglected. Sutton [100] considers the design of engine limiters to prevent overspeeding and overheating of the engine; his approach is based on the ideas of Nett & Polley [71], and results in a “multi-mode” control scheme. The term “multi-mode” corresponds to the controller having different modes of operation: the ‘normal’ or thrust control mode, and the various limiting modes, which are switched between, depending on which output is the most significant at a given time. A similar multi-mode scheme is developed in this thesis. Sutton [100] and Greig [37] demonstrate their designs by engine tests. They however, do not consider the full flight envelope operation of the engine.

It is apparent from the literature survey presented here that the majority of the work in the field of aero-engine control is based on simplified and often unrealistic definitions of the control problem, and not all essential control requirements are considered. Most researchers have presented case studies in order to illustrate a particular design technique, and in the process have over-simplified the problem. The more realistic design studies all employ classical PI controllers. Such controllers have been successfully used in the industry, however, new engines under development are expected to require more sophisticated

methods of control. These engines will have an increased number of variable inputs, and the existing approaches to controller design are likely to be inadequate; engine designs at present being undertaken by Rolls Royce have as many as nine control variables. The application of modern techniques to contemporary engines, and then proving these by engine tests, will demonstrate a capability and provide experience in design to meet the likely challenge of forthcoming control requirements.

The aero-engine control problem considered here is a challenging one. The dynamics of the engine vary considerably with the thrust it produces, and also with the operating altitude and the forward speed of the aircraft. The controller should either be robust to the change in dynamics, or be adapted accordingly; all existing schemes use gain-scheduling to cover the full operating envelope of the engine. Secondly, the requirement that certain variables (apart from the ones being primarily controlled) must not exceed pre-set limits adds to the complexity of the problem. Moreover, the engine is inherently nonlinear and multivariable, future engines will have an increased number of manipulated and controlled variables. There is thus, a need to apply state-of-the-art techniques to this problem, and to analyse the benefits these techniques can offer over existing control schemes. This need motivates the work described in this thesis.

## 1.2 Structure of thesis

This thesis consists of nine chapters and is organized as follows.

**Chapter 2** briefly reviews the ideas and concepts fundamental to the theory of  $H_\infty$  control. The use and need of robust multivariable control is motivated. It is argued that the Nyquist-like techniques of multivariable design (such as the Characteristic Locus and Nyquist array methods) can lead to designs that have poor stability margins. Moreover, since the question of optimality is not addressed, it is not clear if the design can be improved or not.  $H_\infty$ -optimization is presented as a complete theory which explicitly addresses the issue of robustness in feedback design. The ‘small gain theorem’ is presented and the use of singular values in quantifying robustness described. Different representations of uncertainty are discussed and conditions for robust stability derived. The normalized coprime factor representation of transfer functions is presented and the

merits of modelling uncertainty in this framework discussed. It is shown that this framework allows a relatively broad class of perturbed systems to be modelled. The standard formulation for posing  $H_\infty$ -optimization problems is presented. Most design problems can be formulated in this standard form, for which standard solutions exist.

**Chapter 3** introduces the aero-engine control problem. The working and operation of the aero-engine is discussed in detail. The characteristics of the individual components of the engine are described. The design specifications and closed-loop objectives are discussed. The plant inputs, and the parameters to be controlled or limited are listed: three parameters require control while two outputs need to be limited, there being three control inputs. Since the number of outputs is greater than the number of available inputs, a multi-mode scheme is developed in which separate controllers are designed for different sets of outputs. These controllers are arranged to be switched between in an appropriate manner, depending on which output is the most significant at a given time. The main sources of nonlinearity in the engine are described. Discretization of linear engine models is discussed. Formulae are derived for discretizing general linear state-space models with different time delays in different input channels, assuming a zero-order hold on the inputs. The discrete time engine model is to be used later for designing discrete time controllers. Direct discrete design is important in our case since the sample time we had to choose is barely sufficient for the application at hand. The delays associated with the digital implementation are thus significant and cannot be neglected. These delays are modelled exactly in discrete time, there is no need for continuous time approximations, and hence direct discrete design is preferable.

**Chapter 4** presents a systematic methodology to deal with the problem of ‘control structure design’. For the case of the aero-engine, some of the parameters to be controlled, such as thrust and the compressor surge margin, are not directly measurable. Instead, a number of related measurements are available which can be used to represent these parameters. For example, there are five measurements which can represent thrust, and three which can represent the compressor surge margin. The problem is then to choose from among these available measurements, the ones that are in some sense better for closed-loop control. This task of choosing appropriate outputs and then deciding on how to pair them with the inputs, is referred to as control structure design. Different techniques

to tackle this problem are presented and demonstrated by application to the aero-engine example. The importance of input output scaling is discussed. The limitations in closed-loop performance arising from slow right half-plane zeros of the plant are described. The relative-gain array is discussed and its role in structure design elaborated. It is shown that large entries in the relative-gain array indicate a plant which is poorly conditioned with respect to inversion. Also such plants can result in the closed-loop system having poor stability robustness in the presence of actuator uncertainty. The plant condition number and its role in structure selection is then discussed. It is shown that for ill-conditioned plants, robust performance can be very poor, even if the closed-loop system has good robust stability and nominal performance properties. Moreover, high condition numbers indicate potentially poor robustness in the face of additive or input multiplicative uncertainty. The Hankel singular values and their role in structure design is introduced. Finally the problem of input output pairing based on the steady-state relative-gain array is briefly reviewed. The main part of the chapter has been published in [90].

**Chapter 5** discusses in detail different methods of obtaining reduced order models using balanced realizations. The issue of model reduction has obtained great importance over the last fifteen years. Optimal design methods, such as  $H_\infty$  or LQG, produce controllers of order at least equal to that of the plant, if not higher. The designer has no direct control over the state dimension of the resulting controllers. As a result, these methods are generally considered by practitioners to be too complex with regards to practical implementation. The problem of complexity becomes even more pronounced when dealing with multi-mode systems, where a number of controllers, each corresponding to a different mode of operation, are run in parallel. Moreover, gain-scheduling requirements further increase the computational load. Hence, there is always a need for obtaining low order, yet accurate approximations of high order systems. The balanced truncation technique has been widely used for model reduction, owing to its simplicity and ease of use. The basic idea is to discard the less controllable and observable states of a system. This idea can be extended so that the less controllable and observable states are ‘residualized’ instead of being truncated. The resulting method, referred to as ‘balanced residualization’, is shown to enjoy some favourable properties. It is shown that this method preserves the steady-state gain of the system. An error bound for this method is also derived, and

this turns out to be the same as the bound for balanced truncation. This error bound has previously been derived by Liu & Anderson [61] using a different approach, they refer to the technique as ‘singular perturbation approximation’. The optimal Hankel-norm approximation technique of Glover [30] is also discussed. The three techniques are demonstrated and compared on two detailed examples. The first example is about reduction of an aero-engine model, and the other about reduction of an  $H_\infty$  controller. The bulk of this chapter has been published in [93, 39, 92].

**Chapter 6** describes an  $H_\infty$  two degrees-of-freedom discrete time controller synthesis procedure. Special importance is given to the structure of the controller. This is because it not only provides a deeper understanding of the working of the controller, but is also vital for the acceptance of the technique into mainstream industrial usage. The robust stabilization problem in the normalized coprime factor framework is reviewed. The importance of loop-shaping in  $H_\infty$  design is described. The loop-shaping design procedure (LSDP) of McFarlane & Glover [64] is discussed in detail. It is shown that common closed-loop transfer function objectives are easily incorporated into the design procedure. Moreover, the LSDP ensures that these closed-loop objectives are well-behaved, and can be shaped as desired at low and high frequencies by appropriately choosing the weighting functions. The two degrees-of-freedom design configuration is presented, which includes a model matching problem in addition to the coprime factor robust stabilization problem. The problem is cast into the standard form introduced in Chapter 2. Explicit state-space formulae for the corresponding controller are derived. This is done by breaking down the problem into two parts: the full information problem and the disturbance feedforward problem, and using standard results to solve these problems. The structure of the controller is presented. It is shown that the controller consists of an observer for the (shaped) plant, the chosen reference model, and a generalized state feedback law associated with the plant and model states. Finally the controller design procedure is presented. The major part of this chapter has been published in [89].

**Chapter 7** works through the design details of the aero-engine multi-mode controller and discusses important implementation issues. Design considerations for plants with more outputs than inputs are discussed. It is shown that for good tracking and disturbance rejection on some outputs, the loop gain associated with these outputs has to be rela-

tively high. The design of the thrust controller and the two limiters is described in detail, thus illustrating the design procedure proposed in Chapter 6. The performance of the controllers is verified using linear simulations. An efficient form for controller implementation is presented. This resolves potential stability problems which can arise from a high bandwidth local feedback loop inside the controller. The controller structure is shown to be utilized to yield considerable real time computational savings. The structure of the overall switched controller is described. Anti-windup and bumpless transfer issues are discussed. The conditioning technique of Hanus et al. [41], and the observer-based approach of Åström & Wittenmark [4] are described in detail. These approaches are applied to the aero-engine multi-mode controller to provide anti-windup action in case of actuator saturation, and bumpless transfer when switching between different controller modes of operation.

**Chapter 8** presents and discusses the results of the engine tests carried out at the Defence Research Agency's engine test facility. The tests are carried out at sea-level static conditions. All the three controller modes of operation are tested. The controller is tested over the entire thrust range of the engine. A way of improving the speed of response of the closed-loop system is suggested by changing slightly the implementation of the anti-windup compensation. Full flight envelope evaluation of the controller is carried out using the nonlinear thermodynamic simulation of the engine. The controller is tested at ten different flight points in the flight envelope. The performance at seven of the ten points is deemed acceptable, large interaction between the controlled outputs is observed for the other three points. Filtering of the reference signals is proposed to reduce the interaction, and the simulations repeated to demonstrate the improvement offered by the pre-filter. Part of Chapters 7 and 8 has been published in [84].

**Chapter 9** draws together the main conclusions and contributions of the thesis. Suggestions for further work are given.

### 1.3 Notation

All systems considered are linear, time-invariant and finite-dimensional. A (proper) transfer function (matrix) is represented in terms of state-space data as:

$$\left[ \begin{array}{c|c} A & B \\ \hline C & D \end{array} \right] := C(sI - A)^{-1}B + D,$$

alternatively written as  $(A, B, C, D)$ , where  $A$ ,  $B$ ,  $C$  and  $D$  are real valued matrices, and  $I$  is the identity matrix of appropriate dimension. If  $D = 0$ , the zero matrix, then the system is strictly proper, and we shall write  $(A, B, C)$ . The system is *asymptotically stable* if and only if each of the eigenvalues of the matrix  $A$  has a strictly negative real part. For discrete time systems, the condition is for all the eigenvalues of  $A$  to lie inside the unit disk.

#### 1.3.1 Mathematical notation

$\mathfrak{R}$	the field of real numbers
$\mathfrak{R}^{m \times n}$	the set of real matrices with $m$ rows and $n$ columns
$\mathcal{C}^{m \times n}$	the set of complex matrices with $m$ rows and $n$ columns
dB	decibels: $x$ dB represents a gain of $10^{x/20}$
$\cdot*$	element-by-element multiplication (the Schur or Hadamard product)
$ a $	the absolute value of the real number $a$
$A^T$	the transpose of the matrix $A$
$A^H$	the transpose of the complex conjugate of matrix $A$
$\det(A)$	the determinant of the square matrix $A$
$[A]_{ij}$ or $a_{ij}$	the $(i, j)$ element of the matrix $A$
$A^{-1}$	the inverse of the square matrix $A$
$\lambda_i(A)$	the $i$ th eigenvalue of the square matrix $A$
$\lambda_{max}(A)$	the largest eigenvalue of the square matrix $A$
$\lambda_{min}(A)$	the smallest eigenvalue of the square matrix $A$
$\rho(A)$	the spectral radius of the square matrix $A$ , i.e., $\max_i  \lambda_i(A) $
$\sigma_i(A)$	the $i$ th singular value of the matrix $A$
$\bar{\sigma}(A)$	the largest singular value of the matrix $A$

$\underline{\sigma}(A)$	the smallest singular value of the matrix $A$
$\kappa(A)$	the condition number of $A$ , $\bar{\sigma}(A)/\underline{\sigma}(A)$
$diag\{\sigma_i\}$	a diagonal matrix with $\sigma_i$ on the main diagonal
$I$	identity matrix of unspecified dimension
$I_n$	the $n \times n$ identity matrix
$j$	$\sqrt{-1}$ ; sometimes an index, as in $a_{ij}$
$\log$ or $\log_{10}$	logarithm to base 10
$\delta(A)$	the number of eigenvalues of $A$ on the imaginary axis
$A > 0$	symmetric matrix $A$ is positive definite
$A \geq 0$	symmetric matrix $A$ is positive semi-definite
$\ x\ $	Euclidean norm of vector, $(x^H x)^{1/2}$
$\ x\ _2$	$\left(\int_{-\infty}^{\infty} x^T(t)x(t)dt\right)^{1/2}$ , if $x(t)$ is a real continuous time signal $\left(\sum_{k=-\infty}^{\infty} x^T(k)x(k)\right)^{1/2}$ , if $x(k)$ is a real discrete time signal
$\ A\ _2$	the spectral norm of $A$ , $\bar{\sigma}(A)$
$G(s)$	a continuous time transfer function (matrix)
$G(z)$	a discrete time transfer function (matrix)
$\ G\ _{\infty}$	$\sup_{\omega} \bar{\sigma}(G(j\omega))$ , if $G$ is a continuous time transfer function (matrix) $\sup_{\theta \in (-\pi, \pi]} \bar{\sigma}(G(e^{j\theta}))$ , if $G$ is a discrete time transfer function (matrix)
$RH_{\infty}$	set of asymptotically stable transfer functions $G$ , with $\ G\ _{\infty} < \infty$
$\ G\ _H$	Hankel norm, if $G$ is a transfer function (matrix)
$T_{zw}$	transfer function from signal $w$ to signal $z$
$\exists$	‘there exists’
$\in$	‘an element of’
$\forall$	‘for all’
$\neq$	‘not equal to’

### 1.3.2 Abbreviations

AWBT	anti-windup bumpless transfer
CAD	computer aided design
DARE	discrete algebraic Riccati equation

DCU	digital control unit
DOF	degrees-of-freedom
DRA	Defence Research Agency
HP	high pressure
LFT	linear fractional transformation
LHP	left half-plane
LP	low pressure
LQG	linear quadratic Gaussian
LTR	loop transfer recovery
LSDP	loop-shaping design procedure
FDLTI	finite-dimensional linear time-invariant
MIMO	multi-input multi-output
PI	proportional plus integral
PID	proportional-integral-derivative
RGA	relative-gain array
RHP	right half-plane
SISO	single-input single-output

### 1.3.3 List of variable names

AJ	nozzle area (percent of maximum)
BOV	blow-off valve position (percent of maximum)
DPUP	Mach number measurement at LP compressor's exit to bypass
IGV	inlet guide vane angle (degrees)
NHPCSL	HP compressor's non-dimensional percent spool speed
NL	LP compressor's percent spool speed
NLPCSL	LP compressor's non-dimensional percent spool speed
OPRS	engine's overall static pressure ratio
OPRT	engine's overall total pressure ratio
PS6PS1	ratio of HP compressor's static outlet pressure to the static pressure at engine inlet
PT6PT1	ratio of HP compressor's total outlet pressure to the total pressure

	at engine inlet
PS21PS1	static pressure ratio across the LP compressor
PT21PT1	total pressure ratio across the LP compressor
TBT	turbine blade temperature (degrees Kelvin)
TT15	total temperature at LP turbine's outlet (degrees Kelvin)
WFE	fuel flow (cc/sec)

## Chapter 2

### Background and preliminaries

#### 2.1 Introduction

In this chapter the concepts and ideas basic to the field of  $H_\infty$ -optimal control are briefly reviewed. §2.2 motivates the use of robust control for tackling uncertain multivariable design problems. §2.3 discusses the use of singular values and the  $L_\infty$ -norm to quantify robustness for multi-input multi-output (MIMO) systems. §2.4 introduces the normalized coprime factor uncertainty representation and discusses its advantages over other models of uncertainty. §2.5 describes the standard form for formulating  $H_\infty$  design problems, and §2.6 summarises the main points of the chapter.

#### 2.2 Motivation for robust multivariable control

A mathematical model of any physical system is always an approximation of the true system dynamics. The difference between the model and the true system, i.e., the *plant uncertainty* depends on various factors. Typical sources of uncertainty include unmodelled (high frequency) dynamics, neglected nonlinearities, effects of deliberate reduced order modelling, and plant parameter changes due to environmental factors and with time. A feedback system (in which the controller design is based on an imperfect plant model) is required to be *robust* to such perturbations: it must maintain stability and some level of performance in the face of uncertainty. In classical single-input single-output (SISO) control, gain and phase margins have been used as measures of robustness. It is now

well known that these measures (taken one loop at a time) are not good indicators of robustness for multivariable feedback systems (as shown, for example, in [36]).

Many SISO design techniques have been generalized to tackle multivariable problems. Examples are the Characteristic Locus and Nyquist Array design methods. These techniques have also been applied to some design problems, an example is the aircraft control problem discussed by Maciejowski [62]. The main drawback of these design methods is that they rely mainly on the notion of gain and phase margins to address robustness, and these measures, as indicated above, can be poor indicators of robust stability. Moreover if designs obtained through such methods do not yield satisfactory closed-loop behaviour, it is often not clear what can be done for improvement. Furthermore, since the question of optimality is not addressed, one does not know if the design can even be improved or not. Hence when faced with the design of controllers for complex multivariable systems, one is motivated to look towards techniques which are inherently multivariable and which provide a degree of robustness to modelling errors and uncertainties. In this thesis, one such approach is considered.

### 2.3 Singular values and the small gain theorem

In addition to plant uncertainties, a control system is also subject to command and/or disturbance input uncertainties. Stability and performance is desired for every disturbance and command input in a prescribed set, under all possible plant perturbations. In fact plant perturbations can also be modelled as external disturbances acting on the system. These external input signals are usually not known precisely but can be classified so as to belong to a prescribed norm-bounded (energy-bounded) set. The design engineer then strives to minimize the maximum error (which is a measure of performance/stability degradation) that can occur subject to all possible input signals belonging to this set. This is achieved by minimizing the *maximum singular value* (or the maximum gain) of the corresponding transfer function(s) [19].

The notion of gain and phase margins turned out to be a poor indicator of robustness for multivariable systems primarily because it doesn't allow for coupling between the loops. The idea of using the maximum singular value however, captures not only the worst-case

scenario, but is also natural in a multivariable setting. A very general result known as the *small gain theorem* forms the basis for the use of the maximum singular value for evaluating robustness of multivariable feedback systems. It states that a feedback loop composed of stable (linear or nonlinear) operators will remain (internally) stable if the product of all the operator gains is less than unity [12]. As an example let  $A, B \in RH_\infty$  form a closed-loop system, where  $RH_\infty$  denotes the space of all real rational asymptotically stable transfer functions. Then according to the small gain theorem, the condition for stability of the feedback system is:

$$\bar{\sigma}(A(j\omega)) \cdot \bar{\sigma}(B(j\omega)) < 1 \quad \forall \omega \in \mathfrak{R}. \quad (2.3.1)$$

Here  $\bar{\sigma}(\cdot)$  denotes the maximum singular value, and  $\mathfrak{R}$  the field of real numbers.

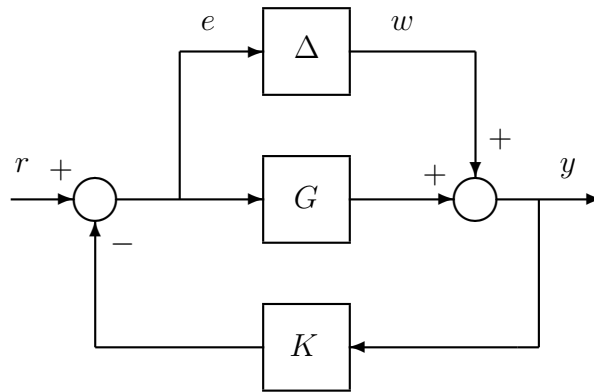


Figure 2.1: Feedback loop containing plant with additive uncertainty.

This theorem can be applied to yield sufficient conditions for robust stability for any representation of uncertainty. Let us consider Figure 2.1. The  $\Delta$ -block represents the (stable) additive uncertainty associated with the nominal plant model  $G$ . If the uncertainty is bounded in the sense that

$$\bar{\sigma}(\Delta(j\omega)) < \epsilon \quad \forall \omega, \quad (2.3.2)$$

then it follows from the small gain theorem that the closed-loop system will remain stable provided the transfer function from  $w$  to  $e$  is stable and has gain less than or equal to  $1/\epsilon$ , i.e.,

$$\bar{\sigma}(K(I + GK)^{-1}) \leq 1/\epsilon \quad \forall \omega. \quad (2.3.3)$$

Defining the  $L_\infty/H_\infty$ -norm of a transfer function  $H$  (where  $H$  has no poles on the imaginary axis) as:

$$\|H\|_\infty \triangleq \sup_\omega \bar{\sigma}(H(j\omega)), \quad (2.3.4)$$

we can rewrite (2.3.3) in more compact notation as:

$$\|K(I + GK)^{-1}\|_\infty \leq 1/\epsilon. \quad (2.3.5)$$

(2.3.5) is thus a sufficient condition for stability of the feedback system of Figure 2.1. If however, all possible perturbations can occur for which (2.3.2) holds, then the condition (2.3.5) is necessary as well as sufficient for robust stability. Similar conditions can be obtained for other representations of uncertainty, e.g., the input multiplicative perturbation, or the output multiplicative perturbation etc., as discussed by Doyle et al. [20]. It should be noted however, that the small gain theorem imposes a restriction on the allowable perturbation  $\Delta$ : it must be stable. This restriction can be relaxed somewhat by using the generalized Nyquist stability theorem instead; however the set of allowable perturbations is still restricted by the condition that the number of closed right half-plane poles of the nominal and perturbed plants be the same. This assumption is retained for such representations of uncertainty because it simplifies the theory and allows the use of homotopy arguments in robust stability analysis<sup>1</sup>. Furthermore in order to have a finite  $L_\infty$ -norm,  $\Delta(s)$  must not have any poles on the  $j\omega$ -axis. Such restrictions can seriously limit the set of perturbed plants that can be modelled, and hence guaranteed to be robustly stabilized. As an example we consider a system with a pair of resonant poles on the  $j\omega$ -axis, i.e., let  $G = \frac{5}{s^2 + \omega_o^2}$ . If the perturbed plant  $G_\Delta$  is given by  $\frac{5}{s^2 + (\omega_o + \alpha)^2}$  indicating uncertainty in the resonant frequencies of the poles, then the additive uncertainty  $G_\Delta - G$  is found to be  $\frac{-5(\alpha^2 + 2\alpha\omega_o)}{[s^2 + (\omega_o + \alpha)^2](s^2 + \omega_o^2)}$ , which is unbounded in the  $L_\infty$ -norm. The same can be verified for the multiplicative uncertainty models for this example. Thus these uncertainty descriptions can, in some cases, fail to capture simple perturbations on the nominal system model. An alternate representation of uncertainty, known as the normalized coprime factor perturbation, can represent a much wider class of systems than the additive or multiplicative models, and is discussed next.

---

<sup>1</sup>More general tests are infact available which allow the nominal and perturbed plants to have different numbers of right half-plane poles and zeros, such tests are however, generally complicated and require the uncertainty to be represented in different forms simultaneously [79].

## 2.4 Normalized coprime factors and uncertain models

This section introduces the normalized coprime factor perturbation which, as indicated above, is capable of modelling a broader range of systems than some other uncertainty descriptions. For a detailed discussion on coprime factorization, refer to Vidyasagar [102].

The pair  $(\tilde{M}, \tilde{N})$  constitutes a *left coprime factorization* of a transfer function  $G$  if:

- $G = \tilde{M}^{-1}\tilde{N}$ ,
- $\tilde{M}, \tilde{N} \in RH_\infty$  and there exist  $X, Y$  also  $\in RH_\infty$  such that  $\tilde{M}X + \tilde{N}Y = I$ , and
- $\det(\tilde{M}) \neq 0$  ( $\det(\cdot)$  denotes the determinant).

A left coprime factorization of  $G$  is said to be *normalized* if  $\tilde{M}, \tilde{N}$  satisfy

$$\tilde{M}\tilde{M}^* + \tilde{N}\tilde{N}^* = I,$$

where  $\tilde{M}^*$  denotes the complex conjugate transpose of  $\tilde{M}$ , etc. If  $G$  is a plant transfer function, then the perturbations or uncertainties in the plant are represented as additive perturbations on the normalized coprime factors of the plant. The perturbed plant  $G_\Delta$  is then given by:

$$G_\Delta = (\tilde{M} + \Delta_{\tilde{M}})^{-1}(\tilde{N} + \Delta_{\tilde{N}}),$$

where  $\Delta_{\tilde{M}}, \Delta_{\tilde{N}}$  are unknown transfer functions representing uncertainty in the plant model  $G = \tilde{M}^{-1}\tilde{N}$ ; see Figure 2.2.

It is important to note that the perturbation  $\Delta_{\tilde{M}}, \Delta_{\tilde{N}}$  will always be stable since  $\tilde{M}, \tilde{N}, (\tilde{M} + \Delta_{\tilde{M}})$  and  $(\tilde{N} + \Delta_{\tilde{N}})$  are stable by the definition of coprime factors. Thus this uncertainty representation imposes no restriction on the number of right half-plane poles of the nominal and perturbed plants:  $\Delta_{\tilde{M}}, \Delta_{\tilde{N}}$  are always stable, and hence the small gain theorem can be applied to any perturbed model. The family of perturbed plants (or the model set) for the normalized coprime factor perturbation is given by:

$$\mathcal{G}_\epsilon = \left\{ (\tilde{M} + \Delta_{\tilde{M}})^{-1}(\tilde{N} + \Delta_{\tilde{N}}) : \Delta_{\tilde{M}}, \Delta_{\tilde{N}} \in RH_\infty; \quad \|\begin{bmatrix} \Delta_{\tilde{M}} & \Delta_{\tilde{N}} \end{bmatrix}\|_\infty < \epsilon \right\}. \quad (2.4.1)$$

The robust stabilization problem is now to find the maximum achievable value of  $\epsilon$ ,  $\epsilon_{max}$ , and the controller that achieves it (i.e., which stabilizes the model set  $\mathcal{G}_{\epsilon_{max}}$ ). It follows

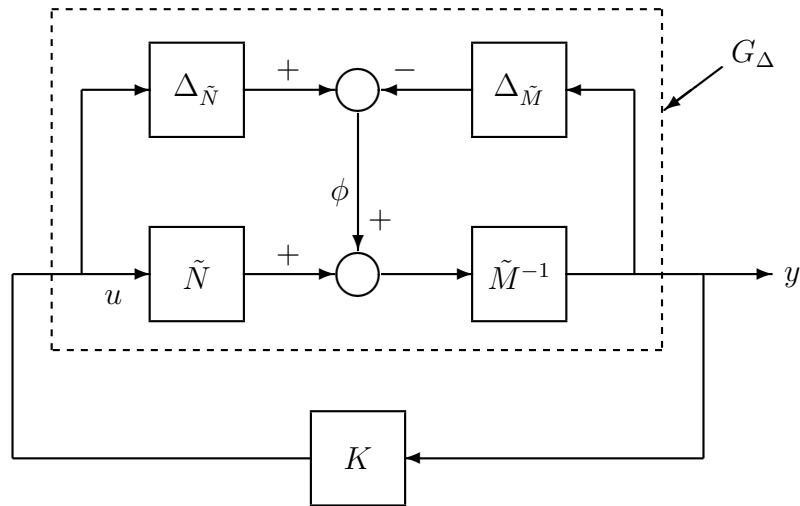


Figure 2.2: Left coprime factor perturbation.

from the small gain theorem that if the transfer function from  $\phi$  to  $\begin{bmatrix} u \\ y \end{bmatrix}$  is less than or equal to  $1/\epsilon$ , i.e., if

$$\left\| \begin{bmatrix} K \\ I \end{bmatrix} (I - GK)^{-1} \tilde{M}^{-1} \right\|_{\infty} \leq 1/\epsilon, \quad (2.4.2)$$

then this ensures that the feedback loop will be stable for all plants in the model set (2.4.1). Therefore in order to maximize the robust stability of the feedback system of Figure 2.2, one seeks a controller that stabilizes the nominal plant  $G$  and minimizes  $\gamma \triangleq 1/\epsilon$ . This problem has been formulated and solved for the continuous time case by McFarlane & Glover [64]; the solution is particularly attractive because the optimal  $\gamma$  can be found without iteration and the controller has an observer-state feedback structure [94]. The discrete time version of this problem has been studied by Walker [106]. Analytical expressions for the optimal  $\gamma$  and state-space formulae for the corresponding central optimal and sub-optimal controllers are available for both the continuous and discrete time cases [32, 106].

McFarlane & Glover [63] have proposed a design procedure which allows performance specifications to be incorporated into the robust stabilization problem outlined above. This is done by first translating the performance specifications into the frequency domain, and then giving the open-loop plant's singular values the desired shape. The singular values are shaped by augmentation of the nominal plant model  $G$  by pre- and/or post-

compensators (or weighting functions)  $W_1$  and  $W_2$  respectively. The shaped plant  $G_s = W_2GW_1$  is then robustly stabilized against coprime factor uncertainty, and the controller  $K$  thus obtained is cascaded with the weights to obtain the final controller  $W_1KW_2$ . It can be shown that the controller does not significantly alter the specified loop shape provided a sufficiently small value of  $\gamma$  is achieved.

## 2.5 The $H_\infty$ standard plant

As discussed in the preceding sections, robustness problems can be formulated as minimization problems where the  $L_\infty$ -norm of transfer functions relating various signals in the feedback loop is to be minimized. Performance specifications can be similarly formulated, e.g., attenuation of output disturbances at the plant output requires minimization of the  $L_\infty$ -norm of the sensitivity function. Thus both performance and robustness problems can be treated by specifying a set of (external) inputs and a set of outputs that define a set of suitable transfer functions to be minimized. Let all the external inputs be denoted by  $w$ , and let  $z$  denote the error or the outputs that are to be minimized; see Figure 2.3. Note that  $z$  includes both performance and robustness measures and hence characterizes fully the behaviour of the closed-loop system.  $P$  is called the generalized plant,  $u$  is the vector of control signals, and  $q$  the vector of measurements available to the controller.

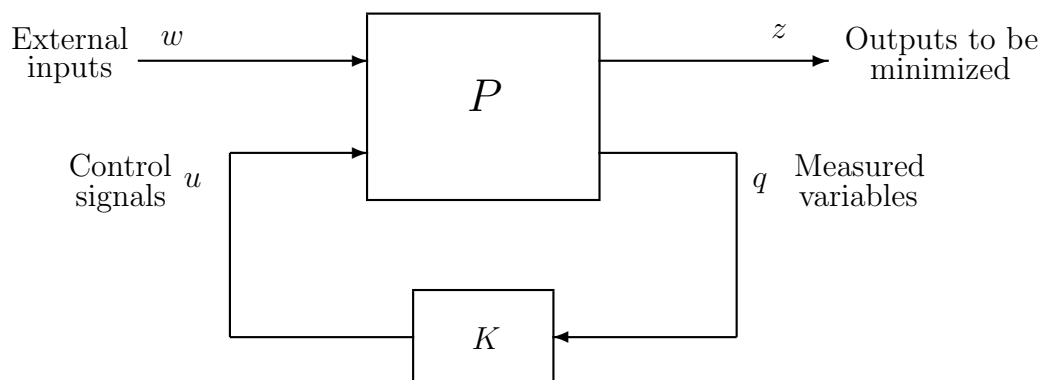


Figure 2.3: The  $H_\infty$  standard plant.

Partitioning the generalized plant  $P$  as:

$$P = \begin{bmatrix} P_{11} & P_{12} \\ P_{21} & P_{22} \end{bmatrix},$$

one can write

$$z = \left[ P_{11} + P_{12}K(I - P_{22}K)^{-1}P_{21} \right] w. \quad (2.5.1)$$

This is called the *lower linear fractional transformation* of  $P$  and  $K$  and is denoted by  $\mathcal{F}_l(P, K)$ . Thus (2.5.1) can be rewritten as:

$$z = \mathcal{F}_l(P, K)w. \quad (2.5.2)$$

The design objective now becomes:

$$\text{minimize } \|\mathcal{F}_l(P, K)\|_\infty,$$

where the minimization is over all linear, realizable controllers  $K$  which internally stabilize the closed-loop system. This is referred to as the  $H_\infty$ -*optimization problem*. Much research during the last decade has gone into finding efficient solutions to this problem. Formulae are now available for controllers which are internally stabilizing, and which achieve

$$\|\mathcal{F}_l(P, K)\|_\infty < \gamma, \quad (2.5.3)$$

where  $\gamma$  is any real number greater than the optimal value. The continuous time formulae are given by Doyle et al. [17] and Glover & Doyle [31], while the discrete time case is discussed by Walker [107] and Iglesias & Glover [50], and briefly summarized by Limebeer et al. [59]. In both cases the controller can be found by solving two matrix Riccati equations, and has a state dimension equal to that of the weighted plant. Having obtained a stabilizing, norm-bounding controller (i.e., one which satisfies (2.5.3) for a particular value of  $\gamma$ ), the solution to the  $H_\infty$ -optimization problem, in general, is obtained iteratively by searching over  $\gamma$  until a controller which yields a value sufficiently close to the optimal is obtained. This is referred to as the  $\gamma$ -*iteration* in  $H_\infty$  design.

Note that to put the robust stabilization problem of Figure 2.2 into the standard form of Figure 2.3, the output  $z$  and the external input  $w$  will consist of the signals  $\begin{bmatrix} u \\ y \end{bmatrix}$  and  $\phi$  of Figure 2.2 respectively.

## 2.6 Summary

In this chapter the use of robust multivariable control has been motivated for the design of controllers for complex MIMO systems. It has been stressed that methods which are extensions of classical SISO control, and which essentially rely on gain and phase margins and on shaping of the characteristic loci to satisfy the generalized Nyquist criterion, may lead to poor robust stability properties. The use of the maximum singular value and the  $L_\infty$ -norm as a measure of robustness was introduced and it was argued that this is more appropriate as it allows for coupling between the loops and considers the worst-case scenario. The small gain theorem was presented and applied to obtain sufficient stability conditions for different uncertainty representations. The concept of normalized coprime factor perturbation was introduced and its potential advantages over other uncertainty models discussed. Finally the standard framework for posing  $H_\infty$ -optimization problems was presented.

## Chapter 3

### A multivariable multi-mode design problem

#### 3.1 Introduction to high performance aero-engines

The purpose of this chapter is to describe in simple physical terms the fundamental characteristics of gas turbines, and associated control problems. The understanding of engine characteristics and operation will aid in the choice of appropriate output variables and the design of a control system that meets the desired specifications. §3.2 gives specifications for controller design in terms of steady-state and transient accuracy, disturbance rejection, and robustness requirements. §3.3 describes the engine parameters to be controlled and the available measurements. The non-linear behaviour of the engine is also discussed. §3.4 discusses discretization of the engine linearized model with pure time delays in input channels driven by zero-order hold circuits. Finally §3.5 summarizes the main points of the chapter.

All gas turbine aero-engines are heat engines, in which thermal energy derived from the combustion of fuel with air is converted to useful work. The transfer of energy from the fire in the combustion chamber to the actual hardware (i.e., propulsion of the aircraft) is achieved by the appropriate use of the *working fluid*, or air, which is made to flow through the engine. The working fluid is handled by the *thermodynamic cycle* of induction, compression, combustion, expansion and exhaust.

The engine considered for the purpose of this study is a Rolls Royce Spey. It is a 2-spool reheated turbofan engine, used to power modern military aircraft. The engine has two compressors: a low pressure (LP) compressor (sometimes also referred to as the fan),

and a high pressure (HP) or core compressor (Figure 3.1). The LP compressor draws air into the engine and raises its pressure. A small portion of this air is by-passed to the jetpipe; this portion does not pass through the thermodynamic cycle of the engine. The remaining portion goes through to the HP compressor where it is compressed to a much higher pressure and smaller volume. The high pressure flow at the exit of the HP compressor flows to the combustor into which fuel is injected in spray form, mixed with the air-stream and ignited. The resultant combustion causes an increase in the gas temperature, proportional to the amount of fuel being injected. The hot gases released from the combustor partially expand through two stages of turbine: the HP turbine and the LP turbine. The turbines extract some of the energy from the expanding combusted gases and drive the two compressors. The still hot and compressed gases at the output of the LP turbine flow into the jetpipe where they mix with the by-pass flow, coming direct from the LP compressor. This mixed flow then expands (almost) to atmospheric pressure in the nozzle, thus producing thrust for propulsion. The main components of the aero-engine are now discussed in more detail.

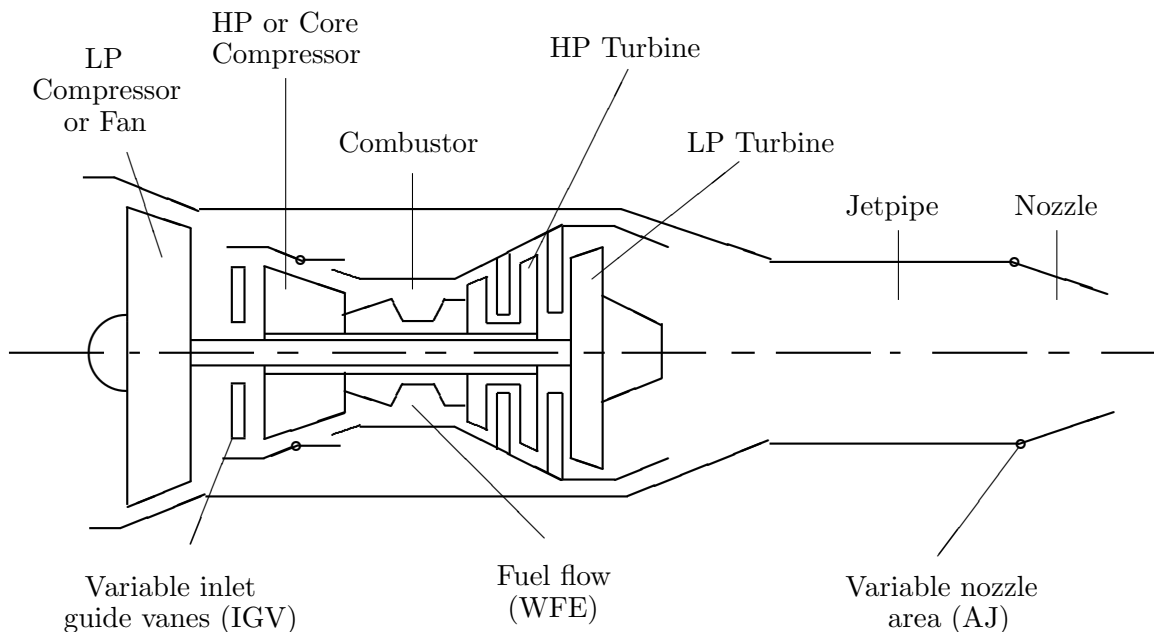


Figure 3.1: Schematic of the aero-engine.

In the sequel pressure and temperature measurements will be frequently referred to as

being *total* or *static*. Total measurements are absolute, *stagnation* values, measured by instruments which face into the approaching flow to give an indication of the energy in the flow at any point. These measurements are taken when a steadily flowing fluid is stagnated (brought to rest) without any transfer of heat. In contrast static conditions apply normal to the flow and would be measured by an instrument moving with the flow. For more details refer to [11].

### 3.1.1 The compressor

Both the compressors of the Spey engine are of the *axial-flow* type, i.e., in which the air flows mainly parallel to the rotational axis of the engine (as opposed to the *radial-flow* or *centrifugal* type). The LP compressor or fan is situated at the front end of the engine as shown in Figure 3.1. It acts to drive air into the engine system, and at the same time provides some compression. As indicated above, part of the air delivered by the LP compressor by-passes the core of the engine (HP compressor, combustion chamber and turbines) to form an annular propulsive jet of cooler air surrounding the hot engine. This results in a final jet of lower mean velocity which provides not only a better propulsive efficiency, but also significantly reduced exhaust noise [11]. The main compression of air takes place in the HP or core compressor.

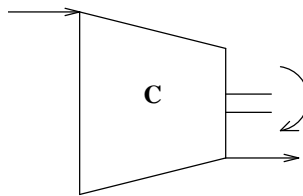


Figure 3.2: Diagrammatic representation of a compressor.

The axial compressor, represented diagrammatically in Figure 3.2, is normally built up from a number of stages, like a series of fans of reducing flow area. It can generate a pressure ratio of 10 or more provided sufficient stages are used [42]. Each stage comprises of a row of rotor blades followed by a row of stator blades. The working fluid (air) is initially accelerated by the rotor blades, and then decelerated in the stator blade passages wherein the kinetic energy transferred by the rotor is converted to potential energy in the

form of raised pressure. The process is repeated in a number of stages, the working fluid thus flows continuously into a region of higher pressure. This flow pattern may, in some cases, break down or even become unstable, particularly if the outlet to inlet pressure ratio becomes very large. Such a condition must be avoided by the use of adequate means of control.

The steady-speed characteristic for a multi-stage axial compressor is shown in Figure 3.3, in terms of pressure ratio and mass flow. The characteristic is obtained by varying the mass flow through the compressor, say by placing a valve in its outlet, and keeping the compressor speed constant. As the valve is steadily closed, the pressure ratio across the compressor starts to build up until the maximum possible value is attained (the peak of the curve in Figure 3.3).

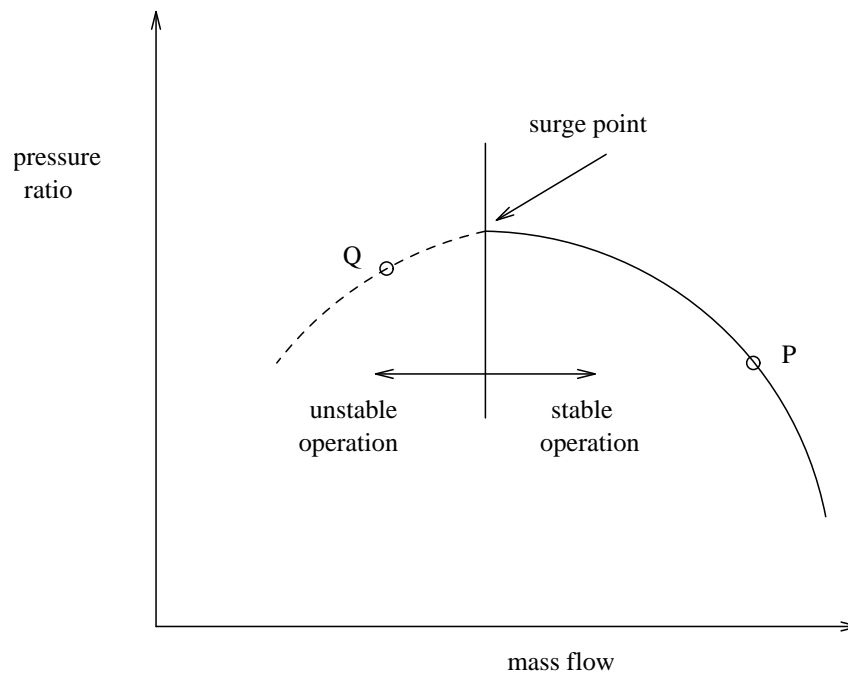


Figure 3.3: Constant speed characteristic of an axial compressor.

The compressor operation is stable only to the right of the maximum pressure ratio. This is because if the flow were to drop slightly while operating at point P, the operating point would move up the curve to a higher pressure ratio; this increased pressure would increase the flow through the outlet valve, thus returning to point P. The dashed part of the curve, on the other hand, represents the unstable region of operation. A slight drop in flow when operating at point Q for example, would result in a slight loss of outlet pressure,

a further loss of flow, greater pressure loss, etc. This is unstable, there being nothing to stop the operating point from accelerating off the bottom of the curve. This happens in practice; when the pressure ratio across the compressor at a certain speed exceeds the maximum for that speed, it is no longer able to hold the pressure head generated and the flow reverses its direction. This is however only a momentary effect. When the back pressure has cleared itself, positive flow is re-established but, if flow conditions do not change, the pressure builds up causing flow reversal again. Thus the flow surges back and forth at high frequency, the phenomenon being referred to as *surge* and the limit of stability called the *surge point*. Surging causes excessive aerodynamic pulsations which are transmitted through the whole machine and must be avoided at all costs. For more details on compressor stability and the phenomenon of surge, refer to [55].

When all the individual, steady-speed characteristics are plotted together, the overall compressor characteristic is obtained as shown in Figure 3.4. The surge points are joined by the *surge line*, and only the stable region of operation is shown. In practice the compressor is made to operate below the surge line, as indicated by its *working line* (Figure 3.4). The separation between the two lines is referred to as the *surge margin*.

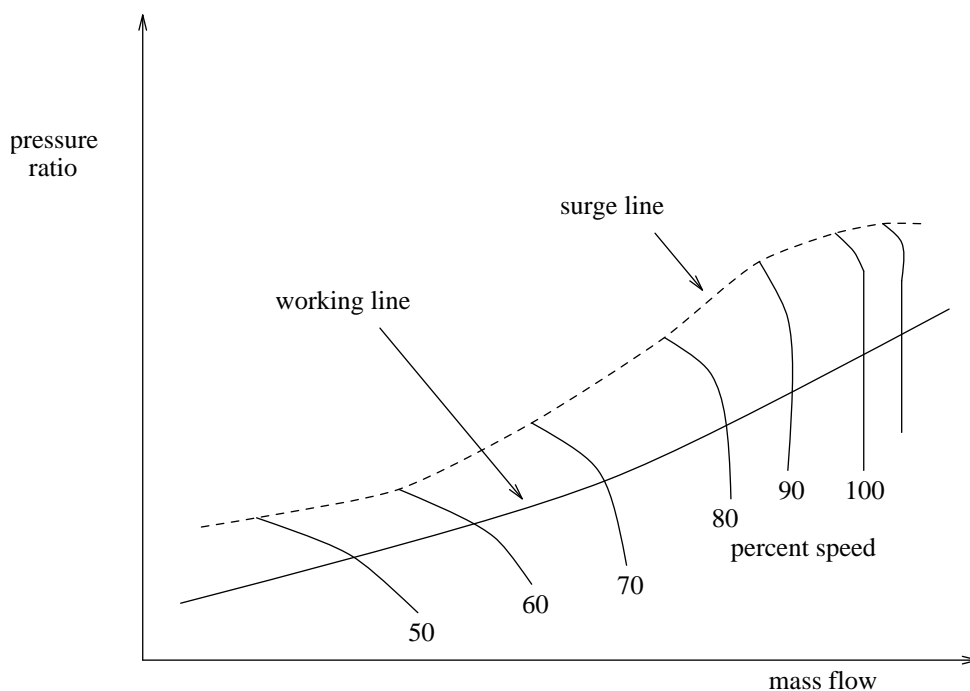


Figure 3.4: Overall compressor characteristic, covering the operational speed range.

The efficiency of the engine and the thrust produced depends on the pressure ratios

generated by the two compressors. For higher performance the compressors should be operated close to their surge lines, i.e., at low surge margins. One of the main objectives of the engine control system is thus not only to avoid surge, but also to ensure that the compressors operate at their specified surge margins at all times. Indeed the regulation of compressor surge margins is one of the most important issues in the field of aero-engine control. In addition to this, compressor rotational speeds need also be limited so that they do not exceed pre-specified maximum values for reasons of mechanical safety and durability.

### 3.1.2 The combustor

The combustor makes possible the reaction of air with fuel at compressor outlet conditions. Its main purpose is to add heat to the compressed flow, and thereby raise its temperature. This is important because the heated compressed flow is capable of doing much more work during expansion than was done initially on its compression. Part of this work is extracted by the turbines which drive the compressors, while the remainder is used to provide thrust. In a combustion chamber, a steady supply of fuel and air mixes and burns as it flows through a flame zone. The flame does not touch its container, being stabilized by the inlet air-flow pattern which also cools the container walls. The combustion process involves very highly developed control of flame stability and can be tuned to emit very low levels of smoke and pollutants.

Gas turbine combustion is a continuous process and usually takes place at a temperature above the melting point of its container [42]. The incoming air is slowed down and a stable flow pattern is generated, to provide adequate residence time for the fuel mixing and chemical processes to take place before the outlet flow is accelerated into the turbine. The combustion chamber is designed so that the process is maintained in a moving stream of air which, although slowed down, still has a velocity in the range of 30–60 m/sec [11]. Another design consideration is the requirement for the process to remain stable over a wide range of air/fuel ratio from full load to idling conditions. Note that full load implies that maximum thrust is being produced whereas idle corresponds to the engine running just at self-sustaining speed, producing very little or no thrust. In addition, the

combustion process must also be stable over a wide range of chamber pressure because this parameter changes with altitude and forward speed.

The main input to the combustion process, the fuel, is one of the control inputs available to the engine control system. By manipulating the fuel flow, the controller can directly vary the amount of combustion taking place and hence, can indirectly vary many other parameters that are important for control purposes and that are influenced by the combustion process.

### 3.1.3 The turbine

The turbine, represented diagrammatically in Figure 3.5, is used to extract energy from a flowing stream of combusted gases, and hence drive the compressor. The loss of energy causes the pressure and temperature of the flow to fall from turbine inlet to outlet, and necessitates the use of an increasing passage area to restrain the flow to a constant velocity.

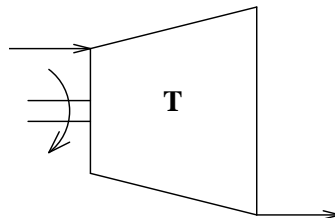


Figure 3.5: Diagrammatic representation of a turbine.

The Spey engine under consideration has two turbines: the HP turbine which is located just after the combustor and drives the HP compressor, and the LP turbine which drives the LP compressor. Apart from extracting energy from the flow, the HP turbine design is also concerned with protecting all components from the heat of the inlet gas. Higher temperature of the inlet gas provides better *specific fuel consumption* (i.e., the fuel consumption per unit net work output). Also, the higher the turbine inlet temperature, the higher the *specific thrust*, defined as the thrust obtained per unit of air flow. Thus it is desirable to have a high turbine inlet temperature for improved system efficiency, but this also poses some serious problems: the life of the turbine is greatly affected by the temperature of the incoming flow. The main influence on maintenance costs and engine life is the condition of the turbine blades which, as indicated above, is dependent on the

turbine inlet temperature. Typically the blade life is halved for every 20°C increase in temperature near its rated operating point [42]. Limiting the turbine temperature to a safe value is therefore of great importance with regards to engine life and durability, and this is one of the main objectives of the aero-engine control system.

#### 3.1.4 The nozzle

The exhaust gases from the LP turbine flow into the nozzle where they are expanded to atmospheric pressure to produce a high velocity jet. The nozzle on the Spey engine has a variable area: hydraulic jacks can be controlled to open or close the nozzle, thus giving a desired outlet flow area. The nozzle area is one of the inputs that would be used by the engine control system.

## 3.2 Design specifications

In this section, design specifications and control objectives for the Spey aero-engine are drawn up based on the information supplied in [98]. In broad terms, the aim is to achieve a range control of engine thrust, from idle to maximum engine speed, whilst regulating compressor stability (surge) margins and minimizing the effects of external disturbances. In addition, the controller is also required to regulate the most significant structural limit of the engine, i.e., the turbine blade temperature, HP compressor spool speed and the LP compressor spool speed must all be limited to safe maximum values under all conditions. The control strategy should take into consideration actuator limits (including minimum and maximum position and slew-rate limits) and engine acceleration and deceleration limits.

In the sequel, the HP compressor's percent spool speed will be denoted by  $N_H$  and the LP compressor's spool speed by  $N_L$ . TBT will denote the turbine blade temperature. The performance requirements are given as follows.

### 3.2.1 Steady-state accuracy

The required steady-state accuracies for the different controlled variables are given below:

NH	:	$\pm 0.1\%$ of design speed.
NL	:	$\pm 0.2\%$ of design speed.
TBT	:	$\pm 2^\circ\text{C}$ .

It should be noted that these values are indicative of the level of accuracy desired from the controller; other variables may be chosen as controlled outputs with similar requirements for steady-state accuracy.

### 3.2.2 Transient accuracy

The maximum allowable closed-loop command response overshoots are as follows:

NH	:	0.5% of design speed.
NL	:	1.0% of design speed.
TBT	:	$10^\circ\text{C}$ .
Engine pressures	:	1.0% of design pressure.

Cross-coupling between controlled outputs is to be minimized so that a change in the demand of one controlled variable should result in little change in the controlled variables whose demands are held stationary.

### 3.2.3 Disturbance rejection

Rejection of disturbances to parameters around which loops are closed should be substantially complete within one second so that the pilot noticing the disturbance would not need to intervene. More specifically, the requirement is that 50% of the maximum amplitude of the response to a discrete disturbance should be removed within 0.5 sec, and 80% of the amplitude removed within 1 sec of the advent of the disturbance.

### 3.2.4 Stability

Stability margins should be such that oscillations in parameters about which loops are closed should be attenuated by at least a factor of four per cycle. Fuel oscillation should be minimized to avoid rapid engine temperature changes (in order to minimize thermal fatigue).

### 3.2.5 Limiter loop exchange

Change over in control loops when limiting different variables should be smooth and should not give rise to oscillations or disturbances.

### 3.2.6 Robustness requirements

Whilst meeting performance requirements, the controller should also exhibit good robustness properties. In the absence of detailed knowledge of uncertainty in the plant, a robustness measure which captures a broad enough class of perturbations should be used. The controller should be robust to the differences between the actual engine dynamics and the linearized models on which the design is based. Also the dynamics of the engine vary not only with the level of thrust it produces, but also with flight conditions as defined by altitude and forward speed. Hence (performance) robustness across the operating envelope is desired in order to eliminate or minimize gain-scheduling requirements.

## 3.3 The aero-engine control problem

Based on the discussion in the preceding sections, the control problem can now be defined in more specific terms. This section lists the variables that need to be controlled and the available measurements and control inputs.

### 3.3.1 Parameters to be controlled/limited and available measurements

For the purpose of this study, the parameters considered for closed-loop control are listed below. Note that the notation used for engine variables is that which is commonly used in the industry, and the numbers refer to different stations in the engine body, e.g., PS6 is the static pressure measurement at the outlet of the HP compressor.

1. Engine thrust. This cannot be measured directly during flight. There are however a number of related measurements which can be used to represent thrust. These include:

- (i) ratio of HP compressor's static outlet pressure to the static pressure at engine inlet (PS6PS1),
- (ii) ratio of HP compressor's total outlet pressure to the total pressure at engine inlet (PT6PT1),
- (iii) LP compressor's non-dimensional<sup>1</sup> percent spool speed (NLPCSL),
- (iv) the engine's overall static pressure ratio (OPRS). This is defined as PS32/PS1, where PS32 and PS1 are the static pressures at the nozzle entry and engine inlet respectively, and
- (v) the engine's overall total pressure ratio (OPRT).

Engine thrust is thus to be controlled indirectly by controlling one of these five measurements; the problem of choosing between them is dealt with in Chapter 4.

2. LP compressor's surge margin. This parameter is also to be controlled indirectly by controlling one of three representative measurements:
  - (i) ratio of LP compressor's static outlet pressure (at the by-pass) to static inlet pressure (PS21PS1),
  - (ii) ratio of LP compressor's total outlet pressure (at the by-pass) to total inlet pressure (PT21PT1), or
  - (iii) LP compressor's mach number measurement at the by-pass exit (DPUP). This is defined in terms of the total and static pressures in the by-pass, PT21 and PS21 respectively, as:  $DPUP=(PT21-PS21)/PS21$ .
3. HP compressor's non-dimensional percent spool speed (NHPCSL).
4. LP compressor's percent spool speed (NL). This has to be limited to a safe value.
5. The total temperature at LP turbine's outlet (TT15). This is limited in order to indirectly limit to a safe value the turbine blade temperature which is very hard to

---

<sup>1</sup>It is usual to work with engine variables in non-dimensional form in order to simplify graphical presentation and understanding of data. Compressor spool speed is expressed in dimensionless form as  $NL/\sqrt{TT1}$ , where TT1 is the total inlet temperature; for details refer to [42].

measure. A temperature (TT15) is thus measured downstream at the LP turbine's outlet which is an indirect measure of the critical blade temperature.

There are thus five outputs which are to be controlled. The next section lists the available control inputs.

### 3.3.2 The control inputs

The control inputs available to the control system are:

- fuel flow,
- variable nozzle area, and
- a variable guide vane angle setting.

The fuel control consists of an engine driven fixed displacement pump, a fuel metering valve whose position is determined by the control computer's output, and a spill valve which controls the pressure drop across the metering valve. The nozzle area control is a hydraulic jack servo controlled from the control computer. The hydraulic fluid is supplied by an independent pump. A similar system controls the guide vanes using the high pressure fuel supply as power source.

### 3.3.3 The multi-mode (switching) strategy

It should be noted that with three inputs one can independently control only three outputs. To control independently the five engine outputs mentioned in §3.3.1 above, three separate controllers will be designed: a primary thrust controller, an NL limiter, and a TT15 limiter. Representing LP compressor's surge margin by LPCSM, the thrust controller will control outputs [thrust,LPCSM,NHPCSL], the NL limiter will control outputs [NL,LPCSM,NHPCSL], while the TT15 limiter will control outputs [TT15,LPCSM, NHPCSL], respectively. These three controllers will then be switched between, depending upon which controlled output is more significant at any given time. The rationale behind this strategy is that it is the large reference demands on the thrust output which cause the

NL and/or TT15 limits to be exceeded. Higher thrust levels require greater fuel flow, and hence higher temperatures and speeds. We shall therefore, set the reference demands for NL and TT15 to their maximum values for the two limiters, and then use a lowest-wins logic to select the controller that demands the lowest fuel. Thus while the thrust controller asks for the least fuel, as will normally be the case, it will be on-line, but when its fuel demand exceeds that of either one of the limiters, the implication is that the particular limit is about to be violated, and hence that limiter will be selected on-line. The limiter will hold the engine constant at the maximum value until the thrust demand is relaxed and the thrust controller resumes control. The controller will thus have three modes of operation, a primary or thrust control mode, an NL limiting mode, and a TT15 limiting mode; the strategy is illustrated in Figure 3.6. Switching schemes like the one proposed here have been considered previously for multi-mode operation, see for example [71].

### 3.3.4 Engine non-linearities

Gas turbine aero-engines by their very nature are highly non-linear in operation. The non-linearity arises mainly from change in the dynamic response of the engine with certain internal and external parameters. The chief internal parameter which affects engine dynamics is the amount of thrust being produced. The dynamics vary considerably as the engine is accelerated from idle to maximum thrust and because of this classical engine controllers need gain-scheduling to meet performance requirements.

The external parameters which influence the dynamic behaviour of the engine are, as mentioned previously, the operating altitude and forward speed. Changes in altitude and speed cause the engine's inlet and outlet conditions (such as pressures, temperatures etc.) to change, thereby affecting its dynamic response.

Other sources of non-linearity include actuator position and slew-rate limits and non-linear thermodynamic effects such as heat soakage.

It should be noted here that the incorporation of the knowledge of these non-linearities into the control design process is not straightforward. The parameters affecting the dynamics do not appear directly in the state-equations. The change in the state-space description of the system as key variables change can however still be modelled as structured uncertainty

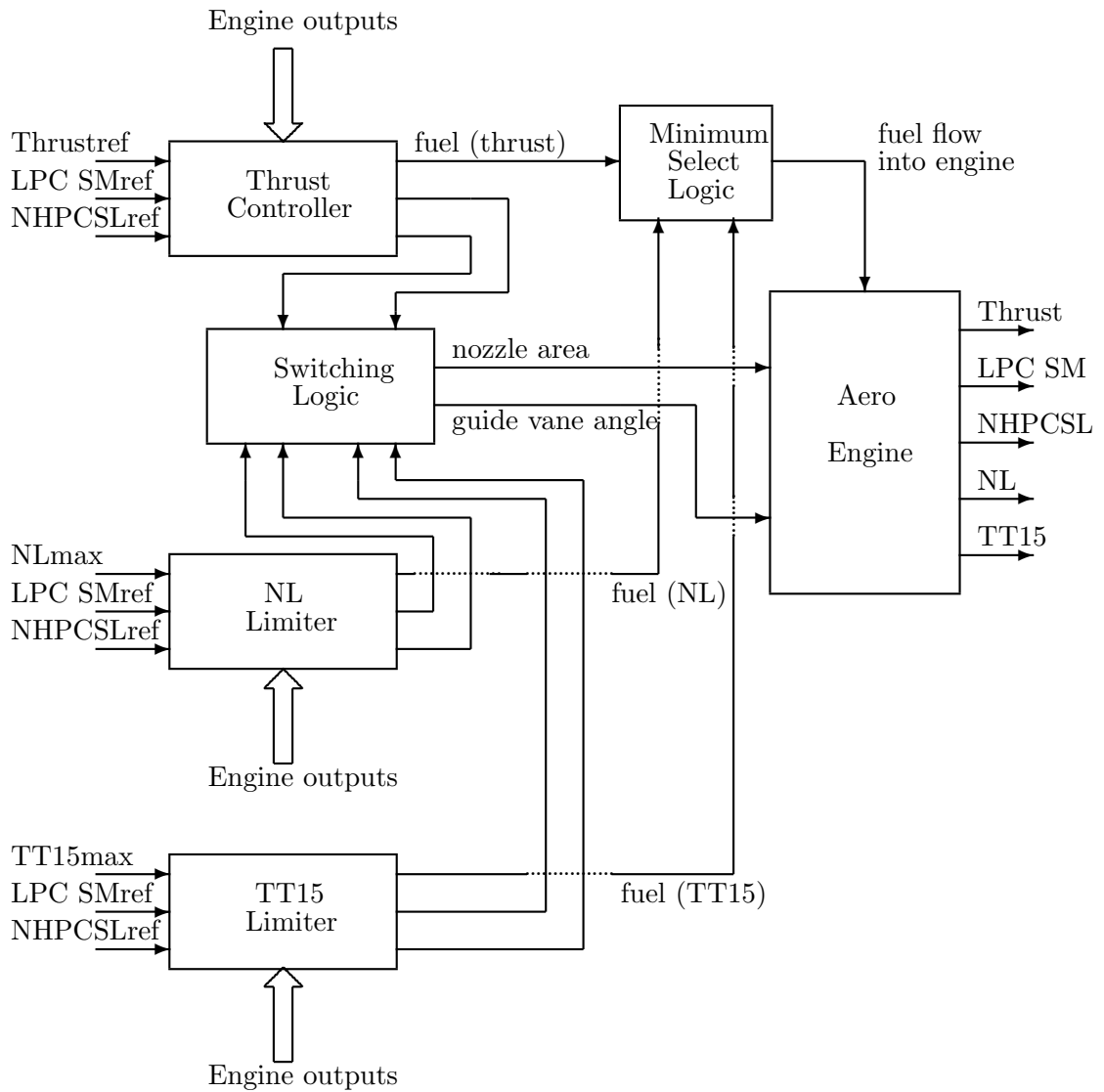


Figure 3.6: Illustration of the switching scheme.

(as discussed in [72]). Once in this form, the state-space uncertainty can be used in structured singular value analysis and also for design with  $D$ - $K$  iteration [16]. In practice however there is a trade-off to be made between how much knowledge is incorporated into the control law, and keeping controller complexity within reasonable limits. For the purpose of this study, the non-linearities as described above are not modelled in the structured uncertainty form. This could nevertheless be a subject for future research.

### 3.4 The aero-engine model

This section describes the linear model development of the aero-engine. Since the controller will be synthesized directly in discrete time, discretization of the model is also discussed.

A detailed non-linear simulation of the gas turbine aero-engine was made available for the purpose of this study. The non-linear engine model has 15 states. This model is used to obtain a continuous time linearization at a particular operating point. The actuators are modelled as simple first order lags. The linearized engine model including the actuators has state dimension 18.

In the actual implementation of the digital control system, the controller drives the plant through a digital-to-analogue converter, which in this case is a simple zero-order hold circuit. The engine model is thus discretized with a zero-order hold on the inputs.

It should be noted that we will discretize the model only after a selection of appropriate outputs has been made (based on the continuous time model) and the continuous time model has been reduced (Chapters 4 & 5). Below we present the discretization formulae.

#### 3.4.1 Discretization: modelling of input delays

There arises in one of the input channels, namely the fuel flow, a pure time delay of more than one sample period. It represents the time elapsed between the injection of liquid fuel into the combustion chamber and its subsequent vaporization and mixing with air before it burns. The effect of this delay has to be included into the engine's linear model. There is no delay associated with the other two actuators. Formulae are therefore derived for discretization of a multi-input multi-output linear model with different time delays in different input channels, assuming a zero-order hold on the inputs. The derivation presented here is an extension of the single-input single-output case discussed by Franklin et al. [27].

Consider a linear state-space model of a system that contains delays  $\lambda_1, \lambda_2, \dots, \lambda_n$  in the

control inputs  $u_1, u_2, \dots, u_n$  respectively:

$$\dot{x} = Fx + G \begin{bmatrix} u_1(t - \lambda_1) \\ u_2(t - \lambda_2) \\ \vdots \\ u_n(t - \lambda_n) \end{bmatrix}, \quad y = Hx, \quad (3.4.1)$$

where  $G \triangleq [G_1 \ G_2 \ \dots \ G_n]$ . The general solution to (3.4.1) is given by:

$$x(t) = e^{F(t-t_0)}x(t_0) + \int_{t_0}^t e^{F(t-\tau)}G \begin{bmatrix} u_1(\tau - \lambda_1) \\ u_2(\tau - \lambda_2) \\ \vdots \\ u_n(\tau - \lambda_n) \end{bmatrix} d\tau. \quad (3.4.2)$$

Letting  $t_0 = kT$  and  $t = kT + T$ , we have:

$$x(kT + T) = e^{FT}x(kT) + \int_{kT}^{kT+T} e^{F(kT+T-\tau)}G \begin{bmatrix} u_1(\tau - \lambda_1) \\ u_2(\tau - \lambda_2) \\ \vdots \\ u_n(\tau - \lambda_n) \end{bmatrix} d\tau. \quad (3.4.3)$$

Substituting  $\eta = kT + T - \tau$  in the integral gives:

$$x(kT + T) = e^{FT}x(kT) + \int_0^T e^{F\eta}G \begin{bmatrix} u_1(kT + T - \eta - \lambda_1) \\ u_2(kT + T - \eta - \lambda_2) \\ \vdots \\ u_n(kT + T - \eta - \lambda_n) \end{bmatrix} d\eta. \quad (3.4.4)$$

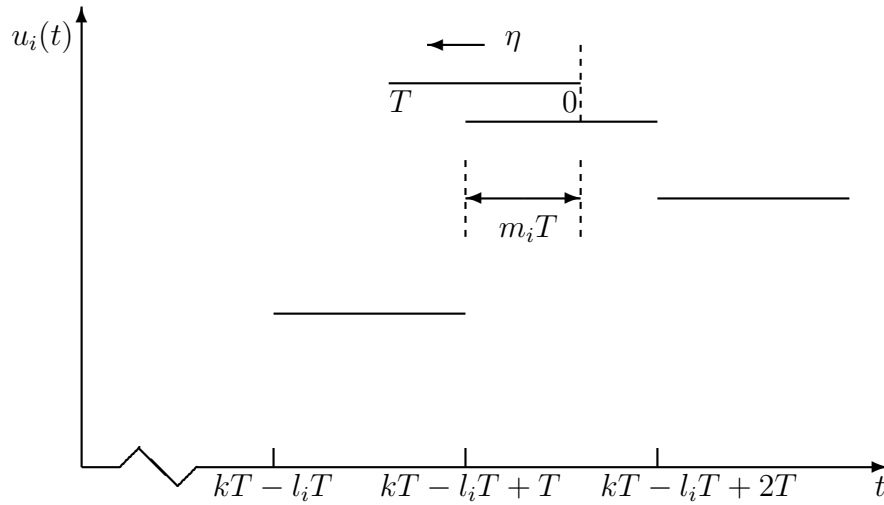
We now separate each delay  $\lambda_i$  into an integral number of sampling periods  $l_i$  and a fraction  $m_i$  of the sample period so that:

$$\lambda_i = l_iT - m_iT, \quad l_i \geq 1, \quad 0 \leq m_i < 1. \quad (3.4.5)$$

With this substitution, the discrete system equation becomes:

$$x(kT + T) = e^{FT}x(kT) + \int_0^T e^{F\eta}G \begin{bmatrix} u_1(kT + T - \eta - l_1T + m_1T) \\ u_2(kT + T - \eta - l_2T + m_2T) \\ \vdots \\ u_n(kT + T - \eta - l_nT + m_nT) \end{bmatrix} d\eta. \quad (3.4.6)$$

Shown in Figure 3.7 is a sketch of the  $i$ th input near time  $t = kT - l_iT$ . Note that the input is piecewise constant because it is being driven by a zero-order hold circuit. It is

Figure 3.7: Sketch of the  $i$  th input with delay  $l_i T - m_i T$ .

seen that as  $\eta$  varies from 0 to  $T$ , time  $t$  runs backwards from  $kT - l_i T + T + m_i T$  to  $kT - l_i T + m_i T$ . We can therefore, for each input  $u_i$ , break the integral into two parts, one where  $u_i$  takes the value  $u_i(kT - l_i T + T)$ , and the other where it has the value  $u_i(kT - l_i T)$ . The integral can now be written as:

$$\begin{aligned}
 x(kT + T) &= e^{FT} x(kT) + \int_0^{m_1 T} e^{F\eta} G_1 u_1(kT - l_1 T + T) d\eta + \int_{m_1 T}^T e^{F\eta} G_1 u_1(kT - l_1 T) d\eta + \\
 &\quad \cdots + \int_0^{m_n T} e^{F\eta} G_n u_n(kT - l_n T + T) d\eta + \int_{m_n T}^T e^{F\eta} G_n u_n(kT - l_n T) d\eta \\
 &= e^{FT} x(kT) + \int_0^{m_1 T} e^{F\eta} d\eta G_1 u_1(kT - l_1 T + T) + \int_{m_1 T}^T e^{F\eta} d\eta G_1 u_1(kT - l_1 T) + \\
 &\quad \cdots + \int_0^{m_n T} e^{F\eta} d\eta G_n u_n(kT - l_n T + T) + \int_{m_n T}^T e^{F\eta} d\eta G_n u_n(kT - l_n T) \\
 &= \Phi x(kT) + \Gamma_1 \begin{bmatrix} u_1(kT - l_1 T) \\ \vdots \\ u_n(kT - l_n T) \end{bmatrix} + \Gamma_2 \begin{bmatrix} u_1(kT - l_1 T + T) \\ \vdots \\ u_n(kT - l_n T + T) \end{bmatrix}, \tag{3.4.7}
 \end{aligned}$$

where

$$\Phi \triangleq e^{FT}, \tag{3.4.8}$$

$$\Gamma_1 \triangleq \left[ \int_{m_1 T}^T e^{F\eta} d\eta G_1 \quad \cdots \quad \int_{m_n T}^T e^{F\eta} d\eta G_n \right] \triangleq [\Gamma_{11} \quad \cdots \quad \Gamma_{1n}], \tag{3.4.9}$$

$$\Gamma_2 \triangleq \left[ \int_0^{m_1 T} e^{F\eta} d\eta G_1 \quad \cdots \quad \int_0^{m_n T} e^{F\eta} d\eta G_n \right] \triangleq [\Gamma_{21} \quad \cdots \quad \Gamma_{2n}]. \tag{3.4.10}$$

For notational convenience we henceforth drop the explicit mention of the sample period

$T$  from the state equation. We now have:

$$x(k+1) = \Phi x(k) + \Gamma_1 \begin{bmatrix} u_1(k-l_1) \\ \vdots \\ u_n(k-l_n) \end{bmatrix} + \Gamma_2 \begin{bmatrix} u_1(k-l_1+1) \\ \vdots \\ u_n(k-l_n+1) \end{bmatrix}. \quad (3.4.11)$$

In order to put this equation in state-space form, we have to eliminate all the past controls up to  $u_i(k)$ . To do this we introduce new state variables defined as  $x_{n+1}(k) \triangleq u_1(k-l_1)$ ,  $x_{n+2}(k) \triangleq u_1(k-l_1+1)$ ,  $\dots$ ,  $x_{n+l_1}(k) \triangleq u_1(k-1)$ ,  $\dots$ ,  $x_{n+l_1+\dots+l_{n-1}+1}(k) \triangleq u_n(k-l_n)$ ,  $x_{n+l_1+\dots+l_{n-1}+2}(k) \triangleq u_n(k-l_n+1)$ ,  $\dots$ ,  $x_{n+l_1+\dots+l_n}(k) \triangleq u_n(k-1)$ . We thus have an increased state dimension, and the equations are:

$$\begin{bmatrix} x(k+1) \\ x_{n+1}(k+1) \\ \vdots \\ x_{n+l_1-1}(k+1) \\ x_{n+l_1}(k+1) \\ \vdots \\ x_{n+l_1+\dots+l_{n-1}+1}(k+1) \\ \vdots \\ x_{n+l_1+\dots+l_{n-1}}(k+1) \\ x_{n+l_1+\dots+l_n}(k+1) \end{bmatrix} = \begin{bmatrix} \Phi & \Gamma_{11} & \Gamma_{21} & 0 & \cdots & 0 & \Gamma_{12} & \Gamma_{22} & 0 & \cdots & \Gamma_{1n} & \Gamma_{2n} & 0 & \cdots & 0 \\ 0 & 0 & 1 & 0 & \cdots & 0 & 0 & 0 & 0 & \cdots & 0 & 0 & 0 & \cdots & 0 \\ \vdots & & & & & & & & & & & & & & & \\ 0 & 0 & 0 & 0 & \cdots & 1 & 0 & 0 & 0 & \cdots & 0 & 0 & 0 & \cdots & 0 \\ 0 & 0 & 0 & 0 & \cdots & 0 & 0 & 0 & 0 & \cdots & 0 & 0 & 0 & \cdots & 0 \\ \vdots & & & & & & & & & & & & & & & \\ 0 & 0 & 0 & 0 & \cdots & 0 & 0 & 0 & 0 & \cdots & 0 & 1 & 0 & \cdots & 0 \\ \vdots & & & & & & & & & & & & & & & \\ 0 & 0 & 0 & 0 & \cdots & 0 & 0 & 0 & 0 & \cdots & 0 & 0 & 0 & \cdots & 1 \\ 0 & 0 & 0 & 0 & \cdots & 0 & 0 & 0 & 0 & \cdots & 0 & 0 & 0 & \cdots & 0 \end{bmatrix} \begin{bmatrix} x(k) \\ x_{n+1}(k) \\ x_{n+2}(k) \\ x_{n+3}(k) \\ \vdots \\ x_{n+l_1}(k) \\ x_{n+l_1+1}(k) \\ x_{n+l_1+2}(k) \\ x_{n+l_1+3}(k) \\ \vdots \\ x_{n+l_1+\dots+l_{n-1}+1}(k) \\ x_{n+l_1+\dots+l_{n-1}+2}(k) \\ x_{n+l_1+\dots+l_{n-1}+3}(k) \\ \vdots \\ x_{n+l_1+\dots+l_n}(k) \end{bmatrix} + \begin{bmatrix} 0 & 0 & \cdots & 0 \\ 0 & 0 & \cdots & 0 \\ \vdots & & & \\ 0 & 0 & \cdots & 0 \\ 1 & 0 & \cdots & 0 \\ \vdots & & & \\ 0 & 0 & \cdots & 0 \\ \vdots & & & \\ 0 & 0 & \cdots & 0 \\ 0 & 0 & \cdots & 1 \end{bmatrix} \begin{bmatrix} u_1(k) \\ u_2(k) \\ \vdots \\ u_n(k) \end{bmatrix}, \quad (3.4.12)$$

and

$$y = [H \quad 0 \quad \cdots \quad 0] \begin{bmatrix} x(k) \\ x_{n+1}(k) \\ \vdots \\ x_{n+l_1+\cdots+l_n}(k) \end{bmatrix}. \quad (3.4.13)$$

It should be noted that if a particular delay  $\lambda_i$  is less than one sample period so that  $l_i = 1$ , then the first row of the matrix coupling the inputs to the states will not all be zero, but will contain a term  $\Gamma_{2i}$  to go with the input  $u_i(k)$ .

For our particular application,  $n = 3$  (since the aero-engine has three inputs), and  $\lambda_2 = \lambda_3 = 0 \Rightarrow l_2 = l_3 = m_2 = m_3 = 0$  (since there are no delays in the second and third input channels). The first channel has a delay slightly greater than one sample period and therefore,  $l_1 = 2$ . The discrete state equation is:

$$x(k+1) = \Phi x(k) + [\Gamma_{11} \quad \Gamma_{12} \quad \Gamma_{13}] \begin{bmatrix} u_1(k-2) \\ u_2(k) \\ u_3(k) \end{bmatrix} + [\Gamma_{21} \quad \Gamma_{22} \quad \Gamma_{23}] \begin{bmatrix} u_1(k-1) \\ u_2(k+1) \\ u_3(k+1) \end{bmatrix}, \quad (3.4.14)$$

where

$$\begin{aligned} [\Gamma_{11} \quad \Gamma_{12} \quad \Gamma_{13}] &= [\int_{m_1 T}^T e^{F\eta} d\eta G_1 \quad \int_0^T e^{F\eta} d\eta G_2 \quad \int_0^T e^{F\eta} d\eta G_3], \\ [\Gamma_{21} \quad \Gamma_{22} \quad \Gamma_{23}] &= [\int_0^{m_1 T} e^{F\eta} d\eta G_1 \quad \int_0^0 e^{F\eta} d\eta G_2 \quad \int_0^0 e^{F\eta} d\eta G_3]. \end{aligned} \quad (3.4.15)$$

It is clear from (3.4.15) that  $\Gamma_{22} = \Gamma_{23} = 0$ , and hence the state equation simplifies to:

$$x(k+1) = \Phi x(k) + [0 \quad \Gamma_{12} \quad \Gamma_{13}] \begin{bmatrix} u_1(k) \\ u_2(k) \\ u_3(k) \end{bmatrix} + \Gamma_{11} u_1(k-2) + \Gamma_{21} u_1(k-1). \quad (3.4.16)$$

Defining new state variables  $x_{n+1}(k) \triangleq u_1(k-2)$ ,  $x_{n+2}(k) \triangleq u_1(k-1)$ , the equations can be put in standard state-space form as:

$$\begin{aligned} \begin{bmatrix} x(k+1) \\ x_{n+1}(k+1) \\ x_{n+2}(k+1) \end{bmatrix} &= \begin{bmatrix} \Phi & \Gamma_{11} & \Gamma_{21} \\ 0 & 0 & 1 \\ 0 & 0 & 0 \end{bmatrix} \begin{bmatrix} x(k) \\ x_{n+1}(k) \\ x_{n+2}(k) \end{bmatrix} + \begin{bmatrix} 0 & \Gamma_{12} & \Gamma_{13} \\ 0 & 0 & 0 \\ 1 & 0 & 0 \end{bmatrix} \begin{bmatrix} u_1(k) \\ u_2(k) \\ u_3(k) \end{bmatrix}, \\ y &= [H \quad 0 \quad 0] \begin{bmatrix} x(k) \\ x_{n+1}(k) \\ x_{n+2}(k) \end{bmatrix}. \end{aligned}$$

To evaluate the integrals in (3.4.15), we first convert  $\Gamma_{11}$  to a form similar to that of the other integrals by setting  $\sigma = \eta - m_1 T$  to get:

$$\Gamma_{11} = e^{Fm_1 T} \int_0^{T-m_1 T} e^{F\sigma} d\sigma G_1. \quad (3.4.17)$$

To compute these integrals, we will use the following two identities which are valid for any positive non-zero scalar number  $a$  [27]:

$$e^{Fa} = \sum_{k=0}^{\infty} \frac{F^k a^k}{k!}, \quad \frac{1}{a} \int_0^a e^{F\sigma} d\sigma = \sum_{k=0}^{\infty} \frac{F^k a^k}{(k+1)!}. \quad (3.4.18)$$

We now define the matrix exponentials:

$$\begin{aligned} S_1 &\triangleq \exp \left( \begin{bmatrix} Fm_1 T & G_1 m_1 T \\ 0 & 0 \end{bmatrix} \right), \quad S_2 \triangleq \exp \left( \begin{bmatrix} F(T - m_1 T) & G_1(T - m_1 T) \\ 0 & 0 \end{bmatrix} \right), \\ S_3 &\triangleq \exp \left( \begin{bmatrix} FT & G_2 T \\ 0 & 0 \end{bmatrix} \right), \quad S_4 \triangleq \exp \left( \begin{bmatrix} FT & G_3 T \\ 0 & 0 \end{bmatrix} \right). \end{aligned}$$

$\Phi$  can now be computed by multiplying the (1,1) block of  $S_1$  on the right-hand side by the (1,1) block of  $S_2$ , i.e.,  $\Phi = e^{Fm_1 T} e^{FT - Fm_1 T}$ . The (1,2) block of  $S_2$  is:

$$\begin{aligned} S_2(1,2) &= G_1(T - m_1 T) + \frac{1}{2!} F(T - m_1 T) G_1(T - m_1 T) \\ &\quad + \frac{1}{3!} F^2(T - m_1 T)^2 G_1(T - m_1 T) + \dots \\ &= \left[ I + \frac{1}{2!} F(T - m_1 T) + \frac{1}{3!} F^2(T - m_1 T)^2 + \dots \right] G_1(T - m_1 T) \\ &= \frac{1}{T - m_1 T} \int_0^{T-m_1 T} e^{F\sigma} d\sigma G_1(T - m_1 T) = \int_0^{T-m_1 T} e^{F\sigma} d\sigma G_1, \end{aligned}$$

where we have made use of the identities given in (3.4.18).  $\Gamma_{11}$  is now simply obtained by left-multiplying the (1,2) block of  $S_2$  with the (1,1) block of  $S_1$ . To compute  $\Gamma_{21}$ , we expand the (1,2) block of  $S_1$ , using the identities in (3.4.18), to get:

$$\begin{aligned} S_1(1,2) &= G_1 m_1 T + \frac{1}{2!} F m_1 T G_1 m_1 T + \frac{1}{3!} (F m_1 T)^2 G_1 m_1 T + \dots \\ &= \left[ I + \frac{1}{2!} F m_1 T + \frac{1}{3!} (F m_1 T)^2 + \dots \right] G_1 m_1 T \\ &= \frac{1}{m_1 T} \int_0^{m_1 T} e^{F\sigma} d\sigma G_1 m_1 T = \int_0^{m_1 T} e^{F\sigma} d\sigma G_1. \end{aligned}$$

$\Gamma_{21}$  is thus equal to the (1,2) block of  $S_1$ . Similarly we can compute  $\Gamma_{12}$  and  $\Gamma_{13}$  from the (1,2) blocks of  $S_3$  and  $S_4$  respectively.

The discrete engine model incorporating the fuel flow input delay is thus given by  $\hat{G}(z) \triangleq \hat{C}(zI - \hat{A})^{-1}\hat{B}$ , where

$$\hat{A} \triangleq \begin{bmatrix} \Phi & \Gamma_{11} & \Gamma_{21} \\ 0 & 0 & 1 \\ 0 & 0 & 0 \end{bmatrix}, \quad \hat{B} \triangleq \begin{bmatrix} 0 & \Gamma_{12} & \Gamma_{13} \\ 0 & 0 & 0 \\ 1 & 0 & 0 \end{bmatrix}, \quad \hat{C} \triangleq [H \quad 0 \quad 0].$$

### 3.4.2 Modelling of output delays

The discrete time implementation causes a delay of one sample period in the measurements available to the controller, i.e., to generate the control at the  $k$  th sample, the controller has access only to the measurements up to and including the  $k - 1$  th sample. This output delay is modelled by pre-multiplying the discrete engine transfer function  $\hat{G}(z)$  by  $z^{-1}I$ , where the dimension of the identity matrix  $I$  is equal to the number of engine outputs. We call the final transfer function  $G(z)$ .

## 3.5 Summary

In this chapter the principle of operation of gas turbine aero-engines and the working of individual components have been briefly discussed. The main objectives of the aero-engine control system were described. Specifications for feedback control design were presented. The parameters required to be controlled or limited, and the available measurements and control inputs were listed. The chief sources of non-linearity in the engine were discussed. Linear model development of the aero-engine was described. Formulae for discretizing multivariable state-space models with different time delays in different input channels were derived. The derivation assumed a zero-order hold on the plant inputs.

## Chapter 4

### Control structure design

#### 4.1 Introduction

An important part of multivariable design is the choice of manipulated and controlled variables (plant inputs and outputs). For many systems, a number of measurements are available for use, and a particular closed-loop specification can be defined in terms of the control of several of these measured variables. However, one can independently control only as many outputs as there are inputs. In the case of the aero-engine, for example, thrust may be represented by the fan spool speed, the engine pressure ratio, or some other appropriate variable. Thus, for thrust regulation, we have the option of choosing from a range of variables, the one we want to control.

Once the choice of output variables has been made, it is frequently necessary to choose appropriate pairs of inputs and outputs. This is of prime importance in decentralized control, but can also produce easier and simpler designs for centralized controllers.

The task of choosing inputs and outputs and deciding on how to pair them is referred to as *control structure design*. A good physical understanding of the plant must be combined with the available analytical tools for an effective structure design.

The purpose of this chapter is to develop a systematic methodology to tackle the structure design problem and apply it to the aero-engine example. As discussed in the previous chapter, engine thrust can be controlled by controlling one of five representative measurements. Similarly LP compressor's surge margin can be represented by any one of three candidate measurements. In this chapter we will address the problem of choosing from

the range of available measurements the ones that are most suitable for control of thrust and the LP compressor's surge margin. In other words, we will perform structure design for the thrust controller, which is to be designed to control thrust, LP compressor's surge margin and NHPCSL (as discussed in §3.3.3). A 15-state continuous time linear model of the engine, derived from the non-linear simulation at 87% of maximum thrust, will be used in the analysis that follows. The 87% thrust point was chosen since it represents the usual operating conditions of the engine. It should be noted that the aero-engine is an asymptotically stable system.

§4.2 describes the importance of plant scaling in control system analysis and design. §4.3 discusses the relevance of physical understanding of the system and practical considerations when choosing outputs for feedback. The importance of right half-plane zeros with regards to structure selection is discussed in §4.4. The relative gain array and the condition number and their roles in structure design are described in §4.5 and §4.6 respectively. §4.7 introduces the use of Hankel singular values in choosing between outputs. The problem of input output pairing is then briefly reviewed and finally §4.9 sums up the main points of the chapter.

## 4.2 Input output scaling

Some of the tools we will be using for structure selection are dependent on the scalings employed. Scaling the inputs and the candidate measurements therefore, is vital before comparisons are made. Scaling also improves the conditioning of the problem, and enables meaningful analysis to be made of the robustness properties of the closed-loop system in the frequency domain. The outputs should be scaled such that equal magnitudes of cross-coupling into each of the outputs are equally undesirable. We have chosen to scale the thrust-related outputs such that one unit of each scaled measurement represents 10% of maximum thrust. A step demand on each of these scaled outputs would thus correspond to a demand of 10% (of maximum) in thrust. The surge margin-related outputs are scaled so that one unit corresponds to 5% surge margin. If the controller designed provides an interaction of less than 10% between the scaled outputs (for unit reference steps), then we would have a 1% or less change in thrust for a step demand of 5% in surge margin,

and a 0.5% or less change in surge margin for a 10% step demand in thrust. The inputs are scaled by 10% of their expected ranges of operation.

### 4.3 Practical considerations

A good physical understanding of the behaviour of the plant is vital for control structure design. This can also simplify the structure design problem. Some candidate outputs may be preferred over others on practical grounds or because of reasons associated with the behaviour of the plant; these engineering considerations should be considered before any analytical tools are employed. Some of the candidate measurements can thus be screened beforehand.

Regarding the aero-engine example, it is known that the static and total pressure ratios behave similarly, and that static pressures are easier to measure than total pressures. Thus it is desirable to choose outputs involving static pressures over those involving total pressures; we therefore drop the total pressure ratio measurements in favour of static pressure ratios.

### 4.4 Right half-plane zeros

Right half-plane (RHP) zeros limit the achievable performance of a feedback loop (both in the SISO and the multivariable cases) by limiting the open-loop gain-bandwidth product. They can be a cause of concern, particularly, if they lie within the closed-loop bandwidth one is aiming for. Choosing different outputs for feedback control can give rise to different numbers of RHP zeros at differing locations. The choice of outputs should be such that a minimum number of RHP zeros are encountered, and these should be as far removed from the imaginary axis as possible.

We can now form sets of outputs (Table 4.1) and analyze their non-minimum phase characteristics. The closed-loop bandwidth requirement for the aero-engine is approximately 10 rad/sec. RHP zeros close to this value or slower, will therefore, cause problems and should be avoided. Table 4.1 shows the RHP zeros slower than 100 rad/sec for all combinations of prospective output variables for the thrust controller. It should be noted that

Set No.	Contents	RHP zeros < 100 rad/sec
1	PS6PS1, PS21PS1, NHPCSL	none
2	NLPCSL, PS21PS1, NHPCSL	none
3	OPRS, PS21PS1, NHPCSL	20.661
4	PS6PS1, DPUP, NHPCSL	none
5	NLPCSL, DPUP, NHPCSL	none
6	OPRS, DPUP, NHPCSL	19.694

Table 4.1: RHP zeros for different sets of outputs for the thrust controller.

measurements involving total pressures have been excluded as discussed in §4.3 above. It is seen from the table that the variable OPRS introduces (relatively) slow RHP zeros. It was observed that these zeros move closer to the origin at higher thrust levels. Thus sets 3 and 6 are dropped as being unfavourable for closed-loop control.

## 4.5 The relative-gain array

The relative-gain array (RGA) has been available for over twenty years and has been widely used for control structure design, specially in the process industry. However, no theoretical explanation of its utility was available until recently, and most of the knowledge was empirical and based on practical experience. A number of results are now available which attempt to provide theoretical justification for the use of the RGA. The RGA is defined as follows.

Suppose that the transfer function from the  $j$ th input to the  $i$ th output of a square plant  $G$  is  $g_{ij}$  when all loops are open, and  $h_{ij}$  when all outputs except the  $i$ th output are tightly controlled. Then the (i,j) element of the RGA  $\Gamma$  is defined as:

$$\gamma_{ij} \triangleq \frac{g_{ij}}{h_{ij}}. \quad (4.5.1)$$

It can be shown that  $h_{ij} = 1/\hat{g}_{ji}$ , where  $\hat{g}_{ji}$  is the (j,i) element of  $\hat{G} \triangleq G^{-1}$  [62]. Thus (4.5.1) becomes:

$$\gamma_{ij} = g_{ij}\hat{g}_{ji}, \quad (4.5.2)$$

and in terms of matrix operations the RGA is written as:

$$\Gamma(G(s)) = G(s) .* \hat{G}^T(s), \quad (4.5.3)$$

where ‘.\*’ denotes element-by-element multiplication (the Schur or Hadamard product). Some interesting properties of the RGA are as follows:

- The RGA is independent of input and output scaling,
- All row and column sums equal one, i.e.,  $\sum_i \gamma_{ij} = \sum_j \gamma_{ij} = 1$ ,
- Any permutation of rows or columns in  $G$  results in the same permutation in  $\Gamma(G)$ , and
- If  $G(s)$  is triangular (and hence also if it is diagonal), then  $\Gamma(G) = I$ .

Hovd & Skogestad [44] show that if  $\Gamma(G) = I \forall \omega$  then stability of the individual loops implies stability of the entire system. Triangular plants yield  $\Gamma = I$ , and plants where  $\Gamma$  is different from  $I$  are termed as interactive [112]. Hoskin et al. [43] show that large off-diagonal elements in the RGA cause greater cross-feed performance degradation. Furthermore it has been known that choosing variables which result in large or negative elements in the RGA leads to difficulties in controlling the plant, and that plant inputs and outputs should be paired so that the diagonal elements of the RGA are as close as possible to unity. It can be shown that [62]:

$$\frac{\partial \hat{g}_{ji}}{\hat{g}_{ji}} = -\gamma_{ij} \frac{\partial g_{ij}}{g_{ij}}. \quad (4.5.4)$$

This implies that a change in  $g_{ij}$  will result in a much larger relative change in  $\hat{g}_{ji}$ , if  $|\gamma_{ij}| \gg 1$ . Thus large entries in the RGA indicate a plant which is poorly conditioned with respect to inversion. An inverse-based controller for such a plant would be very sensitive to changes in the behaviour of the plant. The closed-loop system in such a case is therefore likely to exhibit poor levels of robustness.

It is also known that large elements in the RGA indicate sensitivity to diagonal multiplicative input uncertainty, i.e., if the plant transfer function is  $G_\Delta = G(I + \Delta_I)$ , where  $G$  is the nominal model, and  $\Delta_I = \text{diag}\{\Delta_i\}$ . Such perturbations are always present to some extent because of uncertainty about the exact behaviour of control actuators. If  $K$

is the controller, then the loop-gain matrix  $G_{\Delta}K$  which is closely related to performance, can be written in terms of the nominal  $GK$  as:

$$G_{\Delta}K = GK(I + K^{-1}\Delta_I K) \quad (4.5.5)$$

$$= (I + G\Delta_I G^{-1})GK. \quad (4.5.6)$$

For SISO plants, a relative input uncertainty of magnitude  $\Delta$  will result in the same relative change in  $G_{\Delta}K = GK(I + \Delta)$ . For multivariable plants however, the effect of input uncertainty on the loop-gain may be amplified as shown below. For a plant with two inputs and two outputs, the error term in (4.5.6) can be expressed in terms of the RGA of the plant as [95]:

$$G\Delta_I G^{-1} = \begin{bmatrix} \gamma_{11}\Delta_1 + \gamma_{12}\Delta_2 & -\gamma_{11}\frac{g_{12}}{g_{22}}(\Delta_1 - \Delta_2) \\ \gamma_{11}\frac{g_{21}}{g_{11}}(\Delta_1 - \Delta_2) & \gamma_{21}\Delta_1 + \gamma_{22}\Delta_2 \end{bmatrix}. \quad (4.5.7)$$

For  $n \times n$  plants, the diagonal elements of  $G\Delta_I G^{-1}$  can be written as:

$$[G\Delta_I G^{-1}]_{ii} = \sum_{j=1}^n \gamma_{ij}(G)\Delta_j, \quad (4.5.8)$$

where  $\gamma_{ij}(G)$  is the (i,j) element of the RGA of the nominal model  $G$ . Similarly we have [95]:

$$[K^{-1}\Delta_I K]_{ii} = \sum_{j=1}^n \gamma_{ji}(K)\Delta_j, \quad (4.5.9)$$

where  $\gamma_{ji}(K)$  is the (j,i) element of the RGA of the controller  $K$ . If the nominal plant and the controller *both* have large RGAs, then it follows from (4.5.8) and (4.5.9) above that the error terms  $G\Delta_I G^{-1}$  and  $K^{-1}\Delta_I K$  will be large, and hence the loop-gain  $G_{\Delta}K$  will be significantly different from its nominal value  $GK$ . Thus, we can say that if the RGAs of both the plant and the controller have large elements, then the closed-loop system will have little stability robustness in the face of diagonal multiplicative input uncertainty. Hence for plants with large RGAs, controllers having small RGAs should be used. Such controllers are however, unlikely to give good performance and will not be able to remove interactions in the plant. Large elements in the plant's RGA have also been shown to cause problems in the presence of individual element uncertainty in the plant's transfer function matrix. Hovd & Skogestad [44] show that if the relative uncertainty in an element  $g_{ij}$  of  $G$  at a given frequency is larger than  $|1/\gamma_{ij}(j\omega)|$ , then the plant may have  $j\omega$ -axis and RHP zeros at this frequency.

We therefore conclude that plants with large RGAs are inherently difficult to control, and should be avoided, if possible. We now define a measure of the size of the RGA, which also takes into account interaction in the plant. The RGA number (rnum) defined below is a measure of the deviation of the RGA from the identity matrix:

$$\text{rnum} = \sum_{i=j} |1 - \gamma_{ij}| + \sum_{i \neq j} |\gamma_{ij}|. \quad (4.5.10)$$

The lower the RGA number, the more preferred would be the control structure. Before calculating the RGA number, the output variables should be arranged so that the steady-state RGA matrix is as close as possible to the identity matrix. The RGA numbers for sets 1 and 4 are shown in Figure 4.1. It is clear that set 4 is a preferred choice over set 1. This indicates that the measurement DPUP should be preferred over PS21PS1. Comparing the RGA numbers for sets 2 and 5 gave the same conclusion. The RGA number thus indicates that the sets 1 and 2 should be dropped in favour of sets 4 and 5.

We are now left with sets 4 and 5; their RGA numbers are shown in Figure 4.2, and are seen to be very similar for the two sets. The RGA number in this case therefore, does not yield decisive information.

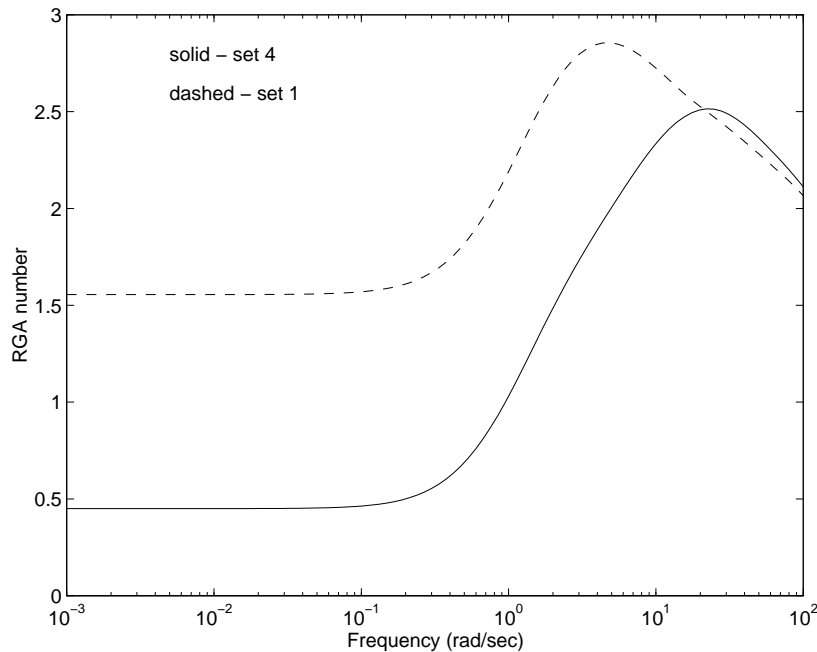


Figure 4.1: RGA numbers for sets 1 and 4.

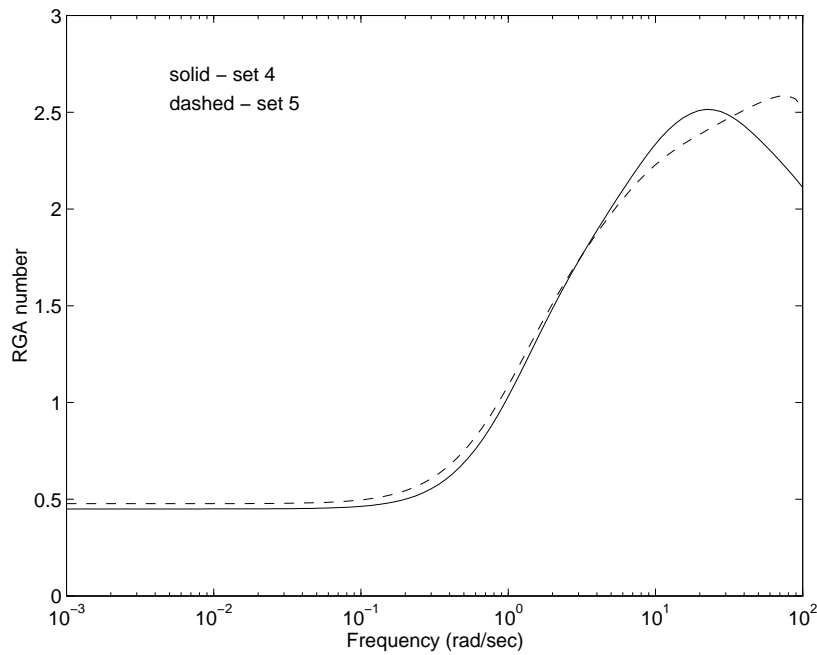


Figure 4.2: RGA numbers for sets 4 and 5.

## 4.6 The condition number

The condition number  $\kappa(G)$  of a plant  $G(s)$  is defined as:

$$\kappa(G(j\omega)) \triangleq \frac{\bar{\sigma}(G(j\omega))}{\underline{\sigma}(G(j\omega))}, \quad (4.6.1)$$

where  $\bar{\sigma}(G)$  and  $\underline{\sigma}(G)$  denote the maximum and minimum singular values of the plant. Ill-conditioned plants are those which have a high condition number, and it is known that such plants can cause control problems [96].

Ill-conditioned plants are characterized by strong directionality because inputs in directions of large plant gains are strongly amplified, while inputs in directions of low plant gains are not. For tight control of such plants, the controller would have to compensate for the directionality of the plant by applying large inputs in the directions corresponding to low gains, i.e., it would have to have a directionality similar to  $G^{-1}$ . However, due to uncertainty in the plant model, the direction of the large input may not match the direction of low plant gain, and the amplification of the large inputs could be much larger than that expected from the model. This could result in large values of the plant output, leading to poor performance or even instability [96].

Morari & Zafiriou [68] have derived sufficient conditions for robust performance in the

presence of unstructured multiplicative uncertainty at the plant input. The perturbed plant is written as:

$$G_{\Delta} = G(I + l_I \Delta_I), \quad (4.6.2)$$

where  $l_I(j\omega)$  is a scalar weight on the normalized perturbation  $\Delta_I$  so that  $\bar{\sigma}(\Delta_I) \leq 1$ . Performance is defined in terms of the sensitivity operator  $S$ , the requirement being  $\bar{\sigma}(S_{\Delta}w) < 1$ , where  $S_{\Delta}$  is the sensitivity function for  $G_{\Delta}$  and  $w(j\omega)$  is the performance weight. Sufficient conditions for robust performance are [68]:

$$\bar{\sigma}(wS) + \kappa(G)\bar{\sigma}(l_I T) < 1 \quad \text{or} \quad (4.6.3)$$

$$\bar{\sigma}(wS) + \kappa(K)\bar{\sigma}(l_I T) < 1. \quad (4.6.4)$$

Here  $\kappa(G)$  and  $\kappa(K)$  denote the plant and controller condition numbers, and  $S$  and  $T$  are the nominal sensitivity and complementary sensitivity functions respectively. We note from (4.6.3) and (4.6.4) that even when robust stability and nominal performance are satisfied with a reasonable margin ( $\bar{\sigma}(l_I T) < 1$  and  $\bar{\sigma}(wS) < 1$ ), the robust performance conditions can be violated by an arbitrarily large amount if *both* the plant  $G$  and the controller  $K$  are ill-conditioned. Thus for ill-conditioned plants, decoupling should be avoided as it can lead to poor robust performance; such plants are thus inherently difficult to control.

It should be noted that for sensitivity to diagonal multiplicative input uncertainty, we found in §4.5, that both the plant and the controller must have large RGA elements. In this section we observe that for unstructured uncertainty to cause poor robust performance, both the plant and controller have to be ill-conditioned. Thus the condition number plays a similar role for unstructured input uncertainty as the RGA does for diagonal input uncertainty [68]; several quantitative relationships between these two measures have been discovered [70].

Chen et al. [9] give an alternate characterization of the condition number with regards to difficulty in robustly controlling the plant. They give estimates for the worst case relative deviations in the open-loop transfer function in the presence of uncertainty. Defining the nominal output open-loop transfer function by  $L$ , i.e.,  $L \triangleq GK$ , the relative error is defined as:  $E \triangleq (L_{\Delta} - L)L^{-1}$ . Here  $L_{\Delta} := G_{\Delta}K$ , with  $G_{\Delta}$  as defined in (4.6.2) with

$l_I = 1$ . It can be shown that [9]:

$$\bar{\sigma}(E(j\omega)) = \kappa(G(j\omega)), \quad (4.6.5)$$

i.e., the maximum relative open-loop deviation in the loop transfer function due to input uncertainty equals the plant condition number. The higher the condition number, the larger the relative deviation  $E$ ; for such a case the open-loop transfer function will deviate far from its nominal value and thus will potentially lead to undesirable closed-loop properties.

Apart from input multiplicative uncertainty, high condition numbers have also been related to robust stability problems in the presence of additive uncertainty. The following theorem is taken from Hoskin et al. [43].

**Theorem 4.6.1** [43] *For a square plant  $G$ , there exists a linear controller  $K$  which stabilizes all  $G_\Delta = G + \Delta$  with*

(i) *the same number of RHP poles as  $G$ , and*

$$(ii) \frac{\bar{\sigma}(\Delta)}{\bar{\sigma}(G)} \leq \delta_{ra},$$

*and achieves  $\bar{\sigma}(S) \leq 0.707 \forall \omega \leq \omega_S$  only if*

$$\kappa(G) < \frac{3.414}{\delta_{ra}} \quad \forall \omega \leq \omega_S.$$

*Here  $\delta_{ra}$  is the relative additive uncertainty margin and  $\omega_S$  is the specified closed-loop 3dB bandwidth of the system.*

This theorem provides a necessary condition for robust stability in the presence of additive uncertainty. The higher the condition number of the plant, the smaller the relative additive perturbation  $\delta_{ra}$  which can be robustly stabilized. Furthermore Freudenberg [28] shows that a feedback system whose plant is ill-conditioned is potentially very sensitive to simultaneous input and output uncertainty. These and the previous results of this section show that plants with high condition numbers are difficult to control and therefore, should be avoided.

Figure 4.3 shows the condition numbers for sets 1 and 4 and indicates that set 4 should be favoured over set 1. The measurement DPUP is thus seen to be better than PS21PS1

for feedback purposes; this supports our earlier conclusions based on the RGA. Condition numbers for sets 2 and 5 (not shown here) led to the same conclusion. Therefore, based on both the RGA and the condition numbers, we drop sets 1 and 2 in favour of sets 4 and 5.

The condition numbers of sets 4 and 5 are shown in Figure 4.4; just like the RGA numbers, the condition numbers are also very similar for the two sets. We therefore need some other criterion to select between these two sets. It should be noted that the condition number which is based on plant input and output scaling, supports the scaling independent RGA in all the cases we considered; this indicates that the scalings chosen were reasonable and physically meaningful.

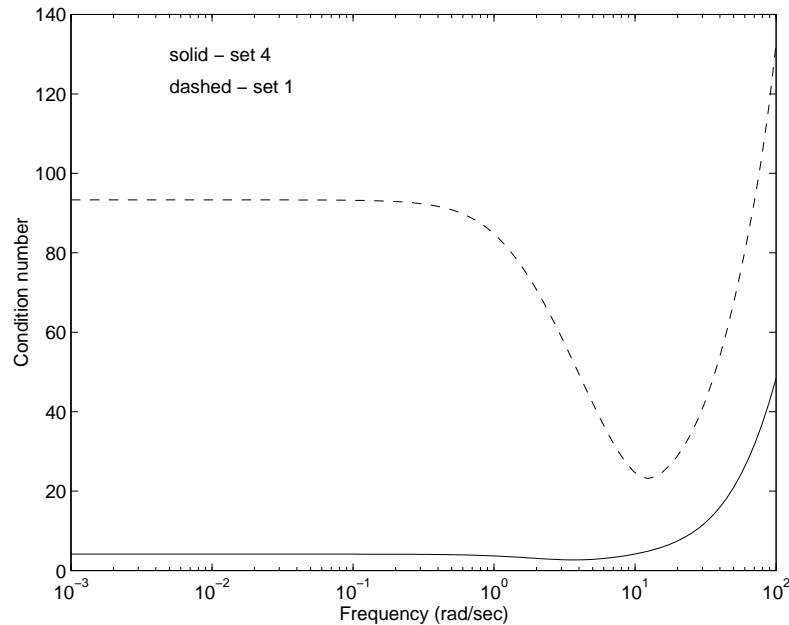


Figure 4.3: Condition numbers for sets 1 and 4.

## 4.7 Hankel singular values

We now present and discuss the use of Hankel singular values in control structure selection. Let  $(A, B, C, D)$  be a minimal realization of an asymptotically stable, rational transfer function  $G(s)$ , then the associated *controllability gramian*  $P$ , and *observability gramian*  $Q$  are defined as:

$$P = \int_0^{\infty} e^{At} B B^T e^{A^T t} dt,$$

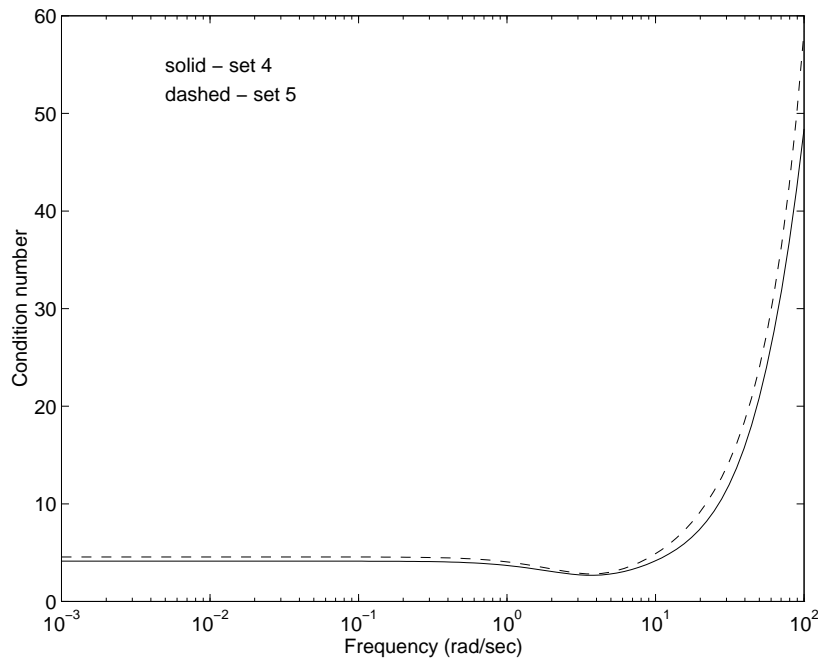


Figure 4.4: Condition numbers for sets 4 and 5.

$$Q = \int_0^{\infty} e^{A^T t} C^T C e^{A t} dt.$$

It can be shown that  $P$  and  $Q$  are given by the unique, positive-definite solutions to the following Lyapunov equations:

$$AP + PA^T + BB^T = 0, \quad (4.7.1)$$

$$A^T Q + QA + C^T C = 0. \quad (4.7.2)$$

The *Hankel singular values* of  $G$  with degree  $n$  (where  $n$  is the number of states of  $G$ ) are given by:

$$\sigma_i = \lambda_i^{1/2}(PQ), \quad i = 1, \dots, n,$$

ordered by convention,  $\sigma_1 \geq \sigma_2 \dots \geq \sigma_n > 0$ . A necessary and sufficient condition for the controllability of the states of a realization is that its controllability gramian be nonsingular. Similarly, the nonsingularity of the observability gramian is a necessary and sufficient condition for the observability of the system states in the particular realization.

The realization for which the controllability and observability gramians are diagonal and equal is called *balanced*. The Hankel singular values defined above reflect the joint controllability and observability (giving equal weight to both) of the states of the balanced realization (since for the balanced case,  $P = Q = \text{diag}\{\sigma_1, \sigma_2, \dots, \sigma_n\}$ ). Note that the

Hankel singular values are invariant under state transformations. They do, however, like the condition number, depend on scaling.

Let the plant transfer function matrix  $G(s)$  be given by:

$$G = \begin{bmatrix} g_{11} & g_{12} & \cdots & g_{1n} \\ \vdots & & & \\ g_{m1} & g_{m2} & \cdots & g_{mn} \end{bmatrix},$$

where  $G$  has  $n$  inputs and  $m$  outputs. Now consider the sub-matrix of  $G$  formed from its first row:

$$G_1 = \begin{bmatrix} g_{11} & g_{12} & \cdots & g_{1n} \end{bmatrix},$$

which relates the first output to all the inputs. The Hankel singular values of  $G_1$  give its combined state controllability and state observability properties. Now consider the sub-matrix  $G_2$  defined as:

$$G_2 = \begin{bmatrix} g_{21} & g_{22} & \cdots & g_{2n} \end{bmatrix},$$

relating the second output to all the inputs. Now if all the Hankel singular values of  $G_2$  are larger than the corresponding values for  $G_1$ , then one can say that the second output is “easier” to control than the first, as it has associated with it better state controllability and observability properties. The Hankel singular values can thus be used to choose between different outputs, the one corresponding to larger Hankel singular values being the one that is more preferable. After a set of outputs has been chosen, the same approach can also be used to pair inputs and outputs by comparing the Hankel singular values of the transfer functions relating the different outputs to a particular input, and so on. It should be noted that Hankel singular values are only defined for asymptotically stable systems.

We now consider the problem of choosing between sets 4 and 5, i.e., choosing between outputs PS6PS1 and NLPCSL. Figure 4.5 shows the Hankel singular values of the two transfer functions relating PS6PS1 and NLPCSL to the three inputs. It is seen from the figure that PS6PS1 has associated with it better state controllability and observability properties as compared to NLPCSL. It would therefore be preferable to use PS6PS1 for control purposes, and hence, set 4 is our final choice.

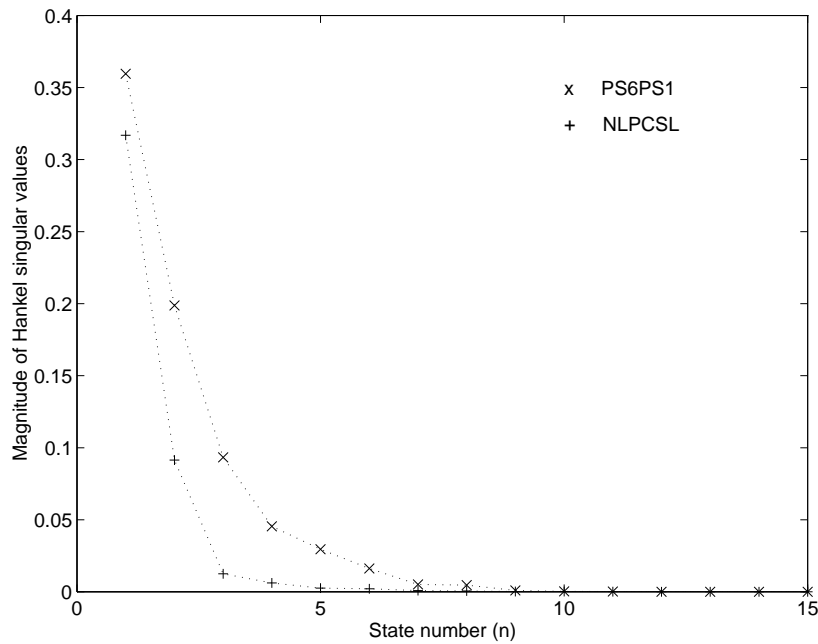


Figure 4.5: Hankel singular values for PS6PS1 and NLPCSL.

## 4.8 Input output pairing

Pairing of inputs and outputs is important in that it makes the design of the pre-filter simpler in some two degrees-of-freedom (DOF) controller design procedures. It is of great importance if a de-centralized control scheme is to be used, and gives insight into the working of the plant. There are several results (see Maciejowski [62]) which show that negative entries on the principal diagonal of the steady-state RGA should be avoided and that it should be close to the identity matrix. Arranging the outputs so that the steady-state RGA meets these conditions gives PS6PS1, DPUP and NHPCSL paired with fuel flow, nozzle area and guide vane angle respectively. The arranged steady-state RGA is shown below:

$$\Gamma(\text{set 4}) = \begin{bmatrix} 1.0783 & 0.0232 & -0.1014 \\ 0.0190 & 0.9737 & 0.0073 \\ -0.0973 & 0.0032 & 1.0941 \end{bmatrix}.$$

These pairings are also confirmed using the structured singular value interaction measure of Grosdidier & Morari [38] as described in detail by Samar & Postlethwaite [91].

## 4.9 Summary

This chapter has described different tools for control structure design, and their application to the aero-engine problem. Some of the tools are scaling dependent, i.e., they are affected by the choice of scalings employed on plant inputs and outputs. Hence proper scaling of the plant is vital before applying these tools; this was discussed in §4.2. Different sets of prospective output variables were formed and their non-minimum phase characteristics analyzed. The relative-gain array was discussed in §4.5. It was shown that large elements in the plant's RGA indicate sensitivity to diagonal multiplicative input uncertainty and individual element uncertainty, and that inverse-based controllers should not be used with such plants. The RGA number was defined and used to screen some of the output sets. The condition number and its role in structure design was discussed in §4.6. Ill-conditioned plants were shown to be prone to robust performance problems in the face of input uncertainty, and to robust stability problems in the presence of additive perturbations. The condition number was shown to support earlier conclusions based on the RGA number. The Hankel singular values and their use in structure selection was introduced in §4.7. Finally the problem of input output pairing based on the steady-state RGA was briefly reviewed in §4.8.

## Chapter 5

### Model reduction with balanced realizations

#### 5.1 Introduction

After deciding on a set of suitable output variables, one is faced with the task of designing robust controllers for the plant. Modern controller design methods such as  $H_\infty$ -optimization (which is the subject of this thesis) and LQG, produce controllers of order at least equal to that of the plant, if not higher. These control laws are typically too complex with regards to practical implementation and simpler designs are sought. In the aero-engine control problem at hand, a number of parameters, apart from the ones being primarily controlled, are to be kept within specified limits, as discussed in Chapter 3. The number of parameters to be controlled or limited exceeds the number of available inputs, and hence all these parameters cannot be controlled independently at the same time. The problem is to be tackled by designing a number of controllers, each for a different set of output variables, which are then switched between, depending on the most significant limit at any given time. The switching is to be done by means of a lowest-wins gate, which serves to propagate the output of the most suitable controller to the plant input. The calculations for all these controllers have to be done and the selection made before each control signal update. This places a high computational demand on the digital controller. In addition, since the aero-engine is highly non-linear, a number of designs may have to be done at various operating points, which would then be scheduled. This would further increase the computational requirements. Hence there is always a great motivation for obtaining low order controllers. For this purpose, one could either reduce the order of

the plant model prior to controller design, or reduce the controller in the final stage, or both. For the aero-engine case, we have chosen to reduce the order of the plant model before design; the reason for this is that controller scheduling is expected to be required to compensate for the non-linear behaviour of the engine. In order to be scheduled, the controllers need to have a well-defined structure, and the change in parameters from one controller to the next is required to be smooth. Reducing the controllers can result in loss of structure and smooth variation between controllers.

In many applications, it is required that the steady-state gain of the system model is not changed after reduction. Examples are internal model-based (IMC) and 2-DOF controllers. If the dc-gain of the controller is changed, a steady-state error between the reference inputs and the outputs will be introduced, which is not desirable. Furthermore when the plant is non-square, the dc-gain of the plant must be accurately known for perfect steady-state tracking (Chapter 7), hence it is desirable that the dc-gain of the plant remains unchanged after reduction. Some popular methodologies for model reduction, such as balanced truncation and optimal Hankel-norm approximation, do not preserve the dc-gain of the system. The reduced system, thus needs to be scaled, and then it no longer enjoys the error bounds guaranteed by these reduction algorithms.

The balanced truncation technique was originally proposed by Moore [66], and later studied by many other researchers, see for example [75, 23]. It consists of balancing the system and then discarding the states corresponding to small Hankel singular values. This idea has been extended such that instead of discarding the states, their derivatives are put to zero. The less controllable and observable states are thus residualized, instead of being truncated. This preserves the dc-gain of the system, and retains more “information” about the original system than the truncation method.

The concept of residualization has been used previously in removing fast system modes and approximating them by a constant term added to the  $D$  matrix of the state-space model. The idea of using residualization with balanced realizations can be found in [33], but no reference is made to any error bound. Such a bound is derived in this thesis, but it is lately discovered that this bound had already been derived by Liu & Anderson [61], where the technique is referred to as *singular perturbation approximation*. The derivation of the error bound has therefore, been relegated to the appendix. The approach taken

here, however, is quite different and follows closely that of Glover [30], and important connections between balanced residualization and optimal Hankel-norm approximation are established.

This chapter is organized as follows. §5.2 contains the necessary background, and introduces the idea of balanced residualization. It is shown that residualization maintains the dc-gain of the system. §5.3 presents some relevant results from [30] and briefly reviews the optimal Hankel-norm approximation technique for stable systems. The error bound for balanced residualization is presented in §5.4. §5.5 works through two examples to demonstrate and compare the balanced residualization approach with the truncation and Hankel-norm approximation techniques for plant and controller reduction. It should be noted that all the results presented in this chapter are developed in continuous time. We will therefore apply these results to the continuous time aero-engine model before discretizing it for discrete time controller design. The controller reduction example is included because of its tutorial value and since it nicely illustrates the importance of dc-gain matching in controller order reduction. §5.6 summarizes the main conclusions of the chapter.

## 5.2 Truncation and residualization

Let  $(A, B, C, D)$  be a minimal realization of an asymptotically stable, rational transfer function  $G(s)$ . The realization  $(A, B, C, D)$  is called *balanced* (as mentioned in §4.7), if the solutions to the following Lyapunov equations

$$AP + PA^T + BB^T = 0 \quad (5.2.1)$$

$$A^TQ + QA + C^TC = 0 \quad (5.2.2)$$

are  $P = Q = \text{diag}\{\sigma_1, \sigma_2, \dots, \sigma_n\} \triangleq \Sigma$ , and  $\sigma_1 \geq \sigma_2 \geq \dots \geq \sigma_n > 0$ .  $\Sigma$  is the *gramian* and  $\sigma_i$  the *ordered Hankel singular values* of the system. The notation  $A^T$  stands for transpose of the matrix  $A$ .

Let the balanced  $A, B, C$  and the corresponding  $\Sigma$  be partitioned compatibly as:

$$A = \begin{bmatrix} A_{11} & A_{12} \\ A_{21} & A_{22} \end{bmatrix}, \quad B = \begin{bmatrix} B_1 \\ B_2 \end{bmatrix}, \quad C = \begin{bmatrix} C_1 & C_2 \end{bmatrix}, \quad \Sigma = \begin{bmatrix} \Sigma_1 & 0 \\ 0 & \Sigma_2 \end{bmatrix},$$

where  $\Sigma_1 = \text{diag}\{\sigma_1, \sigma_2, \dots, \sigma_k\}$ ,  $\Sigma_2 = \text{diag}\{\sigma_{k+1}, \sigma_{k+2}, \dots, \sigma_n\}$  and  $\sigma_k > \sigma_{k+1}$ . Then the reduced order model given by  $(A_{11}, B_1, C_1, D)$  is called a *balanced truncation* of the full order system  $G(s)$ , and the infinity-norm of the error between  $G(s)$  and the reduced order system is bounded by twice the sum of the last  $n - k$  Hankel singular values (trace of  $\Sigma_2$ ) [30, 24]. For the case of repeated Hankel singular values, Glover [30] shows that each repeated Hankel singular value is to be counted only once in calculating the sum; his bound in such a case is therefore better than that of Enns [24].

Let  $\begin{bmatrix} x_1 \\ x_2 \end{bmatrix}$  denote the state vector partitioned compatibly with the balanced  $(A, B, C, D)$  above. To residualize the state vector  $x_2$ , we put  $\dot{x}_2 = 0$  in the state equations and solve for  $x_2$  in terms of  $x_1$  and the input  $u$ . Backsubstitution of  $x_2$  gives:

$$\dot{x}_1 = (A_{11} - A_{12}A_{22}^{-1}A_{21})x_1 + (B_1 - A_{12}A_{22}^{-1}B_2)u, \quad (5.2.3)$$

$$y = (C_1 - C_2A_{22}^{-1}A_{21})x_1 + (D - C_2A_{22}^{-1}B_2)u. \quad (5.2.4)$$

Since  $(A, B, C, D)$  is a minimal and balanced realization of an asymptotically stable system,  $A_{22}$  has negative eigenvalues only (Theorem 4.2 in [30]). This implies that  $A_{22}$  is invertible. (5.2.3) and (5.2.4) are therefore, well-defined. Let us define:

$$A_r \triangleq A_{11} - A_{12}A_{22}^{-1}A_{21}, \quad (5.2.5)$$

$$B_r \triangleq B_1 - A_{12}A_{22}^{-1}B_2, \quad (5.2.6)$$

$$C_r \triangleq C_1 - C_2A_{22}^{-1}A_{21}, \quad (5.2.7)$$

$$D_r \triangleq D - C_2A_{22}^{-1}B_2. \quad (5.2.8)$$

$(A_r, B_r, C_r, D_r)$  is called a *balanced residualization* of the system  $G(s)$ . Liu & Anderson [61] have shown that it enjoys the same error bound as balanced truncation. An alternate proof is presented in Appendix 5B.

We shall now show that balanced residualization preserves the system dc-gain. The dc-gain of the full order balanced system  $(A, B, C, D)$  partitioned as above is given by:

$$-CA^{-1}B + D = -\begin{bmatrix} C_1 & C_2 \end{bmatrix} \begin{bmatrix} A_{11} & A_{12} \\ A_{21} & A_{22} \end{bmatrix}^{-1} \begin{bmatrix} B_1 \\ B_2 \end{bmatrix} + D. \quad (5.2.9)$$

Because

$$\begin{bmatrix} I & 0 \\ -A_{22}^{-1}A_{21} & I \end{bmatrix} \begin{bmatrix} I & 0 \\ A_{22}^{-1}A_{21} & I \end{bmatrix} = I,$$

and

$$\begin{bmatrix} I & A_{12}A_{22}^{-1} \\ 0 & I \end{bmatrix} \begin{bmatrix} I & -A_{12}A_{22}^{-1} \\ 0 & I \end{bmatrix} = I,$$

(5.2.9) can be written as:

$$\begin{aligned} & -[C_1 \quad C_2] \begin{bmatrix} I & 0 \\ -A_{22}^{-1}A_{21} & I \end{bmatrix} \begin{bmatrix} I & 0 \\ A_{22}^{-1}A_{21} & I \end{bmatrix} \begin{bmatrix} A_{11} & A_{12} \\ A_{21} & A_{22} \end{bmatrix}^{-1} \begin{bmatrix} I & A_{12}A_{22}^{-1} \\ 0 & I \end{bmatrix} \\ & \begin{bmatrix} I & -A_{12}A_{22}^{-1} \\ 0 & I \end{bmatrix} \begin{bmatrix} B_1 \\ B_2 \end{bmatrix} + D \\ = & -[C_1 - C_2A_{22}^{-1}A_{21} \quad C_2] \left( \begin{bmatrix} I & -A_{12}A_{22}^{-1} \\ 0 & I \end{bmatrix} \begin{bmatrix} A_{11} & A_{12} \\ A_{21} & A_{22} \end{bmatrix} \begin{bmatrix} I & 0 \\ -A_{22}^{-1}A_{21} & I \end{bmatrix} \right)^{-1} \\ & \begin{bmatrix} B_1 - A_{12}A_{22}^{-1}B_2 \\ B_2 \end{bmatrix} + D. \end{aligned}$$

From (5.2.6) and (5.2.7), the above expression becomes:

$$\begin{aligned} & -[C_r \quad C_2] \left( \begin{bmatrix} A_{11} - A_{12}A_{22}^{-1}A_{21} & 0 \\ A_{21} & A_{22} \end{bmatrix} \begin{bmatrix} I & 0 \\ -A_{22}^{-1}A_{21} & I \end{bmatrix} \right)^{-1} \begin{bmatrix} B_r \\ B_2 \end{bmatrix} + D \\ = & -[C_r \quad C_2] \begin{bmatrix} A_{11} - A_{12}A_{22}^{-1}A_{21} & 0 \\ 0 & A_{22} \end{bmatrix}^{-1} \begin{bmatrix} B_r \\ B_2 \end{bmatrix} + D \\ = & -[C_r \quad C_2] \begin{bmatrix} (A_{11} - A_{12}A_{22}^{-1}A_{21})^{-1} & 0 \\ 0 & A_{22}^{-1} \end{bmatrix} \begin{bmatrix} B_r \\ B_2 \end{bmatrix} + D \\ = & -[C_r \quad C_2] \begin{bmatrix} A_r^{-1} & 0 \\ 0 & A_{22}^{-1} \end{bmatrix} \begin{bmatrix} B_r \\ B_2 \end{bmatrix} + D, \end{aligned}$$

where we have used the definition of  $A_r$  as given in (5.2.5). Further manipulation of this gives:

$$\begin{aligned} -[C_r A_r^{-1} \quad C_2 A_{22}^{-1}] \begin{bmatrix} B_r \\ B_2 \end{bmatrix} + D &= -C_r A_r^{-1} B_r + (D - C_2 A_{22}^{-1} B_2) \\ (5.2.8) \implies &= -C_r A_r^{-1} B_r + D_r, \end{aligned}$$

which is the dc-gain of the residualized system  $(A_r, B_r, C_r, D_r)$ . Thus we see that balanced residualization preserves the steady-state gain of the system. This is exactly as one would expect since we are discarding derivative terms which are zero anyway in the steady-state.

### 5.3 Optimal approximations of stable transfer functions

Theorem 6.3 by Glover [30] gives a particular construction for optimal approximations of stable transfer functions. Here we give a slightly less general statement of the same theorem, specific to our requirements here.

**Theorem 5.3.1** [30] *Let  $(A, B, C, D)$  with  $A \in \mathfrak{R}^{n \times n}$ ,  $B \in \mathfrak{R}^{n \times m}$ ,  $C \in \mathfrak{R}^{m \times n}$ ,  $D \in \mathfrak{R}^{m \times m}$  (where  $\mathfrak{R}^{n \times m}$  denotes the space of  $n \times m$  real matrices) be a balanced realization of a stable, rational transfer function  $G(s)$  which satisfies*

$$AP + PA^T + BB^T = 0 \quad (5.3.1)$$

$$A^T Q + QA + C^T C = 0 \quad (5.3.2)$$

for

$$P = Q = \text{diag}\{\Sigma_1, \sigma I_l\} \quad (5.3.3)$$

with  $\Sigma_1$  diagonal ( $\Sigma_1 > \sigma I$  is implied as the realization is balanced),  $\sigma \neq 0$  and  $\delta(\Sigma_1 - \sigma I) = 0$ , where  $\delta(\cdot)$  represents the number of eigenvalues on the imaginary axis. Partition  $(A, B, C)$  conformally with  $P$  and define:

$$\hat{A} \triangleq \Gamma^{-1}(\sigma^2 A_{11}^T + \Sigma_1 A_{11} \Sigma_1 - \sigma C_1^T U B_1^T), \quad (5.3.4)$$

$$\hat{B} \triangleq \Gamma^{-1}(\Sigma_1 B_1 + \sigma C_1^T U), \quad (5.3.5)$$

$$\hat{C} \triangleq C_1 \Sigma_1 + \sigma U B_1^T, \quad (5.3.6)$$

$$\hat{D} \triangleq D - \sigma U, \quad (5.3.7)$$

where  $U$  is a unitary matrix satisfying

$$B_2 = -C_2^T U, \quad (5.3.8)$$

and

$$\Gamma \triangleq \Sigma_1^2 - \sigma^2 I. \quad (5.3.9)$$

Also define the error system:

$$A_e \triangleq \begin{bmatrix} A & 0 \\ 0 & \hat{A} \end{bmatrix}, \quad B_e \triangleq \begin{bmatrix} B \\ \hat{B} \end{bmatrix}, \quad C_e \triangleq \begin{bmatrix} C & -\hat{C} \end{bmatrix}, \quad D_e \triangleq D - \hat{D}.$$

Then  $(A_e, B_e, C_e, D_e)$  satisfy

$$A_e P_e + P_e A_e^T + B_e B_e^T = 0 \quad (5.3.10)$$

$$A_e^T Q_e + Q_e A_e + C_e^T C_e = 0 \quad (5.3.11)$$

with

$$P_e = \begin{bmatrix} \Sigma_1 & 0 & I \\ 0 & \sigma I & 0 \\ I & 0 & \Sigma_1 \Gamma^{-1} \end{bmatrix}, \quad (5.3.12)$$

$$Q_e = \begin{bmatrix} \Sigma_1 & 0 & -\Gamma \\ 0 & \sigma I & 0 \\ -\Gamma & 0 & \Sigma_1 \Gamma \end{bmatrix}, \quad (5.3.13)$$

$$P_e Q_e = \sigma^2 I. \quad (5.3.14)$$

On defining  $E(s) \triangleq C_e(sI - A_e)^{-1} B_e + D_e$ , we have:

$$E(s)E^T(-s) = \sigma^2 I. \quad (5.3.15)$$

■

An optimal Hankel-norm approximation of a stable transfer function  $G(s)$  is defined as one that minimizes the Hankel-norm of the error between the full order and reduced systems. One class of solutions to this problem has been shown by Glover [30] to be obtained as follows. Let  $G$  have Hankel singular values  $\sigma_1 \geq \sigma_2 \geq \dots \geq \sigma_k > \sigma_{k+1} = \sigma_{k+2} = \dots = \sigma_{k+l} > \sigma_{k+l+1} \geq \dots \geq \sigma_n > 0$ , and construct a balanced realization of  $G$  but with the gramian reordered as  $\Sigma = \text{diag}\{\sigma_1, \sigma_2, \dots, \sigma_k, \sigma_{k+l+1}, \dots, \sigma_n, \sigma_{k+1}, \dots, \sigma_{k+l}\}$ . Denote the balanced realization by  $(A, B, C)$  and the gramian by  $\Sigma = \begin{bmatrix} \Sigma_1 & 0 \\ 0 & \sigma_{k+1} I_l \end{bmatrix}$ . Now partition  $(A, B, C)$  conformally with  $\Sigma$  and define  $(\hat{A}, \hat{B}, \hat{C}, \hat{D})$  by equations (5.3.4)–(5.3.7), and write:

$$G_h + F = \hat{C}(sI - \hat{A})^{-1} \hat{B} + \hat{D}, \quad (5.3.16)$$

where  $G_h$  is a stable transfer function and  $F$  is an anti-stable transfer function (i.e., poles in the right half-plane).  $G_h$  is an optimal Hankel-norm approximation to  $G$  of McMillan degree  $k$  (the McMillan degrees of  $G_h$  and  $F$  depend on the  $\sigma$  chosen). If  $\sigma_{k+1}$  is the

smallest Hankel singular value then  $F = 0$ , otherwise  $(\hat{A}, \hat{B}, \hat{C}, \hat{D})$  has a non-zero anti-stable part. In such a case  $G_h$  has to be separated from  $F$ . The Hankel-norm of the error between  $G$  and  $G_h$  is equal to  $\sigma_{k+1}$ , i.e., the  $(k + 1)$  th Hankel singular value of  $G$ .

The Hankel-norm does not depend on the  $D$  matrix of the state-space model. The choice of the  $D$  matrix of  $G_h$  is, therefore, arbitrary except when  $F = 0$  as in that case it is just equal to  $\hat{D}$ . The  $L_\infty$ -norm however, does depend on  $D$ . A particular choice of  $D$ , say  $D_o$ , has been shown to give the following  $L_\infty$ -norm bound on the error [30]:

$$\|G - G_h - D_o\|_\infty \leq \sigma_{k+1} + \delta, \quad (5.3.17)$$

where

$$\begin{aligned} \delta &= \sigma_1(F(-s)) + \sigma_2(F(-s)) + \dots \\ &\leq \sigma_{k+2}(G(s)) + \dots + \sigma_n(G(s)). \end{aligned}$$

## 5.4 Error bound for balanced residualization

As already mentioned, the  $L_\infty$ -norm of the difference between a balanced full order system  $G(s)$  of McMillan degree  $n$  and its reduced order approximation of degree  $k$  obtained via balanced residualization is bounded by twice the sum of the last  $n - k$  Hankel singular values of  $G$ . To be more precise and to take into consideration the case where one might have repeated Hankel singular values, we present here the statement of Theorem 5B.3 (Appendix 5B).

**Theorem 5B.3** *Let  $G(s)$  be a stable, rational,  $p \times m$ , transfer function with Hankel singular values  $\sigma_1 > \sigma_2 > \dots > \sigma_N$ , where each  $\sigma_i$  has multiplicity  $r_i$  and let  $\tilde{G}_k(s)$  be obtained by residualizing the balanced realization of  $G(s)$  to the first  $(r_1 + r_2 + \dots + r_k)$  states. Then*

1.  $\|G(s) - \tilde{G}_k(s)\|_\infty \leq 2(\sigma_{k+1} + \sigma_{k+2} + \dots + \sigma_N)$
2.  $\|G(s) - \tilde{G}_k(s)\|_H \leq 2(\sigma_{k+1} + \sigma_{k+2} + \dots + \sigma_N)$ . ■

The proof is detailed in Appendix 5B.

## 5.5 Some multivariable examples

In this section we demonstrate the balanced residualization procedure on different examples and make comparisons with balanced truncation and optimal Hankel-norm approximation methods. The first example is about reduction of the aero-engine plant model and the second example considers reduction of a 2-DOF  $H_\infty$  controller. As mentioned earlier, the controller reduction example is included because of its tutorial value; only the engine plant model is reduced in the context of this project.

### 5.5.1 Reduction of the aero-engine model

For the first example, we consider the reduction of a continuous time model of the aero-engine. The model has 3 inputs, 3 outputs, and 18 states; the outputs being PS6PS1, DPUP and NHPCSL. The model is reduced to 6 states via balanced residualization, balanced truncation, and optimal Hankel-norm approximation, and the results compared in both the frequency and time domains.

Figures 5.1, 5.2 and 5.3 show the singular values of the reduced and full order models plotted against frequency for the residualized, truncated and optimal Hankel-norm approximated cases, respectively. The  $D$  matrix used for optimal Hankel-norm approximation is such that the error bound given in (5.3.17) is met. It can be seen that the residualized system matches perfectly at steady-state. The singular values of the three error systems (defined as the difference between the full order and reduced models) are shown in Figure 5.4. The  $L_\infty$ -norm of the error system is computed to be 0.1863 for balanced residualization and occurs at infinite frequency; the corresponding error norms for balanced truncation and optimal Hankel-norm approximation are 0.2931 and 0.1501 occurring at 181.9 rad/sec and zero respectively. The theoretical upper bounds for these error norms are 0.6285 (twice the sum of the tail) for residualization and truncation, and 0.1724 (using (5.3.17)) for optimal Hankel-norm approximation respectively. It should be noted that the plant under consideration is desired to have a closed-loop bandwidth of around 10 rad/sec. The error close to this frequency, therefore, should be as small as possible. Figure 5.4 shows that the error for balanced residualization is the smallest at low and medium frequencies (i.e., close up to the bandwidth), but at high frequencies,

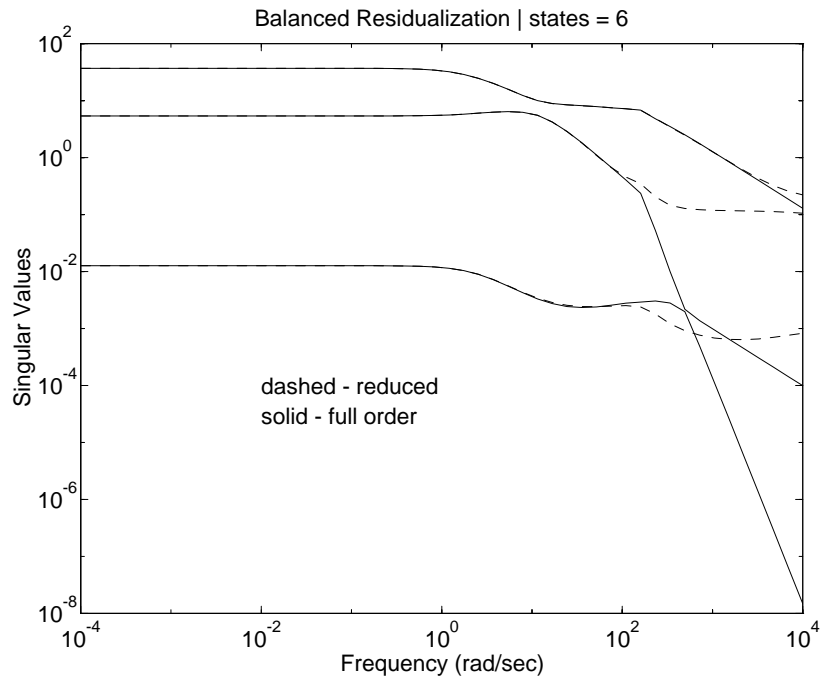


Figure 5.1: Aero-engine: Balanced residualization.

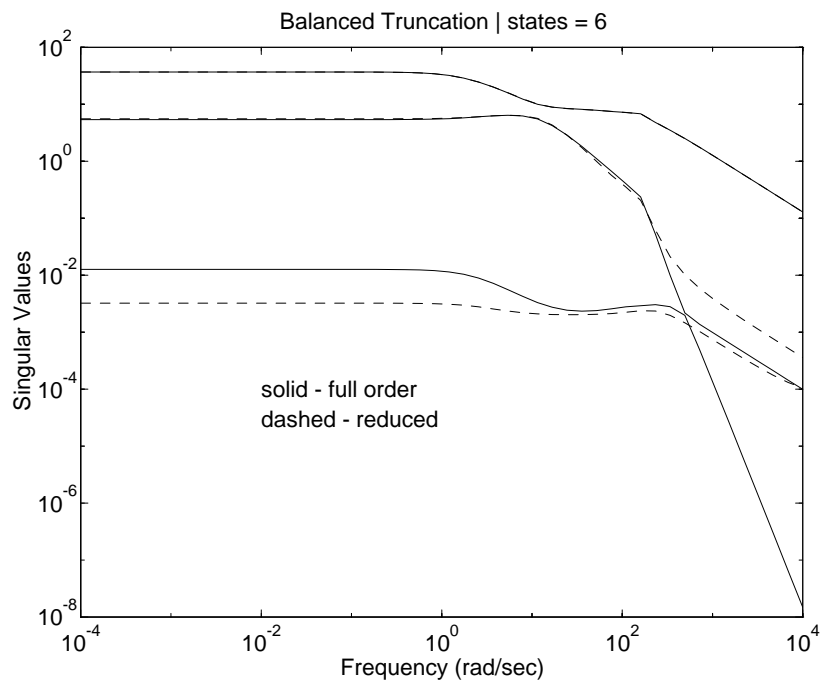


Figure 5.2: Aero-engine: Balanced truncation.

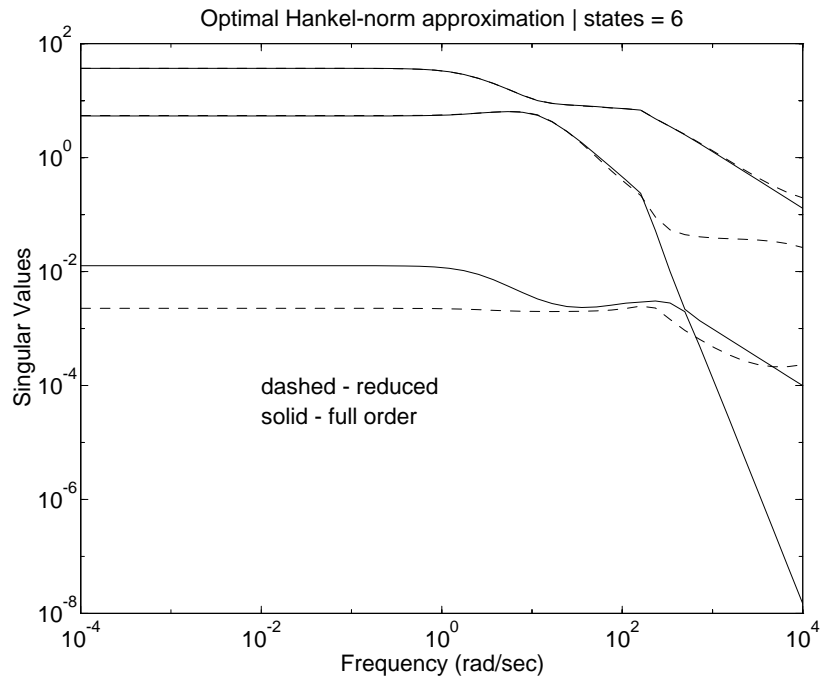


Figure 5.3: Aero-engine: Optimal Hankel-norm approximation.

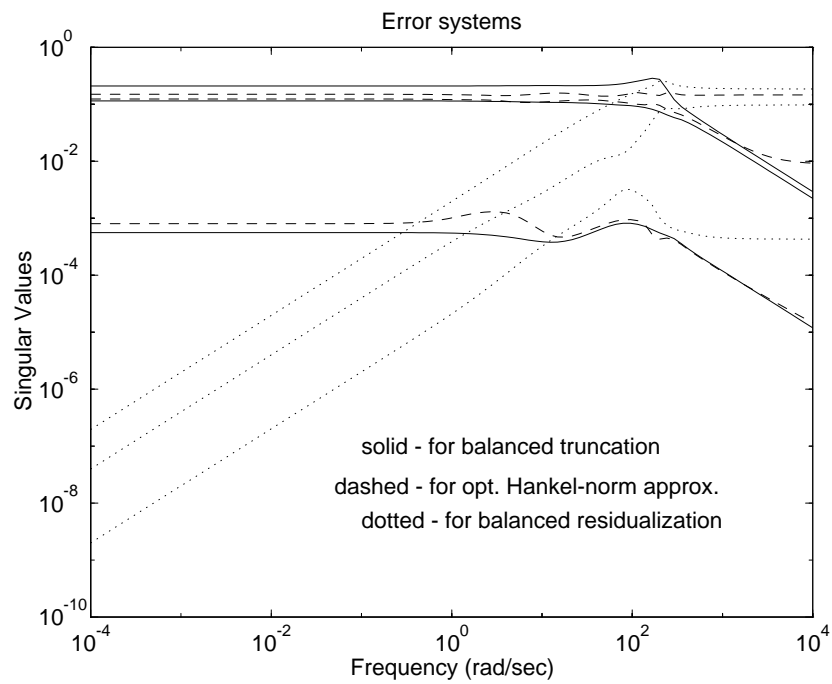


Figure 5.4: Aero-engine: Singular values of the error systems.

the error is greater than for the other two reduced systems.

It is sometimes desirable to have the steady-state gain of the reduced plant model the same as the full order model. This is true for non-square plants, in which case accurate knowledge of the plant's dc-gain is essential for perfect tracking (Chapter 7). The truncated and optimal Hankel-norm approximated systems do not preserve the dc-gain and have to be scaled, i.e., the reduced model  $G_{reduced}$  is replaced by  $G_{reduced}S$ , where  $S = G_{reduced}(0)^{-1}G(0)$ ,  $G$  being the full order model. The scaled systems no longer enjoy the bounds guaranteed by these methods and  $\|G - G_{reduced}S\|_{\infty}$  can be quite large. The singular values of the scaled reduced order systems are shown in Figures 5.5 and 5.6 for the two cases. The singular values of the error systems for balanced residualization, and for the other two scaled systems are shown in Figure 5.7. Note that the residualized system does not need scaling, and the error system for this case has been shown again only for ease of comparison. The  $L_{\infty}$ -norms of these errors are computed and are found to degrade to 4.542 (at 12.14 rad/sec) for the scaled truncated system and 5.703 (at 11.65 rad/sec) for the scaled optimal Hankel-norm approximated system. The truncated and Hankel-norm approximated systems are clearly worse after scaling since the errors in the critical frequency range around cross-over become large despite the improvement at steady-state. Hence residualization is to be preferred over these other techniques whenever good low frequency matching is desired.

Impulse and step responses from the second input to all the outputs for the three reduced systems (with the truncated and optimal Hankel-norm approximated systems scaled) are shown in Figures 5.8 and 5.9 respectively. The responses for the other inputs were found to be similar. The residualized model's response is seen to be closer to the full order model's response.

We have observed that balanced residualization performs closer to the full order system (i.e., the error is smaller) at low and medium frequencies, whereas the other two methods perform better at high frequencies. It should be noted that plant models are inherently inaccurate at high frequencies, and it is the low to medium frequency behaviour which is more important. Thus, residualization may be a preferable choice over the other methods in the context of plant model reduction.

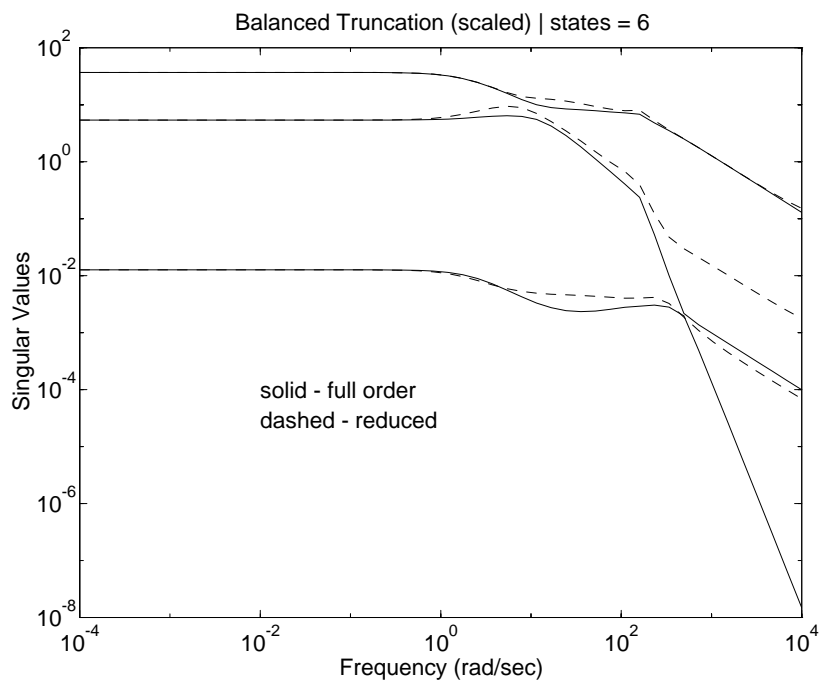


Figure 5.5: Aero-engine: Truncation (scaled).

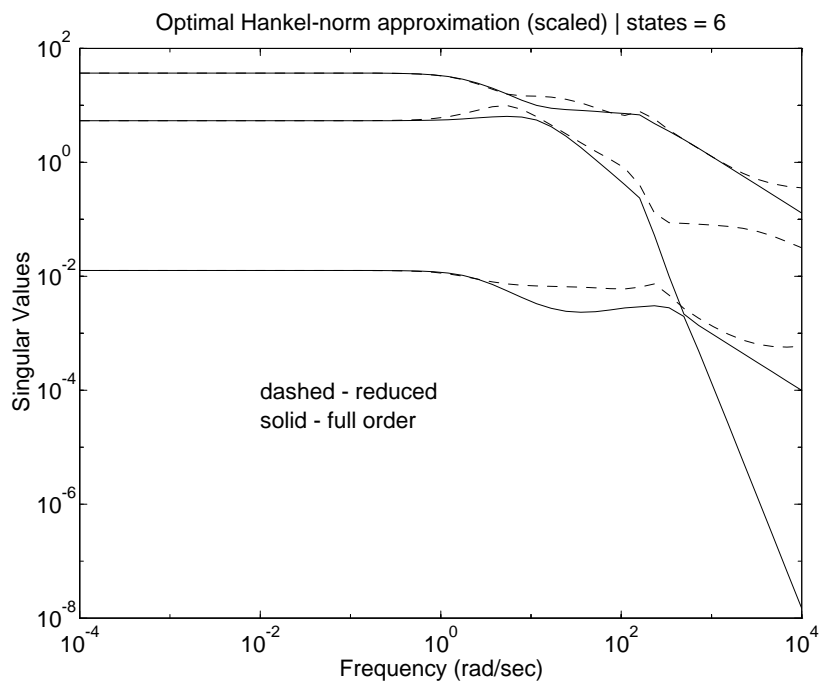


Figure 5.6: Aero-engine: Optimal Hankel-norm approximation (scaled).

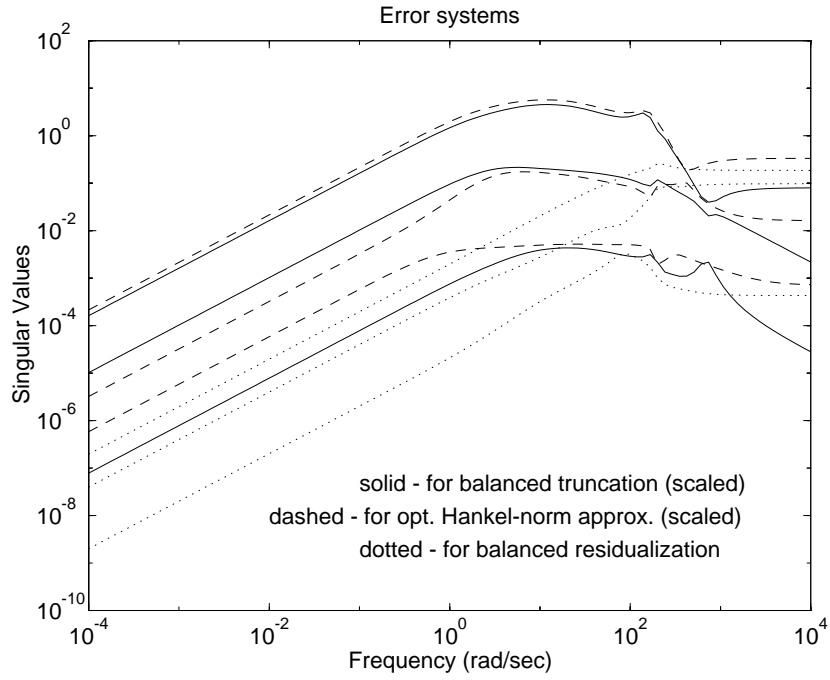


Figure 5.7: Aero-engine: Singular values of the error systems (scaled).

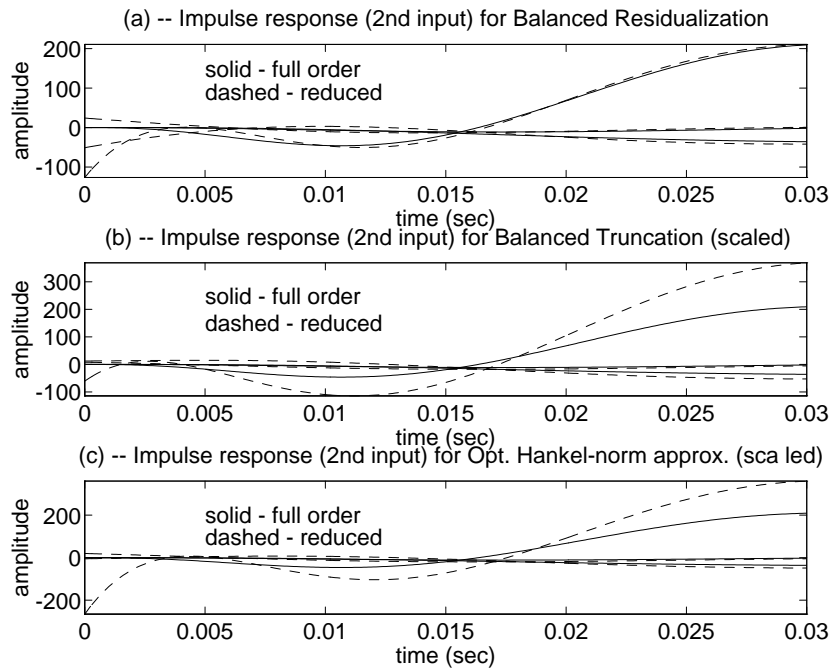


Figure 5.8: Aero-engine: Impulse response (2nd input).

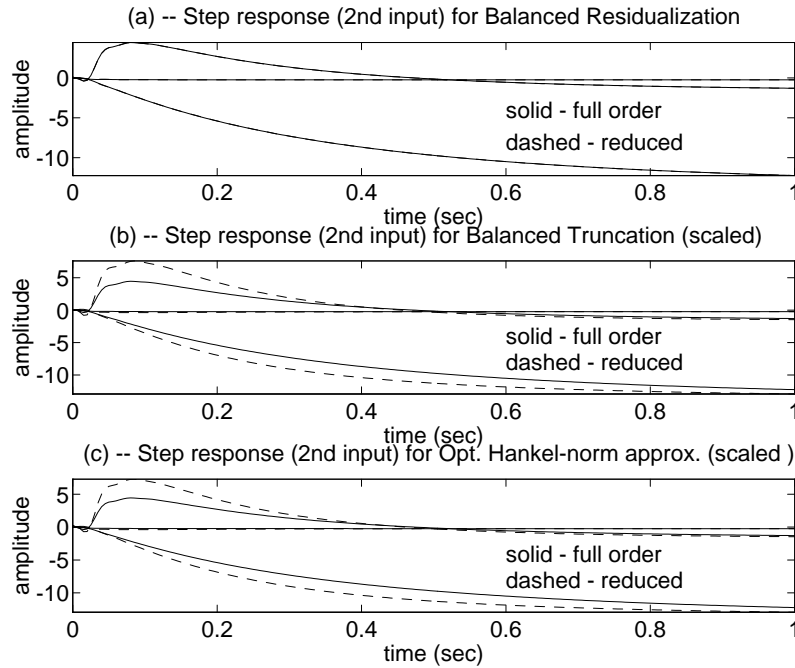


Figure 5.9: Aero-engine: Step response (2nd input).

Finally, scaling can pose problems for non-square plants. Consider, for example, a plant with more outputs than inputs. Suppose that it is reduced by some method, whereby the dc-gain has been lost, and it is required to scale the reduced system to restore the steady-state value. Normally scaling is done by post-multiplying (pre-compensating) the plant with the inverse of its dc-gain and then with the desired dc-gain matrix. For the plant under discussion, however, such an inverse (i.e., the right inverse) does not exist, and the scaling procedure is not clear. It should be noted that accurate dc-gain information is needed for such plants in order to achieve perfect steady-state tracking; it is therefore desirable that the reduced models do not lose the system dc-gain. In such cases, the residualization method for reduction is preferable.

### 5.5.2 Reduction of an aero-engine controller

We now consider reduction of a 2-DOF controller designed via  $H_\infty$ -optimization. The plant for which the controller is designed is the full order gas turbine engine model described in Example 5.5.1 above.

A robust controller was designed using the procedure outlined by Hoyle et al. [45]. The

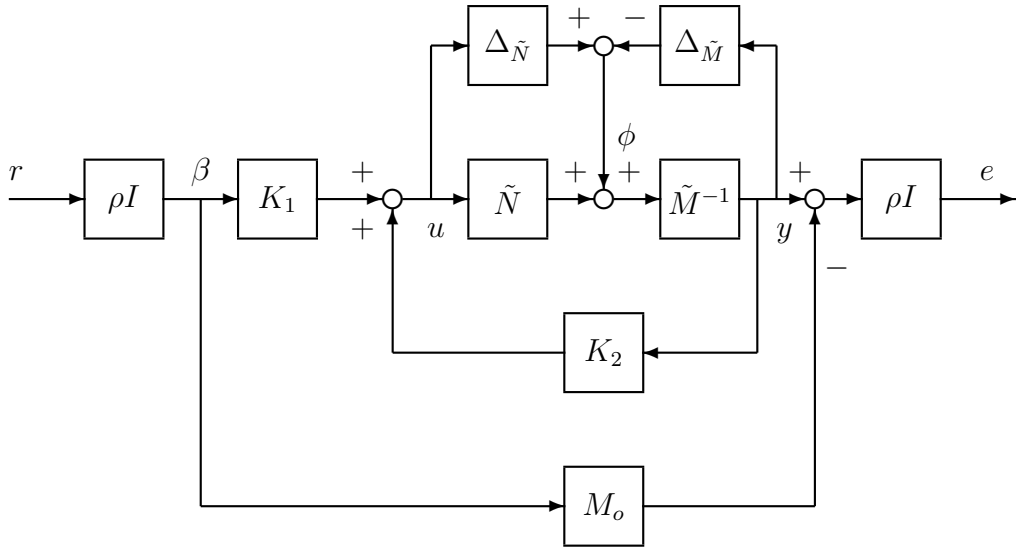


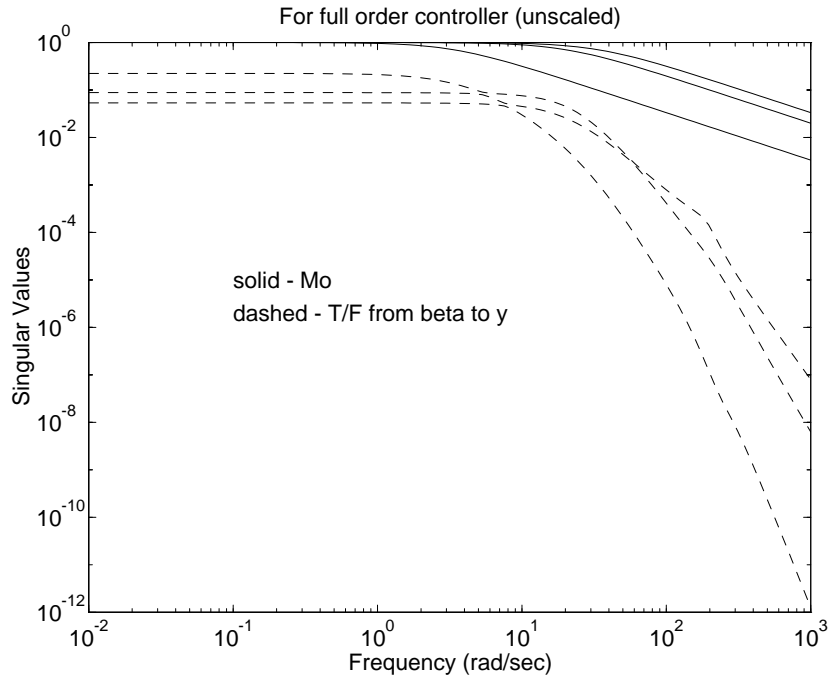
Figure 5.10: 2-DOF design configuration.

procedure is based on robust stabilization in the normalized coprime factor framework with model matching, using a 2-DOF control configuration. The discrete time version of this procedure is discussed in the next chapter, and in Chapter 7 this is used to design robust controllers for the aero-engine. We therefore leave the details of the design procedure for subsequent chapters and concentrate here on controller order reduction.

The framework for posing the  $H_\infty$ -optimization problem is illustrated in Figure 5.10.  $(\tilde{M}, \tilde{N})$  are the normalized coprime factors of the shaped plant model  $G_s$ , i.e.,  $G_s = \tilde{M}^{-1}\tilde{N}$ .  $M_o$  is a reference model chosen to have ideal closed-loop time response characteristics. The controller  $K$  is partitioned as  $K = [K_1 \ K_2]$ , where  $K_1$  is the pre-filter and  $K_2$  the feedback controller. The problem is formulated as a standard  $H_\infty$ -optimization problem such that the  $L_\infty$ -norm of the transfer function relating  $u, y, e$  to  $r, \phi$ , namely

$$\left[ \begin{array}{c|c} \rho(I - K_2 G_s)^{-1} K_1 & K_2 (I - G_s K_2)^{-1} \tilde{M}^{-1} \\ \rho(I - G_s K_2)^{-1} G_s K_1 & (I - G_s K_2)^{-1} \tilde{M}^{-1} \\ \hline \rho^2 ((I - G_s K_2)^{-1} G_s K_1 - M_o) & \rho(I - G_s K_2)^{-1} \tilde{M}^{-1} \end{array} \right] \quad (5.5.1)$$

is minimized. The (1,2) partition of (5.5.1) is associated with robust stability optimization, while the (2,1) partition is associated with model matching. The pre-filter  $K_1$  ensures

Figure 5.11:  $M_o$  and  $R_{y\beta}$  for  $[K_1 \ K_2]$ .

that

$$\| R_{y\beta} - M_o \|_{\infty} \leq \gamma \rho^{-2}, \quad (5.5.2)$$

where  $R_{y\beta} = (I - G_s K_2)^{-1} G_s K_1$  is the closed-loop transfer function mapping  $\beta \rightarrow y$  and  $\gamma$  is the  $L_{\infty}$ -norm achieved for the transfer function given in (5.5.1). For further details refer to [45] or [60]. A 2-DOF controller was designed using this procedure. The controller has 6 inputs (because of the 2-DOF structure), 3 outputs, and 27 states. It has not been scaled (i.e., the dc-gain of  $R_{y\beta}$  has not been matched to that of  $M_o$  by scaling the pre-filter). It is to be reduced to 7 states in each of the cases that follow.

Let us first compare the magnitude of  $R_{y\beta}$  with that of the specified model  $M_o$ . This is shown in Figure 5.11. The  $L_{\infty}$ -norm of the difference is computed to be 0.9475 and occurs at zero frequency. Note that we have  $\rho = 1$  and the  $\gamma$  achieved is 2.8603, so that (5.5.2) is satisfied. The pre-filter is now scaled so that  $R_{y\beta}$  matches  $M_o$  exactly at steady-state, i.e., we replace  $K_1$  by  $K_1 S$  where  $S = R_{y\beta}(0)^{-1} M_o(0)$ . It is argued by Hoyle et al. [45] that this scaling produces better model matching at all frequencies, because the  $H_{\infty}$ -optimization process has already given  $R_{y\beta}$  the same magnitude frequency response shape as the model  $M_o$ . The scaled transfer function is shown in Figure 5.12, and the

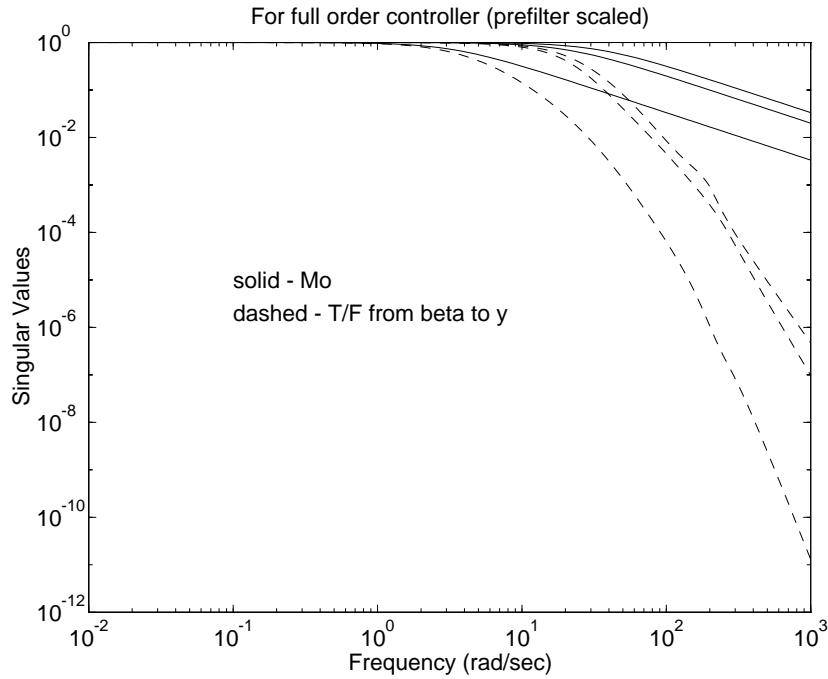


Figure 5.12:  $M_o$  and  $R_{y\beta}$  for  $[K_1 S \ K_2]$ .

$L_\infty$ -norm of the difference ( $R_{y\beta} - M_o$ ) computed to be 1.126 (at 17.17 rad/sec). It can be seen that this scaling has not degraded the  $L_\infty$ -norm of the error significantly as was claimed in [45]. To ensure perfect steady-state tracking the controller is always scaled in this way. We are now in a position to discuss ways of reducing the controller. We shall look at the following two approaches:

1. The scaled controller  $[K_1 S \ K_2]$  is reduced. A balanced residualization of this controller preserves the controller's steady-state gain and would not need to be scaled again. Reductions via truncation and optimal Hankel-norm approximation techniques, however, lose the dc-gain. The pre-filters of these reduced controllers would therefore need to be scaled.
2. The full order controller  $[K_1 \ K_2]$  is directly reduced without first scaling the pre-filter. In which case, scaling is done after reduction.

We now consider the first approach. A balanced residualization of  $[K_1 S \ K_2]$  is obtained. The theoretical upper bound on the  $L_\infty$ -norm of the error (twice the sum of the tail) is

0.5416, i.e.,

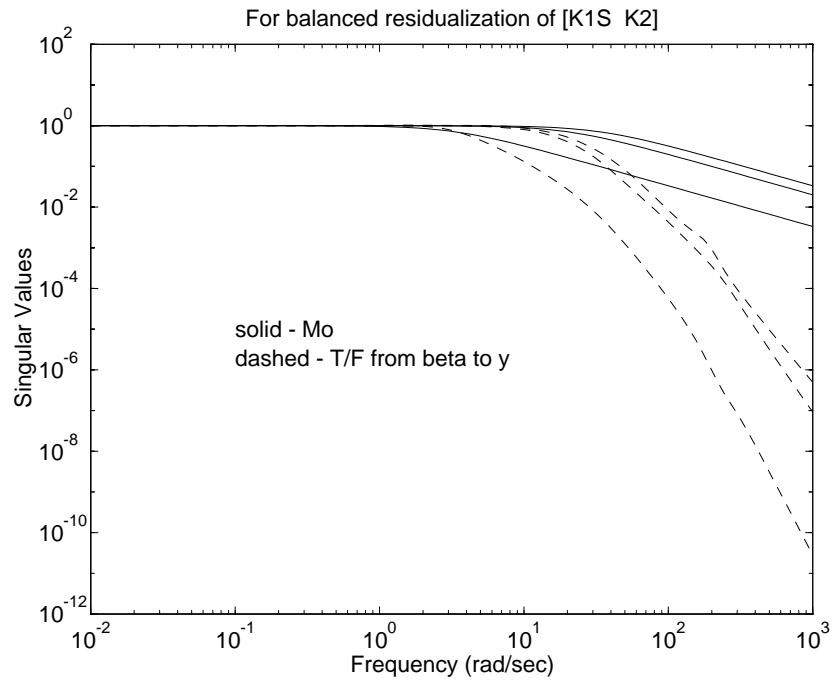
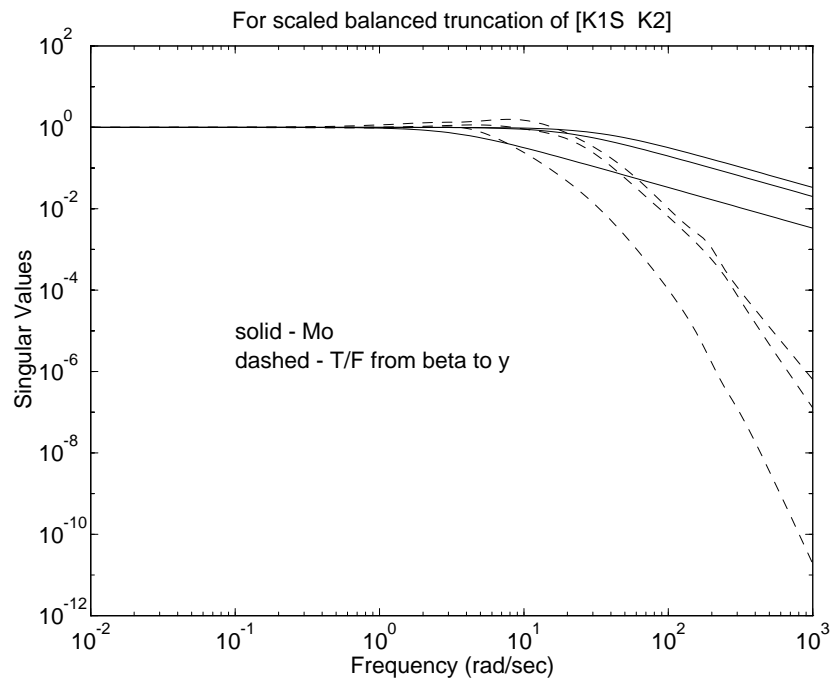
$$\| K_1 S - (K_1 S)_{reduced} \quad K_2 - K_{2_{reduced}} \|_{\infty} \leq 0.5416. \quad (5.5.3)$$

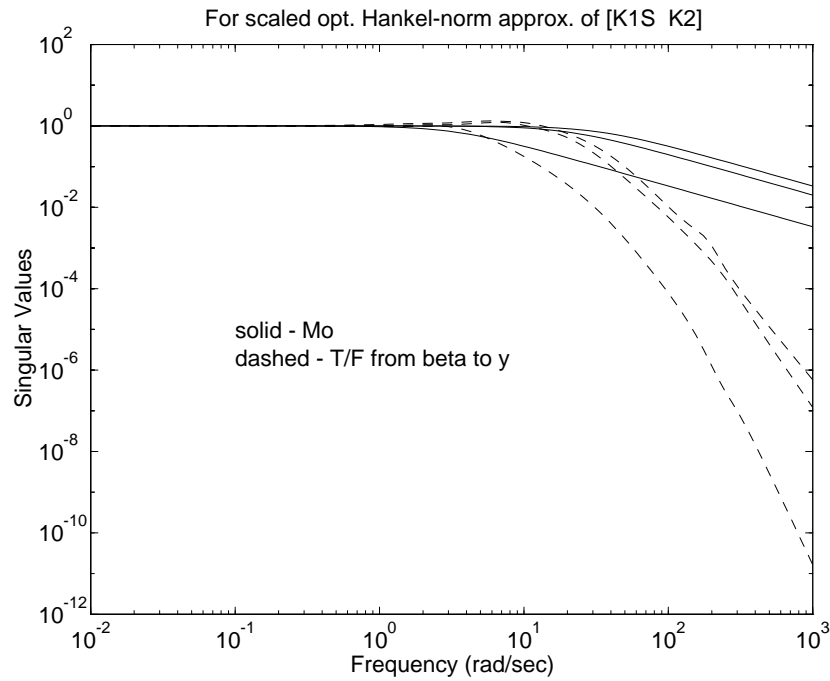
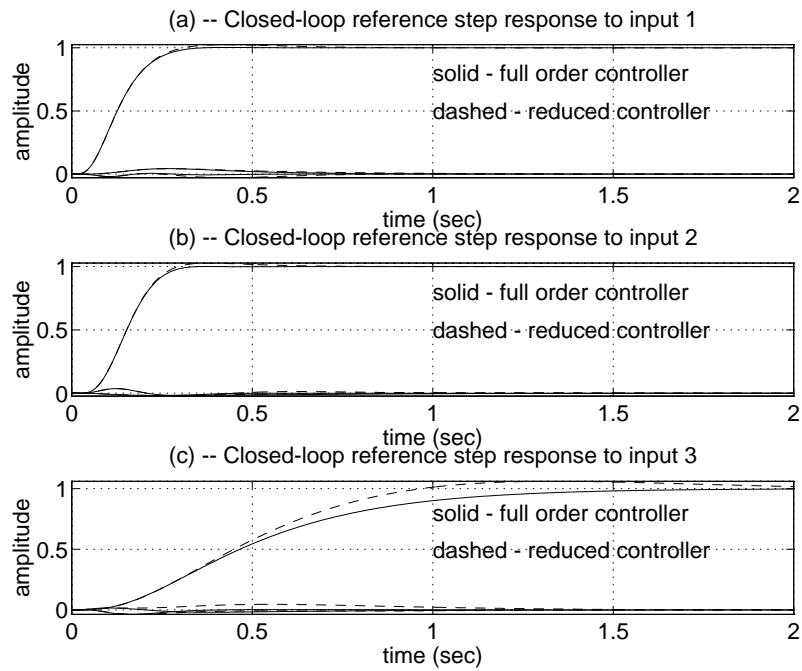
The actual error norm is computed to be 0.2574.  $R_{y\beta}$  for this residualization is computed and its magnitude plotted in Figure 5.13. The  $L_{\infty}$ -norm of the difference ( $R_{y\beta} - M_o$ ) is computed to be 1.124 (at 15.52 rad/sec). This value is very close to that obtained with the full order controller  $[K_1 S \quad K_2]$ , and so the closed-loop response of the system with this reduced controller is expected to be very close to that with the full order controller. Next  $[K_1 S \quad K_2]$  is reduced via balanced truncation. The  $L_{\infty}$ -norm bound given in (5.5.3) still holds. The dc-gain however, falls below the adjusted level, and the pre-filter of the truncated controller is thus scaled. The bound given in (5.5.3) can no longer be guaranteed for the pre-filter (it is in fact found to degrade to 1.56), but it holds for  $K_2 - K_{2_{reduced}}$ . Singular values of  $M_o$  and  $R_{y\beta}$  for the scaled truncated controller are shown in Figure 5.14. The  $L_{\infty}$ -norm of the difference is computed to be 1.476 and this maximum occurs at 14 rad/sec. Finally  $[K_1 S \quad K_2]$  is reduced by optimal Hankel-norm approximation. The following error bound is theoretically guaranteed:

$$\| K_1 S - (K_1 S)_{reduced} \quad K_2 - K_{2_{reduced}} \|_{\infty} \leq 0.1326. \quad (5.5.4)$$

Again the reduced pre-filter needs to be scaled and the above bound can no longer be guaranteed; it actually degrades to 0.9806. Magnitude plots of  $R_{y\beta}$  and  $M_o$  are shown in Figure 5.15 and the  $L_{\infty}$ -norm of the difference is computed to be 1.316, and occurs at 15.43 rad/sec.

It has been observed that both balanced truncation and optimal Hankel-norm approximation cause a lowering of the system dc-gain. In the process of adjustment of these dc-gains, the  $L_{\infty}$ -error bounds are destroyed. In the case of the 2-DOF controller, where the pre-filter has been optimized to give closed-loop responses within a tolerance of a chosen ideal model, large deviations may be incurred. Closed-loop responses for the three reduced controllers discussed above are shown in Figures 5.16, 5.17 and 5.18. It is seen that the residualized controller performs much closer to the full order controller and exhibits better performance in terms of interactions and overshoots. It may not be possible to use the other two reduced controllers if the deviation from the specified model becomes larger than the allowable tolerance, in which case the number of states by which the controller

Figure 5.13:  $M_o$  and  $R_{y\beta}$  for  $[K_1 S \ K_2]$  residualized.Figure 5.14:  $M_o$  and  $R_{y\beta}$  for  $[K_1 S \ K_2]$  truncated and scaled.

Figure 5.15:  $M_o$  and  $R_{y\beta}$  for  $[K_1 S \ K_2]$  optimal Hankel-norm approximated and scaled.Figure 5.16: Closed-loop:  $[K_1 S \ K_2]$  residualized.

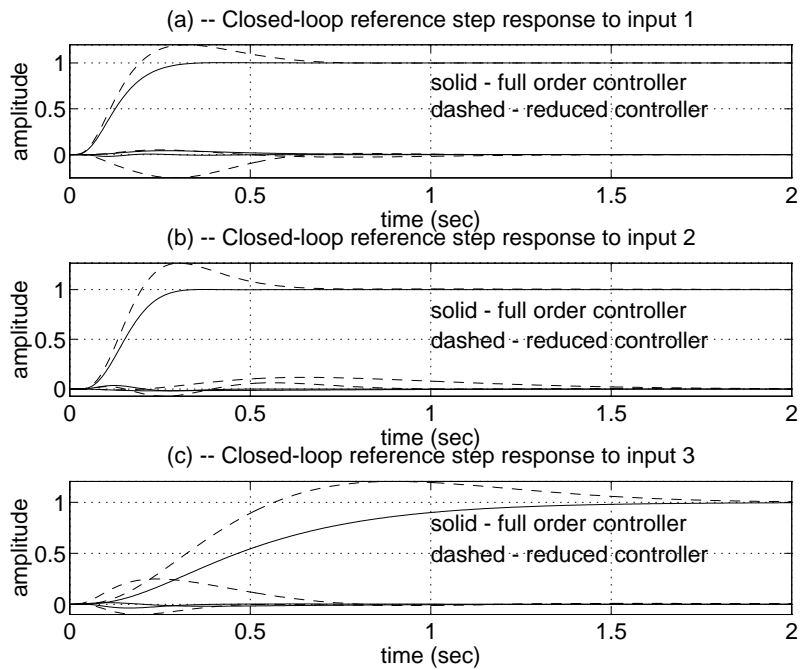


Figure 5.17: Closed-loop:  $[K_1 S \ K_2]$  truncated and scaled.

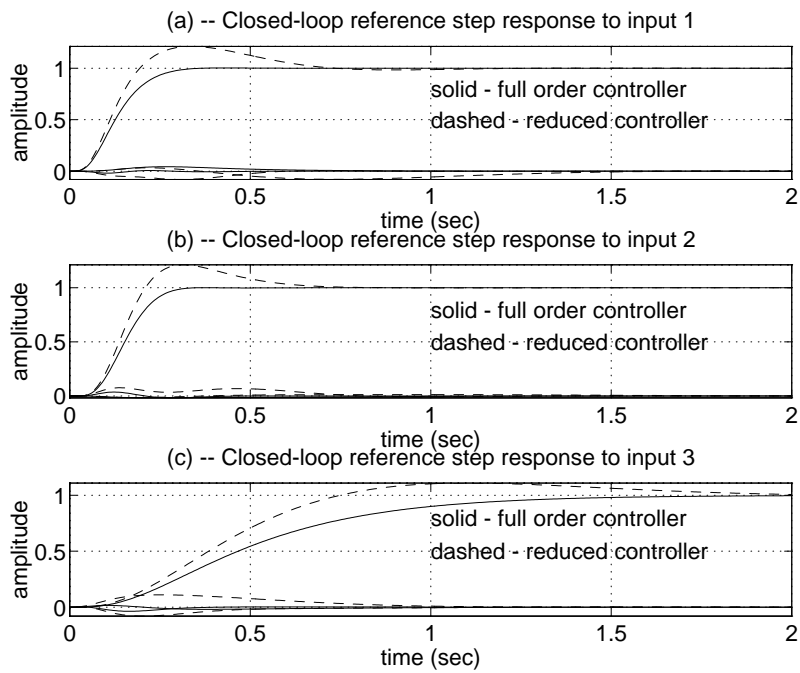


Figure 5.18: Closed-loop:  $[K_1 S \ K_2]$  optimal Hankel-norm approximated and scaled.

is reduced would probably have to be lessened. It should also be noted from (5.5.3) and (5.5.4) that the guaranteed bound for  $K_2 - K_{2_{reduced}}$  is lowest for optimal Hankel-norm approximation.

Let us now consider the second approach. The controller  $[K_1 \ K_2]$  obtained from the  $H_\infty$ -optimization algorithm is reduced directly. The theoretical upper bound on the error for balanced residualization and truncation is:

$$\| [K_1 - K_{1_{reduced}} \ K_2 - K_{2_{reduced}}] \|_\infty \leq 0.1862. \quad (5.5.5)$$

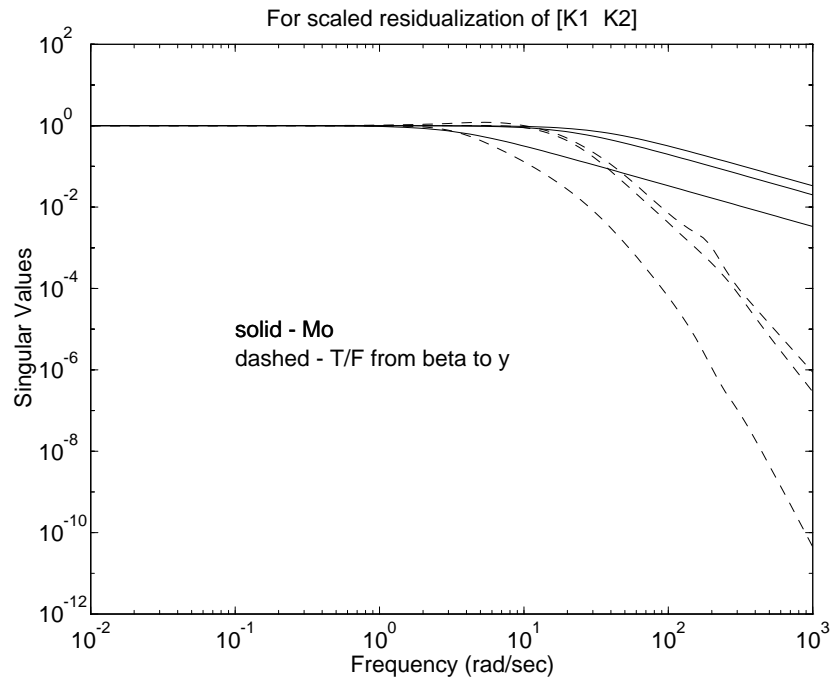
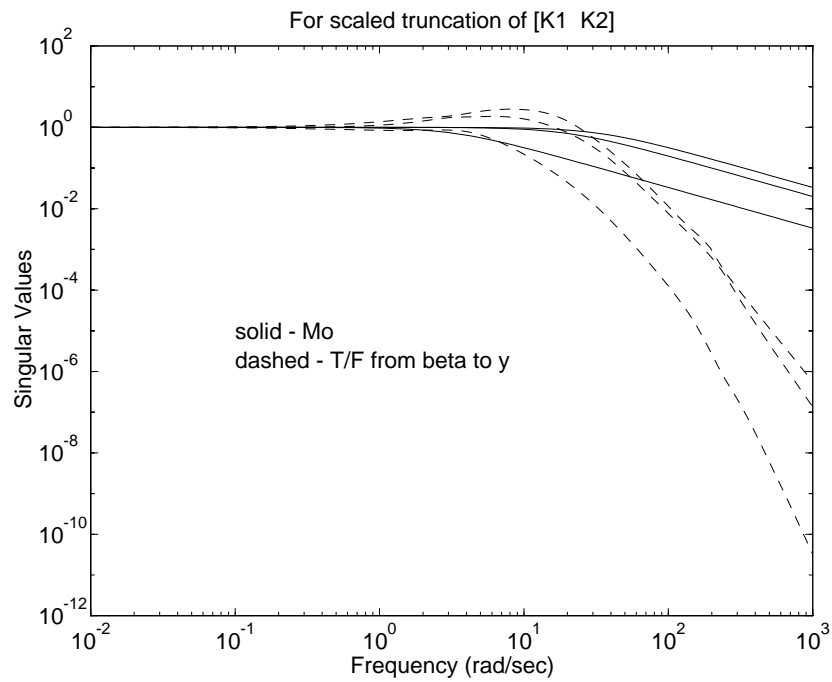
The residualized controller holds to the dc-gain of  $[K_1 \ K_2]$ . It is, therefore, scaled with the same  $S$  as was required for scaling the pre-filter of the full order controller. Singular values of  $M_o$  and  $R_{y\beta}$  for this reduced controller are shown in Figure 5.19, and the  $L_\infty$ -norm of the difference computed to be 1.24 (at 15.15 rad/sec).  $[K_1 \ K_2]$  is next truncated. The dc-gain of the truncated controller is lower than that of  $[K_1 \ K_2]$ , and it turns out that this has the effect of reducing the dc-gain of  $R_{y\beta}$ . Note that the dc-gain of  $R_{y\beta}$  is already less than that of  $M_o$  (Figure 5.11). Thus in scaling the pre-filter of the truncated controller, the dc-gain has to be pulled up from a lower level as compared to the previous (residualized) case. This causes greater degradation at other frequencies. The  $L_\infty$ -norm of  $(R_{y\beta} - M_o)$  in this case is computed to be 3.506 and occurs at 7.165 rad/sec (see Figure 5.20). Finally  $[K_1 \ K_2]$  is reduced by optimal Hankel-norm approximation. The theoretical bound given in (5.3.17) is computed and found to be 0.0448, i.e., we have:

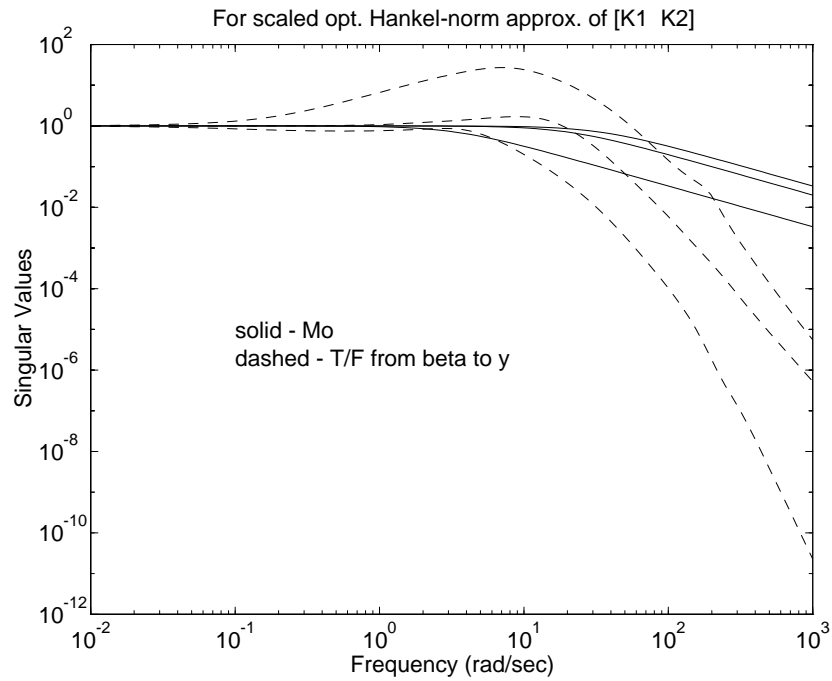
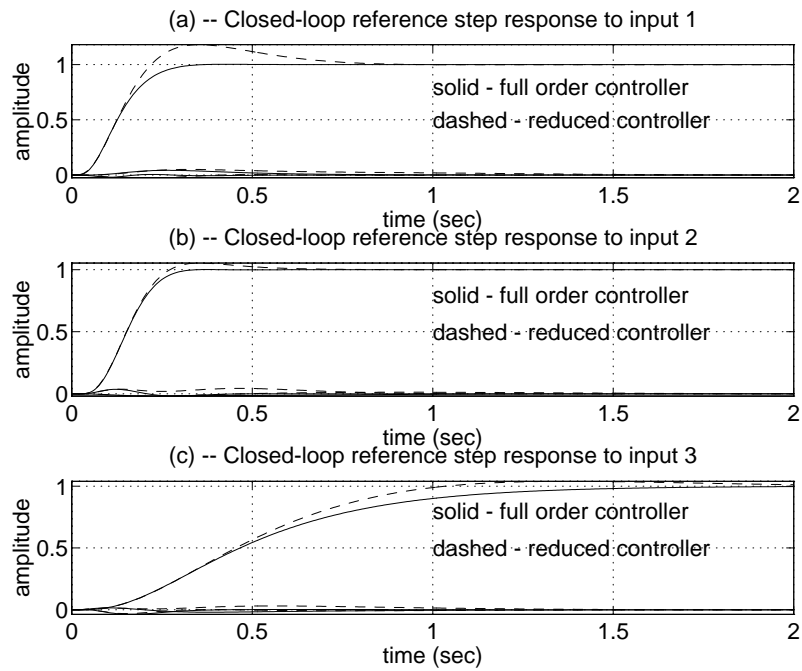
$$\| [K_1 - K_{1_{reduced}} \ K_2 - K_{2_{reduced}}] \|_\infty \leq 0.0448. \quad (5.5.6)$$

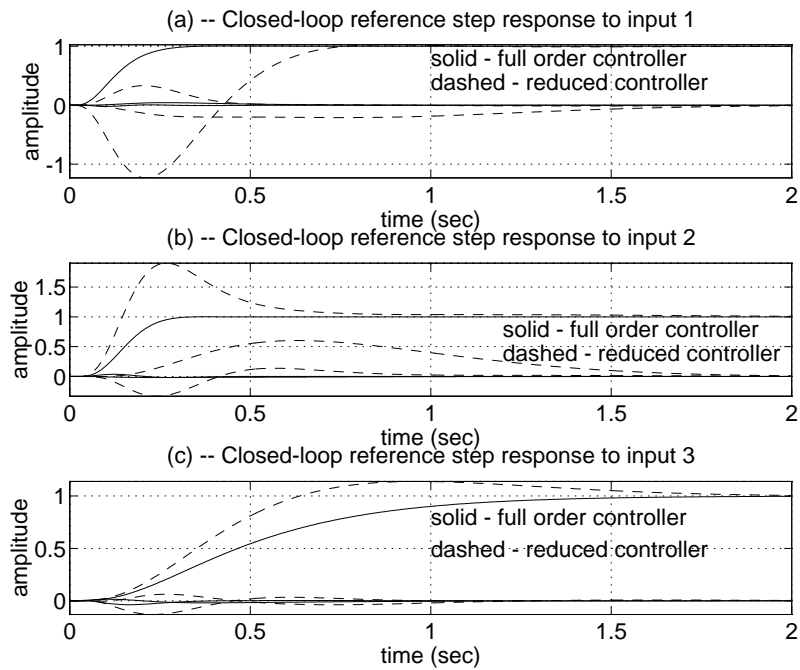
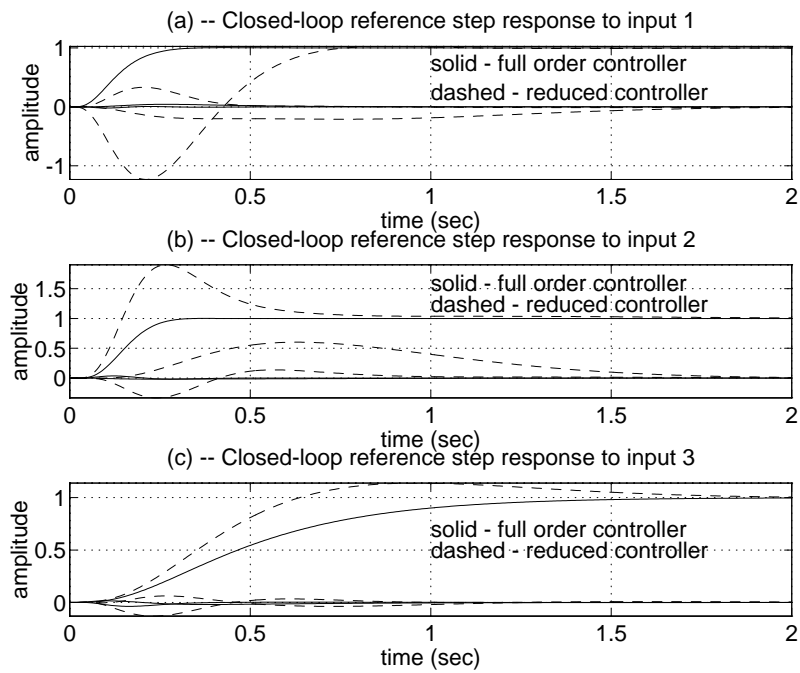
The dc-gain falls once more in the reduction process, and again a larger scaling is required. Singular value plots for  $R_{y\beta}$  and  $M_o$  are shown in Figure 5.21.  $\| R_{y\beta} - M_o \|_\infty$  is computed to be 26.31 and occurs at 7.45 rad/sec.

The closed-loop step response simulations are shown in Figures 5.22, 5.23 and 5.24. It can be seen that the truncated and Hankel-norm approximated systems have deteriorated to an unacceptable level. Only the residualized system maintains an acceptable level of performance.

We have seen that the first approach yields better model matching, though at the expense of a larger  $L_\infty$ -bound on  $K_2 - K_{2_{reduced}}$  (compare (5.5.3) and (5.5.5), or (5.5.4) and

Figure 5.19:  $M_o$  and  $R_{y\beta}$  for  $[K_1 \ K_2]$  residualized and scaled.Figure 5.20:  $M_o$  and  $R_{y\beta}$  for  $[K_1 \ K_2]$  truncated and scaled.

Figure 5.21:  $M_o$  and  $R_{y\beta}$  for  $[K_1 \ K_2]$  optimal Hankel-norm approximated and scaled.Figure 5.22: Closed-loop:  $[K_1 \ K_2]$  residualized and scaled.

Figure 5.23: Closed-loop:  $[K_1 \ K_2]$  truncated and scaled.Figure 5.24: Closed-loop:  $[K_1 \ K_2]$  optimal Hankel-norm approximated and scaled.

(5.5.6)). We have also seen how the scaling of the pre-filter in the first approach gives poorer performance for the truncated and optimal Hankel-norm approximated controllers, relative to the residualized one.

In the second case, all the reduced controllers need to be scaled, but a “larger” scaling is required for the truncated and optimal Hankel-norm approximated controllers. This is an observation only, and there exists no formal proof for it. It is however intuitive in the sense that controllers reduced by these two methods yield poorer model matching at dc as compared to that achieved by the full order controller. A larger scaling is required for them therefore, than that required by the full order or residualized controllers. This larger scaling gives poorer model matching at other frequencies, and only the residualized controller’s performance is deemed acceptable.

## 5.6 Conclusions

Internally balanced realizations have been investigated in the context of model reduction. Residualization of such realizations, unlike truncation and optimal Hankel-norm approximation, preserves the dc-gain of the system. The method, like truncation, is simple and computationally inexpensive. It was observed that truncation and optimal Hankel-norm approximation perform better at high frequencies, whereas residualization performs better at low and medium frequencies, i.e., up to the critical frequencies. Thus for plant model reduction, where models are not accurate at high frequencies to start with, residualization would seem to be a better option. Further, if the dc-gains are to be kept unchanged, truncated and optimal Hankel-norm approximated systems require scaling, which may give large  $L_\infty$ -norms for the errors. In such a case, too, residualization would be a preferred choice.

Frequency weighted model reduction has been the subject of numerous papers over the past few years, see for example, [57, 1, 24]. The idea is to emphasize frequency ranges where better matching is required. This however, has been observed to have the effect of producing larger errors (greater mismatching) at other frequencies [1, 24]. In order to get good steady-state matching, a relatively large weight would have to be used at dc, which would cause poorer matching elsewhere. The choice of weights is not straightforward,

and an error bound is available only for weighted Hankel-norm approximation. The computation of the bound is also not as easy as in the unweighted case [2]. Balanced residualization can in this context, be seen as a reduction scheme with implicit low and medium frequency weighting built into it.

For controller reduction, we have shown in a 2-DOF example, the importance of scaling and dc-gain matching. Two approaches were considered. In the first approach, the pre-filter of the full order controller was scaled beforehand. In this case, the pre-filter of the residualized system does not need to be scaled, and enjoys the guaranteed  $L_\infty$ -error bounds. The pre-filters of the other reduced systems have to be scaled, and can have large  $L_\infty$ -errors (with respect to the scaled full order pre-filter). They were thus, seen to give poorer performance.

In the second approach, the unscaled full order controller  $[K_1 \ K_2]$  was first reduced, and then scaled. The residualized system needed the same scaling matrix as the full order controller. With the other reduced controllers, the model matching at dc deteriorated compared to the full order controller, and hence a larger scaling was needed. This caused very poor matching at other frequencies. The residualized controller thus performed better than the other two. As for the feedback part of the controller ( $K_2$ ), the  $L_\infty$ -error bound given by optimal Hankel-norm approximation was the best.

It is remarked that in general, dc-gain matching may not be crucial. The matching should, however be good near the desired closed-loop bandwidth. Balanced residualization has been seen to perform very close to the full order system in this frequency range. Good approximation at high frequencies may also sometimes be desired. In such a case, using truncation or optimal Hankel-norm approximation with appropriate frequency weightings may yield better results.

## APPENDICES

### 5A All-pass transfer functions

The following theorem is taken from [30]:

**Theorem 5A.1** [30] *Given a realization  $(A, B, C)$  (not necessarily stable) with  $A \in \mathfrak{R}^{n \times n}$ ,  $B \in \mathfrak{R}^{n \times m}$ ,  $C \in \mathfrak{R}^{m \times n}$ , then*

1. *If  $(A, B, C)$  is completely controllable and completely observable, the following two statements are equivalent:*

- (a)  $\exists D$  such that  $G(s)G^T(-s) = \sigma^2 I \forall s$ , where  $G(s) \triangleq C(sI - A)^{-1}B + D$ .

- (b)  $\exists P, Q \in \mathfrak{R}^{n \times n}$  such that

- i.  $P = P^T, Q = Q^T$ ,

- ii.  $AP + PA^T + BB^T = 0$ ,

- iii.  $A^TQ + QA + C^TC = 0$ ,

- iv.  $PQ = \sigma^2 I$ .

2. *Given that part 1(b) is satisfied, then  $\exists D$  satisfying*

$$D^T D = \sigma^2 I,$$

$$D^T C + B^T Q = 0,$$

and

$$DB^T + CP = 0,$$

and any such  $D$  will satisfy part 1(a) (note, observability and controllability are not assumed). ■

### 5B Error bound for balanced residualization

We shall first show that residualization of a balanced realization is balanced and preserves the Hankel singular values. Then we shall use this and several other results to show that

the difference between a residualized balanced realization of degree  $n - l$  and an optimal Hankel-norm approximation of the same degree is all-pass. This can then be used to derive an error bound for balanced residualization.

**Lemma 5B.1** *Let  $(A, B, C)$  be a balanced realization of a stable, rational transfer function  $G(s)$  with gramian  $\Sigma$ , partitioned as in §5.2, and let  $(A_r, B_r, C_r, D_r)$  be defined by equations (5.2.5)–(5.2.8). Then  $\Sigma_1$  satisfies the following Lyapunov equations:*

$$A_r \Sigma_1 + \Sigma_1 A_r^T + B_r B_r^T = 0, \quad (5B.1)$$

$$A_r^T \Sigma_1 + \Sigma_1 A_r + C_r^T C_r = 0. \quad (5B.2)$$

*Proof*

Since  $(A, B, C)$  is balanced, (5.2.1) and (5.2.2) hold. Rewriting (5.2.1) we have:

$$\begin{bmatrix} A_{11} & A_{12} \\ A_{21} & A_{22} \end{bmatrix} \begin{bmatrix} \Sigma_1 & 0 \\ 0 & \Sigma_2 \end{bmatrix} + \begin{bmatrix} \Sigma_1 & 0 \\ 0 & \Sigma_2 \end{bmatrix} \begin{bmatrix} A_{11}^T & A_{21}^T \\ A_{12}^T & A_{22}^T \end{bmatrix} + \begin{bmatrix} B_1 \\ B_2 \end{bmatrix} \begin{bmatrix} B_1^T & B_2^T \end{bmatrix} = 0 \quad (5B.3)$$

Multiplying both sides of the above equation on the left by  $\begin{bmatrix} I & -A_{12}A_{22}^{-1} \\ 0 & I \end{bmatrix}$  and on the right by  $\begin{bmatrix} I & 0 \\ -A_{22}^{-T}A_{12}^T & I \end{bmatrix}$  and picking out the (1,1) block, we have:

$$(A_{11} - A_{12}A_{22}^{-1}A_{21})\Sigma_1 + \Sigma_1(A_{11} - A_{12}A_{22}^{-1}A_{21})^T + (B_1 - A_{12}A_{22}^{-1}B_2)(B_1 - A_{12}A_{22}^{-1}B_2)^T = 0,$$

and thus, equation (5B.1) is satisfied.

To prove (5B.2), we left-multiply both sides of (5.2.2) by  $\begin{bmatrix} I & -A_{21}^T A_{22}^{-T} \\ 0 & I \end{bmatrix}$  and right-multiply by  $\begin{bmatrix} I & 0 \\ -A_{22}^{-1}A_{21} & I \end{bmatrix}$ , and pick the (1,1) block again to give:

$$(A_{11} - A_{12}A_{22}^{-1}A_{21})^T \Sigma_1 + \Sigma_1(A_{11} - A_{12}A_{22}^{-1}A_{21}) + (C_1 - C_2A_{22}^{-1}A_{21})^T(C_1 - C_2A_{22}^{-1}A_{21}) = 0,$$

and the proof is complete. ■

Thus, it is seen that the residualized system, like the truncated system, is balanced (with a positive-definite gramian  $\Sigma_1$ ), and hence stable.

**Lemma 5B.2** *Let  $(A, B, C)$  be a balanced realization of a stable, rational,  $m \times m$  transfer function  $G(s)$ , and let*

$$A = \begin{bmatrix} A_{11} & A_{12} \\ A_{21} & A_{22} \end{bmatrix}, \quad B = \begin{bmatrix} B_1 \\ B_2 \end{bmatrix}, \quad C = \begin{bmatrix} C_1 & C_2 \end{bmatrix}, \quad \Sigma = \begin{bmatrix} \Sigma_1 & 0 \\ 0 & \sigma I \end{bmatrix},$$

with  $\delta(\Sigma_1 - \sigma I) = 0$ . Let  $(A_r, B_r, C_r, D_r)$  and  $(\hat{A}, \hat{B}, \hat{C}, \hat{D})$  be defined by equations (5.2.5)–(5.2.8) and (5.3.4)–(5.3.7) respectively, and define:

$$\begin{aligned} G_r(s) &\triangleq C_r(sI - A_r)^{-1}B_r + D_r, \\ G_h(s) &\triangleq \hat{C}(sI - \hat{A})^{-1}\hat{B} + \hat{D}, \end{aligned}$$

then

1.  $(G_r(s) - G_h(s))/\sigma$  is all-pass.
2.  $\|G(s) - G_r(s)\|_\infty \leq 2\sigma$ .
3.  $\|G(s) - G_r(s)\|_H \leq 2\sigma$  ( $\|\cdot\|_H$  denotes the Hankel-norm).

*Proof*

$G_h$  defined above is an optimal Hankel-norm approximation to  $G$  and is identical to that defined in (5.3.16). Note however that here  $F = 0$  as  $\sigma$  is the smallest Hankel singular value (by definition of balanced realizations).

1. In order to prove that  $(G_r(s) - G_h(s))/\sigma$  is all-pass, we note that  $G_r(s) - G_h(s) = \tilde{C}(sI - \tilde{A})^{-1}\tilde{B} + \tilde{D}$  where

$$\tilde{A} = \begin{bmatrix} A_r & 0 \\ 0 & \hat{A} \end{bmatrix}, \quad \tilde{B} = \begin{bmatrix} B_r \\ \hat{B} \end{bmatrix}, \quad \tilde{C} = [C_r \quad -\hat{C}], \quad \tilde{D} = D_r - \hat{D}.$$

We shall prove the all-pass property by first showing that the solutions to the Lyapunov equations

$$\tilde{A}\tilde{P} + \tilde{P}\tilde{A}^T + \tilde{B}\tilde{B}^T = 0 \tag{5B.4}$$

$$\tilde{A}^T\tilde{Q} + \tilde{Q}\tilde{A} + \tilde{C}^T\tilde{C} = 0 \tag{5B.5}$$

are

$$\tilde{P} = \begin{bmatrix} \Sigma_1 & I \\ I & \Sigma_1 \Gamma^{-1} \end{bmatrix}, \quad \tilde{Q} = \begin{bmatrix} \Sigma_1 & -\Gamma \\ -\Gamma & \Sigma_1 \Gamma \end{bmatrix}, \quad (5B.6)$$

(where  $\Gamma$  is defined as in (5.3.9)), and then using Theorem 5A.1 to show that  $\tilde{D}$  is an appropriate choice. To prove (5B.4), we rewrite it as follows:

$$\begin{aligned} & \begin{bmatrix} A_r & 0 \\ 0 & \hat{A} \end{bmatrix} \begin{bmatrix} \Sigma_1 & I \\ I & \Sigma_1 \Gamma^{-1} \end{bmatrix} + \begin{bmatrix} \Sigma_1 & I \\ I & \Sigma_1 \Gamma^{-1} \end{bmatrix} \begin{bmatrix} A_r^T & 0 \\ 0 & \hat{A}^T \end{bmatrix} \\ & + \begin{bmatrix} B_r \\ \hat{B} \end{bmatrix} \begin{bmatrix} B_r^T & \hat{B}^T \end{bmatrix} \end{aligned} \quad (5B.7)$$

$$= \begin{bmatrix} A_r \Sigma_1 & A_r \\ \hat{A} & \hat{A} \Sigma_1 \Gamma^{-1} \end{bmatrix} + \begin{bmatrix} \Sigma_1 A_r^T & \hat{A}^T \\ A_r^T & \Sigma_1 \Gamma^{-1} \hat{A}^T \end{bmatrix} + \begin{bmatrix} B_r B_r^T & B_r \hat{B}^T \\ \hat{B} B_r^T & \hat{B} \hat{B}^T \end{bmatrix} \quad (5B.8)$$

The (1,1) block of the above expression has been proved to be equal to zero in Lemma 5B.1, the (1,2) and (2,1) blocks are proved to be zero in Appendix 5C.1. The (2,2) block is zero from equation (5C.1), block (3,3).

To prove (5B.5), we rewrite it as:

$$\begin{aligned} & \begin{bmatrix} A_r^T & 0 \\ 0 & \hat{A}^T \end{bmatrix} \begin{bmatrix} \Sigma_1 & -\Gamma \\ -\Gamma & \Sigma_1 \Gamma \end{bmatrix} + \begin{bmatrix} \Sigma_1 & -\Gamma \\ -\Gamma & \Sigma_1 \Gamma \end{bmatrix} \begin{bmatrix} A_r & 0 \\ 0 & \hat{A} \end{bmatrix} \\ & + \begin{bmatrix} C_r^T \\ -\hat{C}^T \end{bmatrix} \begin{bmatrix} C_r & -\hat{C} \end{bmatrix} \end{aligned} \quad (5B.9)$$

$$= \begin{bmatrix} A_r^T \Sigma_1 & -A_r^T \Gamma \\ -\hat{A}^T \Gamma & \hat{A}^T \Sigma_1 \Gamma \end{bmatrix} + \begin{bmatrix} \Sigma_1 A_r & -\Gamma \hat{A} \\ -\Gamma A_r & \Sigma_1 \Gamma \hat{A} \end{bmatrix} + \begin{bmatrix} C_r^T C_r & -C_r^T \hat{C} \\ -\hat{C}^T C_r & \hat{C}^T \hat{C} \end{bmatrix} \quad (5B.10)$$

The (1,1) block of the above expression is proved to equal zero in Lemma 5B.1, and the (1,2) and (2,1) blocks are proved to be zero in Appendix 5C.2. The (2,2) block is readily seen to be equal to zero from equation (5C.2), block (3,3).

Now it can be seen that  $\tilde{P}$  and  $\tilde{Q}$  also satisfy  $\tilde{P}\tilde{Q} = \sigma^2 I$  and by Theorem 5A.1, there exists a  $\tilde{D}$  such that  $(G_r(s) - G_h(s))/\sigma$  is all-pass. We can now show that  $\tilde{D} = D_r - \hat{D}$  is an appropriate choice from Theorem 5A.1, part 2, by showing that  $\tilde{D}$  satisfies the equations:

$$\tilde{D}^T \tilde{D} = \sigma^2 I, \quad (5B.11)$$

$$\tilde{D}^T \tilde{C} + \tilde{B}^T \tilde{Q} = 0, \quad (5B.12)$$

$$\tilde{D} \tilde{B}^T + \tilde{C} \tilde{P} = 0. \quad (5B.13)$$

The proofs of these equations can be found in Appendices 5C.3, 5C.4 and 5C.5 respectively.

2.  $(G(s) - G_r(s))/\sigma = ((G(s) - G_h(s))/\sigma + (G_h(s) - G_r(s))/\sigma)$ , but the first term on the right-hand side is all-pass by Theorem 5.3.1 equation (5.3.15), and the second term is all-pass by part 1 above. Hence

$$\|G(s) - G_r(s)\|_\infty \leq 2\sigma.$$

3. Using the fact that all-pass functions have unity Hankel-norms gives:

$$\begin{aligned} \|G(s) - G_r(s)\|_H &\leq \|G(s) - G_h(s)\|_H + \|G_h(s) - G_r(s)\|_H \\ &= 2\sigma. \end{aligned}$$

■

Given the result of Lemma 5B.2, the bound on the error in a residualized balanced realization is easily proved as follows.

**Theorem 5B.3** *Let  $G(s)$  be a stable, rational,  $p \times m$ , transfer function with Hankel singular values  $\sigma_1 > \sigma_2 > \dots > \sigma_N$ , where each  $\sigma_i$  has multiplicity  $r_i$  and let  $\tilde{G}_k(s)$  be obtained by residualizing the balanced realization of  $G(s)$  to the first  $(r_1 + r_2 + \dots + r_k)$  states. Then*

1.  $\|G(s) - \tilde{G}_k(s)\|_\infty \leq 2(\sigma_{k+1} + \sigma_{k+2} + \dots + \sigma_N)$ .

2.  $\|G(s) - \tilde{G}_k(s)\|_H \leq 2(\sigma_{k+1} + \sigma_{k+2} + \dots + \sigma_N)$ .

*Proof*

If  $p \neq m$  then augmenting  $B$  or  $C$  by zero columns or rows, respectively, will still give a balanced realization and the same argument is valid. Hence we assume  $p = m$ . We have already seen in Lemma 5B.1 that residualizations of balanced realizations are also balanced, satisfying the smaller (residualized) Lyapunov equations, therefore, the Hankel singular values of  $\tilde{G}_i(s)$  will be  $\sigma_1, \sigma_2, \dots, \sigma_i$  with multiplicities  $r_1, r_2, \dots, r_i$ , respectively. Also  $\tilde{G}_i(s)$  can be obtained by residualizing the balanced realization of  $\tilde{G}_{i+1}(s)$  and hence

by Lemma 5B.2,  $\|\tilde{G}_{i+1}(s) - \tilde{G}_i(s)\| \leq 2\sigma_{i+1}$  for both  $L_\infty$ - and Hankel-norms. Therefore, with the simplifying notation  $\tilde{G}_N(s) \triangleq G(s)$ , we have:

$$\begin{aligned} \|G(s) - \tilde{G}_k(s)\| &= \left\| \sum_{k \leq i \leq N-1} (\tilde{G}_{i+1}(s) - \tilde{G}_i(s)) \right\| \\ &\leq 2(\sigma_{k+1} + \sigma_{k+2} + \dots + \sigma_N). \end{aligned}$$

for both norms, and the proof is complete.  $\blacksquare$

It is therefore seen that the  $L_\infty$ -norm of the error in residualized balanced realizations is bounded by twice the sum of the Hankel singular values of the states that have been residualized. This is identical to the bound on balanced truncation.

## 5C Manipulation of equations and some useful results

We will first give detailed expressions for equations (5.3.10) and (5.3.11). Substituting  $A_e$ ,  $B_e$  and  $P_e$  in (5.3.10), we get:

$$\begin{aligned} \begin{bmatrix} A_{11}\Sigma_1 & \sigma A_{12} & A_{11} \\ A_{21}\Sigma_1 & \sigma A_{22} & A_{21} \\ \hat{A} & 0 & \hat{A}\Sigma_1\Gamma^{-1} \end{bmatrix} &+ \begin{bmatrix} \Sigma_1 A_{11}^T & \Sigma_1 A_{21}^T & \hat{A}^T \\ \sigma A_{12}^T & \sigma A_{22}^T & 0 \\ A_{11}^T & A_{21}^T & \Sigma_1\Gamma^{-1}\hat{A}^T \end{bmatrix} \\ &+ \begin{bmatrix} B_1 B_1^T & B_1 B_2^T & B_1 \hat{B}^T \\ B_2 B_1^T & B_2 B_2^T & B_2 \hat{B}^T \\ \hat{B} B_1^T & \hat{B} B_2^T & \hat{B} \hat{B}^T \end{bmatrix} = 0. \end{aligned} \quad (5C.1)$$

Substituting  $A_e$ ,  $C_e$  and  $Q_e$  in (5.3.11), we get:

$$\begin{aligned} \begin{bmatrix} A_{11}^T \Sigma_1 & \sigma A_{21}^T & -A_{11}^T \Gamma \\ A_{12}^T \Sigma_1 & \sigma A_{22}^T & -A_{12}^T \Gamma \\ -\hat{A}^T \Gamma & 0 & \hat{A}^T \Sigma_1 \Gamma \end{bmatrix} &+ \begin{bmatrix} \Sigma_1 A_{11} & \Sigma_1 A_{12} & -\Gamma \hat{A} \\ \sigma A_{21} & \sigma A_{22} & 0 \\ -\Gamma A_{11} & -\Gamma A_{12} & \Sigma_1 \Gamma \hat{A} \end{bmatrix} \\ &+ \begin{bmatrix} C_1^T C_1 & C_1^T C_2 & -C_1^T \hat{C} \\ C_2^T C_1 & C_2^T C_2 & -C_2^T \hat{C} \\ -\hat{C}^T C_1 & -\hat{C}^T C_2 & \hat{C}^T \hat{C} \end{bmatrix} = 0. \end{aligned} \quad (5C.2)$$

### 5C.1 Expression (5B.8): (1,2)/(2,1) blocks

Using equation (5.2.6), we can write:

$$B_r \hat{B}^T = (B_1 - A_{12} A_{22}^{-1} B_2) \hat{B}^T$$

$$\begin{aligned}
&= B_1 \hat{B}^T - A_{12} A_{22}^{-1} B_2 \hat{B}^T \\
(5C.1) \text{ block}(1, 3) &\implies = -A_{11} - \hat{A}^T - A_{12} A_{22}^{-1} B_2 \hat{B}^T \\
(5C.1) \text{ block}(2, 3) &\implies = -A_{11} - \hat{A}^T + A_{12} A_{22}^{-1} A_{21} \\
&= -A_r - \hat{A}^T. \tag{5C.3}
\end{aligned}$$

Therefore, we have:

$$A_r + \hat{A}^T + B_r \hat{B}^T = 0.$$

### 5C.2 Expression (5B.10): (1,2)/(2,1) blocks

Using equation (5.2.7), we can write:

$$\begin{aligned}
C_r^T \hat{C} &= (C_1^T - A_{21}^T A_{22}^{-T} C_2^T) \hat{C} \\
&= C_1^T \hat{C} - A_{21}^T A_{22}^{-T} C_2^T \hat{C} \\
(5C.2) \text{ block}(1, 3) &\implies = -A_{11}^T \Gamma - \Gamma \hat{A} - A_{21}^T A_{22}^{-T} C_2^T \hat{C} \\
(5C.2) \text{ block}(2, 3) &\implies = -A_{11}^T \Gamma - \Gamma \hat{A} + A_{21}^T A_{22}^{-T} A_{12}^T \Gamma \\
&= -(A_{11}^T - A_{21}^T A_{22}^{-T} A_{12}^T) \Gamma - \Gamma \hat{A} \\
&= -A_r^T \Gamma - \Gamma \hat{A}. \tag{5C.4}
\end{aligned}$$

Thus we have:

$$A_r^T \Gamma + \Gamma \hat{A} + C_r^T \hat{C} = 0.$$

### 5C.3 Proof of equation (5B.11)

Note that the (2,2) blocks of (5.3.1) and (5.3.2) give:

$$\sigma A_{22} + \sigma A_{22}^T + B_2 B_2^T = 0, \tag{5C.5}$$

$$\sigma A_{22}^T + \sigma A_{22} + C_2^T C_2 = 0. \tag{5C.6}$$

Using (5.2.8) and (5.3.7), we can write:

$$\begin{aligned}
\tilde{D}^T \tilde{D} &= (\sigma U^T - B_2^T A_{22}^{-T} C_2^T) (\sigma U - C_2 A_{22}^{-1} B_2) \\
&= -\sigma U^T C_2 A_{22}^{-1} B_2 + \sigma^2 U^T U + B_2^T A_{22}^{-T} C_2^T C_2 A_{22}^{-1} B_2 - \sigma B_2^T A_{22}^{-T} C_2^T U \\
(5.3.8) \ \&\ (5C.6) \implies &= \sigma B_2^T A_{22}^{-1} B_2 + \sigma^2 I + \sigma B_2^T A_{22}^{-T} (-A_{22}^T - A_{22}) A_{22}^{-1} B_2 + \sigma B_2^T A_{22}^{-T} B_2 \\
&= \sigma^2 I.
\end{aligned}$$

### 5C.4 Proof of equation (5B.12)

The (2,1) block of equation (5.3.2) gives:

$$A_{12}^T \Sigma_1 + \sigma A_{21} + C_2^T C_1 = 0. \quad (5C.7)$$

Rewriting (5B.12), we have:

$$(D_r - \hat{D})^T [C_r \quad -\hat{C}] + [B_r^T \quad \hat{B}^T] \begin{bmatrix} \Sigma_1 & -\Gamma \\ -\Gamma & \Sigma_1 \Gamma \end{bmatrix} = 0. \quad (5C.8)$$

Let us first prove the (1,1) block of the above equation. Substituting the values of  $D_r$ ,  $C_r$  and  $B_r$ , we get:

$$\begin{aligned} & (D_r - \hat{D})^T C_r + B_r^T \Sigma_1 - \hat{B}^T \Gamma \\ &= (D - \hat{D})^T C_1 - (D - \hat{D})^T C_2 A_{22}^{-1} A_{21} - (C_2 A_{22}^{-1} B_2)^T C_1 + (C_2 A_{22}^{-1} B_2)^T C_2 A_{22}^{-1} A_{21} + \\ & \quad B_1^T \Sigma_1 - (A_{12} A_{22}^{-1} B_2)^T \Sigma_1 - \hat{B}^T \Gamma. \end{aligned}$$

It can easily be verified that  $(D - \hat{D})^T C_1 + B_1^T \Sigma_1 - \hat{B}^T \Gamma = 0$ . Using this and (5.3.7), we can write the above as:

$$\begin{aligned} & -\sigma U^T C_2 A_{22}^{-1} A_{21} - (C_2 A_{22}^{-1} B_2)^T C_1 + B_2^T A_{22}^{-T} C_2^T C_2 A_{22}^{-1} A_{21} \\ & - (A_{12} A_{22}^{-1} B_2)^T \Sigma_1 \\ (5.3.8) \ \& \ (5C.6) \implies &= \sigma B_2^T A_{22}^{-1} A_{21} - (C_2 A_{22}^{-1} B_2)^T C_1 - (A_{12} A_{22}^{-1} B_2)^T \Sigma_1 \\ & - \sigma B_2^T A_{22}^{-T} (A_{22}^T + A_{22}) A_{22}^{-1} A_{21} \\ &= -B_2^T A_{22}^{-T} C_2^T C_1 - (A_{12} A_{22}^{-1} B_2)^T \Sigma_1 - \sigma B_2^T A_{22}^{-T} A_{21} \\ (5C.7) \implies &= B_2^T A_{22}^{-T} (A_{12}^T \Sigma_1 + \sigma A_{21}) - (A_{12} A_{22}^{-1} B_2)^T \Sigma_1 - \sigma B_2^T A_{22}^{-T} A_{21} \\ &= 0. \end{aligned}$$

We now prove the (1,2) block of (5C.8). Using the definitions of  $B_r$  and  $D_r$ , we have:

$$\begin{aligned} & -(D_r - \hat{D})^T \hat{C} - B_r^T \Gamma + \hat{B}^T \Sigma_1 \Gamma \\ &= -(D - \hat{D})^T \hat{C} + (C_2 A_{22}^{-1} B_2)^T \hat{C} - B_1^T \Gamma + (A_{12} A_{22}^{-1} B_2)^T \Gamma + \hat{B}^T \Sigma_1 \Gamma. \end{aligned}$$

It can readily be verified that  $-(D - \hat{D})^T \hat{C} - B_1^T \Gamma + \hat{B}^T \Sigma_1 \Gamma = 0$ . Thus the above expression becomes:

$$B_2^T A_{22}^{-T} C_2^T \hat{C} + (A_{12} A_{22}^{-1} B_2)^T \Gamma$$

$$\begin{aligned}
(5C.2)block(2, 3) \implies &= -B_2^T A_{22}^{-T} A_{12}^T \Gamma + B_2^T A_{22}^{-T} A_{12}^T \Gamma \\
&= 0.
\end{aligned}$$

### 5C.5 Proof of equation (5B.13)

Left-multiplying (5B.12) by  $\tilde{D}$  and right-multiplying by  $\tilde{P}$  yields

$$\tilde{D}\tilde{D}^T\tilde{C}\tilde{P} + \tilde{D}\tilde{B}^T\tilde{Q}\tilde{P} = 0. \quad (5C.9)$$

It can be verified that  $\tilde{Q}\tilde{P} = \sigma^2 I$  and, since  $\tilde{D}$  is square, (5B.11) implies  $\tilde{D}\tilde{D}^T = \sigma^2 I$ .

Now (5C.9) becomes:

$$\tilde{D}\tilde{B}^T + \tilde{C}\tilde{P} = 0,$$

and (5B.13) is proved.

## Chapter 6

# Robust two degrees-of-freedom discrete time controller synthesis

### 6.1 Introduction

Over the past few years, there has been considerable progress towards the design of robust controllers for multi-input multi-output systems. Design methods, such as  $H_\infty$ -optimization and  $\mu$ -synthesis, have been developed and translated into commercial software packages. These modern techniques are powerful in that they are inherently multi-variable and guarantee a degree of robustness against a specified uncertainty structure. They are thus best suited to address the control problems associated with ever more complex multivariable systems, such as high performance aero-engines.

However, there has been a very limited acceptance of these methods by the industrial sector. High state dimension of the resulting controllers together with the absence of any readily recognizable controller structure have both contributed to this cause. Control solutions provided by these methods are generally considered by practitioners to be too complex with regards to implementation. This problem of complexity becomes even more pronounced when dealing with multi-mode problems where a number of controllers have to be run in parallel. This could make the structure of the overall controller very obscure and the computational load associated with it can easily get out of hand. If however, all these controllers have a well-defined basic structure, considerable simplifications in the overall switched controller can be made.

The ability to synthesize controllers with a simple and well-defined structure is therefore, of great engineering importance and motivates the work described in this chapter. Since the control law is finally to be implemented in discrete time, the results presented here are developed in a discrete time framework.

This chapter is organized as follows. §6.2 contains the necessary background to robust stabilization in the normalized coprime factor framework. In §6.3 the idea of loop-shaping in the context of  $H_\infty$ -optimization is motivated. §6.4 describes the two degrees-of-freedom controller configuration that we use and formulates the problem as a standard  $H_\infty$ -optimization problem. Results on  $H_\infty$  full information control and the disturbance feedforward problem are presented in §6.6 and §6.7 respectively. In §6.8 we show that the discrete central two degrees-of-freedom  $H_\infty$  loop-shaping controller has an observer-based structure. A similar development in the continuous domain is presented in [105]. §6.9 outlines the design procedure and §6.10 summarizes the main points of the chapter.

## 6.2 Robust stabilization in the normalized coprime factor framework

In the sequel, we will denote by  $RH_\infty$ , the space of all rational functions which are analytic and bounded for all  $|z| > 1$ . The notation

$$G(z) = C(zI - A)^{-1}B + D \stackrel{s}{=} \left[ \begin{array}{c|c} A & B \\ \hline C & D \end{array} \right]$$

will be used to denote the state-space representation of a transfer function.

We will concentrate on the  $H_\infty$  loop-shaping design procedure introduced by McFarlane & Glover [64] and later extended to the two degrees-of-freedom case by Hoyle et al. [45]. The procedure is intuitive in that it is based on the multivariable generalization of classical loop-shaping ideas. The open-loop plant, once given the desired loop-shape, is robustly stabilized against coprime factor uncertainty. The resulting controller has been shown to enjoy some favourable properties, such as no pole-zero cancellation occurs in the closed-loop system (except for a certain special class of plants) [101]. In addition, the controllers thus designed have been successful in various applications; examples are those

described in [103, 104], [69] and [46, 111]. Moreover, the two degrees-of-freedom structure allows performance specifications to be explicitly introduced into the  $H_\infty$ -optimization framework.

Representing uncertainty in the plant model in terms of perturbations on its normalized coprime factors has advantages over other representations, as discussed in Chapter 2. We now give a state-space construction for the normalized left coprime factorization [107]. Given  $G(z) = C(zI - A)^{-1}B + D$ , let  $R_1 \triangleq I + D^T D$ ,  $R_2 \triangleq I + DD^T$ , and let  $P = P^T$  be the non-negative definite stabilizing solution to the algebraic Riccati equation:

$$BR_1^{-1}B^T - P + \Phi P \Phi^T - \Phi P C^T (R_2 + C P C^T)^{-1} C P \Phi^T = 0, \quad (6.2.1)$$

then

$$[\tilde{N} \quad \tilde{M}] \stackrel{s}{=} \left[ \begin{array}{c|cc} A + HC & B + HD & H \\ \hline Z_2 C & Z_2 D & Z_2 \end{array} \right] \quad (6.2.2)$$

is a normalized left coprime factorization of  $G$ , where  $\Phi = A - BR_1^{-1}D^T C$ ,  $H = -(APC^T + BD^T)(R_2 + CPC^T)^{-1}$ , and  $Z_2$  satisfies

$$Z_2^T Z_2 = (R_2 + CPC^T)^{-1}.$$

If  $G$  is a plant transfer function, then the perturbations or uncertainties in the plant are represented as perturbations on the normalized coprime factors of the plant (Chapter 2). The perturbed plant  $G_\Delta$  is then given by

$$G_\Delta = (\tilde{M} + \Delta_{\tilde{M}})^{-1}(\tilde{N} + \Delta_{\tilde{N}}),$$

where  $\Delta_{\tilde{M}}, \Delta_{\tilde{N}}$  are stable unknown transfer functions representing uncertainty in the plant model  $G = \tilde{M}^{-1}\tilde{N}$ ; see Figure 2.2. We saw in Chapter 2 that robust stability to coprime factor perturbations is maximized by a controller  $K$  which stabilizes the nominal plant  $G$ , and minimizes

$$\gamma = \left\| \left[ \begin{array}{c} K \\ I \end{array} \right] (I - GK)^{-1} \tilde{M}^{-1} \right\|_\infty. \quad (6.2.3)$$

The perturbed closed-loop system is then guaranteed to remain stable in the face of all  $\Delta_{\tilde{M}}, \Delta_{\tilde{N}}$  such that

$$\|[\Delta_{\tilde{M}} \quad \Delta_{\tilde{N}}]\|_\infty < \gamma^{-1}.$$

An analytical expression for the lowest achievable value of  $\gamma$  referred to as  $\gamma_{opt}$  has been derived in [106] and is given by:

$$\gamma_{opt} = \sqrt{1 + \lambda_{max}(PQ)}, \quad (6.2.4)$$

where  $Q = Q^T$  is the non-negative definite stabilizing solution to the algebraic Riccati equation:

$$C^T R_2^{-1} C - Q + \Phi^T Q \Phi - \Phi^T Q B (R_1 + B^T Q B)^{-1} B^T Q \Phi = 0,$$

$\lambda_{max}(\cdot)$  denotes the largest eigenvalue, and  $R_1$ ,  $R_2$ ,  $\Phi$  and  $P$  are as defined above. State-space formulae for the central optimal and sub-optimal controllers are also presented in [106].

### 6.3 $H_\infty$ loop-shaping

The technique of loop-shaping has been used extensively in SISO feedback design. Over the last few years, the loop-shaping process has been successfully generalized to multi-variable design problems by using singular values as appropriate measures of magnitude for matrix-valued transfer functions [19]. However, it has been argued that singular value loop-shaping is an effective<sup>1</sup> MIMO design paradigm only for problems involving *spatially round* (i.e., well-conditioned) specifications on closed-loop transfer functions [97]. Stein [97] considers the problem of output sensitivity reduction in the presence of uncertainty and derives sufficient conditions for robust performance. It is seen that these conditions, which are in terms of acceptable shapes for the nominal sensitivity function, can be arbitrarily conservative for *skewed* problems, i.e., problems for which specifications are not spatially round. Such problems arise when the plant is ill-conditioned, and performance and robustness requirements are levied at different points in the feedback loop, e.g., performance required at the plant's output, uncertainties applied at its input, and vice versa. Freudenberg [29] has given some guidelines on how to shape the open-loop transfer function so that performance at one point is insensitive to uncertainty at another, given that the plant is ill-conditioned. His results, however, are based on several assumptions, such

---

<sup>1</sup>By effective we mean effective in designing for robust performance.

as the plant is assumed to have a natural partition into high- and low-gain sub-systems, and the gain within each sub-system is assumed to be uniform. The structured singular value [20, 13] has been put forward as a more effective tool to deal with such problems; it is however computationally expensive and results in controllers of high state dimension [111, 109].

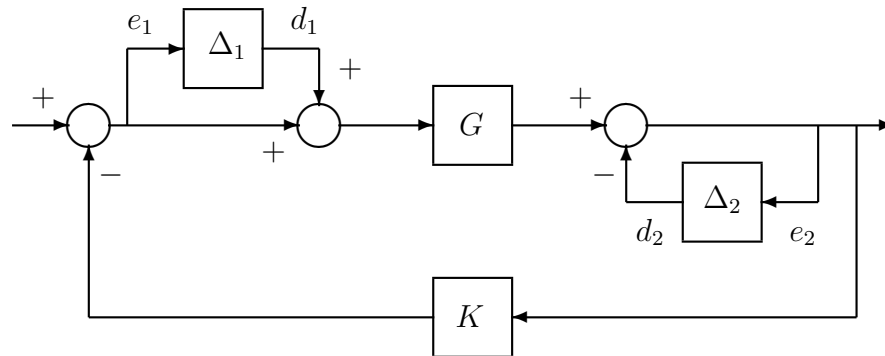


Figure 6.1: Simultaneous uncertainty at plant input and output.

Freudenberg [28] also considers the robust performance problem for ill-conditioned plants. He shows that the robust performance problem is synonymous to the *simultaneous uncertainty* problem, i.e., when modelling errors occur at different points in the feedback loop. Figure 6.1 illustrates simultaneous uncertainty at two different points in the loop, i.e., at the plant input and output. The perturbed plant  $G_\Delta$  is given by:

$$G_\Delta = (I + \Delta_2)^{-1}G(I + \Delta_1).$$

The transfer functions  $\Delta_1$  and  $\Delta_2$ , used to model the system uncertainty, represent the input and output perturbations respectively and are assumed to be stable and proper.  $\Delta_1$  is used to model actuator uncertainty and high frequency plant modelling errors.  $\Delta_2$  can represent modelling errors at the plant output but, as is more often, it is used to represent a performance specification, such as output disturbance rejection. The simultaneous uncertainty problem can thus be viewed as a robust performance problem where performance at the plant output has to be maintained in the presence of uncertainty at its input.

We now consider the loop-shaping approach in the context of coprime factor robust stabi-

lization, as developed by McFarlane & Glover [64]. In this case, performance specifications are translated into the frequency domain, and the open-loop plant's singular value frequency response is given the desired shape. This is achieved by augmentation of the nominal plant model  $G$  by pre- and/or post-compensators (or weighting functions)  $W_1$  and  $W_2$  respectively. Recently the use of numerical optimization techniques has been suggested for automating the choice of the weighting functions [86, 110, 109]. Having chosen the weights, the shaped plant  $G_s = W_2GW_1 = \tilde{M}^{-1}\tilde{N}$  is robustly stabilized against coprime factor uncertainty, and the controller  $K$  thus obtained is cascaded with the weights to obtain the final controller  $K_f = W_1KW_2$ . It can be shown that the controller does not significantly alter the specified loop-shape provided a sufficiently small value of  $\gamma$  is achieved. Note that  $W_1$  and  $W_2$  must be chosen such that  $G_s$  contains no hidden unstable modes.

We now look at the advantages the loop-shaping approach of McFarlane & Glover [64] has to offer over some of the other approaches to  $H_\infty$  design. During the last few years, several formulations for  $H_\infty$  controller synthesis have been proposed, the most widely used being the  $S/KS$  [83] and the  $S/T$  design procedures [87, 88]. A potential problem with these methods is that all the emphasis is placed at the output of the plant, and this can give rise to poor properties at the plant input. Also the choice of weighting functions is not always obvious and undesirable cancellation of plant poles can occur [94, 85].

With the loop-shaping design procedure (LSDP) of McFarlane & Glover [64], the designer specifies the open-loop shape  $W_2GW_1$ . The choice of weights is intuitive and relatively straightforward. The actual loop shape achieved, however, is given by  $W_1KW_2G$  at the plant input and  $GW_1KW_2$  at the plant output,  $K$  being the  $H_\infty$  controller. McFarlane & Glover [64] show that at frequencies where  $\underline{\sigma}(W_2GW_1) \gg 1$  or  $\bar{\sigma}(W_2GW_1) \ll 1$ , the deterioration in the loop shape due to  $K$  is bounded by a function of  $\gamma$  and the condition numbers of the weights only, a small value of  $\gamma$  and well-conditioned weights indicate minimal deterioration in the loop shape, *both* at the plant input and output. Thus with this approach, good nominal properties can be achieved easily at both points. Further it can be shown that the robust stabilization objective (6.2.3) is equivalent to the more standard  $H_\infty$  4-block problem of minimizing the  $L_\infty$ -norm of the frequency-weighted gain from disturbances on the plant input and output to the controller input and output as

follows [63]:

$$\left\| \begin{bmatrix} I \\ K \end{bmatrix} (I - G_s K)^{-1} \tilde{M}^{-1} \right\|_{\infty} \quad (6.3.1)$$

$$= \left\| \begin{bmatrix} I \\ K \end{bmatrix} (I - G_s K)^{-1} \begin{bmatrix} I & G_s \end{bmatrix} \right\|_{\infty} \quad (6.3.2)$$

$$= \left\| \begin{bmatrix} W_2 \\ W_1^{-1} K_f \end{bmatrix} (I - G K_f)^{-1} \begin{bmatrix} W_2^{-1} & G W_1 \end{bmatrix} \right\|_{\infty} \quad (6.3.3)$$

$$= \left\| \begin{bmatrix} I \\ G_s \end{bmatrix} (I - K G_s)^{-1} \begin{bmatrix} I & K \end{bmatrix} \right\|_{\infty} \quad (6.3.4)$$

$$= \left\| \begin{bmatrix} W_1^{-1} \\ W_2 G \end{bmatrix} (I - K_f G)^{-1} \begin{bmatrix} W_1 & K_f W_2^{-1} \end{bmatrix} \right\|_{\infty}. \quad (6.3.5)$$

This shows how the common closed-loop transfer function objectives are incorporated into the loop-shaping design procedure. From (6.3.2) and (6.3.4) it is seen that solving the normalized coprime factor robust stabilization problem is equivalent to achieving good feedback properties both at the input and output of the shaped plant  $G_s$ . Thus important closed-loop transfer functions relating to both points in the feedback loop are incorporated into the design, e.g., the input and output sensitivities  $(I - K G_s)^{-1}$  and  $(I - G_s K)^{-1}$ , the gain from input disturbance to the plant output  $(I - G_s K)^{-1} G_s$ , and robustness measures for additive, input multiplicative, and output multiplicative perturbations  $K(I - G_s K)^{-1}$ ,  $K(I - G_s K)^{-1} G_s$ , and  $G_s(I - K G_s)^{-1} K$ , respectively. It can easily be seen that this incorporates the closed-loop transfer function from  $\begin{bmatrix} d_1 \\ d_2 \end{bmatrix}$  to  $\begin{bmatrix} e_1 \\ e_2 \end{bmatrix}$  in Figure 6.1, provided we take  $G$  in the figure to represent the shaped plant. Thus output disturbance rejection on the shaped plant is achieved in the face of input multiplicative uncertainty; this is a conservative solution to the simultaneous uncertainty problem and therefore, the loop-shaping design procedure is seen to provide a degree of robust performance.

It should be noted that we have so far considered performance and robustness objectives on the shaped plant  $W_2 G W_1$ , and not the nominal plant  $G$ . For implementation, however, the weights  $W_1$  and  $W_2$  are absorbed into the controller, and hence in the final analysis, closed-loop objectives involving the unshaped nominal plant  $G$  are the ones that must be satisfactory. McFarlane & Glover [63] show that the loop-shaping design procedure ensures that these closed-loop objectives are well-behaved. More specifically they show

that if

$$\left\| \begin{bmatrix} K \\ I \end{bmatrix} (I - G_s K)^{-1} \tilde{M}^{-1} \right\|_{\infty} \leq \gamma,$$

then

$$\bar{\sigma}(K_f(I - GK_f)^{-1}) \leq \gamma \bar{\sigma}(\tilde{M}) \bar{\sigma}(W_1) \bar{\sigma}(W_2), \quad (6.3.6)$$

$$\bar{\sigma}((I - GK_f)^{-1}) \leq \gamma \bar{\sigma}(\tilde{M}) \kappa(W_2), \quad (6.3.7)$$

$$\bar{\sigma}(K_f(I - GK_f)^{-1}G) \leq \gamma \bar{\sigma}(\tilde{N}) \kappa(W_1), \quad (6.3.8)$$

$$\bar{\sigma}((I - GK_f)^{-1}G) \leq \frac{\gamma \bar{\sigma}(\tilde{N})}{\underline{\sigma}(W_1) \underline{\sigma}(W_2)}, \quad (6.3.9)$$

$$\bar{\sigma}((I - K_f G)^{-1}) \leq 1 + \gamma \bar{\sigma}(\tilde{N}) \kappa(W_1), \quad (6.3.10)$$

$$\bar{\sigma}(G(I - K_f G)^{-1}K_f) \leq 1 + \gamma \bar{\sigma}(\tilde{M}) \kappa(W_2), \quad (6.3.11)$$

where  $(\tilde{M}, \tilde{N})$  is a normalized coprime factorization of  $G_s = W_2 G W_1$ ,  $K_f = W_1 K W_2$ , and  $\kappa(\cdot)$  denotes the condition number. (6.3.6), (6.3.8) and (6.3.11) above are bounds on the additive, input multiplicative and output multiplicative robustness measures respectively for the unshaped plant  $G$ , while (6.3.7), (6.3.9) and (6.3.10) give bounds on various performance measures. Given that  $\bar{\sigma}(\tilde{M}) \leq 1$  and  $\bar{\sigma}(\tilde{N}) \leq 1$ , it follows that if  $\gamma$  is small and the weights are well-conditioned, then all the above closed-loop objectives are well-behaved, i.e., they have bounded magnitude. Further it can be shown that these objectives can be shaped at low and high frequencies by appropriate choice of the weights  $W_1$  and  $W_2$ . We therefore see that the LSDP ensures good feedback properties both at the input and output of the plant  $G$ . Also the selection of weights is relatively simple and pole-zero cancellations are avoided in most cases. In conclusion, we can therefore say that the LSDP is an intuitive and effective design technique.

## 6.4 Two degrees-of-freedom configuration

We will now discuss the two degrees-of-freedom configuration (Figure 5.10) which we briefly considered in §5.5.2. The formulation includes a model matching problem in addition to the robust stability maximization problem outlined above. This is discussed for the continuous time case in [45, 60]. The controller  $K$  is partitioned as  $K = [K_1 \quad K_2]$  where  $K_1$  is the pre-filter, and  $K_2$  the feedback controller.  $M_o(z)$  is a reference model chosen to

have ideal time-domain response characteristics, which the closed-loop system is desired to follow.  $G_s = GW_1 = \tilde{M}^{-1}\tilde{N}$  is the shaped plant. For the two degrees-of-freedom configuration, we assume in the first instance the plant to have no post-compensation as part of the weighting, i.e.,  $W_2 = I$ . We will later consider the case where  $W_2$  may also be used in shaping the plant gains. The problem is now formulated as a standard  $H_\infty$ -optimization problem such that  $L_\infty$ -norm of the transfer function relating  $u, y, e$  to  $r, \phi$ , namely

$$\left[ \begin{array}{c|c} \rho(I - K_2G_s)^{-1}K_1 & K_2(I - G_sK_2)^{-1}\tilde{M}^{-1} \\ \rho(I - G_sK_2)^{-1}G_sK_1 & (I - G_sK_2)^{-1}\tilde{M}^{-1} \\ \hline \rho^2((I - G_sK_2)^{-1}G_sK_1 - M_o) & \rho(I - G_sK_2)^{-1}\tilde{M}^{-1} \end{array} \right] \quad (6.4.1)$$

is minimized. As discussed in §5.5.2, the (1,2) partition of (6.4.1) is associated with robust stabilization and the (2,1) partition with model matching. The aim is thus to provide robust stability and model following in face of the uncertainty  $\Delta_{\tilde{M}}, \Delta_{\tilde{N}}$ . The parameter  $\rho$  is a scaling used to emphasize the (2,1) partition of (6.4.1), thus emphasizing the model matching part of the problem.

To set the problem in an  $H_\infty$ -optimization framework, we will first put it into the standard regulator form given in §2.5 (Figure 2.3). As shown in the figure,  $w$  is the vector of all external signals ( $[r^T \ \phi^T]^T$  for our two degrees-of-freedom case) and  $z$  is a vector of all signals to be minimized ( $[u^T \ y^T \ e^T]^T$  for our case, as is apparent from the choice of the transfer function (6.4.1) we seek to minimize).  $u$  is the vector of control signals and  $q$  is the vector of measurements available to the controller ( $[\beta^T \ y^T]^T$  for our case, see Figure 5.10). The generalized plant  $P$  is thus given by

$$\begin{bmatrix} u \\ y \\ e \\ \beta \\ y \end{bmatrix} = \left[ \begin{array}{c|c} P_{11} & P_{12} \\ \hline P_{21} & P_{22} \end{array} \right] \begin{bmatrix} r \\ \phi \\ u \end{bmatrix}$$

$$= \left[ \begin{array}{cc|c} 0 & 0 & I \\ 0 & \tilde{M}^{-1} & G_s \\ -\rho^2 M_o & \rho \tilde{M}^{-1} & \rho G_s \\ \hline \rho I & 0 & 0 \\ 0 & \tilde{M}^{-1} & G_s \end{array} \right] \begin{bmatrix} r \\ \phi \\ u \end{bmatrix}. \quad (6.4.2)$$

Let the shaped plant  $G_s(z)$  and the reference model  $M_o(z)$  have state-space realizations  $G_s \stackrel{s}{=} \left[ \begin{array}{c|c} A & B \\ \hline C & 0 \end{array} \right]$  and  $M_o \stackrel{s}{=} \left[ \begin{array}{c|c} A_o & B_o \\ \hline C_o & D_o \end{array} \right]$  respectively, with  $M_o$  chosen stable, and let the normalized coprime factors of  $G_s$  be given by (6.2.2). A state-space realization for  $P$  is then given as follows:

$$P \stackrel{s}{=} \left[ \begin{array}{c|c|c} \tilde{A} & B_1 & B_2 \\ \hline C_1 & D_{11} & D_{12} \\ \hline C_2 & D_{21} & D_{22} \end{array} \right] = \left[ \begin{array}{cc|cc|c} A & 0 & 0 & -HZ_2^{-1} & B \\ 0 & A_o & B_o & 0 & 0 \\ \hline 0 & 0 & 0 & 0 & I \\ C & 0 & 0 & Z_2^{-1} & 0 \\ \hline \rho C & -\rho^2 C_o & -\rho^2 D_o & \rho Z_2^{-1} & 0 \\ 0 & 0 & \rho I & 0 & 0 \\ C & 0 & 0 & Z_2^{-1} & 0 \end{array} \right]. \quad (6.4.3)$$

The state vector  $x$  of  $P$  can be partitioned as  $\begin{bmatrix} x_G \\ x_o \end{bmatrix}$ , where  $x_G$  is the state of the shaped plant and  $x_o$  the state of the reference model. Note that we have assumed the shaped plant  $G_s$  to be strictly proper (no direct feedthrough). This is true for most physical systems, and the direct feedthrough term remains zero even after the system is discretized, assuming a zero-order hold on the inputs. The controller formulae are more complicated for systems that are not strictly proper, and these will not be considered here.

We now consider the case where the post-compensator  $W_2$  is also used in shaping the open-loop plant, i.e., the shaped plant is given by  $G_s = W_2 G W_1 = \tilde{M}^{-1} \tilde{N}$ . We will assume  $W_2$  to be invertible. The signal  $y$  in Figure 5.10 is now the output of the shaped plant, i.e., the actual plant output post-compensated by  $W_2$ . Hence it is the transfer function from the reference input  $r$  to the output of the shaped plant, denoted  $T_{r \rightarrow y}$ , that is being matched to the model  $M_o$ . It is, however, desired that the transfer function  $T_{r \rightarrow \tilde{y}}$  be matched to the chosen model,  $\tilde{y}$  being the actual plant output (i.e.,  $\tilde{y} = W_2^{-1} y$ ). This

can be done as follows. We define the model matching error  $e$  to be  $\rho(\tilde{y} - y_o)$  where  $y_o$  is the output of the reference model. Given  $y = Cx + Z_2^{-1}\phi$  (see (6.4.3)) and  $W_2$ , an expression for  $\tilde{y} = W_2^{-1}y$  can be obtained easily. The state-space realization for  $P$  as given in (6.4.3) can then be modified slightly to accommodate this new definition of  $e$ . This will be illustrated by an example in Chapter 7.

## 6.5 $H_\infty$ two degrees-of-freedom controller synthesis

We will now derive a state-space realization for the two degrees-of-freedom controller (Figure 5.10) that internally stabilizes the generalized plant given in (6.4.3), and achieves a given (sub-optimal)  $L_\infty$ -norm for the closed-loop transfer function relating the error signals ( $u$ ,  $y$  and  $e$ ) to the external inputs ( $r$  and  $\phi$ ). First however, we present some relevant results on full information control and the disturbance feedforward problem.

## 6.6 $H_\infty$ full information control

The full information control is characterized by the structure shown in Figure 6.2 where the controller  $K$  has access to both the present dynamic state  $x$  of the generalized plant  $P$ , and to the current disturbance input  $w$ . The discrete time full information control problem is discussed in detail by Walker [107]. Here we will briefly review the main results.

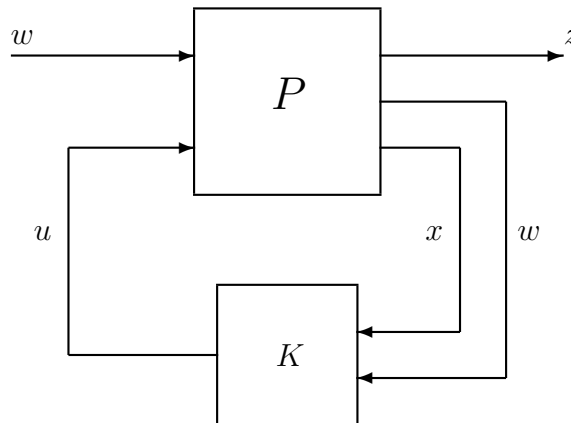


Figure 6.2: Full information control structure.

Let the general system for the full information problem (Figure 6.2) be described by the equations:

$$\begin{aligned}x_{k+1} &= \tilde{A}x_k + B_1w_k + B_2u_k, \\z_k &= C_1x_k + D_{11}w_k + D_{12}u_k.\end{aligned}\tag{6.6.1}$$

The notation is simplified using the ‘ $J$ ’ notation of Green et al. [35], defining:

$$\left[ \begin{array}{c|cc} \tilde{A} & \tilde{B} & \\ \hline \tilde{C} & \tilde{D} & \end{array} \right] \triangleq \left[ \begin{array}{c|cc} \tilde{A} & B_1 & B_2 \\ \hline C_1 & D_{11} & D_{12} \\ 0 & I & 0 \end{array} \right],\tag{6.6.2}$$

and

$$J_{pq}(\gamma) \triangleq \begin{bmatrix} I_p & 0 \\ 0 & -\gamma^2 I_q \end{bmatrix}.\tag{6.6.3}$$

The latter will simply be denoted by  $J$ . The full information control problem has a game-like nature. The disturbance  $w$  influences  $P$  so as to make the magnitude of the cost  $z$  large (in the sense of the 2-norm). The control input  $u$ , on the other hand, tries to keep  $z$  small. These conflicting aims are embodied in a cost (or performance) functional  $V$  associated with the game, which has the general form

$$V = \|z\|_2^2 - \gamma^2 \|w\|_2^2.$$

For the system described by (6.6.1), the cost functional is defined as:

$$V = \sum_{k=0}^{N-1} (z_k^T z_k - \gamma^2 w_k^T w_k) + x_N^T P_N x_N.$$

where the horizon is later on extended to infinity ( $N \rightarrow \infty$ ). Note that in order to prevent the state vector from possibly becoming unbounded in the limit as  $N$  tends to infinity, the cost functional includes a terminal state weighting  $P_N$ . Lagrange multipliers  $\lambda_k$  are now introduced to determine stationary values of the cost functional:

$$V = \sum_{k=0}^{N-1} \left( (z_k^T z_k - \gamma^2 w_k^T w_k) - 2\lambda_{k+1}^T (x_{k+1} - \tilde{A}x_k - B_1w_k - B_2u_k) \right) + x_N^T P_N x_N.$$

Assuming  $(C_1, \tilde{A})$  to be detectable (no unobservable unstable modes), input-output stability effectively implies internal stability, hence  $P_N$  can be made zero and the above

expression for the cost rewritten as:

$$V = \sum_{k=0}^{N-1} \left( \begin{bmatrix} z_k^T & w_k^T \end{bmatrix} J \begin{bmatrix} z_k \\ w_k \end{bmatrix} - 2\lambda_{k+1}^T (x_{k+1} - \tilde{A}x_k - \tilde{B}\delta_k) \right),$$

where  $\delta_k \triangleq [w_k^T \ u_k^T]^T$ . Note that this assumption of detectability remains in force throughout the rest of the chapter. Also

$$\begin{bmatrix} z_k \\ w_k \end{bmatrix} = \begin{bmatrix} C_1 & D_{11} & D_{12} \\ 0 & I & 0 \end{bmatrix} \begin{bmatrix} x_k \\ w_k \\ u_k \end{bmatrix} = \begin{bmatrix} \tilde{C} & \tilde{D} \end{bmatrix} \begin{bmatrix} x_k \\ \delta_k \end{bmatrix},$$

in which case we have:

$$V = \sum_{k=0}^{N-1} \left( (\tilde{C}x_k + \tilde{D}\delta_k)^T J (\tilde{C}x_k + \tilde{D}\delta_k) - 2\lambda_{k+1}^T (x_{k+1} - \tilde{A}x_k - \tilde{B}\delta_k) \right).$$

The first-order necessary conditions for a stationary point:

$$\begin{aligned} \frac{\partial V}{\partial x_k} &= 0, & k = 1, 2, \dots, N, \\ \frac{\partial V}{\partial \delta_k} &= 0, & k = 0, 1, \dots, N-1, \end{aligned}$$

lead as  $N$  is made infinite, to the following discrete time algebraic Riccati equation:

$$X_\infty = \tilde{A}^T X_\infty \tilde{A} + \tilde{C}^T J \tilde{C} - (\tilde{C}^T J \tilde{D} + \tilde{A}^T X_\infty \tilde{B}) (\tilde{D}^T J \tilde{D} + \tilde{B}^T X_\infty \tilde{B})^{-1} (\tilde{D}^T J \tilde{C} + \tilde{B}^T X_\infty \tilde{A}). \quad (6.6.4)$$

This can be rearranged to give:

$$X_\infty = \tilde{A}^T X_\infty \tilde{A} + \tilde{C}^T J \tilde{C} - F^T (\tilde{D}^T J \tilde{D} + \tilde{B}^T X_\infty \tilde{B}) F, \quad (6.6.5)$$

where

$$F \triangleq (\tilde{D}^T J \tilde{D} + \tilde{B}^T X_\infty \tilde{B})^{-1} (\tilde{D}^T J \tilde{C} + \tilde{B}^T X_\infty \tilde{A}). \quad (6.6.6)$$

The term  $(\tilde{D}^T J \tilde{D} + \tilde{B}^T X_\infty \tilde{B})$  may be factorized [34], with  $W = \begin{bmatrix} W_{11} & W_{12} \\ W_{21} & 0 \end{bmatrix}$ , as:

$$\begin{aligned} \tilde{D}^T J \tilde{D} + \tilde{B}^T X_\infty \tilde{B} &= W^T J W \\ &= \begin{bmatrix} W_{11}^T & W_{21}^T \\ W_{12}^T & 0 \end{bmatrix} \begin{bmatrix} I & 0 \\ 0 & -\gamma^2 I \end{bmatrix} \begin{bmatrix} W_{11} & W_{12} \\ W_{21} & 0 \end{bmatrix} \\ &= \begin{bmatrix} -\gamma^2 I + B_1^T X_\infty B_1 + D_{11}^T D_{11} & D_{11}^T D_{12} + B_1^T X_\infty B_2 \\ D_{12}^T D_{11} + B_2^T X_\infty B_1 & D_{12}^T D_{12} + B_2^T X_\infty B_2 \end{bmatrix}. \end{aligned} \quad (6.6.7)$$

The terms of  $W$  are found by solving the two Cholesky factorizations:

$$W_{12}^T W_{12} = D_{12}^T D_{12} + B_2^T X_\infty B_2, \quad (6.6.8)$$

$$W_{21}^T W_{21} = \gamma^{-2} \left[ (D_{11}^T D_{12} + B_1^T X_\infty B_2)(D_{12}^T D_{12} + B_2^T X_\infty B_2)^{-1} (D_{12}^T D_{11} + B_2^T X_\infty B_1) - D_{11}^T D_{11} + \gamma^2 I - B_1^T X_\infty B_1 \right], \quad (6.6.9)$$

and then

$$W_{11} = W_{12}^{-T} (D_{12}^T D_{11} + B_2^T X_\infty B_1). \quad (6.6.10)$$

(6.6.6) may now be rewritten as:

$$\begin{aligned} F &= W^{-1} J^{-1} W^{-T} (\tilde{D}^T J \tilde{C} + \tilde{B}^T X_\infty \tilde{A}) \\ &= \begin{bmatrix} 0 & W_{21}^{-1} \\ W_{12}^{-1} & -W_{12}^{-1} W_{11} W_{21}^{-1} \end{bmatrix} \begin{bmatrix} W_{12}^{-T} \Gamma_2 \\ -\gamma^{-2} W_{21}^{-T} \Gamma_1 + \gamma^{-2} W_{21}^{-T} W_{11}^T W_{12}^{-T} \Gamma_2 \end{bmatrix} \\ &= \begin{bmatrix} 0 & W_{21}^{-1} \\ W_{12}^{-1} & -W_{12}^{-1} W_{11} W_{21}^{-1} \end{bmatrix} \begin{bmatrix} L_1 \\ L_2 \end{bmatrix}, \end{aligned} \quad (6.6.11)$$

where  $\Gamma_1 \triangleq (D_{11}^T C_1 + B_1^T X_\infty \tilde{A})$ ,  $\Gamma_2 \triangleq (D_{12}^T C_1 + B_2^T X_\infty \tilde{A})$ ,  $L_1 \triangleq W_{12}^{-T} \Gamma_2$  and  $L_2 \triangleq -\gamma^{-2} W_{21}^{-T} \Gamma_1 + \gamma^{-2} W_{21}^{-T} W_{11}^T W_{12}^{-T} \Gamma_2$ . The following theorem summarizes the results on the full information problem.  $T_{zw}$  is used to denote the closed-loop transference from the disturbance  $w$  to the error  $z$  (Figure 6.2).

**Theorem 6.6.1 [107]** *Given  $\gamma$  such that*

$$-\gamma^2 I + B_1^T X_\infty B_1 + D_{11}^T D_{11} - (D_{11}^T D_{12} + B_1^T X_\infty B_2)(D_{12}^T D_{12} + B_2^T X_\infty B_2)^{-1} (D_{12}^T D_{11} + B_2^T X_\infty B_1) < 0,$$

where  $X_\infty = X_\infty^T \geq 0$  is the stabilizing solution to the discrete algebraic Riccati equation (6.6.4), all finite-dimensional linear time-invariant (FDLTI) full information controls which guarantee  $\|T_{zw}\|_\infty < \gamma$  and which are internally stabilizing are generated by

$$u_k = -W_{12}^{-1} L_1 x_k - W_{12}^{-1} W_{11} w_k + \gamma W_{12}^{-1} \Theta \{ \gamma W_{21} w_k + \gamma L_2 x_k \}, \quad (6.6.12)$$

where  $\Theta(z)$  is an arbitrary stable transfer function satisfying  $\|\Theta(z)\|_\infty < \gamma^{-1}$ . The plant state-space realization is assumed to be stabilizable and detectable. The central full information control law, obtained by setting  $\Theta = 0$  is given by

$$u_k = -W_{12}^{-1} L_1 x_k - W_{12}^{-1} W_{11} w_k. \quad (6.6.13)$$

■

Assuming full information, this theorem can be applied to the generalized plant of (6.4.3). The matrices  $\tilde{A}$ ,  $\tilde{B}$ ,  $\tilde{C}$  and  $\tilde{D}$  can be fully defined by the matrices  $\tilde{A}$ ,  $[B_1 \ B_2]$ ,  $C_1$  and  $[D_{11} \ D_{12}]$  (see (6.6.2)) as given in (6.4.3), and hence only these are required for the computation of the full information control. The central control law thus obtained will simply be a constant gain matrix to be used with the state and disturbance measurements.

## 6.7 The disturbance feedforward problem

For the realization of the full information control, as discussed above, the state and disturbance measurements are required. In the event that these measurements are not available, an estimate has to be generated, and the estimated state  $\hat{x}$  and disturbance  $\hat{w}$  substituted for their actual values in (6.6.12) to obtain the so-called ‘*Certainty Equivalence*’ control [107]. If the matrix  $D_{21}$  is square, as is the case for the two degrees-of-freedom configuration considered above (see (6.4.3)), the measurement equation  $q = C_2x + D_{21}w + D_{22}u$  can be inverted, and an estimate of  $w$  obtained in terms of  $u$ ,  $q$  and an estimate of  $x$ . This characterizes what is referred to as the *disturbance feedforward problem*. We will henceforth be specific to the generalized plant  $P$  of (6.4.3), for which state and disturbance estimates can be obtained as follows.

Noting that  $D_{22} = 0$  for our case, the measurement equation becomes:

$$q = C_2x + D_{21}w. \quad (6.7.1)$$

The observer will be designed so that its state vector  $\hat{x}$ , which is an estimate of  $P$ ’s true state  $x$ , evolves according to the following equation:

$$\hat{x}_{k+1} = \tilde{A}\hat{x}_k + B_1\hat{w}_k + B_2u_k, \quad (6.7.2)$$

where  $\hat{w}$  is the observer estimate of  $w$ , given by the inversion of (6.7.1) as:

$$\hat{w}_k = D_{21}^{-1}(q_k - C_2\hat{x}_k). \quad (6.7.3)$$

On substituting for  $q$  from (6.7.1), the above equation can be written for the disturbance estimation error as:

$$\hat{w} - w = D_{21}^{-1}C_2(x - \hat{x}). \quad (6.7.4)$$

Also subtracting  $x_{k+1} = \tilde{A}x_k + B_1w_k + B_2u_k$  from (6.7.2) and substituting from (6.7.4), we get:

$$(\hat{x} - x)_{k+1} = (\tilde{A} - B_1D_{21}^{-1}C_2)(\hat{x} - x)_k. \quad (6.7.5)$$

This equation describes the propagation of the state estimation error. We can show that the estimation error dynamics are stable by showing the stability of  $(\tilde{A} - B_1D_{21}^{-1}C_2)$  as follows. From (6.4.3) we have:

$$\begin{aligned} \tilde{A} - B_1D_{21}^{-1}C_2 &= \begin{bmatrix} A & 0 \\ 0 & A_o \end{bmatrix} - \begin{bmatrix} 0 & -HZ_2^{-1} \\ B_o & 0 \end{bmatrix} \begin{bmatrix} \rho I & 0 \\ 0 & Z_2^{-1} \end{bmatrix}^{-1} \begin{bmatrix} 0 & 0 \\ C & 0 \end{bmatrix} \\ &= \begin{bmatrix} A + HC & 0 \\ 0 & A_o \end{bmatrix}, \end{aligned} \quad (6.7.6)$$

which is stable because  $A + HC$  is stable from the definition of coprime factors and (6.2.2), and  $A_o$  is chosen to have eigenvalues inside the unit circle. Thus if  $\hat{x}_0 = x_0$ , (6.7.5) shows that the observer state will be identically equal to  $P$ 's true state vector  $x$  for all  $k$ , and hence from (6.7.4),  $\hat{w} \equiv w$  for all  $k$ . Thus if initialized properly, the observer will be able to reconstruct full information concerning  $P$  from  $q$ . Even if the observer is not initialized with the right initial state, the estimation error is guaranteed to decay to zero. We can therefore incorporate the observer with the full information control law, where the observer provides an estimate of state and disturbance information regarding the plant  $P$  from the measurement  $q$ . Rearranging the above equations, the observer dynamics can be expressed as:

$$\hat{x}_{k+1} = (\tilde{A} - B_1D_{21}^{-1}C_2)\hat{x}_k + B_1D_{21}^{-1}q_k + B_2u_k. \quad (6.7.7)$$

Now substituting the observer estimates of state  $x$  and disturbance  $w$  for the actual values in the central full information control law (6.6.13), the following certainty equivalence control is obtained:

$$u_k = -W_{12}^{-1}L_1\hat{x}_k - W_{12}^{-1}W_{11}\hat{w}_k. \quad (6.7.8)$$

It can be shown that such a control is norm-bounding as well as internally stabilizing as follows.

**Theorem 6.7.1** *Given a stabilizable and detectable realization of the FDLTI plant  $P$  described by*

$$x_{k+1} = \tilde{A}x_k + B_1w_k + B_2u_k,$$

$$\begin{aligned}
e_k &= C_1 x_k + D_{11} w_k + D_{12} u_k, \\
q_k &= C_2 x_k + D_{21} w_k,
\end{aligned} \tag{6.7.9}$$

with  $D_{21}$  square and  $D_{12}$  tall:

1. There exist internally stabilizing FDLTI controls of the form  $u = Kq$  satisfying  $\|T_{zw}\|_\infty < \gamma$  if and only if
$$-\gamma^2 I + B_1^T X_\infty B_1 + D_{11}^T D_{11} - (D_{11}^T D_{12} + B_1^T X_\infty B_2)(D_{12}^T D_{12} + B_2^T X_\infty B_2)^{-1}(D_{12}^T D_{11} + B_2^T X_\infty B_1) < 0,$$
where  $X_\infty = X_\infty^T \geq 0$  is the stabilizing solution to the discrete Riccati equation (6.6.4).
2. When the above condition is satisfied, all internally stabilizing FDLTI controls  $u = Kq$  achieving  $\|T_{ew}\|_\infty < \gamma$  are generated by

$$u_k = -W_{12}^{-1} L_1 \hat{x}_k - W_{12}^{-1} W_{11} \hat{w}_k + \gamma W_{12}^{-1} \Theta \{ \gamma W_{21} \hat{w}_k + \gamma L_2 \hat{x}_k \}, \tag{6.7.10}$$

where  $\hat{w}_k$  is given by (6.7.3) and  $\hat{x}_k$  evolves according to (6.7.7).  $\Theta(z)$  is an arbitrary stable transfer function satisfying  $\|\Theta(z)\|_\infty < \gamma^{-1}$ . The central certainty equivalence control law obtained by setting  $\Theta = 0$  is given by (6.7.8).

*Proof*

1. By Theorem 6.6.1, the condition of part 1 above is necessary and sufficient for the existence of internally stabilizing full information controls for which  $\|T_{zw}\|_\infty < \gamma$ . If there exists a norm-bounding output feedback control of the form  $u = Kq$ , then there also exists a norm-bounding full information control [107], in which case the condition must be satisfied. Conversely, since the observer construction reconstructs full information from the measurement  $q$ , existence of an internally stabilizing norm-bounding full information control implies existence of an internally stabilizing norm-bounding measurement feedback control.
2. Since  $\hat{x} = x$  and  $\hat{w} = w$ , combining the observer with the generator of all internally stabilizing norm-bounding full information controls captures all controls of the form  $u = Kq$ . ■

The overall structure of the controller is depicted in Figure 6.3.

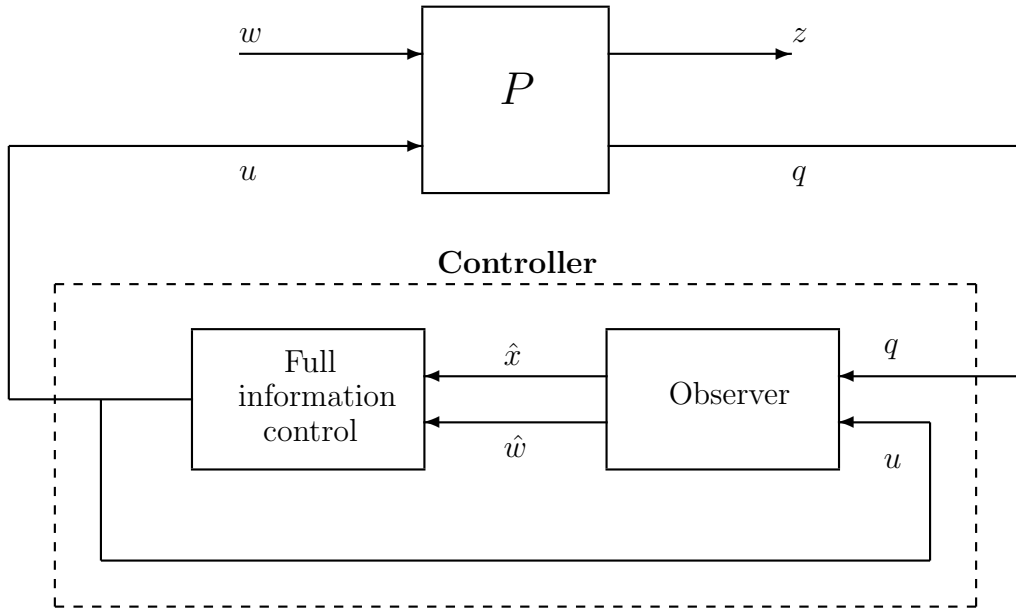


Figure 6.3: Controller separation structure.

## 6.8 Controller formulae and structure

We will now derive a state-space realization of the central sub-optimal controller for the two degrees-of-freedom control configuration under consideration. First, however, we make the following observations. From (6.4.3) we have:

$$D_{12}^T D_{11} = 0, \quad D_{12}^T C_1 = 0, \quad D_{12}^T D_{12} = I. \quad (6.8.1)$$

Now from (6.6.10) we have:

$$\begin{aligned} W_{12}^{-1} W_{11} &= W_{12}^{-1} W_{12}^{-T} (D_{12}^T D_{11} + B_2^T X_\infty B_1) \\ (6.8.1) \implies &= (W_{12}^T W_{12})^{-1} B_2^T X_\infty B_1 \\ (6.6.8) \implies &= (D_{12}^T D_{12} + B_2^T X_\infty B_2)^{-1} B_2^T X_\infty B_1 \\ (6.8.1) \implies &= (I + B_2^T X_\infty B_2)^{-1} B_2^T X_\infty B_1. \end{aligned} \quad (6.8.2)$$

From (6.6.11) we can write:

$$\begin{aligned} W_{12}^{-1} L_1 &= W_{12}^{-1} W_{12}^{-T} (D_{12}^T C_1 + B_2^T X_\infty \tilde{A}) \\ (6.8.1) \implies &= (W_{12}^T W_{12})^{-1} B_2^T X_\infty \tilde{A} \end{aligned}$$

$$(6.6.8) \implies = \left( D_{12}^T D_{12} + B_2^T X_\infty B_2 \right)^{-1} B_2^T X_\infty \tilde{A}$$

$$(6.8.1) \implies = \left( I + B_2^T X_\infty B_2 \right)^{-1} B_2^T X_\infty \tilde{A}. \quad (6.8.3)$$

The central sub-optimal controller given in (6.7.8) can now be written as:

$$\begin{aligned} u_k &= -W_{12}^{-1} L_1 \hat{x}_k - W_{12}^{-1} W_{11} \hat{w}_k \\ (6.8.2) \&(6.8.3) \implies u_k &= - \left( I + B_2^T X_\infty B_2 \right)^{-1} B_2^T X_\infty \tilde{A} \hat{x}_k - \\ &\quad \left( I + B_2^T X_\infty B_2 \right)^{-1} B_2^T X_\infty B_1 \hat{w}_k \\ &= - \left( I + B_2^T X_\infty B_2 \right)^{-1} B_2^T X_\infty \left( \tilde{A} \hat{x}_k + B_1 \hat{w}_k \right) \\ (6.7.3) \implies &= - \left( I + B_2^T X_\infty B_2 \right)^{-1} B_2^T X_\infty \left[ \tilde{A} \hat{x}_k + B_1 D_{21}^{-1} (q_k - C_2 \hat{x}_k) \right] \\ &= - \left( I + B_2^T X_\infty B_2 \right)^{-1} B_2^T X_\infty \left[ \left( \tilde{A} - B_1 D_{21}^{-1} C_2 \right) \hat{x}_k + B_1 D_{21}^{-1} q_k \right] \\ &= C_k \hat{x}_k + D_k q_k, \end{aligned} \quad (6.8.4)$$

where

$$C_k \triangleq - \left( I + B_2^T X_\infty B_2 \right)^{-1} B_2^T X_\infty \left( \tilde{A} - B_1 D_{21}^{-1} C_2 \right), \quad (6.8.5)$$

$$D_k \triangleq - \left( I + B_2^T X_\infty B_2 \right)^{-1} B_2^T X_\infty B_1 D_{21}^{-1}. \quad (6.8.6)$$

Now substituting for  $u_k$  from (6.8.4) in (6.7.7), the observer dynamics can be written as:

$$\begin{aligned} \hat{x}_{k+1} &= \left( \tilde{A} - B_1 D_{21}^{-1} C_2 \right) \hat{x}_k + B_1 D_{21}^{-1} q_k + B_2 (C_k \hat{x}_k + D_k q_k) \\ &= \left( \tilde{A} - B_1 D_{21}^{-1} C_2 + B_2 C_k \right) \hat{x}_k + \left( B_1 D_{21}^{-1} + B_2 D_k \right) q_k \\ &= A_k \hat{x}_k + B_k q_k, \end{aligned} \quad (6.8.7)$$

where

$$A_k \triangleq \tilde{A} - B_1 D_{21}^{-1} C_2 + B_2 C_k, \quad (6.8.8)$$

$$B_k \triangleq B_1 D_{21}^{-1} + B_2 D_k. \quad (6.8.9)$$

The solution  $X_\infty$  of the discrete Riccati equation can be partitioned conformally with  $\tilde{A} = \left[ \begin{array}{c|c} A & 0 \\ \hline 0 & A_o \end{array} \right]$ , i.e.,  $X_\infty = \left[ \begin{array}{c|c} X_{\infty 11} & X_{\infty 12} \\ \hline X_{\infty 21} & X_{\infty 22} \end{array} \right]$ . We can thus write from (6.4.3):

$$B_2^T X_\infty = [B^T \quad 0] \begin{bmatrix} X_{\infty 11} & X_{\infty 12} \\ X_{\infty 21} & X_{\infty 22} \end{bmatrix} = [B^T X_{\infty 11} \quad B^T X_{\infty 12}],$$

and

$$B_2^T X_\infty B_2 = [B^T \quad 0] \begin{bmatrix} X_{\infty 11} & X_{\infty 12} \\ X_{\infty 21} & X_{\infty 22} \end{bmatrix} \begin{bmatrix} B \\ 0 \end{bmatrix} = B^T X_{\infty 11} B,$$

so that (6.8.5) becomes:

$$\begin{aligned} C_k &= -(I + B^T X_{\infty 11} B)^{-1} [B^T X_{\infty 11} \quad B^T X_{\infty 12}] (\tilde{A} - B_1 D_{21}^{-1} C_2) \\ (6.7.6) \implies &= -(I + B^T X_{\infty 11} B)^{-1} [B^T X_{\infty 11} \quad B^T X_{\infty 12}] \begin{bmatrix} A + HC & 0 \\ 0 & A_o \end{bmatrix} \\ &= -(I + B^T X_{\infty 11} B)^{-1} \left[ B^T X_{\infty 11} (A + HC) \mid B^T X_{\infty 12} A_o \right] \\ &\triangleq \left[ C_{k11} \mid C_{k12} \right]. \end{aligned} \quad (6.8.10)$$

Similarly substituting for  $B_2^T X_\infty$  and  $B_2^T X_\infty B_2$  from above and for  $B_1$  and  $D_{21}$  from (6.4.3) in (6.8.6), we get:

$$\begin{aligned} D_k &= -(I + B^T X_{\infty 11} B)^{-1} [B^T X_{\infty 11} \quad B^T X_{\infty 12}] \begin{bmatrix} 0 & -HZ_2^{-1} \\ B_o & 0 \end{bmatrix} \begin{bmatrix} \rho I & 0 \\ 0 & Z_2^{-1} \end{bmatrix}^{-1} \\ &= -(I + B^T X_{\infty 11} B)^{-1} \left[ \frac{1}{\rho} B^T X_{\infty 12} B_o \mid -B^T X_{\infty 11} H \right] \\ &\triangleq \left[ D_{k11} \mid D_{k12} \right]. \end{aligned} \quad (6.8.11)$$

By using (6.4.3), (6.7.6) and (6.8.10), (6.8.8) can be written as:

$$\begin{aligned} A_k &= \begin{bmatrix} A + HC & 0 \\ 0 & A_o \end{bmatrix} + \begin{bmatrix} B \\ 0 \end{bmatrix} [C_{k11} \quad C_{k12}] \\ &= \begin{bmatrix} A + HC + BC_{k11} & BC_{k12} \\ 0 & A_o \end{bmatrix}. \end{aligned} \quad (6.8.12)$$

Similarly for  $B_k$  substituting from (6.4.3) and (6.8.11) into (6.8.9), we have:

$$\begin{aligned} B_k &= \begin{bmatrix} 0 & -HZ_2^{-1} \\ B_o & 0 \end{bmatrix} \begin{bmatrix} \rho I & 0 \\ 0 & Z_2^{-1} \end{bmatrix}^{-1} + \begin{bmatrix} B \\ 0 \end{bmatrix} [D_{k11} \quad D_{k12}] \\ &= \begin{bmatrix} BD_{k11} & -H + BD_{k12} \\ \frac{1}{\rho} B_o & 0 \end{bmatrix}. \end{aligned} \quad (6.8.13)$$

Using  $A_k$  and  $B_k$  from above, the observer dynamics (6.8.7) can be written as:

$$\begin{bmatrix} \hat{x}_{G_{k+1}} \\ x_{o_{k+1}} \end{bmatrix} = \begin{bmatrix} A + HC + BC_{k11} & BC_{k12} \\ 0 & A_o \end{bmatrix} \begin{bmatrix} \hat{x}_{G_k} \\ x_{o_k} \end{bmatrix} + \begin{bmatrix} BD_{k11} & -H + BD_{k12} \\ \frac{1}{\rho} B_o & 0 \end{bmatrix} \begin{bmatrix} \beta_k \\ y_k \end{bmatrix},$$

where we have split the observer state vector into the estimated state  $\hat{x}_G$  of the shaped plant  $G_s$ , and the state  $x_o$  of the reference model  $M_o$ . Recall that the measurement  $q$

available to the controller consists of the scaled reference input  $\beta$  and the plant output  $y$  (as can be seen from (6.4.2)), and hence  $q$  has been replaced above by  $[\beta^T \quad y^T]^T$ . Using  $\beta = \rho r$  (see Figure 5.10), we can rewrite the observer state equation as:

$$\begin{bmatrix} \hat{x}_{G_{k+1}} \\ x_{o_{k+1}} \end{bmatrix} = \begin{bmatrix} A + HC + BC_{k11} & BC_{k12} \\ 0 & A_o \end{bmatrix} \begin{bmatrix} \hat{x}_{G_k} \\ x_{o_k} \end{bmatrix} + \begin{bmatrix} \rho BD_{k11} & -H + BD_{k12} \\ B_o & 0 \end{bmatrix} \begin{bmatrix} r_k \\ y_k \end{bmatrix}. \quad (6.8.14)$$

The controller output equation (6.8.4) can be written as:

$$u_k = [C_{k11} \quad C_{k12}] \begin{bmatrix} \hat{x}_{G_k} \\ x_{o_k} \end{bmatrix} + [\rho D_{k11} \quad D_{k12}] \begin{bmatrix} r_k \\ y_k \end{bmatrix}. \quad (6.8.15)$$

(6.8.14) and (6.8.15) give a state-space realization of the sub-optimal controller that is stabilizing and norm-bounding for the generalized plant of (6.4.3).

The controller state equation (6.8.14) can also be written as:

$$\begin{bmatrix} \hat{x}_{G_{k+1}} \\ x_{o_{k+1}} \end{bmatrix} = \begin{bmatrix} A + HC & 0 \\ 0 & A_o \end{bmatrix} \begin{bmatrix} \hat{x}_{G_k} \\ x_{o_k} \end{bmatrix} + \begin{bmatrix} B & -H & 0 \\ 0 & 0 & B_o \end{bmatrix} \begin{bmatrix} u_k \\ y_k \\ r_k \end{bmatrix}, \quad (6.8.16)$$

which shows clearly the controller structure. It is seen that the controller consists of an observer for the shaped plant  $G_s$ , which provides an estimate  $\hat{x}_G$  for the state  $x_G$  of  $G_s$ ;  $H$  being the observer gain. The observer is driven by the input and output of  $G_s$ ,  $u_k$  and  $y_k$  respectively. Also included in the controller dynamical equation is the state update equation of the reference model  $M_o$ . The model runs autonomously inside the controller, its state  $x_o$  being driven by the reference input  $r$ . Recall that the generalized plant  $P$  given in (6.4.3) has the state vector  $\begin{bmatrix} x_G \\ x_o \end{bmatrix}$ . The controller has information regarding some of the states of  $P$ , i.e., the ones corresponding to the reference model. These states are thus used directly – they need not be estimated. An observer, it turns out from (6.8.16), is constructed only for the estimation of the states of the shaped plant  $G_s$ .

The controller output equation (6.8.15) consists of a generalized state feedback that uses both the plant state estimate, and the reference model state. It is remarked here that in general,  $H_\infty$  sub-optimal control problems cannot be solved by an observer-state feedback combination alone – a worst case disturbance estimate will also be used to generate the control. In the two degrees-of-freedom case under consideration however, it is the special structure of the generalized plant  $P$  ( $D_{21}$  square), that enables the controller to be written simply as an observer plus a state feedback. The controller structure is elaborated in

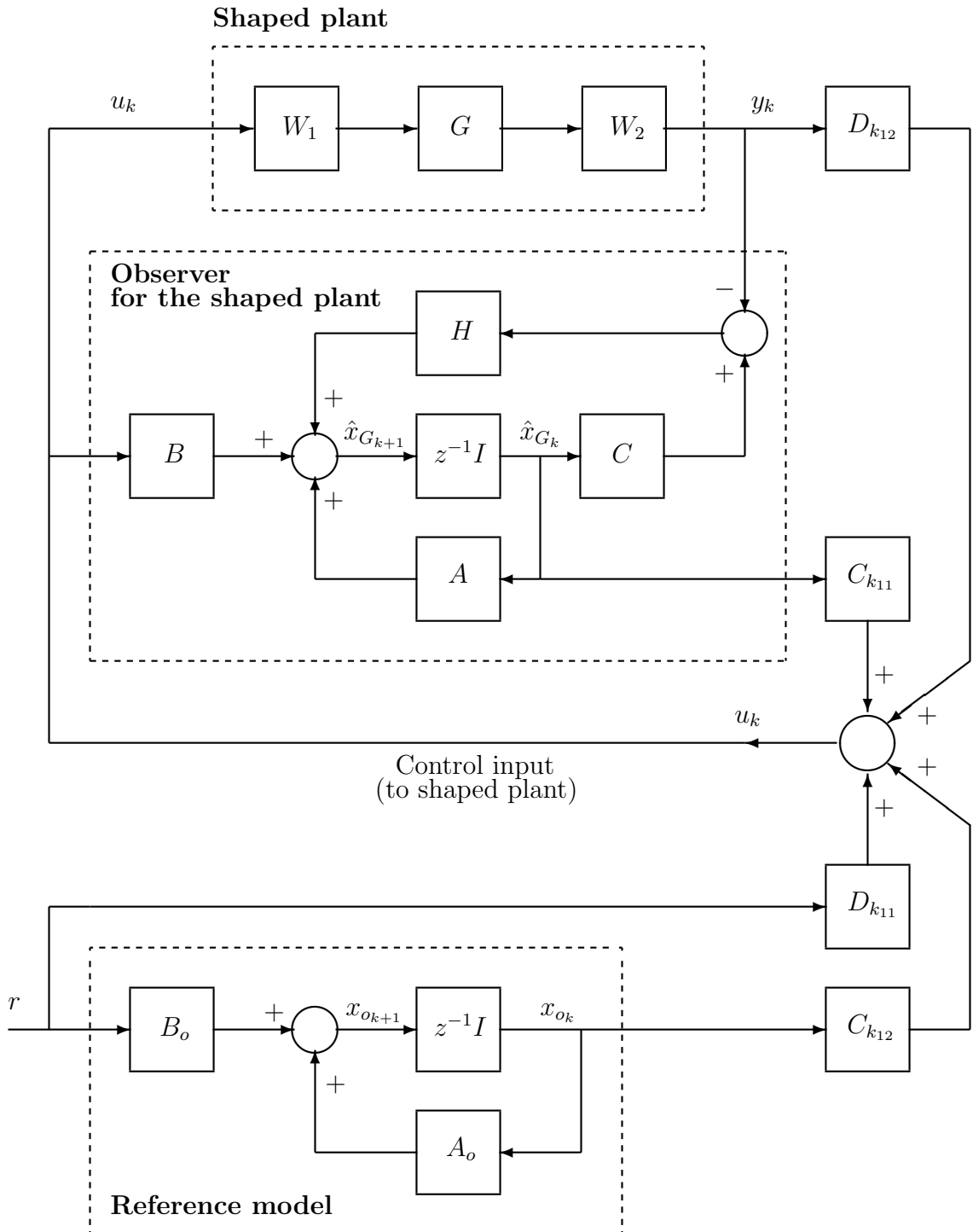


Figure 6.4: Controller structure.

Figure 6.4. For implementation of the control law, the weights  $W_1$  and  $W_2$  are cascaded with  $K \triangleq [K_1 \quad K_2] \stackrel{s}{=} \left[ \begin{array}{c|c} A_k & B_k \\ \hline C_k & D_k \end{array} \right]$  to yield the final controller  $[W_1K_1 \quad W_1K_2W_2]$ . In addition, for perfect steady-state tracking, the pre-filter  $K_1$  is scaled so that the steady-state gain from the reference to the output becomes unity.

## 6.9 Design procedure

In this section we present a design procedure for designing robust two degrees-of-freedom discrete time controllers based on open-loop shaping and robust stabilization of the normalized coprime factors of the plant. The two degrees-of-freedom configuration provides a degree of robust performance in the sense of making the closed-loop system match a pre-specified reference model in the face of coprime factor uncertainty. The procedure was developed for the continuous time case by Hoyle et al. [45]. The procedure consists of the following main steps.

1. Plot the singular value frequency response of the open-loop plant  $G(z)$ . Based on this, select a pre-compensator  $\hat{W}_1$  and/or a post-compensator  $W_2$ , both in the continuous domain, to give the plant a desired open-loop shape. These weights will be discretized later, before being cascaded with the plant  $G(z)$ . It has been found from experience that it is easier and more intuitive to select the weights in continuous time and then discretize them, rather than to choose them directly in the discrete domain. Discretize  $\hat{W}_1$  and  $W_2$  using, for example, Tustin's method, and form the product  $W_2(z)G(z)\hat{W}_1(z)$ .
2. Align the singular values of  $W_2G\hat{W}_1$  at the desired bandwidth. The align gain  $K_a$  is the approximate real inverse of the system at the specified frequency. The cross-over (and hence the bandwidth) is thus adjusted to approximately the align frequency. Alignment should not be used with ill-conditioned plants, this can result in poor robustness properties, as seen earlier in Chapter 4.

An additional constant diagonal matrix  $K_g$  may sometimes be used in front of the align gain to exercise control over actuator usage. It is chosen so that the various actuator rate limits are not exceeded whilst following references or rejecting distur-

bances. The pre-compensator can now be written as  $W_1 = \hat{W}_1 K_a K_g$ ; see Figure 6.5. Build the shaped plant  $G_s(z) = W_2(z)G(z)W_1(z)$  and calculate the optimal value  $\gamma_{opt}$  as given by (6.2.4), for the pure robust stabilization problem. A high value (typically  $> 10$ ) of  $\gamma_{opt}$  indicates that the specified loop-shape is inconsistent with robust stability; in such a case the weights  $W_1$  and  $W_2$  should be modified.

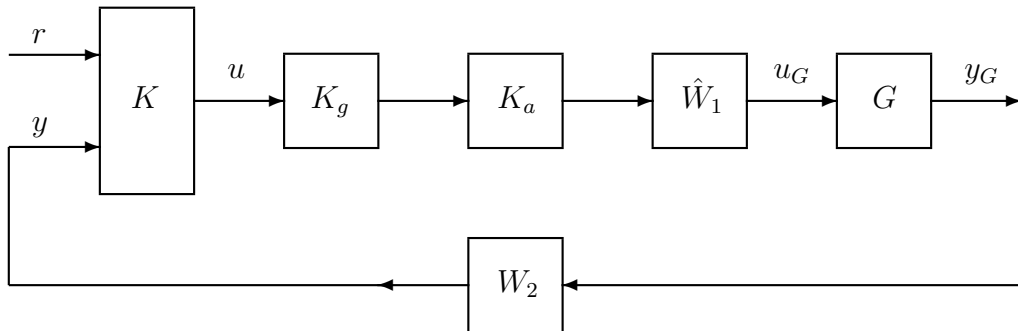


Figure 6.5: The shaped plant and the controller.

3. Select a step response model ( $M_o$ ) for the closed-loop system, again in continuous time, for ease and intuition. The model is usually a diagonal matrix of first or second order lags. Discretize the reference model, set  $\rho$  to be in the range  $1 \leq \rho \leq 3$ , and build the state-space realization of the generalized plant as given in (6.4.3).
4. Perform  $\gamma$ -iterations, find the near to optimal  $\gamma$  and compute the corresponding controller. It should be noted that while iterating for  $\gamma$ , only one Riccati equation needs to be solved, i.e., the  $H_\infty$  full information Riccati equation given in (6.6.4). If for a certain value of  $\gamma$  a stabilizing solution to this Riccati equation exists, an internally stabilizing, norm-bounding full information control law exists, which can then be combined with an observer (§6.7) to yield the corresponding output feedback control.
5. Cascade the controller with the weights  $W_1$  and  $W_2$ , and scale the pre-filter to achieve perfect steady-state model matching.
6. Form the closed-loop and check the appropriate performance and robustness measures against the given specification.

This procedure will be illustrated on the aero-engine designs, presented in the next chapter.

## 6.10 Summary

This chapter has motivated and described the robust 2-DOF discrete time controller synthesis and design procedure based on open-loop shaping and robust stabilization in the normalized coprime factor framework. A state-space construction for the normalized left coprime factorization was given in §6.2. The technique of multivariable loop-shaping in the context of coprime factor robust stabilization was motivated in §6.3. Justification for the loop-shaping design procedure of McFarlane & Glover [64] was given and its connection to the simultaneous uncertainty problem described. It was shown that the LSDP ensures that standard closed-loop transfer function objectives remain well-behaved and that good feedback properties are achieved at both the plant input and output. The extension of the LDSP to the two degrees-of-freedom configuration was discussed in §6.4. The problem was then set up in the generalized regulator framework of Chapter 2. Results on discrete time full information  $H_\infty$  control were summarized in §6.6. The disturbance feedforward problem was discussed in §6.7. It was shown that the two degrees-of-freedom  $H_\infty$  controller synthesis problem posed earlier could be solved by an observer state-feedback combination; controller structure and formulae were presented in §6.8. Finally the controller design procedure was given in §6.9.

## Chapter 7

### Multi-mode controller design and implementation

#### 7.1 Introduction

When faced with the task of control of complex engineering systems, efficient and effective ways of implementing the controller are as important as its design in the first place. Most of the application studies based on  $H_\infty$  controllers to date have been based on computer simulations, and hence very few (such as [48]) have discussed issues regarding implementation. There have been some studies regarding switching and scheduling of  $H_\infty$  controllers (see for example, [49, 47, 54]) to cope with the non-linear behaviour of the plant, but design of multi-mode systems using  $H_\infty$  controllers has been very rare, if not altogether absent. Furthermore, problems can arise from discrete time implementation of the controller, particularly if the sample time is comparable to the system bandwidth. In this chapter we shall look into some of these issues; the emphasis will be on obtaining workable solutions for the aero-engine multi-mode problem.

This chapter is organized as follows. §7.2 describes limitations and design considerations associated with plants having more outputs than inputs. §7.3 works through the details of the controller design for the aero-engine example, based on the procedure outlined in Chapter 6. The controller structure used for implementation, and the associated computational advantages are discussed in §7.4 and §7.5 respectively. The structure of the overall switched controller is given in §7.6. §7.7 discusses the issues of anti-windup and bumpless transfer between controllers and §7.8 summarizes the main points of the chapter.

## 7.2 Design considerations for plants with more outputs than inputs

For the aero-engine under consideration, we plan to design three separate controllers each controlling three outputs independently – a thrust controller for controlling [PS6PS1, DPUP, NHPCSL], an NL limiter for controlling [NL,DPUP,NHPCSL] and a TT15 limiter for controlling [TT15,DPUP,NHPCSL]. There are three control inputs to the engine. Five measurements are available to each controller (Figure 3.6). It shall now be explored whether using measurements in addition to the ones being controlled offer any advantages for each of these controllers.

As already mentioned, one can independently control only as many outputs as there are inputs. Any extra outputs cannot be controlled independently, but may be made effective use of by the controller. For example, low noise rate measurements in position control systems provide improved system damping. For an observer-based controller, the extra measurements if contributed by low noise, high fidelity sensors, can act to improve the state estimate. Extra measurements however, make the plant non-square, and this has an effect on the tracking and disturbance rejection properties of the feedback system. Here we briefly discuss some of these issues.

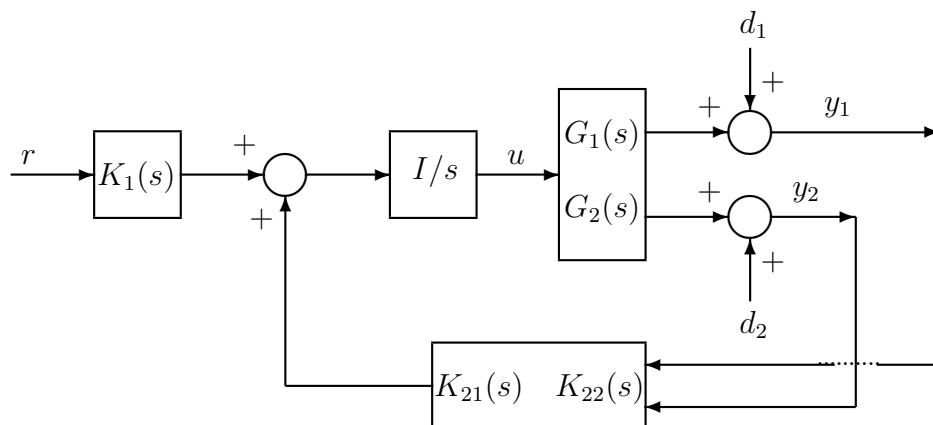


Figure 7.1: Plant with extra measurements.

Let us consider a two degrees-of-freedom control system as shown in Figure 7.1 where extra output measurements  $y_2$  are available to the controller. The plant  $G(s)$  can be

partitioned as  $\begin{bmatrix} G_1(s) \\ G_2(s) \end{bmatrix}$  where  $G_1(s)$  is square,  $y_1$  being the outputs to be controlled. We have shown integral action in the control loop because ideally we want perfect steady-state tracking and disturbance rejection.  $r$  is the reference input for  $y_1$  to follow. Defining  $e$  to be the tracking error, i.e.,  $e \triangleq r - y_1$ , we have:

$$e = \left[ I - G_1(sI - K_{21}G_1 - K_{22}G_2)^{-1}K_1 \right] r - \left[ I + G_1(sI - K_{21}G_1 - K_{22}G_2)^{-1}K_{21} \right] d_1 - G_1(sI - K_{21}G_1 - K_{22}G_2)^{-1}K_{22}d_2. \quad (7.2.1)$$

Thus the transfer function from  $r$  to  $e$  denoted  $T_{er}$  is:

$$T_{er} = I - G_1(sI - K_{21}G_1 - K_{22}G_2)^{-1}K_1.$$

At steady-state (zero frequency) we have:

$$T_{er}(s=0) = I + G_1(K_{21}G_1 + K_{22}G_2)^{-1}K_1 \Big|_{s=0}.$$

For perfect steady-state tracking, we require  $T_{er}(s=0) = 0$  which gives

$$K_1(0) = -[K_{21}(0)G_1(0) + K_{22}(0)G_2(0)]G_1(0)^{-1}. \quad (7.2.2)$$

Thus we have to scale the pre-filter  $K_1$  so that its dc-gain equals that given by (7.2.2). Note that this scaling is dependent on the plant dc-gain, and in cases where the exact plant dc-gain is not known (or it changes with time), there would be discrepancies between  $r$  and  $y_1$  in the steady-state. Now assuming that  $\|K_{21}(0)G_1(0)\|_2 \gg \|K_{22}(0)G_2(0)\|_2$ , (7.2.2) becomes:

$$K_1(0) = -K_{21}(0). \quad (7.2.3)$$

Thus we see that if the steady-state loop gain associated with the controlled outputs is relatively large, the scaling required on the pre-filter becomes independent of the plant dc-gain. Hence for square plants one can always achieve exact tracking in the steady-state whenever there is integral action in the loop.

Now considering the transfer function from  $d_1$  to  $y_1$  denoted  $T_{y_1d_1}$  at dc, we have:

$$T_{y_1d_1}(s=0) = I - G_1(K_{21}G_1 + K_{22}G_2)^{-1}K_{21} \Big|_{s=0}.$$

For perfect disturbance rejection in the steady-state (i.e.,  $T_{y_1d_1}(s=0) = 0$ ), we require

$$(K_{21}(0)G_1(0) + K_{22}(0)G_2(0))^{-1} = (K_{21}(0)G_1(0))^{-1}, \quad (7.2.4)$$

for which again we need that  $\|K_{21}(0)G_1(0)\|_2 \gg \|K_{22}(0)G_2(0)\|_2$ . Thus making the loop gain associated with  $y_1$  much greater than that associated with  $y_2$  will give good disturbance rejection on the controlled outputs  $y_1$ .

We have shown that for good steady-state reference following and disturbance rejection on the controlled outputs, the loop gain associated with these outputs should be relatively large. For the aero-engine example under consideration, we shall have three controllers running in parallel; at any given time one of the three would be on-line and the other two off-line. These controllers should have a high loop gain associated with the outputs they are designed to control so that they may provide good tracking and disturbance rejection on these outputs. The loop gains for the various outputs can be adjusted by an appropriate choice of the post-compensator  $W_2$ . Choosing it to be a constant diagonal matrix with relatively high gains in the channels corresponding to the controlled outputs results in these outputs having higher loop gains. The three controllers can thus either be designed such that they only use the outputs they are designed to control (i.e., for square plants), or if extra outputs are to be used, the post-compensator  $W_2$  should be chosen such that it emphasizes the controlled outputs over the extra measurements.

The improvement offered by the use of additional measurements can be judged from the improvement in the value of the cost function that the controller is designed to minimize. In our case the cost function is the  $L_\infty$ -norm of the transfer function given in (6.4.1), denoted by  $\gamma$ . Several designs were performed, with and without extra outputs, and the values achieved for  $\gamma$  compared. It was found that using additional outputs offered only a marginal improvement in the cost. For example, a design was performed for the thrust controller using only the outputs [PS6PS1,DPUP,NHPCSL], and the value of  $\gamma$  achieved was 2.37. The design was repeated so that the controller now had access to all the five measurements; and with  $W_2 = \text{diag}\{1, 1, 1, 0.2, 0.2\}$ , the value achieved for the cost was 2.32. This improvement is indeed quite marginal and does not justify using additional measurements, particularly if perfect steady-state tracking and disturbance rejection on the controlled outputs are required.

The usual incentive for the use of additional measurements in feedback systems is the improvement they provide in stability margins and damping of the system. In our case, the optimal cost  $\gamma$  is a design indicator; the lower the cost, the better the design. We

have seen that the extra measurements offer no significant improvement in the optimal cost, and hence their use appears to be unjustified in our case. It is discovered, however, that the use of an extra measurement in the PS6PS1 and NL controllers can lead to a considerable simplification in the overall switched controller structure. This simplification is a consequence of the particular relation between the PS6PS1 and NL outputs, and is specific to the aero-engine example under consideration. An extra measurement is thus used in each of the PS6PS1 and NL controllers; this is elaborated further in the following paragraph.

As already discussed, the  $H_\infty$  two degrees-of-freedom controller consists of an observer for the shaped plant, the chosen reference model, and a generalized state feedback law. The thrust controller and the two limiters all share this same basic structure. In effect, thus, we shall be running three observers in parallel. This is indispensable in general because each of the three observers estimates the shaped plant's states from different outputs, and this is crucial for rejecting disturbances acting on these outputs. For the case of the aero-engine however, the knowledge of actual disturbances acting on the engine suggests that these affect the outputs PS6PS1 and NL in a very similar way. That is to say that if the disturbance impinging on the system causes a change  $\Delta PS6PS1$  in the thrust output, and a change  $\Delta NL$  in the LP compressor's spool speed, then rejecting the disturbance on PS6PS1 also causes  $\Delta NL \rightarrow 0$ , and vice versa. This close relationship between PS6PS1 and NL can be exploited so that just a single observer can be used for both the thrust and NL controllers. The TT15 controller however, uses a separate observer. The three controllers thus use only two observers, which significantly reduces the state dimension of the overall switched controller. This is discussed in greater detail in subsequent sections.

### 7.3 Controller design

Here we will describe the design of the three controllers, and hence illustrate the design procedure as proposed in Chapter 6. Since we plan to use the same observer for both PS6PS1 and NL controllers, the linear engine model we will use for the design of these controllers has four outputs, i.e., PS6PS1, DPUP, NHPCSL and NL. The selection of the sample time is dictated by the available computing resources and is chosen to be 30

msec, which is just adequate for the closed-loop bandwidth we are aiming for. The delays associated with the discrete time implementation are therefore significant in this case. These delays arise because the plant output at a particular sampling time is not available to the controller until after one sample period has elapsed. Also there is a half sample delay associated with the zero-order hold at the output of the controller. A time delay is well-known to produce phase lag and generally leads to a less stable design if not taken properly into account. These delays have to be approximated for continuous time design, but can be modelled exactly in discrete time. Direct discrete design is therefore important and will yield superior results as compared to those obtained by discretizing continuous time controllers.

### 7.3.1 PS6PS1 controller design

We now follow the design procedure given in §6.9.

1. Singular values of the open-loop plant  $G(z)$  are plotted and these indicate the need for boosting the low frequency gain for good tracking and disturbance rejection at low frequencies. The weights are thus to be selected with these objectives in mind. The low frequency gain is boosted by introducing integral action in the control loop. We are aiming for a closed-loop bandwidth of approximately 9 rad/sec. We therefore introduce zeros at  $-5$  to reduce the roll-off at the cross-over frequencies.  $\hat{W}_1$  in Figure 6.5 thus becomes  $\frac{s+5}{s}I_3$ . It is discretized using Tustin's method.  $W_2$  is chosen to be  $diag\{1, 1, 1, 0.2\}$  so that it de-emphasizes the NL output relative to the other three.
2.  $W_2G\hat{W}_1$  is now aligned at 6 rad/sec. The cross-over is thus adjusted to approximately 6 rad/sec. Alignment should not be used with ill-conditioned plants, the condition number of the aero-engine is only 2.8 at 6 rad/sec, and hence alignment is not expected to cause problems. An additional gain  $K_g$  is used in front of the align gain to exercise control over actuator usage. It is chosen to be  $diag\{1, 1.1, 0.3\}$ , the third actuator (the guide vane angle) being made to respond slower. The pre-compensator can now be written as  $W_1 = \hat{W}_1K_aK_g$ . The shaped plant  $G_s = W_2GW_1$  is now formed, its singular values are shown in Figure 7.2.

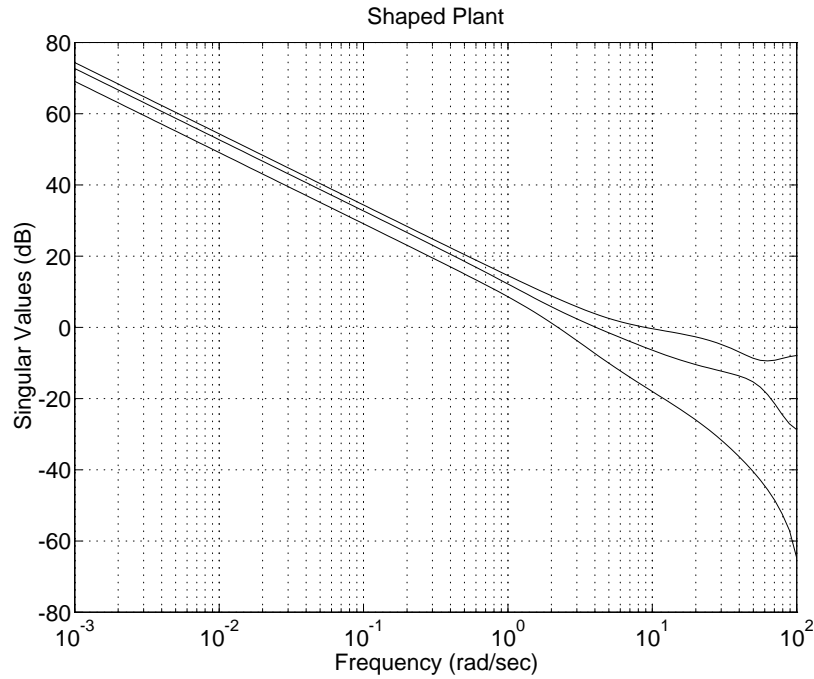


Figure 7.2: Singular values of the shaped plant for the PS6PS1 controller design.

3. A step response model ( $M_o$ ) is selected for the closed-loop system. The model is chosen in continuous time as  $diag\{\frac{1}{0.08s+1}, \frac{1}{0.055s+1}, \frac{1}{0.33s+1}\}$ . The controlled outputs are thus desired to behave as simple first order lags with no interaction. The reference model is discretized using Tustin's method. It should be noted that we are controlling only the first three outputs, i.e., PS6PS1, DPUP and NHPCSL, hence the 3-input 3-output reference model.  $\rho$  is set to 1 and the state-space realization of the generalized plant as given in (6.4.3) formed, except for  $C_1$  and  $D_{11}$ ;  $\rho C$  and  $\rho Z_2^{-1}$  in the third rows of these matrices being replaced by  $\rho TC$  and  $\rho TZ_2^{-1}$ , where  $T = \begin{bmatrix} 1 & 0 & 0 & 0 \\ 0 & 1 & 0 & 0 \\ 0 & 0 & 1 & 0 \end{bmatrix}$ . This corresponds to selecting the first three outputs for model matching, i.e., the error  $e$  (see Figure 5.10) is given by  $\rho(Ty - y_o)$ ,  $y_o$  being the output of the reference model. Note that  $W_2$  does not affect the first three plant outputs, the gain being unity in these channels.
4.  $\gamma$ -iterations are performed, and a slightly sub-optimal controller achieving  $\gamma = 2.3125$  obtained.
5. The controller is cascaded with the weights  $W_1$  and  $W_2$ , and the pre-filter scaled to

achieve perfect steady-state model matching.

Step responses for the linear model are shown in Figure 7.3. The NL output is shown with a dotted line, and not being a controlled output, is not regulated to any specific value. The response times are within the specification, and the decoupling is good with less than 10% interaction. Responses to disturbances are also analysed and shown in Figure 7.4. Each output is given a step disturbance of amplitude  $-1$  at zero time. The NL output can be seen to have no disturbance rejection action, this being expected as it was given a low weighting in the post-compensator  $W_2$ . It should be noted that these disturbances are hypothetical; in real life the disturbances on PS6PS1 and NL would be strongly coupled. The rejection of disturbances on the three controlled outputs is satisfactory and conforms to the specification. The singular values of the sensitivity function are shown in Figure 7.5. One of the singular values, the one that remains flat at low frequencies, corresponds to NL and indicates no disturbance rejection on that output.

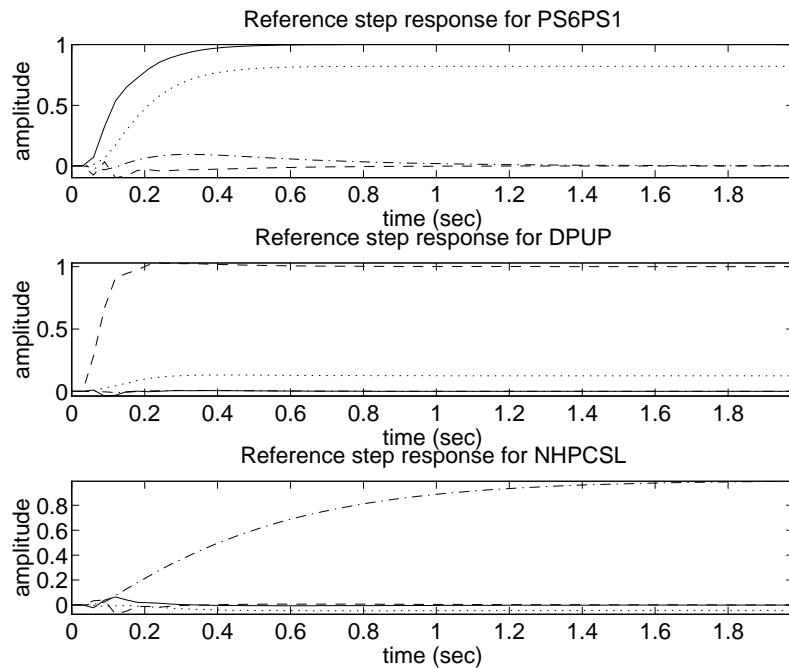


Figure 7.3: Reference step responses for the PS6PS1 controller (PS6PS1 —, DPUP - - -, NHPCSL - · -, NL ···).

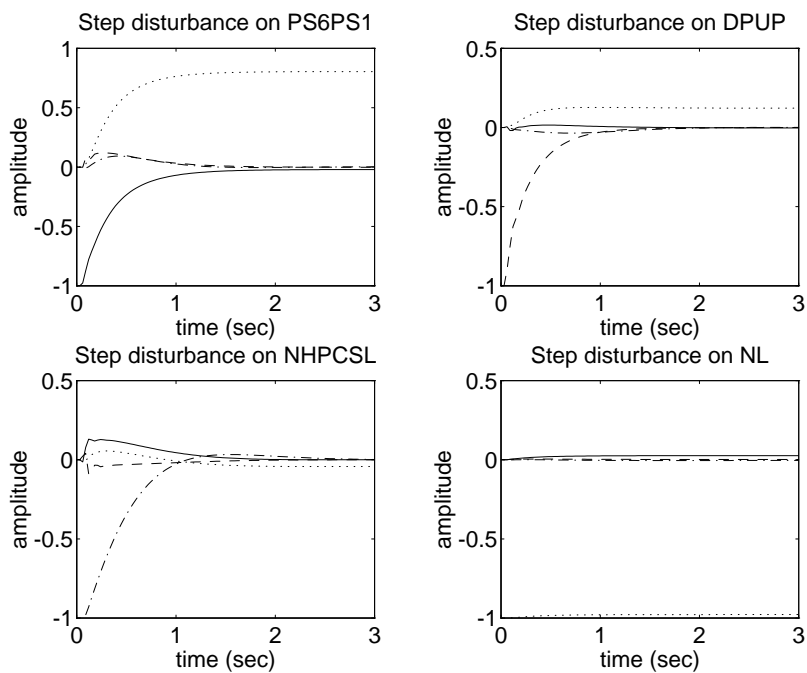


Figure 7.4: Disturbance step responses for the PS6PS1 controller (PS6PS1 —, DPUP - - -, NHPCSL ···, NL ···).

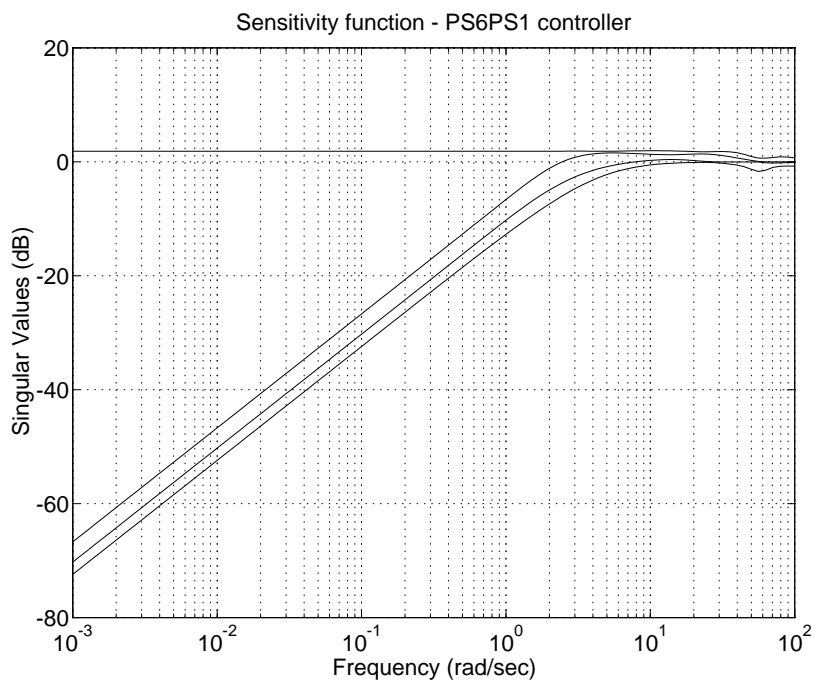


Figure 7.5: Sensitivity function  $(I + GW_1K_2W_2)^{-1}$  for the PS6PS1 controller.

### 7.3.2 NL limiter design

We now consider design of the NL limiter. Since we plan to use the same shaped plant observer as we used for the PS6PS1 controller, the shaped plant must be the same in both cases. We therefore select the same weights  $W_1$  and  $W_2$  as for the previous design. The reference model chosen is however slightly different and is given by  $\text{diag}\{\frac{1}{0.05s+1}, \frac{1}{0.05s+1}, \frac{1}{0.33s+1}\}$ . The model is discretized using Tustin's method.  $\rho$  is chosen to be 1. The generalized plant of (6.4.3) is now built, where  $C_1$  and  $D_{11}$  are changed to

$$C_1 = \begin{bmatrix} 0 & 0 \\ C & 0 \\ \rho T \bar{C} & \rho^2 C_o \end{bmatrix}, \quad D_{11} = \begin{bmatrix} 0 & 0 \\ 0 & Z_2^{-1} \\ -\rho^2 D_o & \rho T \bar{Z}_2^{-1} \end{bmatrix}.$$

The third rows of  $C_1$  and  $D_{11}$  correspond to the difference between the model output and the actual plant output  $\tilde{y} = \bar{C}x + \bar{Z}_2^{-1}\phi$  (and not the plant output after  $W_2$ ).  $\bar{C}$  is given by  $W_2^{-1}C$  and  $\bar{Z}_2^{-1}$  is obtained by solving the normalized coprime factor Riccati equation (6.2.1) for  $GW_1$ . Obtaining  $\bar{Z}_2^{-1}$  in this way was found to give a more realistic representation of the direct feedthrough from  $\phi$  through to the plant output  $\tilde{y}$ , as compared to just taking it as  $W_2^{-1}Z_2^{-1}$ . The output selection matrix  $T$  is chosen so that the fourth, second and third outputs (i.e., NL, DPUP and NHPCSL) are used for model matching, i.e.,  $T = \begin{bmatrix} 0 & 0 & 0 & 1 \\ 0 & 1 & 0 & 0 \\ 0 & 0 & 1 & 0 \end{bmatrix}$ . A slightly sub-optimal stabilizing solution to the discrete full information Riccati equation is iteratively found, the corresponding value of  $\gamma$  being 2.2969. The state-space realization of the controller  $K$  as given in (6.8.14) and (6.8.15) is constructed. Note that the observer part of the controller is the same as for the PS6PS1 controller, the shaped plant used for design being the same in both cases.

As already mentioned, the weight  $W_2$  used in this design is the same as that used for the design of the PS6PS1 controller. It therefore weights the NL output relatively small, thus giving no disturbance rejection on NL. The disturbances on PS6PS1, DPUP and NHPCSL would however be rejected as for the PS6PS1 controller. Moreover, the scaling required on the pre-filter for perfect steady-state reference following will be very much dependent on the plant dc-gain, as discussed previously in §7.2. If the plant's steady-state gain is not exactly known, or in case it changes over time, the tracking on NL

would deteriorate. This latter problem in our case is more pronounced, since disturbance rejection on NL can be provided through disturbance rejection on PS6PS1, as discussed previously. We therefore need a high loop gain associated with NL for robust tracking, and this gain could be traded against that for PS6PS1; PS6PS1 serving here as an extra measurement and no longer being a controlled output.  $W_2$  is therefore changed, the gain in the PS6PS1 channel lowered and that in the NL channel raised until step responses obtained are similar to the ones achieved with the original  $W_2$ . With some trial and error

$W_2$  is finally chosen to be 
$$\begin{bmatrix} 0.05 & 0 & 0 & 0 \\ 0 & 1 & 0 & 0 \\ 0 & 0 & 1 & 0 \\ 0 & -1 & 0 & 7.2 \end{bmatrix}.$$
  $W_1$  and the new  $W_2$  are now cascaded

with the controller  $K = [K_1 \quad K_2]$  to yield the final controller  $[W_1K_1 \quad W_1K_2W_2]$ . The controller now essentially uses the outputs DPUP, NHPCSL and NL for generating the plant state estimate, the PS6PS1 measurement being weighted to be negligible. Note that this effective “replacement” of the PS6PS1 measurement by NL has been possible only because the two outputs have similar response times, it would not be possible if one lagged considerably behind the other. It must be appreciated however that the  $H_\infty$ -optimization problem was solved for the original  $W_2$ , the  $\gamma$  of 2.2969 being achieved for that  $W_2$ . The new  $W_2$  is therefore expected to give a poorer cost; the value of  $\gamma$  achieved with the new  $W_2$  is calculated and is found to deteriorate to 7.17. The stability margins are thus reduced by approximately one third; this is still deemed acceptable given that the limiter would be on-line only for certain specific operating conditions. Linear step and disturbance responses are shown in Figures 7.6 and 7.7 respectively. It can be seen that the disturbance rejection on NL has been traded against that for PS6PS1, the sensitivity function is shown in Figure 7.8.

### 7.3.3 TT15 limiter design

The TT15 limiter is designed for a square plant model with just three outputs, i.e., TT15, DPUP and NHPCSL. The same pre-compensator  $W_1$  as used for the PS6PS1 and NL controllers is found to give an acceptable open-loop frequency response shape, and hence is chosen for this design as well (it need not be the same though).  $W_2$  is taken to be the identity matrix. The singular values of the shaped plant  $G_s = W_2GW_1$

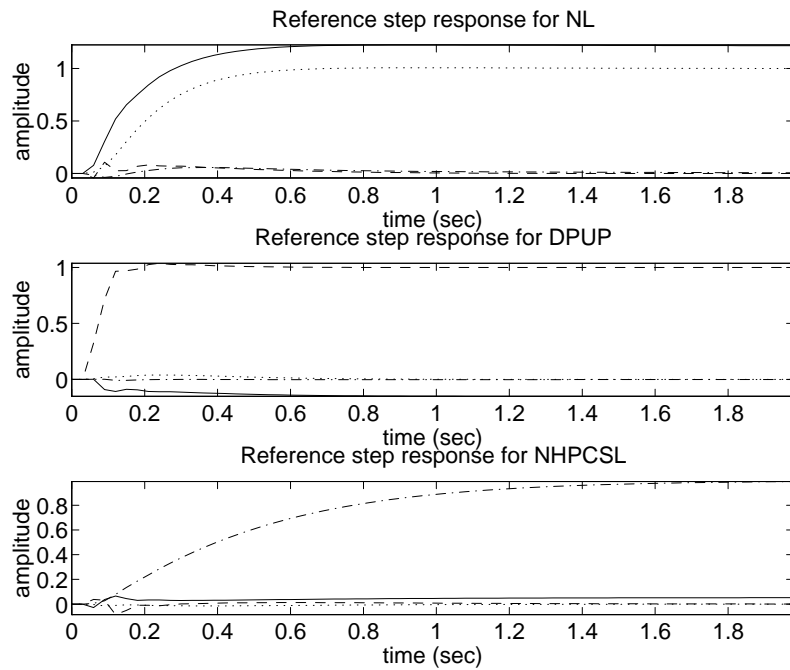


Figure 7.6: Reference step responses for the NL limiter (PS6PS1 —, DPUP ---, NHPCSL ---, NL ...).

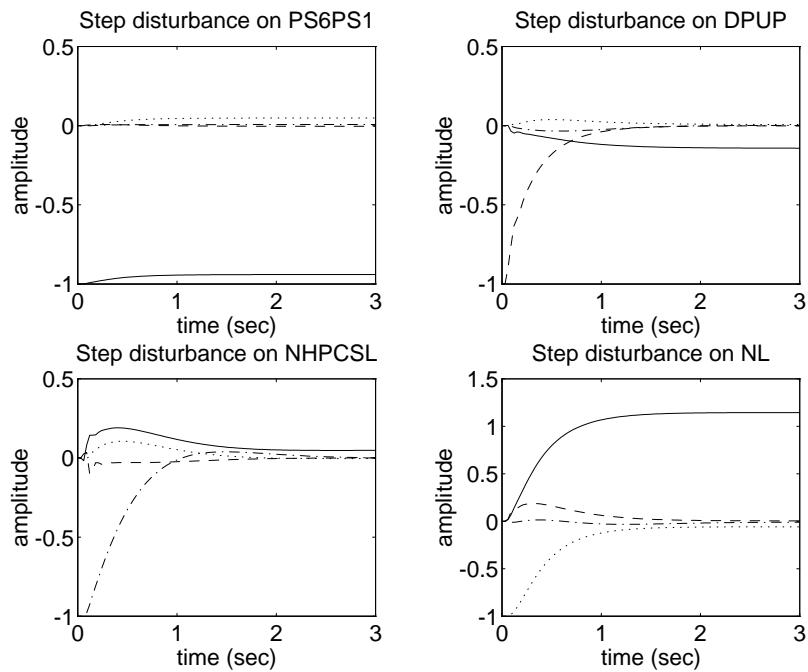


Figure 7.7: Disturbance step responses for the NL limiter (PS6PS1 —, DPUP - - -, NHPCSL ---, NL ...).

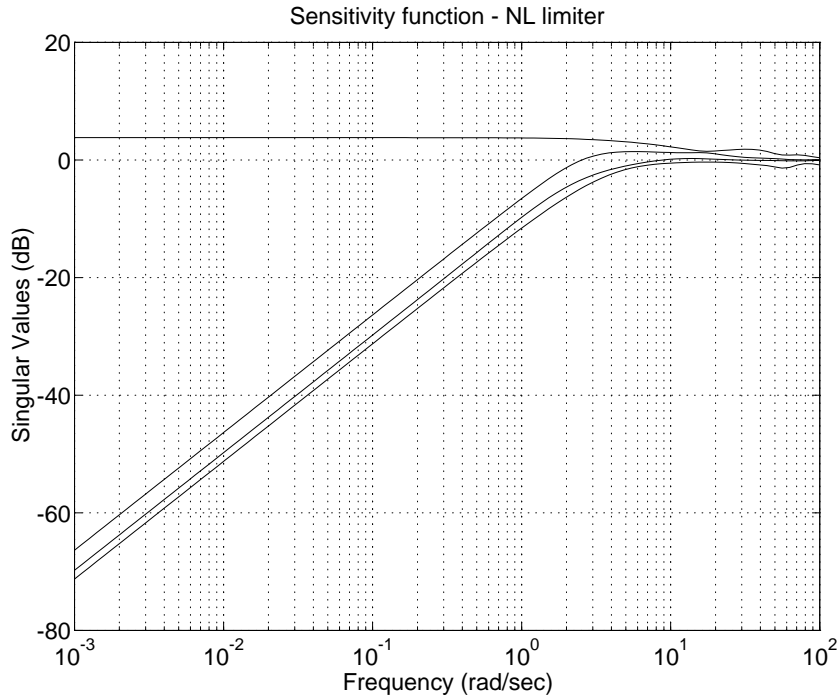


Figure 7.8: Sensitivity function  $(I + GW_1K_2W_2)^{-1}$  for the NL limiter.

are shown in Figure 7.9. The reference model for the closed-loop system is chosen to be  $diag\{\frac{1}{1.3s+1}, \frac{1}{0.05s+1}, \frac{1}{0.33s+1}\}$ . With  $\rho$  set to 1, the generalized plant of (6.4.3) is constructed and a  $\gamma$  of 2.675 achieved. Reference and disturbance step responses on the linear model are shown in Figures 7.10 and 7.11 respectively. The singular values of the sensitivity function are shown in Figure 7.12.

## 7.4 Controller implementation

We now present the controller structure used for implementation. The controller dynamics can be decomposed into an observer for the shaped plant, and the reference model dynamics, as is clear from Chapter 6, equation (6.8.16). Separating the observer and model dynamics, the controller state-space equations can be rewritten as:

$$\hat{x}_{G_{k+1}} = (A + HC) \hat{x}_{G_k} + \begin{bmatrix} -H & B \end{bmatrix} \begin{bmatrix} y_k \\ u_k \end{bmatrix}, \quad (7.4.1)$$

$$x_{o_{k+1}} = A_o x_{o_k} + B_o r_k, \quad (7.4.2)$$

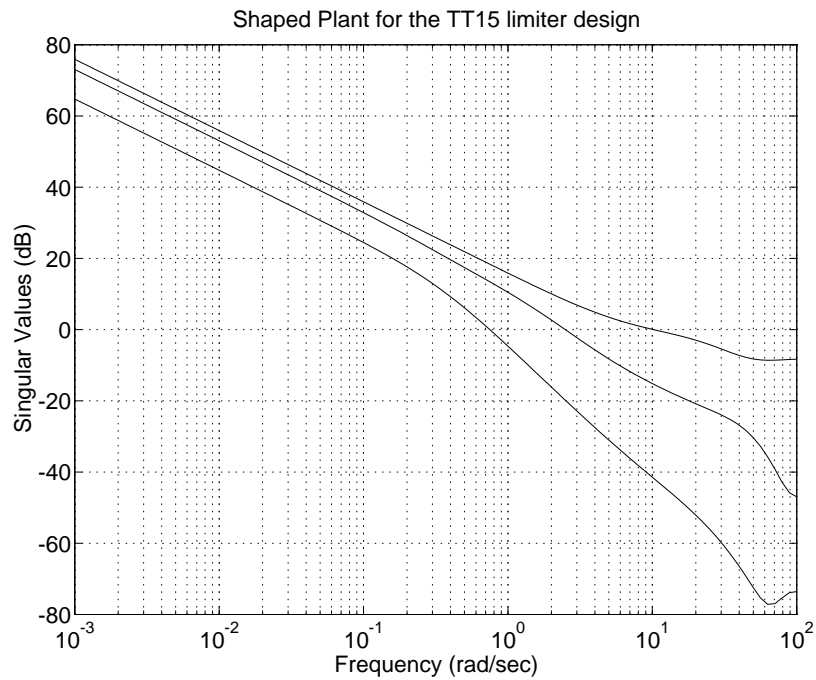


Figure 7.9: Singular values of the shaped plant for the TT15 limiter design.

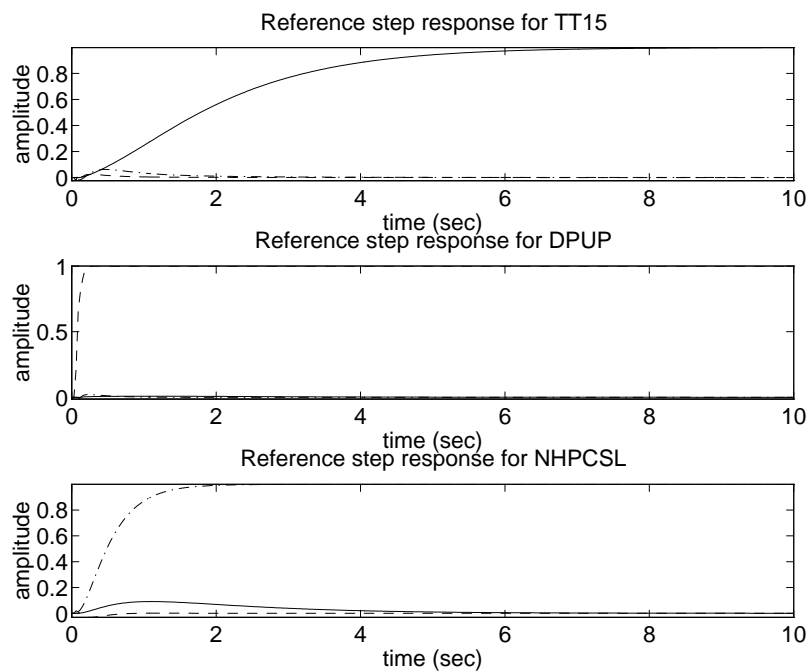


Figure 7.10: Reference step responses for the TT15 limiter (TT15 —, DPUP - - -, NHPCSL ----).

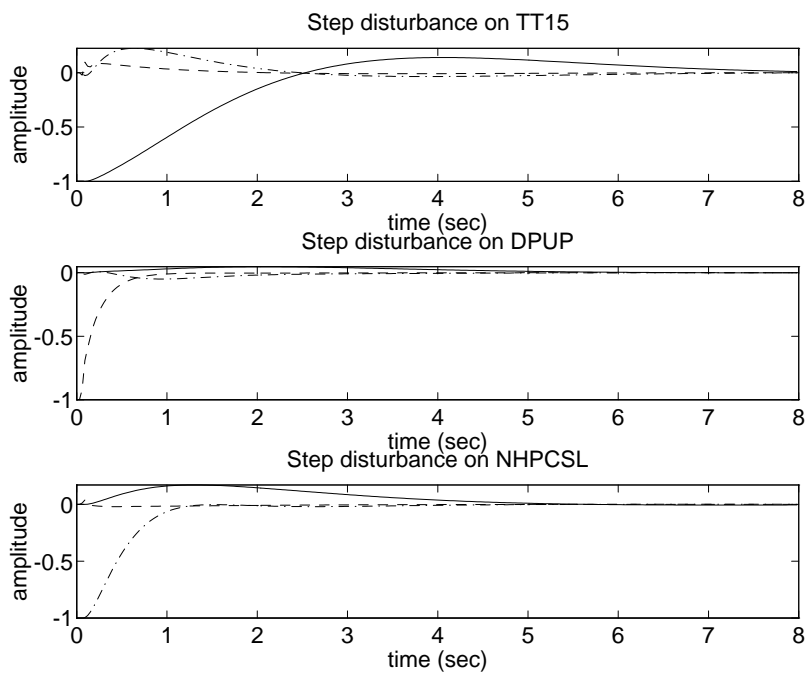


Figure 7.11: Disturbance step responses for the TT15 limiter (TT15 —, DPUP - - -, NHPCSL -.-.).

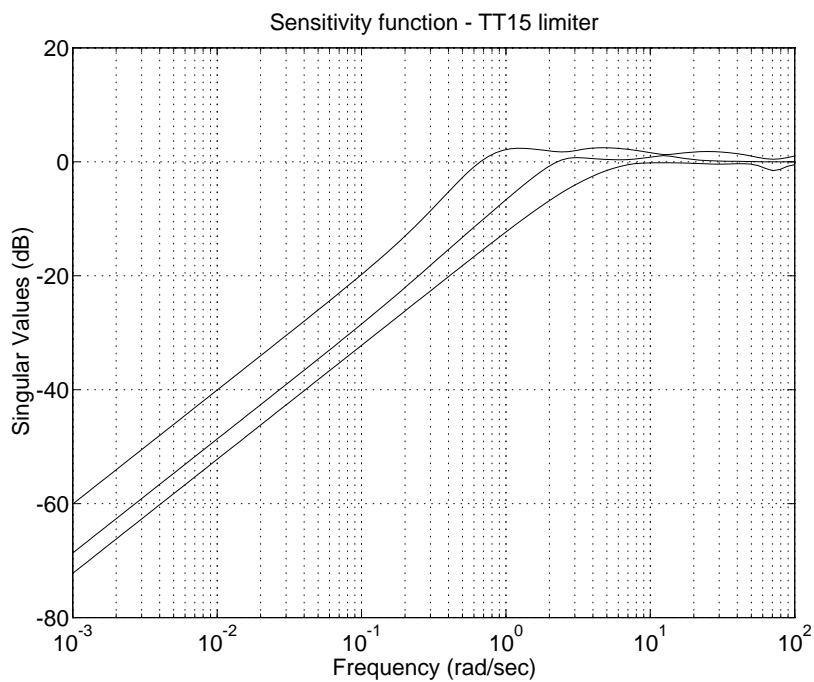


Figure 7.12: Sensitivity function  $(I + GW_1K_2W_2)^{-1}$  for the TT15 limiter.

and

$$\begin{aligned} u_k &= C_{k11}\hat{x}_{G_k} + C_{k12}x_{o_k} + \rho D_{k11}r_k + D_{k12}y_k \\ &= \hat{u}_k + u_{o_k}, \end{aligned} \quad (7.4.3)$$

where

$$\hat{u}_k \triangleq C_{k11}\hat{x}_{G_k} + [D_{k12} \quad 0] \begin{bmatrix} y_k \\ u_k \end{bmatrix}, \quad (7.4.4)$$

$$u_{o_k} \triangleq C_{k12}x_{o_k} + \rho D_{k11}r_k. \quad (7.4.5)$$

The controller is now seen to constitute two sub-systems, one given by equations (7.4.1) and (7.4.4), and the other given by equations (7.4.2) and (7.4.5), connected as in Figure 7.13.

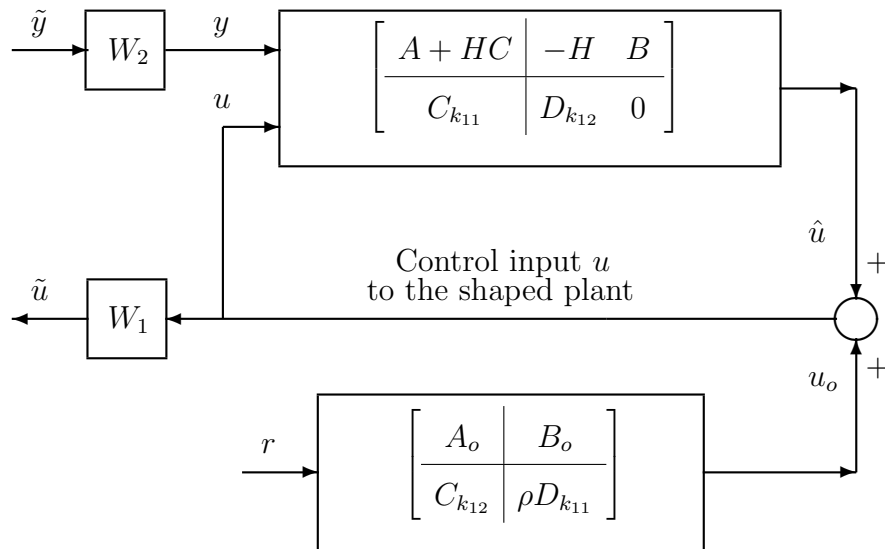


Figure 7.13: Controller partitioning into observer and reference model.

$u$  is the input to the shaped plant while  $\tilde{u}$  represents the actual plant input. Similarly  $y$  and  $\tilde{y}$  represent the shaped plant output and the actual plant output respectively. The separation of the controller as above yields significant computational advantages as discussed in the next section.

The controller was simulated in the form shown in Figure 7.13. It was found that implementing the controller in this form gave rise to stability problems. The instability resulted

from a high bandwidth local feedback loop inside the controller, i.e., from the signal  $\hat{u}$  to the signal  $u$  and back again to  $\hat{u}$  via the observer-state feedback combination. This loop was found to have a much higher bandwidth than that desired for the closed-loop system. The chosen sample time of 30 msec though just adequate for the closed-loop system bandwidth, was definitely inadequate for this much faster observer loop. The solution taken to this problem was to collapse the loop causing the instability and make the feedback implicit in the state-space equations as follows. From (7.4.1) we have:

$$\begin{aligned}
 \hat{x}_{G_{k+1}} &= (A + HC) \hat{x}_{G_k} + Bu_k - Hy_k \\
 (7.4.3) \implies &= (A + HC) \hat{x}_{G_k} + B(C_{k_{11}} \hat{x}_{G_k} + C_{k_{12}} x_{o_k} + \rho D_{k_{11}} r_k + D_{k_{12}} y_k) - Hy_k \\
 &= (A + HC + BC_{k_{11}}) \hat{x}_{G_k} + B(C_{k_{12}} x_{o_k} + \rho D_{k_{11}} r_k) + (-H + BD_{k_{12}}) y_k \\
 (7.4.5) \implies &= (A + HC + BC_{k_{11}}) \hat{x}_{G_k} + [-H + BD_{k_{12}} \quad B] \begin{bmatrix} y_k \\ u_{o_k} \end{bmatrix}. \quad (7.4.6)
 \end{aligned}$$

(7.4.4) can be rewritten as:

$$\hat{u}_k = C_{k_{11}} \hat{x}_{G_k} + [D_{k_{12}} \quad 0] \begin{bmatrix} y_k \\ u_{o_k} \end{bmatrix}. \quad (7.4.7)$$

The two systems, one given by equations (7.4.6) and (7.4.7) and the other described by the state-space equations (7.4.2) and (7.4.5) can now be connected as in Figure 7.14, and this is the final form used for implementation. It can be seen that the local feedback inside the controller is no longer explicit in the block diagram (Figure 7.14), rather it is made implicit in the observer state equation. The stability problems associated with the sample time are therefore resolved.

## 7.5 Computational advantages gained by utilizing the controller structure

Each of the three controllers designed has, excluding the weights, a state dimension of 27. The shaped plant observer contributes 24 states, and the reference model three states. The observer for each controller is reduced to 12 states, so that the reduced controllers have order 15. We will now explore the computational advantages gained by implementing the controllers in the form shown in Figure 7.14.

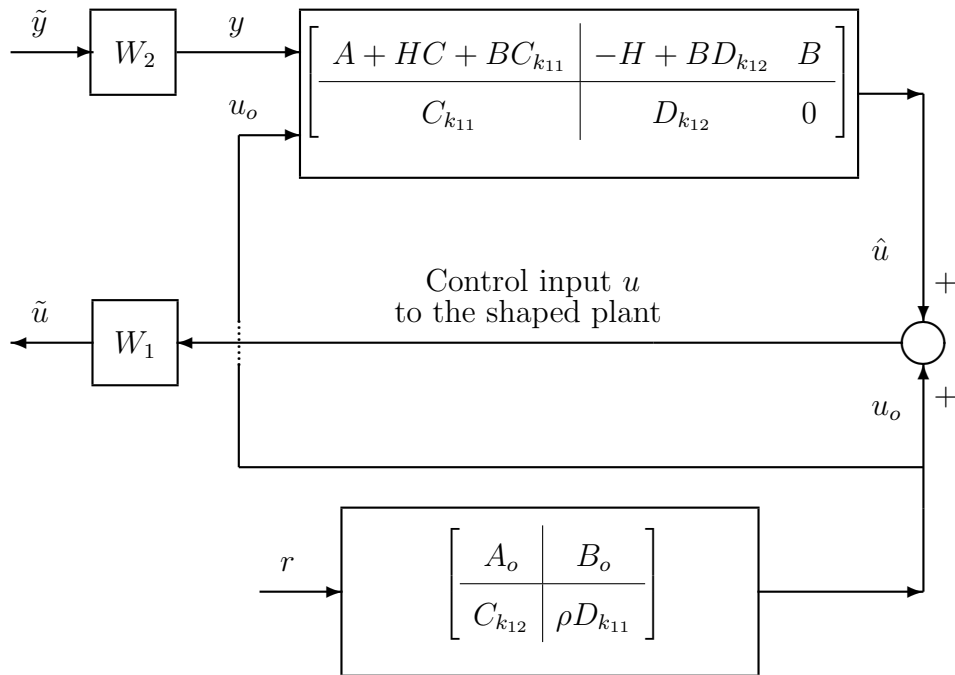


Figure 7.14: Controller structure used for implementation.

First let us calculate the computations required to run a 15 state unstructured controller in real time. The state up-date equation for such a controller (assuming three measurements) requires  $15 \times 15 + 15 \times 3 = 270$  multiplications and  $15 \times 14 + 15 \times 2 = 240$  additions. We now consider the case where the controller is partitioned into a 12 state observer and a 3 state reference model (as in Figure 7.14). The observer state equation requires  $12 \times 12 + 12 \times 3 = 180$  multiplications and  $12 \times 11 + 12 \times 2 = 156$  additions while the model state up-date requires  $3 \times 3 + 3 \times 3 = 18$  multiplications and  $3 \times 2 + 3 \times 2 = 12$  additions. The total number of multiplications required is therefore calculated to be  $180 + 18 = 198$ , and the total additions are  $156 + 12 = 168$ . This corresponds to a reduction of 26% in the number of multiplications and a reduction of 30% in the number of additions required. When running a number of controllers in parallel, implementing each in the form shown in Figure 7.14, can thus yield a significant saving in the amount of real time computation required. The overall switched controller containing all the three controllers running in parallel (§7.6), was implemented on a real time Intel 486-based machine. The controller structure described above was found to be crucial in running the control algorithms within

the desired sample time of 30 msec.

## 7.6 The switched controller structure

We now present the structure of the overall switched controller. In the sequel  $\bar{M}_o(z)$  denotes the reference model dynamics and the associated state feedback gain, i.e.,  $\bar{M}_o(z) \triangleq \left[ \begin{array}{c|c} A_o & B_o \\ \hline C_{k_{12}} & \rho D_{k_{11}} \end{array} \right]$ . The controller structure is illustrated in Figure 7.15. The superscripts “nl” and “tt” refer to parameter values for the NL and TT15 controllers respectively. It can be seen that the PS6PS1 and NL controllers share the same observer. The post-compensator driving the observer is switched, depending on whether the PS6PS1 or NL controllers is on-line, thus giving disturbance rejection and precise tracking on appropriate outputs. Either  $W_2$  or  $W_2^{nl}$  can be used while the TT15 limiter is on-line. The observer states evolve according to equation (7.4.6),  $C_{k_{11}}$  and  $D_{k_{12}}$  being replaced by  $C_{k_{11}}^{nl}$  and  $D_{k_{12}}^{nl}$  respectively when the NL limiter is selected on-line. The second input to the observer (from  $\bar{M}_o(z)$  or  $\bar{M}_o^{nl}(z)$ ) is also switched accordingly. The reference demands  $r^{nl}$  and  $r^{tt}$  for the limiters are set so that maximum values of NL and TT15 are demanded. The pre-compensator  $W_1$  is the same for the three controllers. The selection is made with regards to the amount of fuel demanded by each controller, the one that demands the least fuel is the one that is selected on-line (§3.3.3). The switched control system thus operates in the PS6PS1 mode or in one of the two limiter modes, depending on which controller is on-line at a given time.

## 7.7 Anti-windup and bumpless transfer

The issues of anti-windup and bumpless transfer (AWBT) are of great importance with regards to the practical implementation of a multi-mode control system. There have been many approaches to provide a solution to the AWBT problem, e.g., anti-reset windup [7] or back-calculation and tracking [3], the high gain conventional anti-windup [46, 53], the conditioning technique [41, 40], the observer-based approach [4] and the internal model control based approach [68, 7]; for a survey of these approaches refer to [67, 56]. All these approaches can be summarized as consisting of two parts:

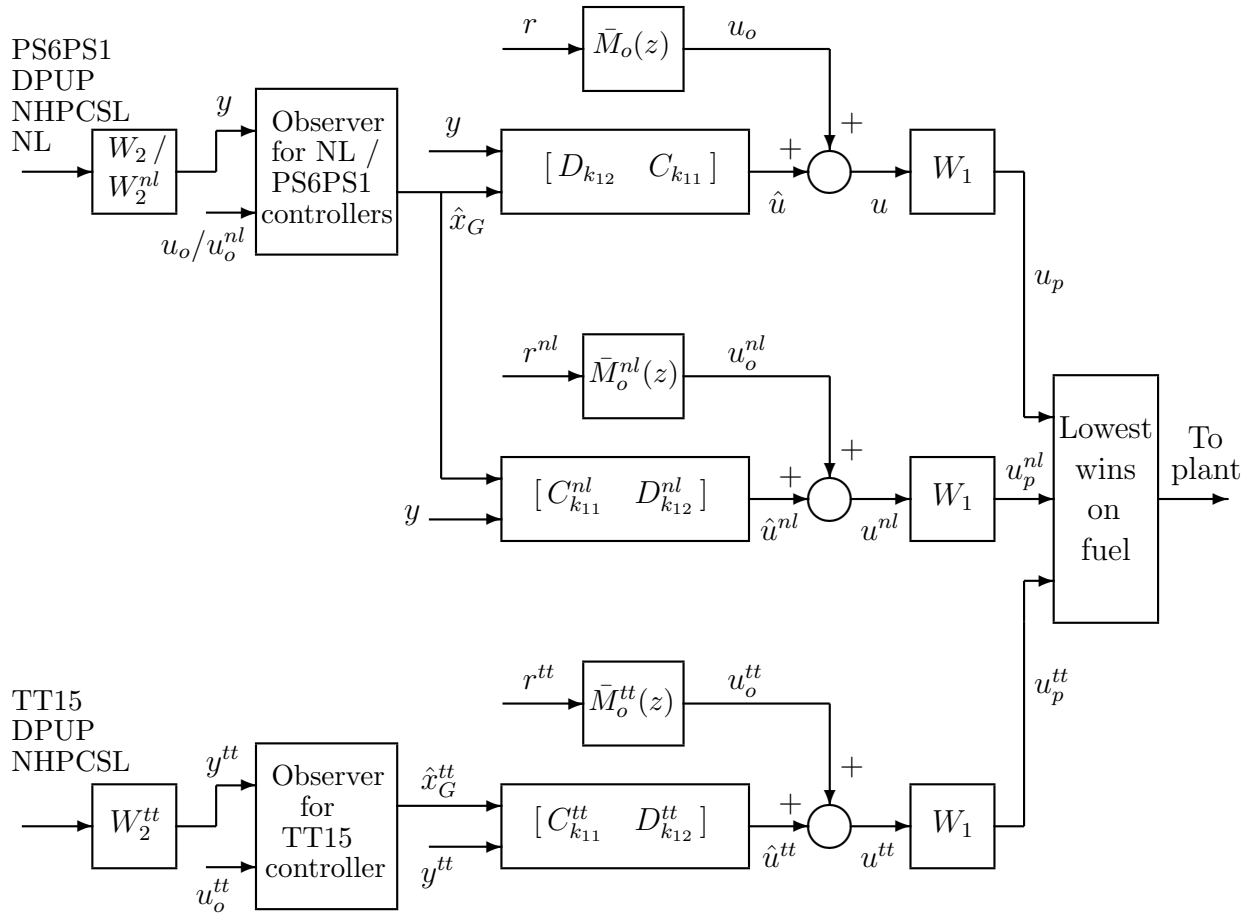


Figure 7.15: Structure of the overall switched controller.

- design the linear controller ignoring control limitations and substitutions, and
- add AWBT compensation to minimize the adverse effects of limitations and substitutions on closed-loop performance.

Recently there have been studies to cast the AWBT problem into a general design framework [8, 7] but this approach is still in the developing stage and synthesis results are not available. Almost all practical designs therefore, employ one of the above-mentioned techniques to provide anti-windup and bumpless transfer action. These techniques though somewhat ad-hoc, have nevertheless been successful in many applications; see for example [46, 53]. Their main strength lies in their simplicity and ease of implementation.

The conditioning technique of Hanus et al. [41] and the observer-based approach of Åström & Wittenmark [4] will be used for the aero-engine designs presented here. Both techniques are inherently multivariable and are simple and intuitive. The conditioning technique has been shown to be a generalization of both classical anti-windup and the internal model control based approach [7]. Campo & Morari [7] also show that the conditioning technique is superior to the other two schemes and can be combined with input directionality compensation to yield an effective anti-windup scheme.

The conditioning technique provides AWBT action by ensuring that the states of the (off-line) controller are always consistent with the input to the plant. Consider a simple error feedback controller  $(A, B, C, D)$  with the non-linearity  $N$  representing a limitation or a substitution:

$$\begin{aligned} \dot{x} &= Ax + B(r - y), \\ u &= Cx + D(r - y), \\ u_m &= N(u). \end{aligned} \tag{7.7.1}$$

Here  $r$  and  $y$  represent the reference input and the plant output respectively, and  $u_m$  represents the actual plant input. Following Hanus et al. [41] we can apply a “realizable reference”  $r^r$  to the controller such that the output of the controller is  $u_m$ , i.e.,  $r^r$  is the reference signal that would make  $u = u_m$  if applied to the controller state and output equations in place of  $r$ . Thus, we have:

$$\dot{x} = Ax + B(r^r - y), \tag{7.7.2}$$

$$u_m = Cx + D(r^r - y). \tag{7.7.3}$$

Using the state  $x$  as given by (7.7.2) and the actual reference input  $r$  to build the control  $u$ , we can write [40]:

$$u = Cx + D(r - y). \tag{7.7.4}$$

From (7.7.3) and (7.7.4) we obtain the expression for  $r^r$  as:

$$r^r = r + D^{-1}(u_m - u), \tag{7.7.5}$$

where we assume that  $D$  is invertible. Combining equations (7.7.1), (7.7.2), (7.7.4) and (7.7.5), we get:

$$\dot{x} = (A - BD^{-1}C)x + BD^{-1}u_m, \tag{7.7.6}$$

$$u = Cx + D(r - y), \quad (7.7.7)$$

$$u_m = N(u). \quad (7.7.8)$$

This is the AWBT *self-conditioned* controller. Using equations (7.7.6) – (7.7.8) we can write the conditioned controller in more compact notation as:

$$u = \left[ \begin{array}{c|cc} A - BD^{-1}C & 0 & BD^{-1} \\ \hline C & D & 0 \end{array} \right] \begin{bmatrix} r - y \\ u_m \end{bmatrix}. \quad (7.7.9)$$

It can be seen from (7.7.9) that during limitations or substitutions, the controller is effectively inverted, while in normal conditions (i.e., when  $u_m = u$ ) the controller dynamics remain unchanged. Hence for this technique to be applied, the controller must be invertible and minimum phase.

We now discuss briefly the idea of providing AWBT action using the observer approach of Åström & Wittenmark [4]. Let the output of an observer-based controller be  $u$ , the observer being driven by  $u$  and the plant output  $y$ . The plant input is given by  $u_m$ . When there is a limitation or a substitution,  $u_m$  is different from  $u$ , and since the observer is not aware of this it computes the state as if the plant input is  $u$ . Thus windup can be prevented simply by making the observer input to be  $[u_m^T \ y^T]^T$  instead of  $[u^T \ y^T]^T$ . Let us define an observer-based controller as:

$$\dot{\hat{x}} = A\hat{x} + Bu + H(C\hat{x} - y), \quad (7.7.10)$$

$$u = F\hat{x}, \quad (7.7.11)$$

$$u_m = N(u). \quad (7.7.12)$$

Here  $(A, B, C, 0)$  is the state-space realization of the plant being controlled, and  $H$  and  $F$  are the observer and state feedback gains respectively. Note that the dynamics of the controller are given by

$$\det(sI - A - BF - HC) = 0$$

in the absence of the non-linearity  $N$  and by

$$\det(sI - A - HC) = 0$$

when  $u_m$  is different from  $u$ . The dynamics of the controller in this case are thus given by the observer dynamics which are designed to be fast and stable, hence preventing windup problems.

With reference to the controller of Figure 7.15, the pre-compensator  $W_1$  provides integral action that is vital for rejecting disturbances acting on the system. However, in case of actuator saturation, or the controller being selected off-line, the integrators continue to integrate the error and hence cause windup problems. An anti-windup scheme is therefore required on the weighting function  $W_1$ . The approach taken here is to implement the weight  $W_1$  in its self-conditioned or Hanus form. Given  $W_1 \stackrel{s}{=} \left[ \begin{array}{c|c} A_{w_1} & B_{w_1} \\ \hline C_{w_1} & D_{w_1} \end{array} \right]$ , we have from Figure 7.15:

$$u_p = W_1 u = \left[ \begin{array}{c|c} A_{w_1} & B_{w_1} \\ \hline C_{w_1} & D_{w_1} \end{array} \right] u. \quad (7.7.13)$$

When implemented in Hanus form, the expression for  $u_p$  becomes:

$$u_p = \left[ \begin{array}{c|cc} A_{w_1} - B_{w_1} D_{w_1}^{-1} C_{w_1} & 0 & B_{w_1} D_{w_1}^{-1} \\ \hline C_{w_1} & D_{w_1} & 0 \end{array} \right] \begin{bmatrix} u \\ u_{p_m} \end{bmatrix}, \quad (7.7.14)$$

where  $u_{p_m}$  is the actual plant input. Note that  $u_{p_m}$  is the measurement at the output of the actuators and hence contains information about possible actuator saturation. As discussed above, the Hanus form (7.7.14) prevents windup by keeping the states of  $W_1$  consistent with the actual plant input at all times. In cases where there is no saturation/substitution (i.e.,  $u_{p_m} = u_p$ ), the dynamics of  $W_1$  remain unaffected as (7.7.14) simplifies to (7.7.13), but when  $u_{p_m} \neq u_p$ , the dynamics are inverted and driven by  $u_{p_m}$  so that the states remain consistent with  $u_{p_m}$ . Note that such an implementation requires  $W_1$  to be invertible and minimum phase.

In addition to  $W_1$ , the model  $\bar{M}_o(z)$  and the observer are also conditioned to ensure smooth transition from one controller to the other (bumpless transfer). The observer is conditioned so that its state always conforms to the actual input to the shaped plant. Thus when on-line, the observer state evolves according to (7.4.6), but when off-line the state equation becomes:

$$\hat{x}_{G_{k+1}} = (A + HC) \hat{x}_{G_k} + B u_m - H y_k, \quad (7.7.15)$$

where  $u_m$  is the actual input to the shaped plant, i.e.,  $u_m = u$  or  $u^{nl}$  or  $u^{tt}$ , depending on which controller drives the plant at a given time. The estimated state thus remains consistent with the actual plant input. The observer for the TT15 controller is also conditioned in a similar way.

For the model  $\bar{M}_o(z)$ , we have (Figure 7.15):

$$u_o = \bar{M}_o r = \left[ \begin{array}{c|c} A_o & B_o \\ \hline C_{k_{12}} & \rho D_{k_{11}} \end{array} \right] r. \quad (7.7.16)$$

In its self-conditioned form the expression for  $u_o$  is written as:

$$u_o = \left[ \begin{array}{cc|cc} A_o - B_o (\rho D_{k_{11}})^{-1} C_{k_{12}} & 0 & B_o (\rho D_{k_{11}})^{-1} & \\ \hline C_{k_{12}} & \rho D_{k_{11}} & 0 & \end{array} \right] \begin{bmatrix} r \\ u_m - \hat{u} \end{bmatrix}. \quad (7.7.17)$$

The conditioning on  $\bar{M}_o(z)$  thus ensures that the input  $\hat{u} + u_o$  to the shaped plant for the (off-line) controllers follows the actual shaped plant input  $u_m$ . It should be noted that we have used identical pre-compensators  $W_1$  for all the three controllers. In cases where these need to be different, one can still partition them such that they share a common factor (provided they have some common dynamics).  $\bar{M}_o^{nl}(z)$  and  $\bar{M}_o^{tt}(z)$  are also conditioned likewise. This helps in making the switching between the controllers smooth and bumpless.

## 7.8 Summary

This chapter has illustrated the design procedure proposed in Chapter 6, and discussed some of the implementation issues associated with multi-mode control systems. Design considerations for non-square (tall) plants were discussed in §7.2. It was shown that extra measurements with large loop-gains, can give poor disturbance rejection on the controlled outputs. Designs for the aero-engine controller were presented in §7.3. An efficient implementation strategy was developed in §7.4. The decoupling of the observer and model states was exploited to yield considerable real-time computational savings. The structure of the overall switched controller was discussed in §7.6. §7.7 described ways of conditioning the controller to provide anti-windup action in case of actuator saturation, and bumpless transfer when switching between different controller modes of operation.

## Chapter 8

### Engine test results

#### 8.1 Introduction

The purpose of this chapter is to evaluate the  $H_\infty$  multi-mode control law developed in Chapter 7 and to present and discuss engine test results. The controller was tested on the Rolls Royce Spey engine in July 1994. The engine is housed at one of the test facilities of the Defence Research Agency (DRA). It is controlled via an Intel 486-based computer, referred to as the digital control unit (DCU). The  $H_\infty$  controller was coded in FORTRAN and implemented on the DCU. Control of engine start-up was not considered, the engine being started and brought to idle<sup>1</sup> using conventional controllers. Arrangements were made so that by toggling a switch, control of the engine could be transferred from and to the conventional controller. This was done in the interests of safety; if anything were to go wrong, the control could quickly be switched to conventional.

This chapter is organized as follows. The test results are presented in §8.2. All the three modes of operation are considered and smooth switching between the modes is demonstrated. New design specifications were set up after the tests; these included requirements on the time response of the controlled system. §8.3 describes how these can be met using the same  $H_\infty$  controller as designed in Chapter 7. The engine tests were carried out at sea-level static conditions. §8.4 evaluates the controller at a range of points across the flight envelope (i.e., at different altitude and forward speeds) using the full non-linear

---

<sup>1</sup>The term ‘idle’ corresponds to the engine running just at self-sustaining speed, producing very little or no thrust (§3.1.2).

engine simulation. Finally §8.5 concludes the chapter.

## 8.2 Engine test results

Here we present engine test results. The output PS6PS1, as mentioned previously, represents engine thrust, and ranges from (approximately) 2.5 to 16 as the engine is accelerated from idle to maximum power. The operating point of the engine for the tests considered here, is therefore defined by PS6PS1.

All the three modes of operation: the thrust control mode, the NL limiting mode and the TT15 limiting mode were tested.

### 8.2.1 PS6PS1 (thrust) control mode

Figure 8.1 shows a positive step demand on PS6PS1, commanding the engine to accelerate from just above idle to about 75% of maximum power. The reference (or command) signals are shown in dashed line and the actual outputs in solid line. The thrust controller is on-line, and the three controlled outputs PS6PS1, DPUP, and NHPCSL are seen to track the reference signals closely. PS6PS1 and DPUP are non-dimensional quantities, while NHPCSL is expressed as percent of maximum speed. Engine thrust is also shown in the figure. The thrust measurement though available on the testbed, is not available during flight; hence we use PS6PS1 to represent and control thrust. The thrust plot serves to illustrate the close correspondence between PS6PS1 and thrust. Figure 8.2 shows the corresponding actuator signals. The fuel flow is measured in cc/sec and ranges from approximately 120 cc/sec to more than 1200 cc/sec. The nozzle area is expressed as percent of the maximum; 0% indicating minimum nozzle area and 100% indicating a fully open nozzle. Larger nozzle areas (30% and above) are required during reheat, when the afterburner is switched on. Control of reheat is not considered here and hence, the nozzle actuator will be seen to operate in the lower range only. The inlet guide vane angle is measured in degrees and ranges from 0 to 40. The fourth actuator, the blow-off valve position, is not used for closed-loop control; it is open-loop scheduled with NHPCSL.

Figure 8.3 shows an acceleration from idle to maximum power, PS6PS1 being commanded

from 2.5 to 16. The control signals are shown in Figure 8.4. Figures 8.5 and 8.6 show deceleration from full power down to idle, and the corresponding actuator signals. The reference tracking is again seen to be good. The tracking of the DPUP output is particularly important, this variable defines the surge margin of the low pressure compressor. Good tracking on DPUP gives good surge margin regulation, which implies that the engine can be operated at lower surge margins (higher efficiency) with greater confidence. This has important implications for future engine design: engines in the future could be designed to operate closer to their surge lines, and thus yield higher efficiency. It is seen that three of the actuators hit their end-stops (limits) during this manoeuvre. The fuel flow saturated at its lower limit of 160 cc/sec, the nozzle area saturated at 2%, and the guide vane angle at 0 degrees. Although the limits for fuel flow and nozzle area could be relaxed a bit more, these were set to conservatively safe values for the purpose of these tests. It is observed however, that all the three actuators come out of saturation gracefully; the AWBT compensation devised in Chapter 7 thus copes with the saturation successfully.

It should be noted that a single controller was used throughout the operating range – no gain-scheduling was used. Existing controllers used to drive such engines are gain-scheduled – six or more controllers are normally scheduled between idle and full power [100, 37, 51, 22]. The  $H_\infty$  two degrees-of-freedom controller thus exhibited a superior level of robust performance.

### 8.2.2 NL limiting mode

We now consider multi-mode operation of the controller. Figure 8.7 shows switching from the PS6PS1 controller to the NL limiter when the NL limit is lowered from 102% to 80%, the PS6PS1 demand being kept constant. It is seen from Figure 8.7(d) that before the limit is lowered, the NL output is at 84.5%, much below the set limit of 102%, and hence the PS6PS1 controller is on-line. Just before time 0 sec, NL limit is lowered to 80%; this caused the limit to be violated, hence the NL limiter comes on-line, bringing NL down to the new limit. The tracking on PS6PS1 is lost and it settles to a value in conformation with the limit on NL. Tracking on NHPCSL and DPUP remains effective. Figure 8.8(a) shows the fuel outputs of the PS6PS1 controller (dotted line) and the NL limiter (dashdot

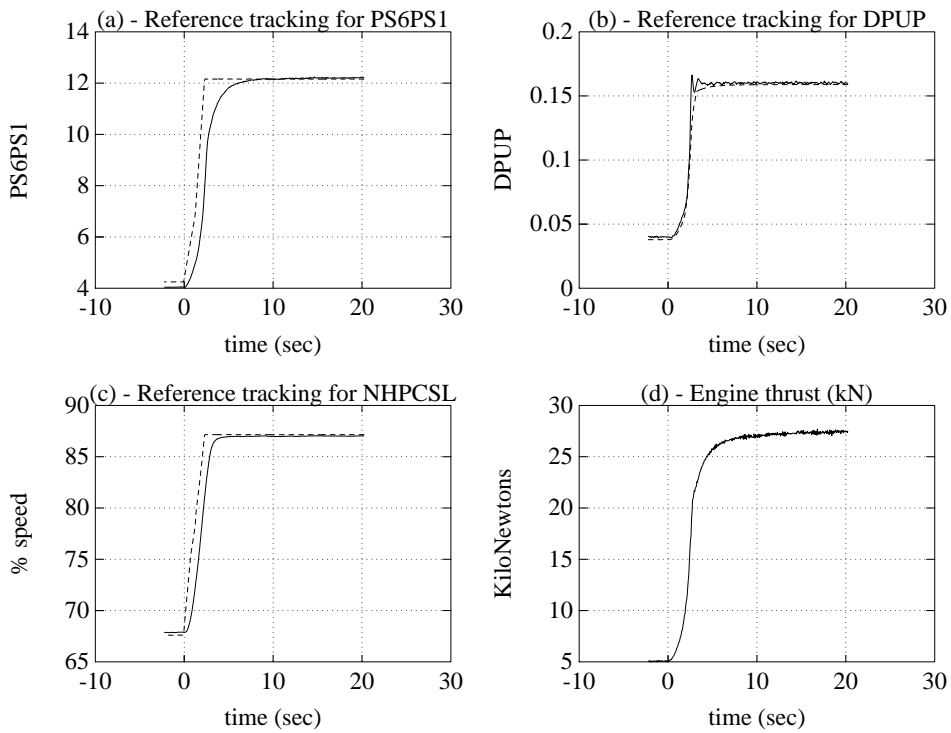


Figure 8.1: (a),(b),(c)–Reference tracking for the controlled outputs (commanded value - - , actual output —). (d)–Engine thrust measurement.

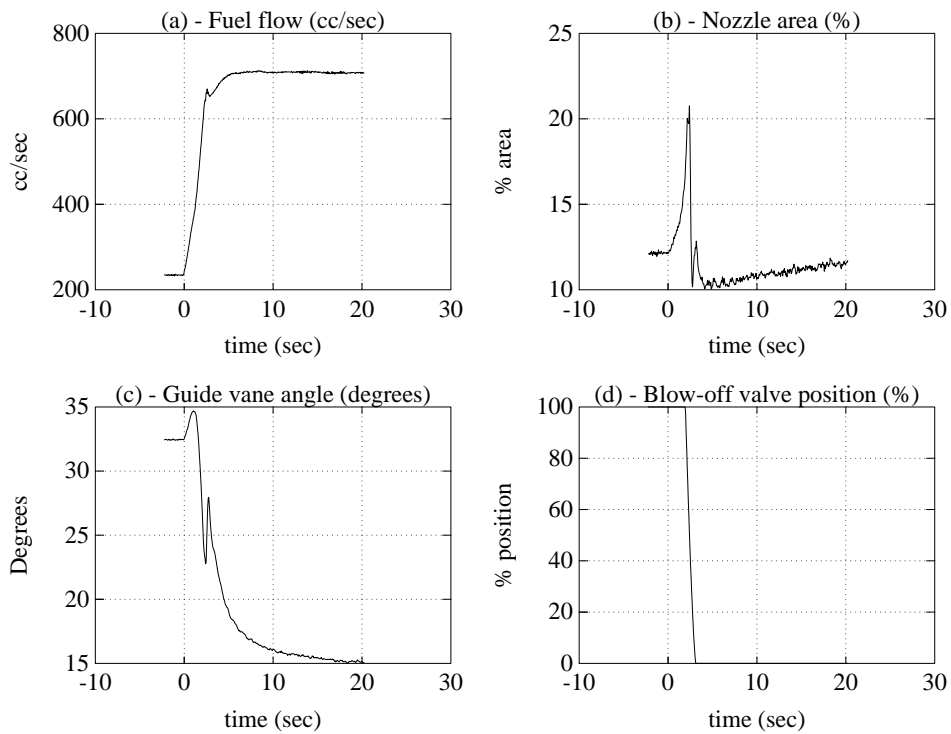


Figure 8.2: Actuator (control) signals.

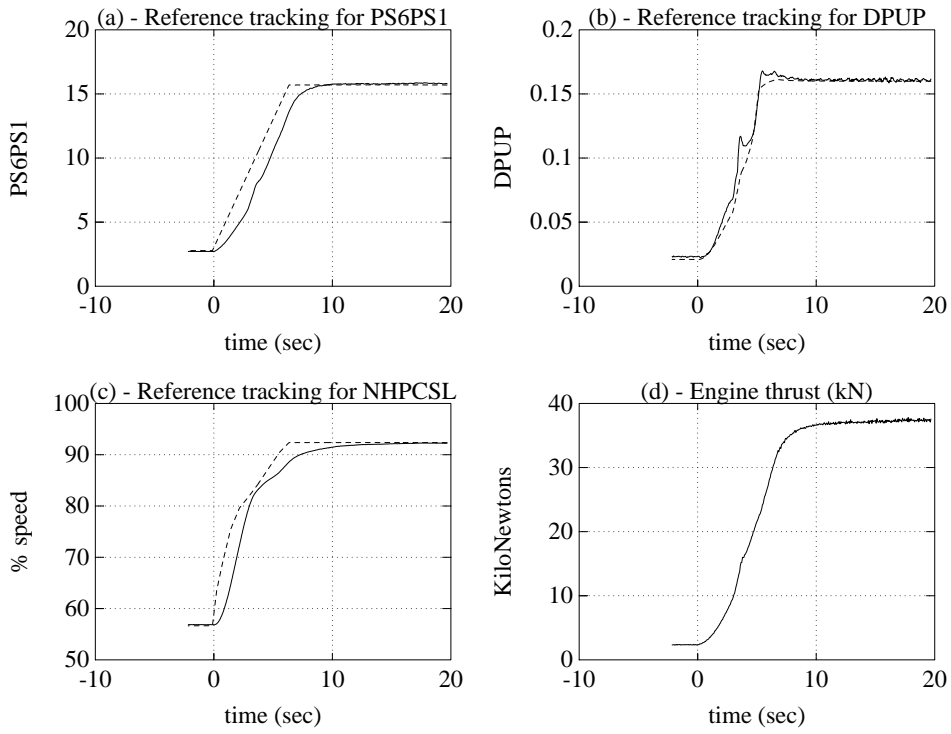


Figure 8.3: (a),(b),(c)–Reference tracking for the controlled outputs: idle to maximum power (commanded value - - -, actual output —). (d)–Engine thrust measurement.

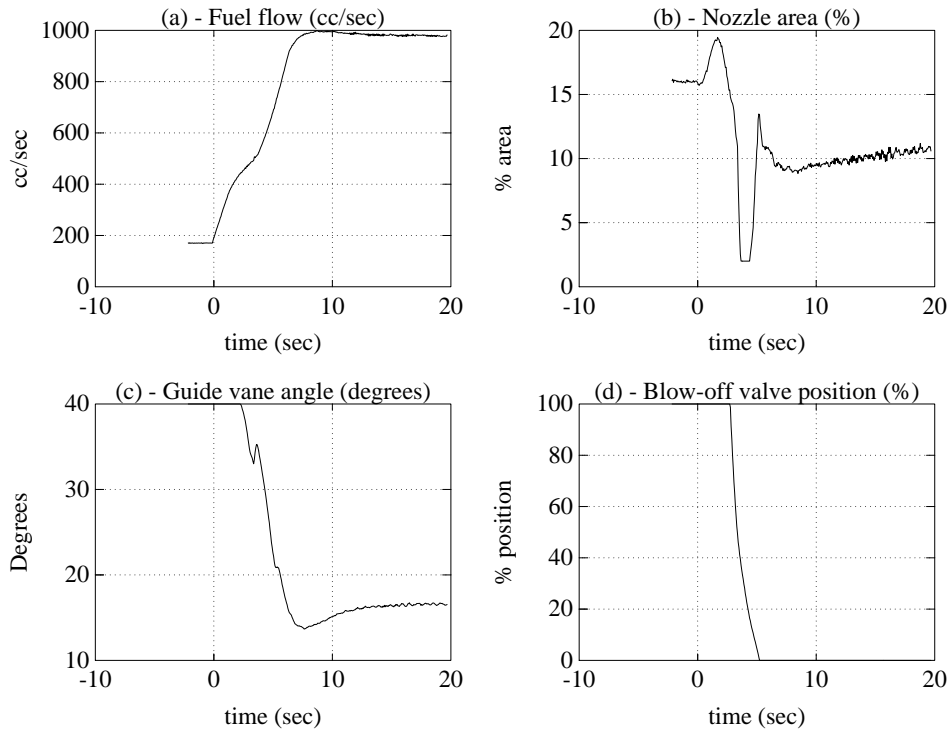


Figure 8.4: Actuator (control) signals: idle to maximum power.

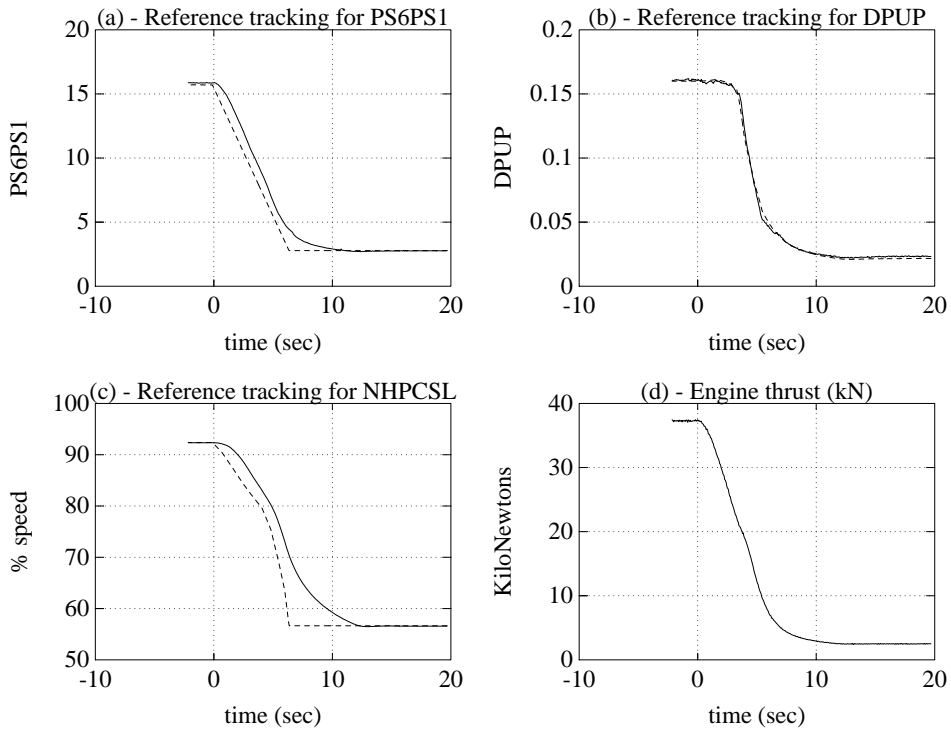


Figure 8.5: (a),(b),(c)–Reference tracking for the controlled outputs: maximum power to idle (commanded value - - -, actual output —). (d)–Engine thrust measurement.

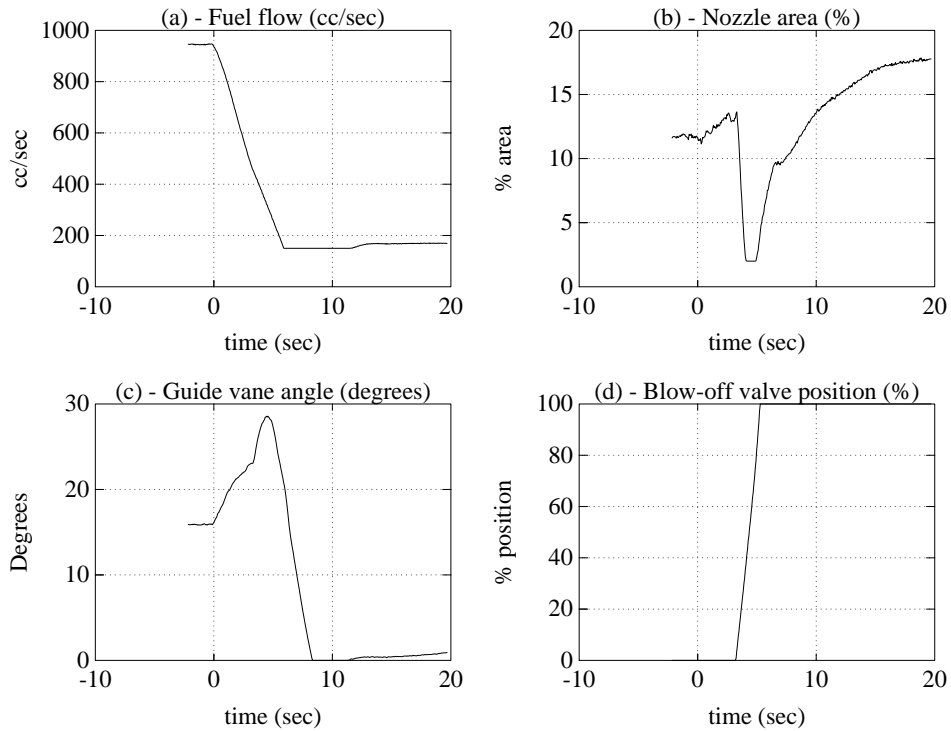


Figure 8.6: Actuator (control) signals: maximum power to idle.

line). The fuel selected to drive the engine is shown in solid line. It is seen that the NL limiter demands a higher fuel initially and so the PS6PS1 controller is selected on-line, but after the limit is lowered, the NL limiter's fuel output becomes smaller and hence it is chosen on-line. The switching from PS6PS1 control mode to the NL limiting mode occurs smoothly without excessive transients or bumps.

Figure 8.9 shows switching to the NL limiter due to an excessive PS6PS1 demand. The NL limit is fixed at 80%. Initially NL is at 70%, and the PS6PS1 controller is on-line. At time 0 sec, the reference for PS6PS1 is raised to a high value so that it would cause NL to exceed its limit. The NL limiter thus switches over and brings NL on to its limit. The limit is overshoot transiently, the overshoot of 1% being within the specification. DPUP and NHPCSL are held at their demanded values. The fuel outputs of the PS6PS1 controller and the NL limiter are shown in Figure 8.10(a). The lower of the two fuels is always selected, as indicated by the solid line. The transition is smooth and takes place at the instant when the fuel demanded by the PS6PS1 controller (dotted line) exceeds that demanded by the NL limiter (dashdot line).

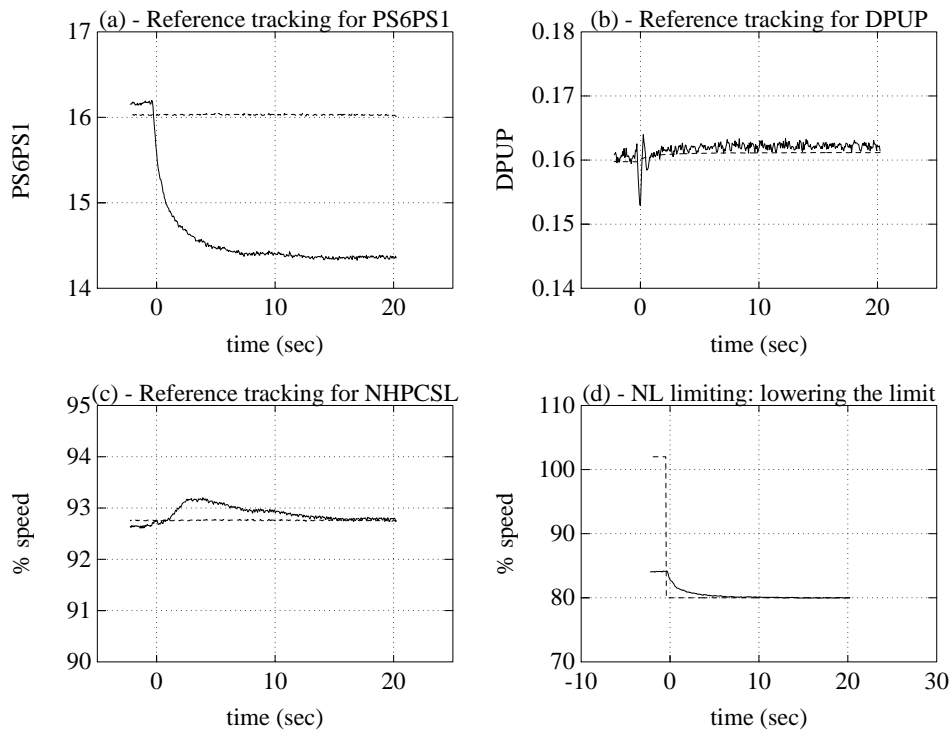


Figure 8.7: Switching from PS6PS1 controller to NL limiter by lowering the limit. (a),(b),(c)–commanded value - - -, actual output —. (d)–NL limit - - -, NL —.

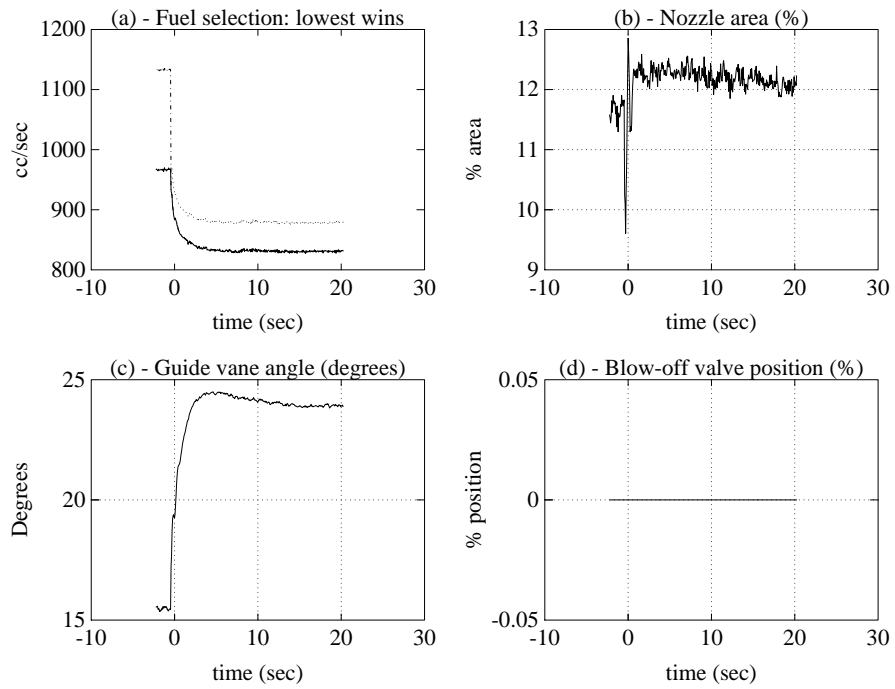


Figure 8.8: Actuator signals: switching to NL limiter by lowering the limit. (a)–Fuel outputs (PS6PS1 controller  $\cdots$ , NL limiter  $\cdots\cdots$ , fuel selected (to engine)  $\text{—}$ ).

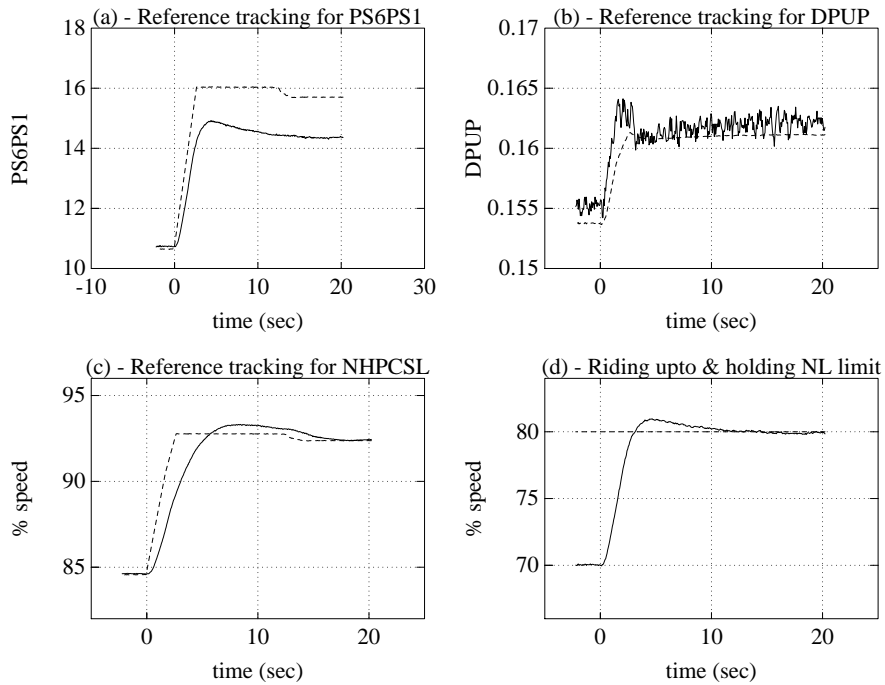


Figure 8.9: Switching from PS6PS1 controller to NL limiter due to excessive PS6PS1 demand. (a),(b),(c)–commanded value  $\text{---}$ , actual output  $\text{—}$ . (d)–NL limit  $\text{---}$ , NL  $\text{—}$ .

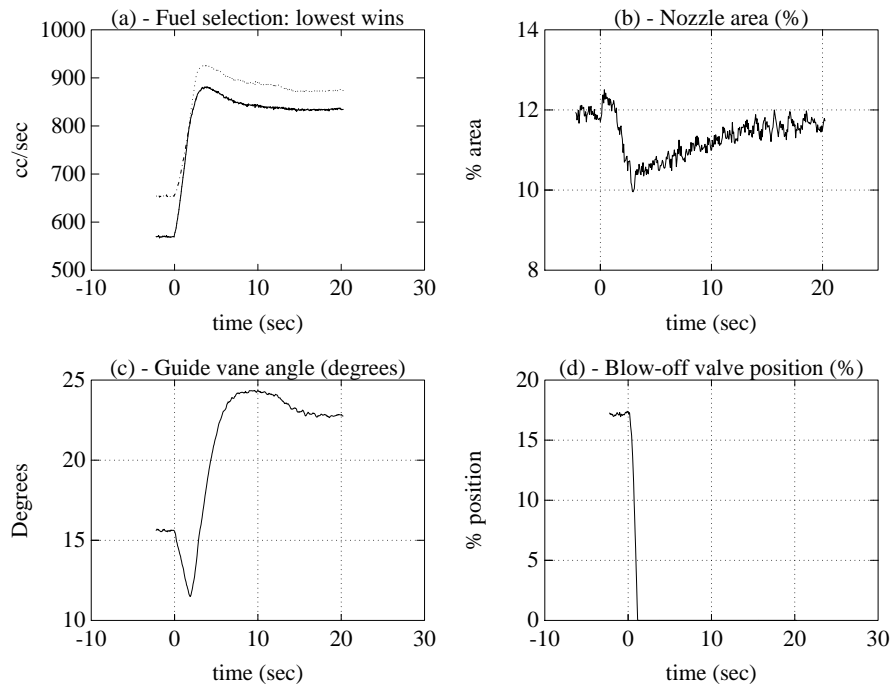


Figure 8.10: Actuator signals: switching to NL limiter due to excessive PS6PS1 demand. (a)–Fuel outputs (PS6PS1 controller  $\cdots$ , NL limiter  $-\cdots-$ , fuel selected (to engine)  $—$ ).

### 8.2.3 TT15 limiting mode

Figure 8.11 shows switching from the PS6PS1 controller to the TT15 limiter due to a lowering of the TT15 limit from  $913^{\circ}\text{K}$  down to  $843^{\circ}\text{K}$ . Initially the PS6PS1 controller is on-line, and TT15 is below the limit. At time 0 sec, the limit is lowered so that TT15 is now higher than the limit; the TT15 limiter is thus selected on-line driving TT15 down to the new limit. The tracking on PS6PS1 is lost as expected, and the other two outputs track their references satisfactorily. The actuator signals are shown in Figure 8.12. The lowest-wins selection on fuel is illustrated, the fuel output of the TT15 limiter (shown in dashdot line) being selected to drive the engine when it falls below the fuel demanded by the PS6PS1 controller (dotted line).

Figure 8.13 shows switching to the TT15 limiter following an excessive thrust demand. The PS6PS1 controller is on-line initially and the TT15 limit is set to  $843^{\circ}\text{K}$ . The reference for PS6PS1 is then raised to a value that would cause the temperature limit to be violated. The control is thus switched to the TT15 limiter, the exact instant of switching can be seen from the controller fuel outputs shown in Figure 8.14(a).

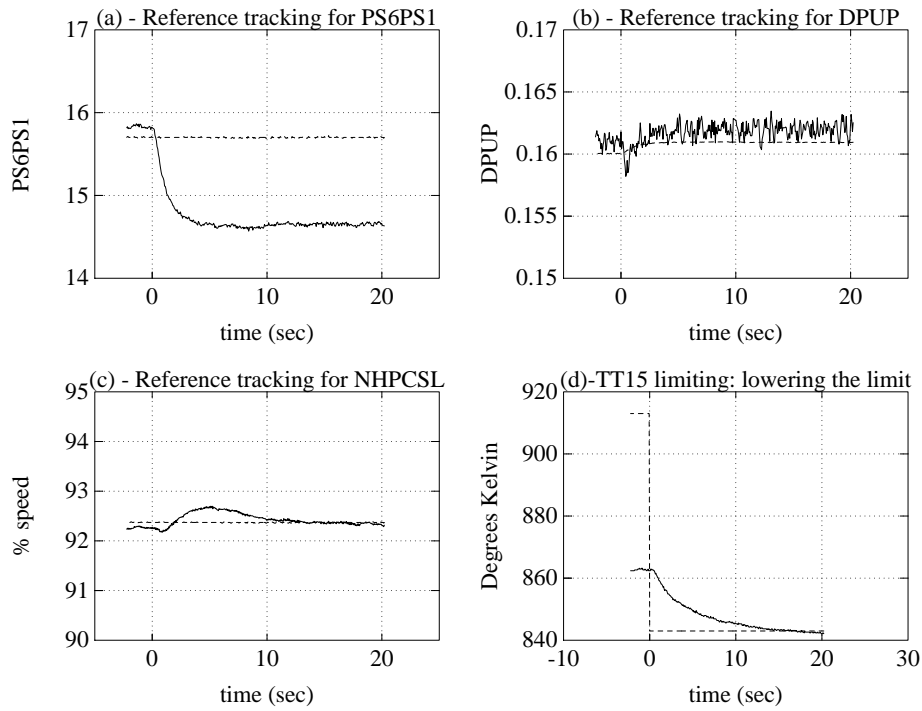


Figure 8.11: Switching from PS6PS1 controller to TT15 limiter by lowering the limit. (a),(b),(c)–commanded value - - -, actual output —. (d)–TT15 limit - - -, TT15 —.

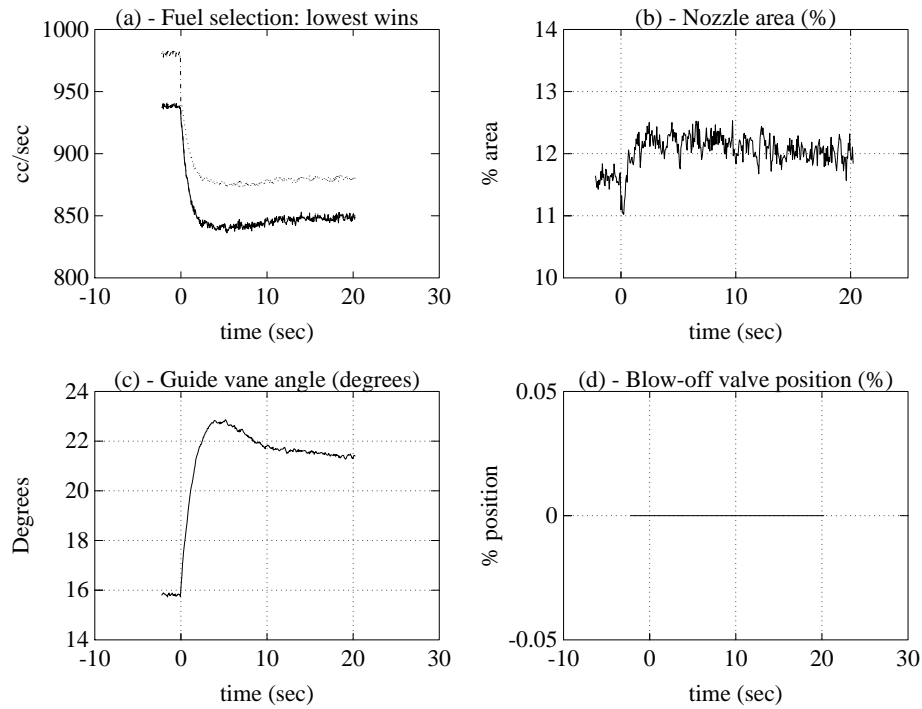


Figure 8.12: Actuator signals: switching to TT15 limiter by lowering the limit. (a)–Fuel outputs (PS6PS1 controller  $\cdots$ , TT15 limiter  $---$ , fuel selected (to engine) —).

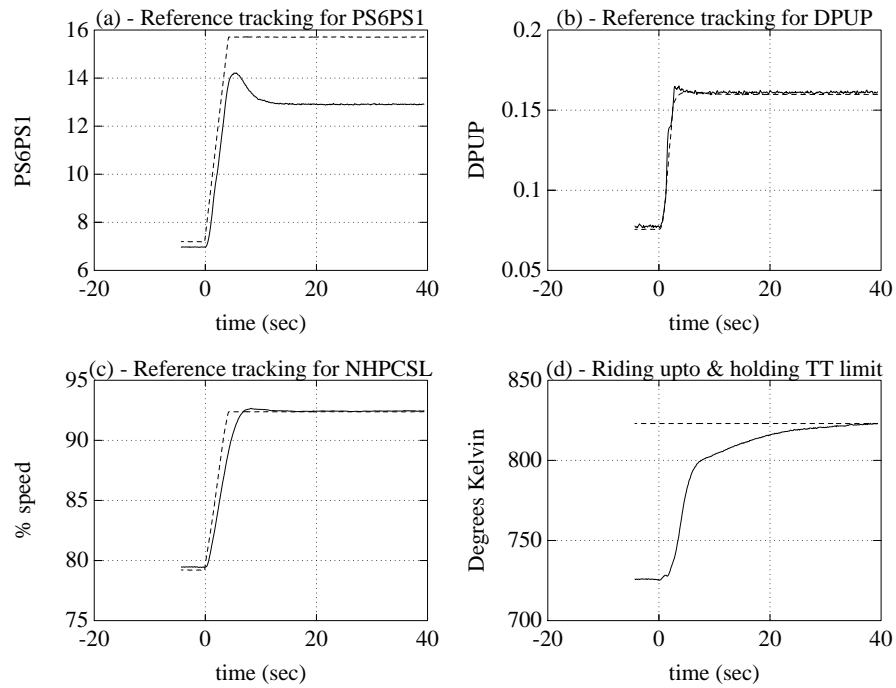


Figure 8.13: Switching from PS6PS1 controller to TT15 limiter due to excessive PS6PS1 demand. (a),(b),(c)–commanded value - - -, actual output —. (d)–TT15 limit - - -, TT15 —.

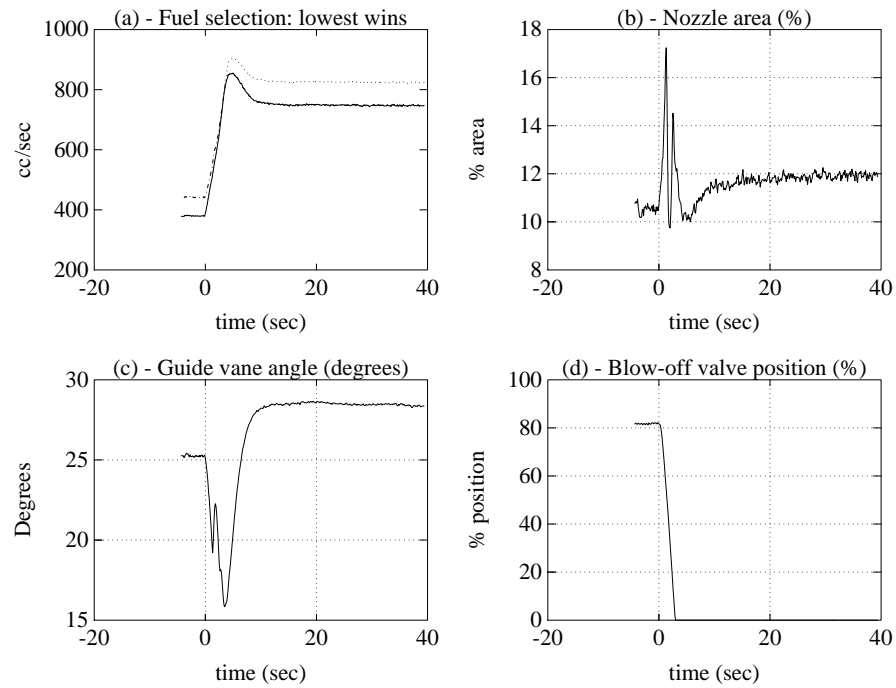


Figure 8.14: Actuator signals: switching to TT15 limiter due to excessive PS6PS1 demand. (a)–Fuel outputs (PS6PS1 controller  $\cdots$ , TT15 limiter  $---$ , fuel selected —.

### 8.3 Improving speed of response

New specifications [99] were provided after the tests; these included requirements on the step response of the closed-loop system. In particular, the requirement given for a small scale step response for thrust was that the response should attain 90% of the demanded change within 0.5 seconds of the initiation of the step and thereafter stay within a band of 10% of the change from the demanded value. The engine test results indicate that this requirement has not been met. We will now show how to improve the speed of response of the closed-loop system so that the specification is achieved; the same controller will be used and no redesign is required.

It should be noted that the  $H_\infty$  controller of Chapter 7 was designed so that it could yield rise times of magnitude similar to that required by the new specification. This can be seen from Figure 7.3, in which the linear PS6PS1 response is seen to settle within the desired time of 0.5 seconds. The sluggishness observed in the engine tests arises from the particular implementation of the anti-windup compensation used. Note that the weight  $W_1$  is conditioned based on the “measured” actuator position ( $u_{p_m}$  in equation (7.7.14)), and is thus influenced by the actuator dynamics. Even when there is no saturation,  $u_{p_m}$  is not equal to  $u_p$  (because of the dynamics of the actuators), and this affects the dynamics of  $W_1$  as (7.7.14) does not simplify to (7.7.13).  $W_1$  is conditioned so that its states (and output  $u_p$ ) conform to the measurement  $u_{p_m}$ , and since  $u_{p_m}$  always lags behind  $u_p$  due to the actuator lag, the effect is to make the control signal sluggish, and the response slow.

It should be noted that engine control systems in general do not use the actual actuator position to produce anti-windup, and in any case such a measurement is not available during flight. The actuator saturation levels are known and in practice the control signal is limited by the control computer itself before giving it to the actuators. In other words, the computed output of the controller is “software limited”, and this limited output is used for conditioning. The sluggishness caused by having the actuator dynamics in the anti-windup loop is therefore removed. In the test results shown, the actual actuator measurement was used since it was desired to be able to switch to and from the conventional controller at any time. In the actual implementation however, this would not be the case, conditioning will be done with respect to the (limited) output of the controller, and the speed of response

will improve. This is seen from Figure 8.15 in which the dashed line shows the (linear) case when the controller is conditioned with the actuator measurement, and the solid line corresponds to conditioning being done with the controller output. In both cases there is no saturation, the sluggishness of the response for the former case is clearly seen. Thus it can be said that the same controller (as was tested on the engine) should be able to meet the time domain specification when conditioned with the ‘proper’ signal. This is confirmed by simulating the controller on the full non-linear engine model; Figure 8.16 shows that the response is well within the specification and faster than that achieved by some existing controllers [100, 37]. It should also be noted that for the engine tests, the reference demands were rate-limited; the rate limit could also be increased to yield faster responses.

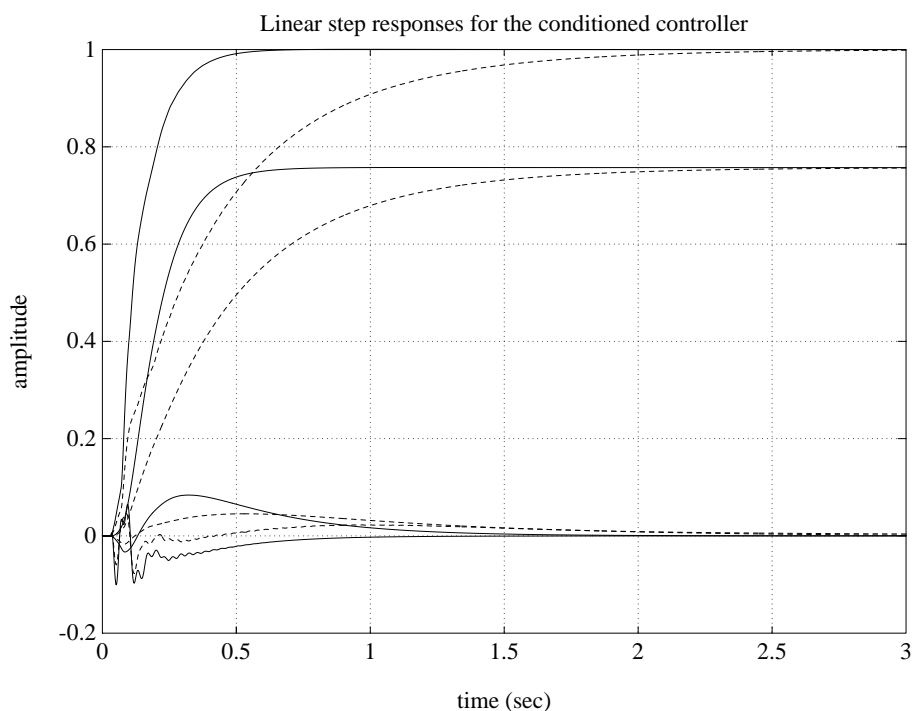


Figure 8.15: Linear step responses: conditioning done with the (limited) output of the controller —, conditioning done with the actuators’ measured output - - -.

## 8.4 Full flight envelope evaluation

The operating point of an aero-engine is defined by its operating altitude, forward speed (or Mach number) and the thrust being produced. The altitude and forward speed cause

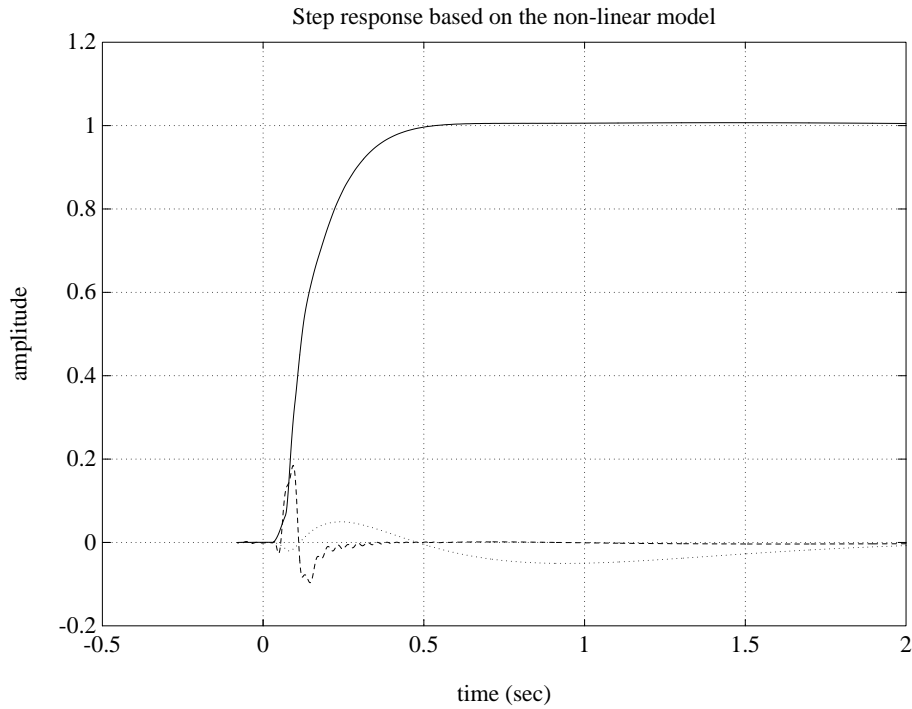


Figure 8.16: Step response for the non-linear model.

the engine's inlet pressure and temperature to change and it is this change in pressure which causes the engine dynamics to vary. In the test results presented earlier, the thrust level varied, but the altitude and speed were fixed to be zero. It was found that the controller's performance was robust enough to cope with the change in engine dynamics due to variation in thrust. We shall now analyse the controller at different combinations of altitude and forward speed, i.e., at different points in the flight envelope.

The flight envelope of the Spey engine is defined in Table 8.1 and depicted graphically in Figure 8.17. Also given in Table 8.1 is the engine inlet pressure which varies from 216 kPa for point 8 to 17.6 kPa for point 7. This variation in pressure causes considerable change in the engine open-loop dynamics, and to cope with this, controllers designed for full flight envelope operation have always had to be gain-scheduled [52, 77, 74].

The  $H_\infty$  controller designed in Chapter 7 was tested over the entire flight envelope using the full non-linear engine simulation. Step responses for the thrust output (PS6PS1) for flight points 1, 2, 3, 4, 6, 8 and 10 are shown in Figure 8.18 and are seen to be acceptable and within the specification. Responses for points 5, 7 and 9 are shown in Figure 8.19; these show excessive cross-coupling from PS6PS1 to the DPUP channel, in particular

Flight point	Mach number	Altitude (kft)	Total Inlet Pressure (kPa)
1	0.0	0	101.325
2	0.0	5	84.3073
3	0.2	5	86.6916
4	0.297	20	49.5023
5	0.4	36	25.3785
6	0.8	20	70.9782
7	0.8	50	17.6782
8	1.1	0	216.3427
9	1.1	36	48.5302
10	1.8	36	130.598

Table 8.1: Flight envelope of the Spey engine – possible flight points for control checks.

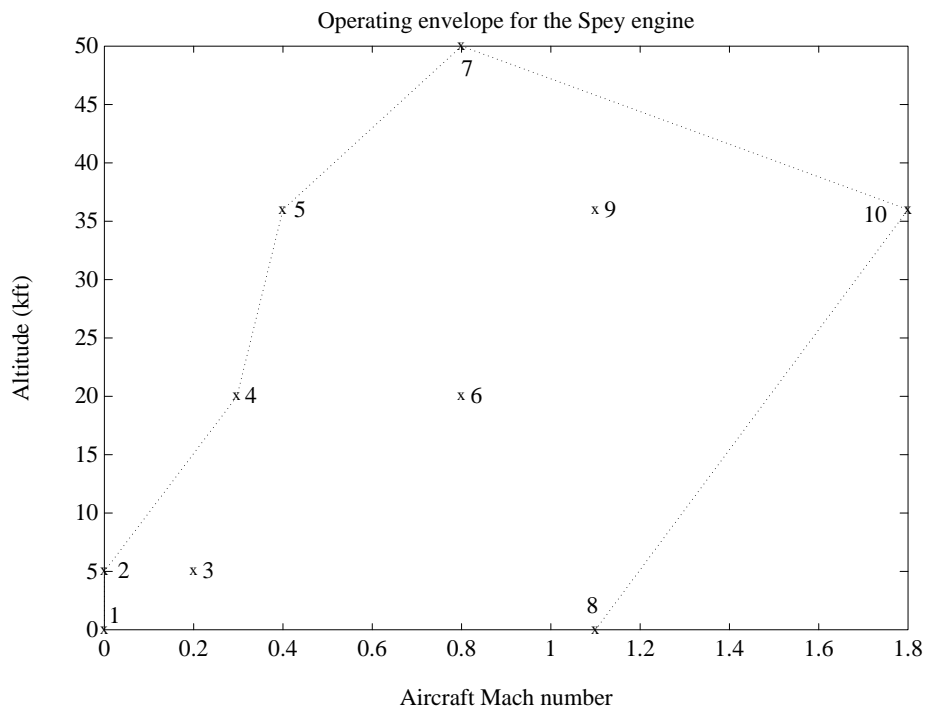


Figure 8.17: Operating envelope for the Spey engine.

DPUP shows 60% coupling for point 7. It is observed that these three points correspond to relatively low engine inlet pressures (Table 8.1). It should be noted that the outputs of the aero-engine are inter-dependent: in practice the reference set-points for the various outputs will be changed in accordance with each other, hence the interaction between the PS6PS1 and DPUP outputs is not as serious as it appears from the figure. Nevertheless this cross-coupling should be reduced and this can be done by appropriately filtering the references before giving them to the controller. As an example, we consider a pre-filter of the form:

$$K_p = \begin{bmatrix} 1 & 0 & 0 \\ \alpha \frac{s}{s^2+15s+50} & 1 & 0 \\ 0 & 0 & 1 \end{bmatrix}, \quad (8.4.1)$$

where  $\alpha$  is a scalar gain which can be scheduled between different points. Step responses for flight points 5 and 7 were repeated with the pre-filter,  $\alpha$  being chosen to be 9 for point 5, and 12 for point 7. These responses are shown in Figure 8.20; it is seen that the interaction has been reduced to an acceptable level. The parameter  $\alpha$  can thus be scheduled with the inlet pressure to reduce the cross-coupling observed at low pressures. The responses are now within the specification, except for the rise time for point 7, the 90% level being achieved in 0.65 seconds, instead of 0.5 seconds. This will require some redesign: the weighting functions  $W_1$  and  $W_2$ , and/or the reference model  $M_o$  may be changed and the controller re-synthesized. It is emphasized however that the specifications [98] and [99] were prepared primarily for sea-level static conditions; for other flight points these may be slightly different.

Disturbance step responses for PS6PS1 are shown in Figures 8.21 and 8.22 for flight points 1 and 7, respectively. The rejection of the disturbance is seen to be satisfactory.

## 8.5 Conclusions

Engine test results were presented and were seen to be very promising. The tests were conducted on the Rolls Royce Spey engine at the DRA at sea-level static conditions. The controller performed all the tasks well, and within the specification. One single controller was used – gain scheduling was not required. Existing controllers [100, 37] need to be scheduled – six or more controllers are normally scheduled between idle and full power.

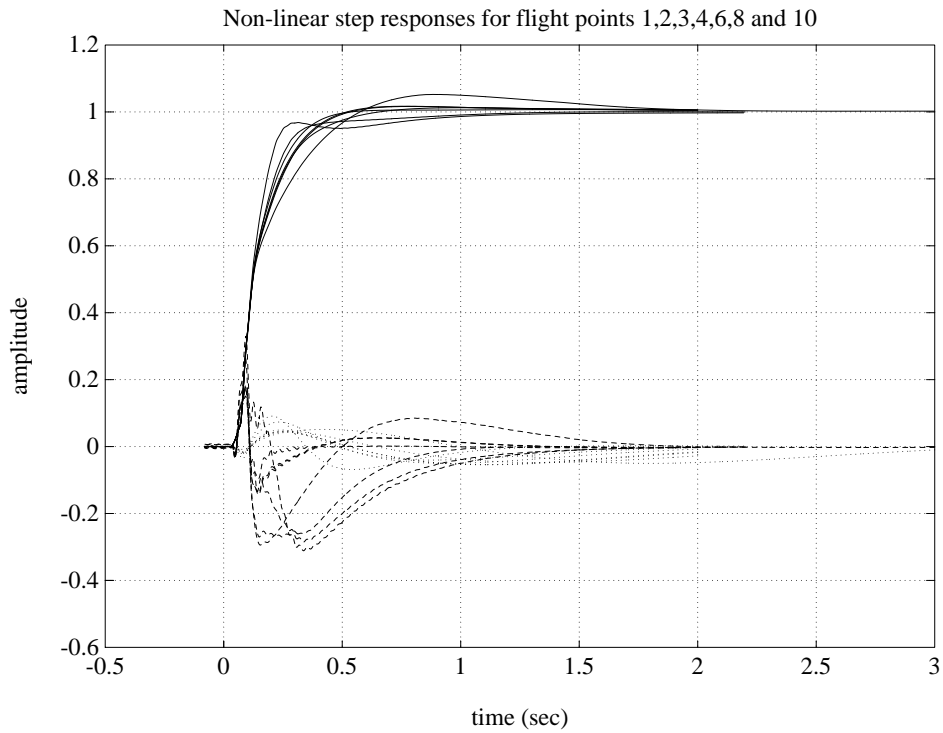


Figure 8.18: Non-linear step responses for flight points 1,2,3,4,6,8 and 10.

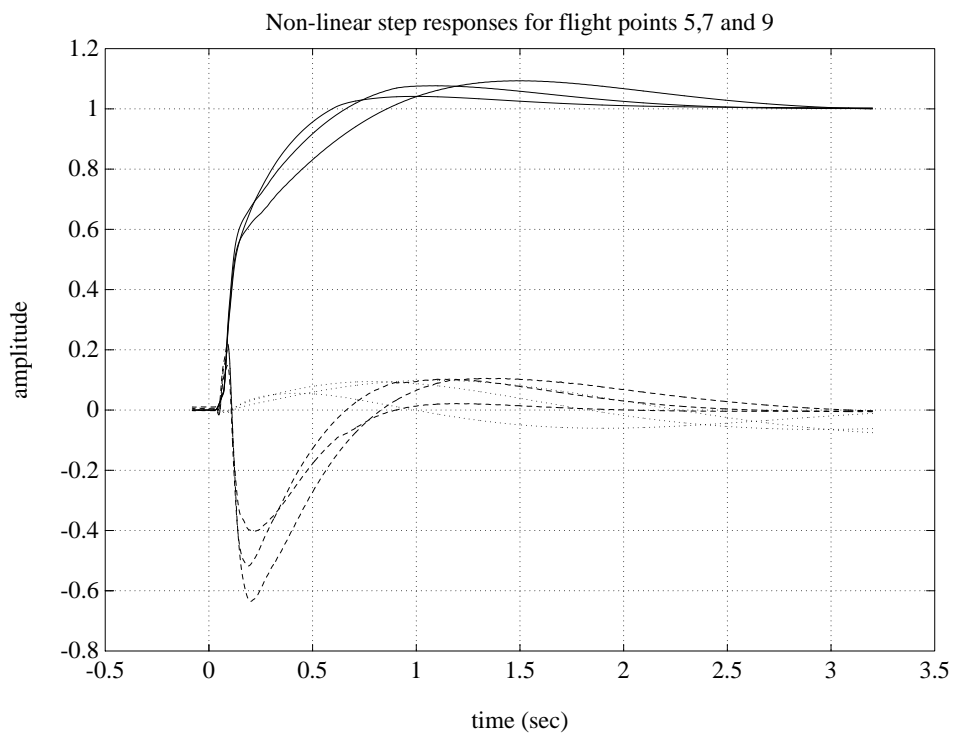


Figure 8.19: Non-linear step responses for flight points 5,7 and 9.

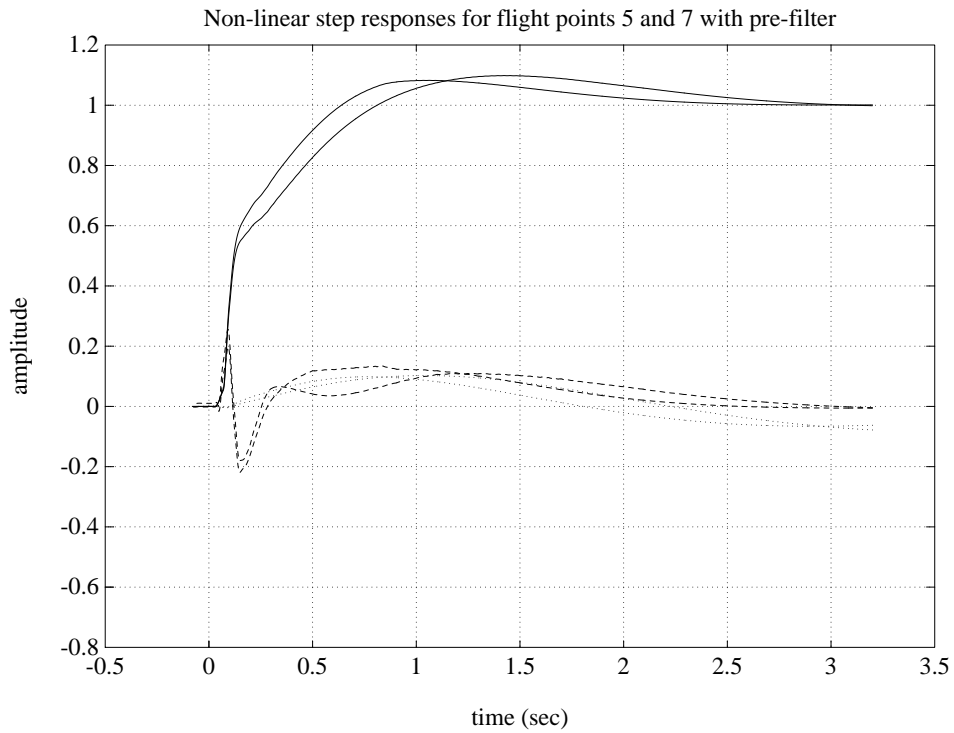


Figure 8.20: Non-linear step responses for flight points 5 and 7 with the pre-filter.

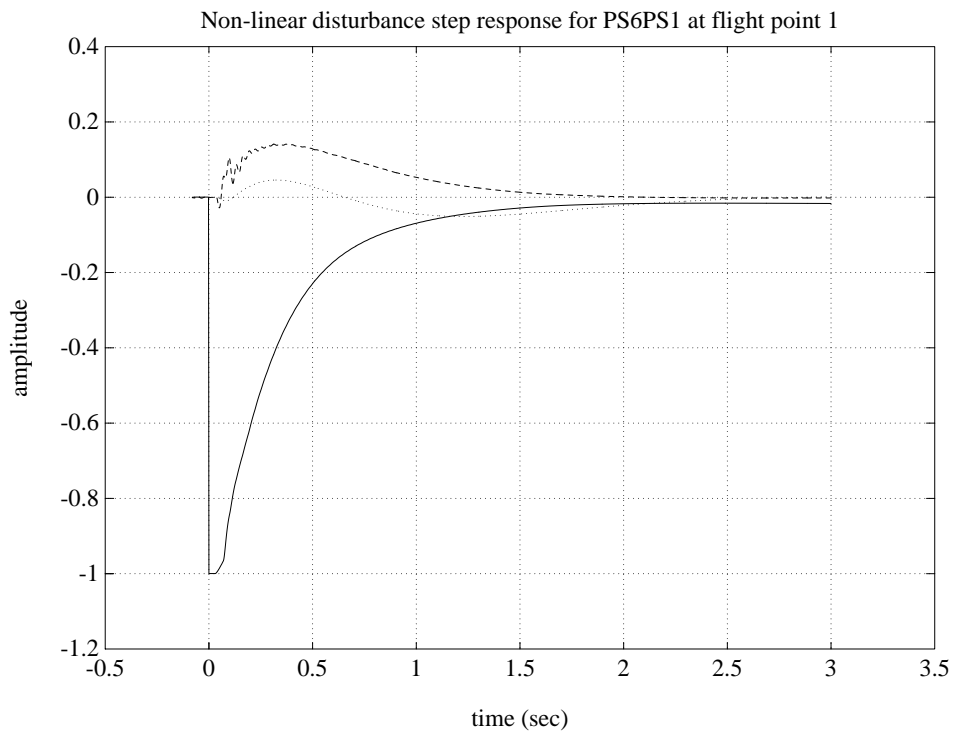


Figure 8.21: Non-linear disturbance step response for PS6PS1 at flight point 1.

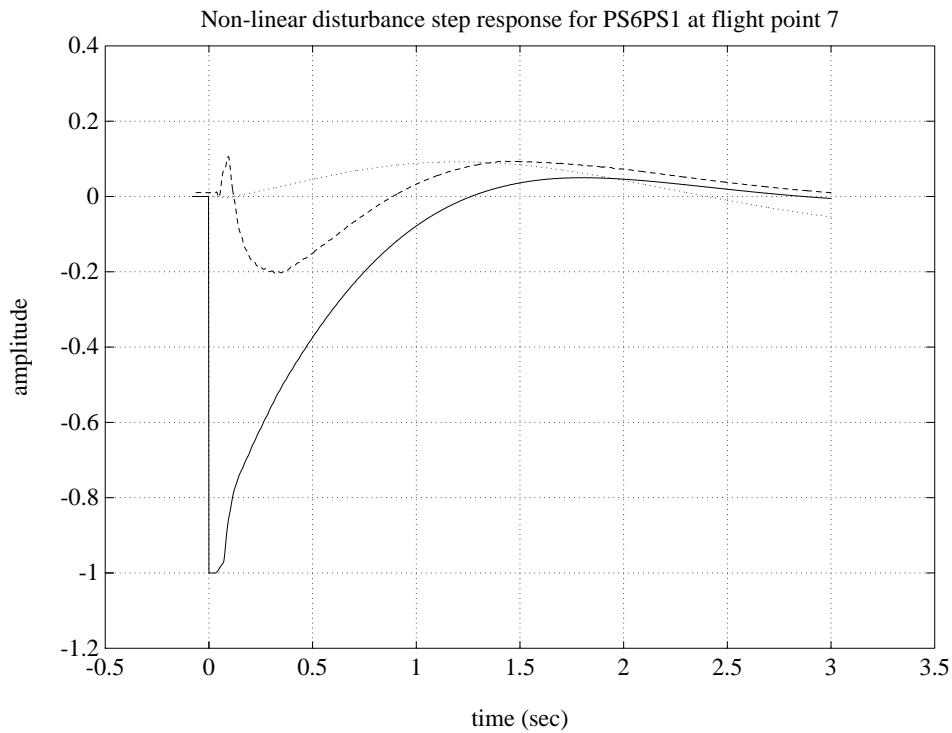


Figure 8.22: Non-linear disturbance step response for PS6PS1 at flight point 7.

Factors affecting the speed of response of the closed-loop system were discussed, and it was shown how the controller could be conditioned to improve the system's rise time. Full flight envelope evaluation of the controller was carried out by using the full non-linear simulation of the aero-engine. The plant dynamics were seen to vary considerably with the engine's inlet pressure. The controller performed satisfactorily at seven of the ten points chosen. The three other points were judged to require some redesign: this could either be a pre-filter for shaping the references, or a separate controller, which could be switched to at low inlet pressures. In any case, more design and test effort is required in this direction. Closed-loop specifications need to be produced for the entire flight envelope, and designing for these will be the subject of future work.

In conclusion of this chapter, it can be said that the controller was seen to provide, in addition to robust stability, a good degree of robust performance, and therefore holds great potential for success in the field of high performance aero-engine control.

## Chapter 9

# Conclusions and suggestions for further research

### 9.1 Conclusions

This thesis demonstrates the applicability of  $H_\infty$  control theory to real engineering problems.  $H_\infty$  control techniques were used to develop robust digital controllers for high performance aero-engines. Engine tests were carried out to demonstrate the design work and to make comparisons with existing control systems. The major conclusion of this work is that  $H_\infty$  control theory is indeed a powerful design tool which can provide practical and workable solutions to the control problems associated with complex multivariable systems.

The design problem tackled here is a challenging one, owing to the highly nonlinear behaviour of the plant, a limited amount of computing power available, and the necessity of preventing violation of several operational constraints. In the process of designing the controller, many issues regarding the design and implementation of robust multi-mode controllers were brought to light. Some answers to these issues have been found and have resulted in an overall design methodology which is fairly generic and which could be applied to a multitude of other problems. The main conclusions and contributions of this thesis are now discussed.

- The working and operation of high performance aero-engines, and associated control problems were discussed in detail. Multi-mode control logic was developed to ensure that engine variables are always limited to specified safe values. Since the controller was to be implemented using a digital computer, the delays associated with such

an implementation were modelled exactly in the discrete domain, and the controller synthesized directly in discrete time.

- Some of the engine parameters which need to be controlled, such as thrust and compressor surge margin, are not directly measurable. Instead, a host of representative measurements are available which can be controlled to provide indirect control of these parameters. A methodology for choosing between the available measurements (control structure design) was presented and demonstrated on the aero-engine example.
- To derive accurate, yet low order models of a physical system from more complicated models is very important for the design of reasonably low order controllers. For this purpose, model reduction using balanced realizations was investigated. Residualization of balanced realizations was considered, and detailed comparisons made with balanced truncation and optimal Hankel-norm approximation. Balanced residualization was shown to preserve the steady-state gain of the system and produce accurate matching at low and medium frequencies. This is favourable for both plant and controller order reduction. The various techniques were demonstrated on two illustrative examples.
- Modern design methods, such as  $H_\infty$ -optimization, are generally considered by practitioners and industrial engineers to produce controllers which are too complex with regards to practical implementation. This is in part due to the high state dimension of the resulting controllers, and also largely due to the fact that the basic structure and operation of these controllers is not as intuitive and readily recognisable as that of say, the more familiar PIDs. Nevertheless, the limitations of single-input single-output control are becoming more and more widely appreciated, and the need for inherently multivariable design procedures has become more accepted. The benefits offered by multivariable control led the aerospace industry, to take up and apply in the 1960s and 70s, the linear quadratic Gaussian based design methods to flight control problems. The notion of control via state feedback combined with a state estimator was thus first taken up by the aerospace industry, and gradually this concept gained familiarity and acceptance from other industries as well. With this in the

background, a particular  $H_\infty$  design formulation was considered, and the structure of the controller investigated. The design technique considered is both powerful and simple to use; the design procedure involves generalization of classical loop-shaping ideas, and provides robust performance in the sense of making the closed-loop system match an ideal time response model. The resulting  $H_\infty$  controller was shown to possess the familiar observer plus state feedback structure. The controller structure was utilized to yield considerable real time computational savings.

- The design procedure was illustrated by working through the design details of the aero-engine controller. The structure of the overall switched multi-mode controller was described. Implementation issues were discussed and an efficient form for implementation presented. The problem of anti-windup and bumpless transfer between different modes of operation was discussed and a simple strategy for dealing with this problem outlined.
- Engine test results were presented and discussed. The engine was operated over its full thrust range. One single controller was used – gain-scheduling was not required. Existing engine controllers need to be gain-scheduled – six or more controllers are normally scheduled between idle and full power [100, 37, 51, 22]. Furthermore, the same controller was evaluated over the entire flight envelope using the full nonlinear engine simulation provided by the DRA. The controller gave good performance for seven of the ten flight points simulated. For the three other points, a high level of interaction was observed, but this was shown to be reduced by appropriately filtering the reference signals. However, some redesign for one of the flight points was still thought to be required to meet the rise time specification. It is however, remarked that the specifications were originally prepared for sea-level static conditions. New specifications therefore, need to be devised for other points in the flight envelope. More design and test effort is required in this area and this should be the subject of future research. The robust performance of the controller was nevertheless demonstrated, and was found to be far superior to that afforded by existing engine control systems. It is reckoned that simple scheduling of the reference pre-filter or at most, one additional controller which could be switched to at low inlet pressures, would be sufficient for the entire flight envelope. Multi-mode operation of the controller was

also engine tested and found to give excellent results. The anti-windup and bumpless transfer compensation worked well – the switching between different modes of operation was smooth and bumpless.

## 9.2 Suggestions for future research

The work presented in this thesis, in terms of both design and implementation, points to a number of areas which require further research. These are discussed below.

- The model reduction approach advocated in Chapter 5 is applicable only to asymptotically stable systems. To tackle unstable systems, one way to proceed is to use a fractional representation of the system, as proposed by McFarlane & Glover [64]. For example, an unstable system  $G$  can be written in terms of its coprime factors as  $G = M^{-1}N$ , where  $M, N \in RH_\infty$ . The balanced residualization technique could then be used to approximate  $\begin{bmatrix} N & M \end{bmatrix}$  of degree  $n$  by  $\begin{bmatrix} N_r & M_r \end{bmatrix}$  of degree  $k$ , where  $k < n$ . The reduced order transfer function  $G_r$  could then be formed as  $G_r = M_r^{-1}N_r$ . Whereas the error bound  $\left\| \begin{bmatrix} N & M \end{bmatrix} - \begin{bmatrix} N_r & M_r \end{bmatrix} \right\|_\infty$  is known, the bound on the error between the full order and reduced systems, i.e.,  $\|G - G_r\|_\infty$  is not available. Deriving this bound could be a subject for future research.
- A more general and challenging problem pertaining to controller reduction is that of finding the *optimal* reduced order controller, where by optimal we mean the controller which best meets the performance and robustness requirements from amongst the set of all possible reduced order controllers of a given degree.
- Multi-mode control logic was developed to preserve the structural integrity of the engine by limiting certain critical variables to specified maximum values. This was done by designing a number of controllers and then switching between them using a lowest-wins gate. The rationale behind this strategy is that a large demand on thrust will require a large amount of fuel, and hence result in higher temperatures and speeds. This can cause the temperature and/or speed limits to be violated. Alternative multi-mode schemes, such as the one shown in Figure 9.1, can also be investigated. With reference to Figure 9.1, the idea is to devise a strategy where the

reference demand for thrust (PS6PS1ref) is “backed off” when a particular limit is about to be violated.

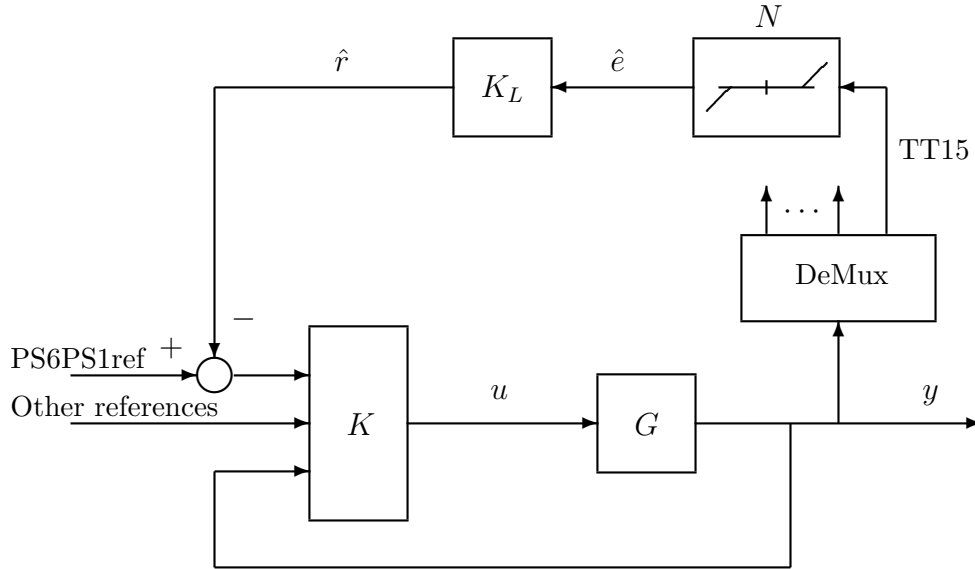


Figure 9.1: An alternative limiting strategy.

The output to be limited, say the temperature TT15 in this case, is passed to a nonlinearity  $N$ , whose output is connected to the linear compensation  $K_L$ . The nonlinearity  $N$  can be designed such that its gain is unity when the input exceeds some specified value, but is zero at all other times. Hence the signal  $\hat{e}$  could be arranged to become non-zero just before the limit is about to be exceeded, and based on this the compensator  $K_L$  can generate a signal  $\hat{r}$  which will serve to lower the demand on thrust. A limiting scheme could be developed based on these ideas. The design of the compensator  $K_L$  and the nonlinear element  $N$  is, however, an open question and requires further research.

- The structure of the  $H_\infty$  loop-shaping controller was shown to be utilized to yield considerable real time computational savings. The computational load could be reduced further by making use of the minimal modal canonical form proposed by Nett & Polley [71], and later used by Hyde [46]. When implemented in this form the  $A$  matrix of the state-space realization ( $A, B, C, D$ ) has elements only on the leading diagonal and the immediate off-diagonals, and the  $B$  matrix consists mainly

of ones and zeros. Finding such a realization is straightforward and just requires an eigenvalue-eigenvector decomposition of the matrix  $A$ . For future implementation, the observer and the reference model parts of the controller could both be implemented in the modal form; this is expected to yield further computational savings.

- Design of anti-windup and bumpless transfer (AWBT) compensators for multivariable systems is quite *ad hoc* at present. A set of guidelines as to which anti-windup scheme is most appropriate for a given situation would be very useful.

The AWBT design problem has almost always been tackled by breaking it down into two separate parts:

- (i) the design of the controller without regard to control limitations and substitutions, and
- (ii) the design of AWBT compensation to minimize the adverse effects of limitations and substitutions on closed-loop performance.

Campo et al. [8] and Campo & Morari [7] have proposed a general framework for the study of anti-windup designs, which has implications for developing synthesis procedures as well; synthesis results are, however, not yet available. A challenging problem for future research could be to further the work of Campo et al. [8] and Campo & Morari [7] and to develop general synthesis methods for AWBT controllers.

- The dynamics of high performance aero-engines have been found to vary considerably over the operating envelope. Different design techniques could be applied to design robust and/or adaptive controllers for such systems. The controllers should provide full flight operation, and should prevent violation of operational constraints. One particular design approach was considered in this thesis, other approaches could be used and the results compared with those presented here.

One of the design methods which could be applied to the aero-engine control problem is  $\mu$ -synthesis. Linear engine models for different operating points could be obtained, and the change in the state-space description of the plant modelled as structured uncertainty [72]. Once in this form, the state-space uncertainty can be used in

structured singular value analysis, and also for design using  $D$ - $K$  iteration [16].  $\mu$ -optimal controllers can thus be designed; this should address explicitly the problem of maintaining acceptable performance over the entire operating range of the engine. The robustness that  $H_\infty$ -optimization provides can thus be “tuned” to the problem at hand. This could be a novel and challenging application for design using  $\mu$ -synthesis techniques.

## References

- [1] B.D.O. Anderson. Weighted Hankel-norm approximation: Calculation of bounds. *Systems & Control Letters*, 7(4):247–255, 1986.
- [2] B.D.O. Anderson and Y. Liu. Controller reduction: Concepts and approaches. *IEEE Transactions on Automatic Control*, 34(8):802–812, 1989.
- [3] K.J. Åström and L. Rundqwist. Integrator windup and how to avoid it. In *Proceedings of American Control Conference*, pages 1693–1698, Pittsburgh, USA, 1989.
- [4] K.J. Åström and B. Wittenmark. *Computer Controlled Systems: Theory and Design*. Prentice-Hall, Englewood Cliffs, NJ 07632, USA, 1984.
- [5] M. Athans, P. Kapsouris, E. Kappos, and H.A. Spang. Linear-quadratic Gaussian with loop transfer recovery methodology for the F-100 engine. *Journal of Guidance, Control, and Dynamics*, 9(1):45–52, 1986.
- [6] G.J. Balas, J.C. Doyle, K. Glover, A. Packard, and R. Smith.  *$\mu$ -Analysis and Synthesis Toolbox: User's Guide*. The MathWorks, Natick, MA 01760, USA, 1991.
- [7] P.J. Campo and M. Morari. Robust control of processes subject to saturation nonlinearities. *Computers & Chemical Engineering*, 14(4/5):343–358, 1990.
- [8] P.J. Campo, M. Morari, and C.N. Nett. Multivariable anti-windup and bumpless transfer: A general theory. In *Proceedings of American Control Conference*, pages 1706–1711, Pittsburgh, USA, 1989.
- [9] J. Chen, J.S. Freudenberg, and C.N. Nett. The role of the condition number and the relative gain array in robustness analysis. *Automatica*, 30(6):1029–1035, 1994.

- [10] R.Y. Chiang and M.G. Safonov. *Robust Control Toolbox: User's Guide*. The MathWorks, Natick, MA 01760, USA, 1992.
- [11] H. Cohen, G.F.C. Rogers, and H.I.H. Saravanamuttoo. *Gas Turbine Theory*. Longman Group UK Limited, Essex, England, third edition, 1987.
- [12] C.A. Desoer and M. Vidyasagar. *Feedback Systems: Input-Output Properties*. Academic Press, New York, 1975.
- [13] J. Doyle. Analysis of feedback systems with structured uncertainties. *IEE Proceedings*, Part D, 129(6):242–250, 1982.
- [14] J. Doyle, K. Lenz, and A. Packard. Design examples using  $\mu$ -synthesis: Space shuttle lateral axis FCS during reentry. In *Proceedings of the 25th IEEE Conference on Decision and Control*, pages 2218–2223, Athens, Greece, 1986.
- [15] J.C. Doyle. Guaranteed margins for LQG regulators. *IEEE Transactions on Automatic Control*, AC-23(4):756–757, 1978.
- [16] J.C. Doyle. Structured uncertainty in control system design. In *Proceedings of the 24th IEEE Conference on Decision and Control*, pages 260–265, Ft. Lauderdale, FL, USA, 1985.
- [17] J.C. Doyle, K. Glover, P.P. Khargonekar, and B.A. Francis. State-space solutions to standard  $H_2$  and  $H_\infty$  control problems. *IEEE Transactions on Automatic Control*, 34(8):831–847, 1989.
- [18] J.C. Doyle and G. Stein. Robustness with observers. *IEEE Transactions on Automatic Control*, AC-24(4):607–611, 1979.
- [19] J.C. Doyle and G. Stein. Multivariable feedback design: Concepts for a classical/modern synthesis. *IEEE Transactions on Automatic Control*, AC-26(1):4–16, 1981.
- [20] J.C. Doyle, J.E. Wall, and G. Stein. Performance and robustness analysis for structured uncertainty. In *Proceedings of the 21st IEEE Conference on Decision and Control*, pages 629–636, Orlando, Florida, USA, 1982.

- [21] J.M. Edmunds. Control system design and analysis using closed-loop nyquist and bode arrays. *International Journal of Control*, 30(5):773–802, 1979.
- [22] S.A. Eisa and H.P. Tyler. Closed loop control of an afterburning F100 gas turbine engine. In *Proceedings of the American Control Conference*, pages 266–272, Seattle, WA, USA, 1986.
- [23] D. Enns. *Model Reduction for Control System Design*. PhD thesis, Department of Electrical Engineering, Stanford University, 1984.
- [24] D.F. Enns. Model reduction with balanced realizations: An error bound and a frequency weighted generalization. In *Proceedings of the 23rd IEEE Conference on Decision and Control*, pages 127–132, Las Vegas, NV, USA, 1984.
- [25] B.A. Francis. *A Course in  $H_\infty$  Control Theory*, volume 88 of *Lecture Notes in Control and Information Sciences*. Springer-Verlag, Berlin, 1987.
- [26] G.F. Franklin, J.D. Powell, and A. Emami-Naeini. *Feedback Control of Dynamic Systems*. Addison-Wesley, second edition, 1991.
- [27] G.F. Franklin, J.D. Powell, and M.L. Workman. *Digital Control of Dynamic Systems*. Addison-Wesley, second edition, 1990.
- [28] J.S. Freudenberg. Analysis and design for ill-conditioned plants—Part 1. Lower bounds on the structured singular value. *International Journal of Control*, 49(3):851–871, 1989.
- [29] J.S. Freudenberg. Plant directionality, coupling and multivariable loop-shaping. *International Journal of Control*, 51(2):365–390, 1990.
- [30] K. Glover. All optimal Hankel-norm approximations of linear multivariable systems and their  $L^\infty$ -error bounds. *International Journal of Control*, 39(6):1115–1193, 1984.
- [31] K. Glover and J.C. Doyle. State-space formulae for all stabilizing controllers that satisfy an  $H_\infty$ -norm bound and relations to risk sensitivity. *Systems & Control Letters*, 11:167–172, 1988.

- [32] K. Glover and D. McFarlane. Robust stabilization of normalized coprime factor plant descriptions with  $H_\infty$ -bounded uncertainty. *IEEE Transactions on Automatic Control*, 34(8):821–830, 1989.
- [33] A. Grace, A.J. Laub, J.N. Little, and C.M. Thompson. *Control System Toolbox for use with Matlab: User's Guide*. The MathWorks, Natick, MA 01760, USA, 1992.
- [34] M. Green.  $H_\infty$  controller synthesis by J-lossless coprime factorization. *SIAM Journal of Control and Optimization*, 30(3):522–547, 1992.
- [35] M. Green, K. Glover, D. Limebeer, and J. Doyle. A  $J$ -spectral factorization approach to  $H_\infty$  control. *SIAM Journal of Control and Optimization*, 28(6):1350–1371, 1990.
- [36] M. Green and D.J.N. Limebeer. *Linear Robust Control*. Prentice-Hall, Englewood Cliffs, NJ 07632, USA, 1995.
- [37] A.W.M. Greig. Multivariable powerplant control - proof of concept. Technical Report DRA/AS/PTD/TR/94067/1, Defence Research Agency, Farnborough, Hampshire, UK, 1994.
- [38] P. Grosdidier and M. Morari. Interaction measures for systems under decentralized control. *Automatica*, 22(3):309–319, 1986.
- [39] D.-W. Gu, R. Samar, B.-W. Choi, and I. Postlethwaite. Model reduction in aero-engine control. In *Proceedings of the 1st Asian Control Conference*, volume 2, pages 457–460, Tokyo, 1994.
- [40] R. Hanus and M. Kinnaert. Control of constrained multivariable systems using the conditioning technique. In *Proceedings of American Control Conference*, pages 1712–1718, Pittsburgh, USA, 1989.
- [41] R. Hanus, M. Kinnaert, and J.-L. Henrotte. Conditioning technique, a general anti-windup and bumpless transfer method. *Automatica*, 23(6):729–739, 1987.
- [42] R.T.C. Harman. *Gas Turbine Engineering: Applications, Cycles and Characteristics*. Macmillan, London, 1981.

- [43] R.F. Hoskin, C.N. Nett, and D.E. Reeves. Control configuration design for a mixed vectored thrust ASTOVL aircraft in hover. In *AIAA Guidance, Navigation and Control Conference: A Collection of Technical Papers*, pages 1625–1642, New Orleans, USA, 1991.
- [44] M. Hovd and S. Skogestad. Simple frequency-dependent tools for control system analysis, structure selection and design. *Automatica*, 28(5):989–996, 1992.
- [45] D.J. Hoyle, R.A. Hyde, and D.J.N. Limebeer. An  $H_\infty$  approach to two degree of freedom design. In *Proceedings of the 30th IEEE Conference on Decision and Control*, pages 1581–1585, Brighton, England, 1991.
- [46] R.A. Hyde. *The Application of Robust Control to VSTOL Aircraft*. PhD thesis, Cambridge University, 1991.
- [47] R.A. Hyde and K. Glover. A comparison of different scheduling techniques for  $H_\infty$  controllers. In *Proceedings of the Institute of Measurement & Control Symposium on Robust Control System Design using  $H_\infty$  and Related Methods*, University of Cambridge, England, 1991.
- [48] R.A. Hyde and K. Glover. Taking  $H_\infty$  control into flight. In *Proceedings of the 32nd IEEE Conference on Decision and Control*, pages 1458–1463, San Antonio, Texas, USA, 1993.
- [49] R.A. Hyde, K. Glover, and S.J. Williams. Scheduling by switching of  $H_\infty$  controllers for a VSTOL aircraft. In *Proceedings of the Institute of Measurement & Control Symposium on Application of Multivariable System Techniques*, University of Bradford, England, 1990.
- [50] P.A. Iglesias and K. Glover. State-space approach to discrete-time  $H_\infty$  control. *International Journal of Control*, 54(5):1031–1073, 1991.
- [51] X. Jiarui, G. Yunho, and Z. Shaoji. Development of QSK-06 full authority digital electronic control for gas turbines. In *Proceedings of the Japan-USA Symposium on Flexible Automation*, pages 805–810, 1986.

- [52] P. Kapsouris. Gain-scheduled multivariable control for the GE-21 turbofan engine using the LQR and LQG/LTR methodologies. Master's thesis, Massachusetts Institute of Technology, Cambridge, MA, USA, 1984.
- [53] E.M. Kasenally, D.J.N. Limebeer, and A. Portone. Robust instability control of ITER plasmas. In *Proceedings of 12th IFAC World Congress on Automatic Control*, volume 4, pages 389–392, Sydney, Australia, 1993.
- [54] M.G. Kellett. Continuous scheduling of  $H_\infty$  controllers for a MS760 Paris aircraft. In *Proceedings of the Institute of Measurement & Control Symposium on Robust Control System Design using  $H_\infty$  and Related Methods*, University of Cambridge, England, 1991.
- [55] J.L. Kerrebrock. *Aircraft Engines and Gas Turbines*. The MIT Press, Cambridge, Massachusetts 02142, USA, second edition, 1992.
- [56] M.V. Kothare, P.J. Campo, M. Morari, and C.N. Nett. A unified framework for the study of anti-windup designs. *Automatica*, 30(12):1869–1883, 1994.
- [57] G.A. Latham and B.D.O. Anderson. Frequency-weighted optimal Hankel-norm approximation of stable transfer functions. *Systems & Control Letters*, 5(4):229–236, 1985.
- [58] W.E. Leithead and J. O'Reilly. Multivariable control by individual channel design: An automotive gas turbine case study. In *Proceedings of the IEE International Conference on Control '91*, pages 1261–1266, Edinburgh, UK, 1991.
- [59] D.J.N. Limebeer, M. Green, and D. Walker. Discrete time  $H_\infty$  control. In *Proceedings of the 28th IEEE Conference on Decision and Control*, pages 392–396, Tampa, Florida, USA, 1989.
- [60] D.J.N. Limebeer, E.M. Kasenally, and J.D. Perkins. On the design of robust two degree of freedom controllers. *Automatica*, 29(1):157–168, 1993.
- [61] Y. Liu and B.D.O. Anderson. Singular perturbation approximation of balanced systems. *International Journal of Control*, 50(4):1379–1405, 1989.

- [62] J.M. Maciejowski. *Multivariable Feedback Design*. Addison-Wesley, Wokingham, U.K., 1989.
- [63] D. McFarlane and K. Glover. A loop shaping design procedure using  $H_\infty$  synthesis. *IEEE Transactions on Automatic Control*, 37(6):759–769, 1992.
- [64] D.C. McFarlane and K. Glover. *Robust Controller Design Using Normalized Coprime Factor Plant Descriptions*, volume 138 of *Lecture Notes in Control and Information Sciences*. Springer-Verlag, Berlin, 1990.
- [65] D.E. Moellenhoff, S.V. Rao, and C.A. Skarvan. Design of robust controllers for gas turbine engines. *Journal of Engineering for Gas Turbines and Power*, 113:283–289, April 1991.
- [66] B.C. Moore. Principal component analysis in linear systems: Controllability, observability, and model reduction. *IEEE Transactions on Automatic Control*, AC-26(1):17–32, 1981.
- [67] M. Morari. Some control problems in the process industries. In H.L. Trentelman and J.C. Willems, editors, *Essays on Control: Perspectives in the Theory and its Applications*, volume 14 of *Progress in Systems and Control Theory*, pages 55–77. Birkhäuser, Boston, 1993.
- [68] M. Morari and E. Zafiriou. *Robust Process Control*. Prentice-Hall, Englewood Cliffs, NJ 07632, USA, 1989.
- [69] G. Murad, I. Postlethwaite, D.-W. Gu, and J. Whidborne. Robust control of a glass tube shaping process. In *Proceedings of the 2nd European Control Conference*, pages 2350–2355, 1993.
- [70] C.N. Nett and V. Manousiouthakis. Euclidean condition and block relative gain: Connections, conjectures, and clarifications. *IEEE Transactions on Automatic Control*, AC-32(5):405–407, 1987.
- [71] C.N. Nett and J.A. Polley. Integrated design/implementation of nonlinear digital controllers. In *Proceedings of the American Control Conference*, pages 1671–1678, 1988.

- [72] A. Packard and J. Doyle. Excerpts from a forthcoming book on  $\mu$ . To appear.
- [73] J.L. Peczkowski and M.K. Sain. Design of nonlinear multivariable feedback controls by total synthesis. In *Proceedings of American Control Conference*, pages 688–697, San Diego, CA, USA, 1984.
- [74] R.A. Perez. A decentralized control scheme for a high performance turbine. In *Proceedings of the 32nd IEEE Conference on Decision and Control*, pages 436–441, San Antonio, Texas, USA, 1993.
- [75] L. Pernebo and L.M. Silverman. Model reduction via balanced state space representations. *IEEE Transactions on Automatic Control*, AC-27(2):382–387, 1982.
- [76] W.H. Pfeil, M. Athans, and H.A. Spang. Multivariable control of the GE T700 engine using the LQG/LTR design methodology. In *Proceedings of American Control Conference*, pages 1297–1312, Seattle, WA, USA, 1986.
- [77] J.A. Polley, S. Adibhatla, and P.J. Hoffman. Multivariable turbofan engine control for full flight envelope operation. In *Proceedings of the 33rd ASME Gas Turbine and Aeroengine Congress and Exposition*, Amsterdam, The Netherlands, June 5-9 1988.
- [78] B. Porter and A.H. Jones. Design of tunable digital set-point tracking PI controllers using step-response matrices for gas turbines. In *Proceedings of the AIAA Guidance, Navigation and Control Conference*, pages 553–558, Williamsburg, 1986.
- [79] I. Postlethwaite and Y.K. Foo. Robustness with simultaneous pole and zero movement across the  $j\omega$ -axis. *Automatica*, 21(4):433–443, 1985.
- [80] I. Postlethwaite and J. Geddes. Gauge control in tandem cold rolling mills: A multivariable case study using  $H_\infty$  optimization. In *Proceedings of the 3rd IEEE Conference on Control Applications*, pages 1551–1556, Strathclyde University, Glasgow, UK, 1994.
- [81] I. Postlethwaite, D.-W. Gu, S.D. O’Young, and M.S. Tombs. Industrial control system design using  $H_\infty$  optimization. In *Proceedings of the 25th IEEE Conference on Decision and Control*, pages 12–13, Athens, Greece, 1986.

- [82] I. Postlethwaite, S.D. O'Young, and D.-W. Gu. *Stable  $H$  – an  $H_\infty$  control-system design package*. *Transactions of the Institute of Measurement and Control*, 10(2):103–109, 1988.
- [83] I. Postlethwaite, S.D. O'Young, D.-W. Gu, and J. Hope.  *$H_\infty$  control system design: A critical assessment based on industrial applications*. In *Proceedings of 10th IFAC World Congress on Automatic Control*, volume 8, pages 328–333, Munich, 1987.
- [84] I. Postlethwaite, R. Samar, B.-W. Choi, and D.-W. Gu. *A digital multi-mode  $H_\infty$  controller for the Spey turbofan engine*. In *Proceedings of the 3rd European Control Conference*, Roma, Italy, 1995.
- [85] I. Postlethwaite, M.-C. Tsai, and D.-W. Gu. *Weighting function selection in  $H_\infty$  design*. In *Proceedings of 11th IFAC World Congress on Automatic Control*, volume 5, pages 104–109, Tallinn, Estonia, 1990.
- [86] I. Postlethwaite, J. Whidborne, G. Murad, and D.-W. Gu. *Robust control of the benchmark problem using  $H_\infty$  methods and numerical optimisation techniques*. In *Proceedings of 12th IFAC World Congress on Automatic Control*, volume 3, pages 193–196, Sydney, 1993.
- [87] M.G. Safonov and R.Y. Chiang. *CACSD using the state-space  $L_\infty$  theory—a design example*. *IEEE Transactions on Automatic Control*, 33(5):477–479, 1988.
- [88] M.G. Safonov, R.Y. Chiang, and H. Flashner.  *$H_\infty$  robust control synthesis for a large space structure*. *Journal of Guidance, Control, and Dynamics*, 14(3):513–520, 1991.
- [89] R. Samar, G. Murad, I. Postlethwaite, and D.-W. Gu. *A discrete time  $H_\infty$  observer-based controller & its application to an aero-engine*. In *Proceedings of American Control Conference*, Seattle, WA, USA, 1995.
- [90] R. Samar and I. Postlethwaite. *Multivariable controller design for a high performance aero-engine*. In *Proceedings of the IEE International Conference on Control '94*, pages 1312–1317, University of Warwick, Coventry, UK, 1994.

- [91] R. Samar and I. Postlethwaite. Multivariable controller design for a turbofan engine. Technical Report 93-58, Leicester University Engineering Department, October 1993.
- [92] R. Samar, I. Postlethwaite, and D.-W. Gu. Applications of the singular perturbation approximation of balanced systems. In *Proceedings of the 3rd IEEE Conference on Control Applications*, pages 1823–1828, Strathclyde University, Glasgow, UK, 1994.
- [93] R. Samar, I. Postlethwaite, and D.-W. Gu. Model reduction with balanced realizations. *International Journal of Control*, 1995. To appear.
- [94] J. Sefton and K. Glover. Pole/zero cancellations in the general  $H_\infty$  problem with reference to a two block design. *Systems & Control Letters*, 14:295–306, 1990.
- [95] S. Skogestad and M. Morari. Implications of large RGA elements on control performance. *Industrial and Engineering Chemistry Research*, 26(11):2323–2330, 1987.
- [96] S. Skogestad, M. Morari, and J.C. Doyle. Robust control of ill-conditioned plants: High-purity distillation. *IEEE Transactions on Automatic Control*, 33(12):1092–1105, 1988.
- [97] G. Stein. Beyond singular values and loop shapes. Technical Report LIDS-P-1504, Massachusetts Institute of Technology, Cambridge, MA, USA, 1985.
- [98] A. Sutton. EPSRC/LUCAS Research Programme: Engine Control Specification. Technical Report B60,702, Lucas Aerospace Limited, Birmingham, UK, 1992.
- [99] A. Sutton. EPSRC/LUCAS Research Programme: Engine Control Specification (Amended). Technical Report B60,702 Amended, Lucas Aerospace Limited, Birmingham, UK, 1994.
- [100] A.E. Sutton. The application of multivariable control to a turbofan engine. Technical Report TM P 1220, Defence Research Agency, Aerospace Division, Farnborough, Hampshire, UK, 1992. Also presented at the IEE International Conference on Control '91, Edinburgh, UK.

- [101] M.C. Tsai, E.J.M. Geddes, and I. Postlethwaite. Pole-zero cancellations and closed-loop properties of an  $H_\infty$  mixed sensitivity design problem. *Automatica*, 28(3):519–530, 1992.
- [102] M. Vidyasagar. *Control System Synthesis: A Factorization Approach*. The MIT Press, Cambridge, Massachusetts 02142, USA, 1985.
- [103] D. Walker and I. Postlethwaite. Discrete time  $H_\infty$  control laws for a high performance helicopter. In *Proceedings of the Institute of Measurement & Control Symposium on Robust Control System Design using  $H_\infty$  and Related Methods*, University of Cambridge, England, 1991.
- [104] D. Walker, I. Postlethwaite, J. Howitt, and N. Foster. Rotorcraft flying qualities improvement using advanced control. In *Proceedings of the American Helicopter Society/NASA Conference*, San Francisco, January, 1993.
- [105] D.J. Walker. On the structure of a 2-degree-of-freedom feedback controller. To be published.
- [106] D.J. Walker. Robust stabilizability of discrete-time systems with normalized stable factor perturbation. *International Journal of Control*, 52(2):441–455, 1990.
- [107] D.J. Walker. *Robust Control of Discrete Time Systems*. PhD thesis, Department of Electrical Engineering, Imperial College of Science, Technology and Medicine, University of London, 1991.
- [108] R. Watanabe, M. Kurosaki, T. Kusakawa, K. Uchida, and M. Fujita.  $H_\infty$  control of gasturbine engines for helicopters. In *Proceedings of American Control Conference*, pages 1123–1127, San Francisco, CA, USA, 1993.
- [109] J.F. Whidborne, G. Murad, D.-W. Gu, and I. Postlethwaite. Robust control of an unknown plant—the IFAC 93 benchmark. *International Journal of Control*, 61(3):589–640, 1995.
- [110] J.F. Whidborne, I. Postlethwaite, and D.-W. Gu. Robust controller design using  $H_\infty$  loop-shaping and the method of inequalities. *IEEE Transactions on Control Systems Technology*, 2(4):455–461, 1994.

- [111] S.J. Williams and R.A. Hyde. A comparison of different  $H_\infty$  methods in VSTOL flight control system design. In *Proceedings of American Control Conference*, pages 2508–2513, San Diego, CA, USA, 1990.
- [112] E.A. Wolff, S. Skogestad, M. Hovd, and K.W. Mathisen. A procedure for controllability analysis. In *Proceedings of the IFAC Workshop on interactions between process design and process control*, Imperial College, London, September 6-8 1992.
- [113] G. Zames. Feedback and optimal sensitivity: Model reference transformations, multiplicative seminorms, and approximate inverses. *IEEE Transactions on Automatic Control*, AC-26(2):301–320, 1981.
- [114] G. Zames and B.A. Francis. Feedback, minimax sensitivity, and optimal robustness. *IEEE Transactions on Automatic Control*, AC-28(5):585–601, 1983.